

https://dspace.org/

Inactivating hepatitis B virus replication using obligate heterodimeric TALEN- encoding mRNA

Smith, Tiffany Shenay

2024

University of the Witwatersrand, Johannesburg

https://hdl.handle.net/10539/47411

Smith, Tiffany Shenay . (2024). Inactivating hepatitis B virus replication using obligate heterodimeric TALEN- encoding mRNA [PhD thesis, University of the Witwatersrand, Johannesburg]. WIReDSpace. https://hdl.handle.net/10539/47411

Downloaded from a DSpace repository. https://dspace.org/

Inactivating hepatitis B virus replication using obligate heterodimeric TALEN-encoding mRNA

Tiffany Shenay Smith

A thesis submitted to the Faculty of Health Sciences, University of the Witwatersrand, in fulfilment of the requirements for the degree of

Doctor of Philosophy in Medicine

Johannesburg, 2024

Declaration

I, Tiffany Shenay Smith, hereby declare that this thesis is my own, unaided work. It is being submitted for the degree of Doctor of Philosophy in Medicine at the University of the Witwatersrand, Johannesburg. This work has not been submitted for any degree or examination at any other university.



5 November 2024

Tiffany Shenay Smith **Date**

Dedication

All Glory to Jesus Christ, my Lord and Saviour

Proverbs 2:6 “It is the Lord who gives wisdom; from Him come knowledge and understanding”

To my family:

My parents, Ernest and Faiza.

My sister Asheline.

My nephews Ruschen and Aaryan.

My partner Decclan.

Thank you for your unconditional love and support.

Publication and presentations

Publications:

- Ely A, Singh P, Smith TS, Arbuthnot P. In vitro transcribed mRNA for expression of designer nucleases: Advantages as a novel therapeutic for the management of chronic HBV infection. Advanced drug delivery reviews. 2021;168:134-46.
- Smith T, Singh P, Chmielewski KO, Bloom K, Cathomen T, Arbuthnot P, Ely A. Improved Specificity and Safety of Anti-Hepatitis B Virus TALENs Using Obligate Heterodimeric Fok I Nuclease Domains. Viruses. 2021;13(7):1344.
- Jacobs R, Singh P, Smith T, Arbuthnot P, Maepa MB. Prospects of viral vector-mediated delivery of sequences encoding anti-HBV designer endonucleases. Gene Therapy. 2022;1-8.
- Kairuz D, Singh P, Smith T, Arbuthnot P, Ely A, Bloom K. Synthetic mRNA gene therapies and hepatotropic non-viral vectors for the treatment of chronic HBV infections. In Messenger RNA Therapeutics. 2022;157-179. Cham: Springer International Publishing.
- Singh P, Smith T, Arbuthnot P, Ely A. In vitro transcription. Handbook of Molecular Biotechnology. 2024;137-151. CRC Press: Taylor & Francis Group.

Oral presentation:

- 4th Sustainable Bio-Innovation Symposium. 28th September 2023, Pretoria, South Africa. Tiffany Smith. Engineering TALENs to permanently disable HBV replication.

Poster presentations:

- Molecular Biosciences research Thrust (MBRT) Postgraduate Research Day. 8th December 2023, Medical School, University of the Witwatersrand, Johannesburg, South Africa. Tiffany Smith, Abdullah Ely, Betty Maepa B and Patrick Arbuthnot. Obligate heterodimeric TALEN-encoding mRNA attenuates hepatitis B virus replication in cultured mammalian cells.
- Virology Africa. 15-18th April 2024, Protea Hotel, Stellenbosch, Western Cape, South Africa. Tiffany Smith, Abdullah Ely, Betty Maepa B and Patrick Arbuthnot. Inhibition of hepatitis B virus replication using obligate heterodimeric TALEN-encoding mRNA.

Abstract

The hepatitis B virus (HBV) poses a significant global health challenge, as chronic infection can lead to cirrhosis and hepatocellular carcinoma, resulting in over 1 million deaths annually. While vaccines exist, they have limitations, particularly in addressing chronic infections or non-responders. Current treatments, including nucleoside/nucleotide analogues and pegylated interferon-α, are inadequate for curing chronic HBV infections because they cannot eliminate covalently closed circular DNA (cccDNA) from infected cell nuclei. cccDNA persists as a viral gene transcription template, sustaining chronic infection and allowing viral reactivation upon treatment cessation. Obligate heterodimeric transcription activator-like effector nucleases (TALENs) have emerged as a promising tool for targeting HBV. These TALENs feature a DNA-binding domain and a second-generation *Fok*I nuclease domain that enable precise DNA cleavage exclusively when heterodimeric TALENs are in close proximity on opposite DNA strands, preventing homodimeric cleavage and minimising off-target effects. This cleavage activates non-homologous end-joining DNA repair, inducing mutations at double-strand break sites. To assess the clinical potential of TALENs targeting HBV *core* and *surface* open reading frames, TALEN-encoding mRNA was synthesised by *in vitro* transcription using T7 RNA polymerase and three distinct cap analogues: anti-reverse cap, post-transcriptional Vaccinia cap, and CleanCap® AG. Immunocytochemistry was first performed in liver-derived cells to detect the haemagglutinin tag located within the TALEN construct. This experiment confirmed that optimal expression of Core and Surface TALENs was achieved using CleanCap® AG. TALEN efficacy was then tested in three *in vitro* models: Huh7 cells with HBV replication-competent plasmid, HepG2-hNTCP cells infected with HBV, and Huh7 cells transduced with adeno-associated virus type 2 (AAV2) containing HBV genome sequences from subgenotype D3. Surface TALENs reduced HBsAg

levels by 40%, 30%, and 90% across the models, with no observed cytotoxicity. *In vivo* studies using lipid nanoparticle-encapsulated Core and Surface TALEN-encoding mRNA in a transgenic HBV murine model showed a 63% reduction in HBsAg and over 99% reduction in viral particle equivalents, with no liver toxicity or significant inflammatory response. While Sanger sequencing did not detect targeted mutations with sufficient sensitivity, next-generation sequencing could offer more detailed insights as observed data indicate a significant difference in viral fitness between mock and TALEN-treated mice. This study represents the first successful production of obligate heterodimeric TALENs as mRNA. It highlights their potential as a therapeutic approach for chronic HBV infection by targeting and permanently inactivating HBV production.

Acknowledgements

I extend my heartfelt thanks to my supervisors, Prof. Patrick Arbuthnot, Prof. Abdullah Ely, and Prof. Betty Maepa, for their invaluable support and mentorship at every stage of my research. This thesis would not have been possible without their guidance.

I would like to express my gratitude to Prashika Singh, Ridhwaanah Jacobs, Dylan Kairuz, and Keila Neves for their invaluable assistance in the many practical aspects of my research. With special mention to Ridhwaanah Jacobs who provided me with AAV-2-D3 virus.

I am eternally thankful for the incredible support system provided by my family. I especially want to mention my parents, Ernest and Faiza, my sister Asheline, and my boyfriend, Decclan Lawrence. Your prayers, guidance, and unwavering support have been my greatest source of encouragement throughout every part of my academic journey.

Finally, I extend my deepest gratitude to these funding bodies for their generous financial support: the National Research Fund (NRF), the Poliomyelitis Research Fund (PRF), and the Antiviral Gene Therapy Research Unit (AGTRU).

Table of Contents

Declaration ii
Dedication iii
Publication and presentations iv
Abstract vi
Acknowledgements viii
List of Figures xiii
List of Tables xvi
List of Abbreviations xvii
Chapter 1- Hepatitis B Virus: Understanding disease mechanisms, evaluating existing therapies and exploring novel treatments 1
1.1 Epidemiology and modes of transmission 1
1.2 Structural and replicative mechanisms of HBV 4
1.3 Persisting cccDNA: A focus on longevity 12
1.4 Existing strategies to combat HBV infection 14
1.5 Recent advances in treating HBV infection with designer nucleases 17
1.6 Employing and modifying TALENs targeted against HBV 24
1.7 TALEN-encoding mRNA as an anti-HBV therapeutic 29
1.8 Encapsulating TALEN-encoding mRNA within lipid nanoparticles 38
1.9 Project aims 41
Chapter 2- Designing anti-HBV TALEN-encoding mRNA and evaluating TALEN expression in cultured mammalian cells 42
2.1 Introduction 42
2.2 Methods 49
2.2.1 Reporter transcripts 49
2.2.1.1 pT7-eGFP 49
2.2.1.2 pT7-mCherry 49
2.2.2 Generation of two distinct plasmid templates for IVT 49
2.2.2.1 Construction of TALEN-encoding mRNA expression plasmids- IVT template design 1 52
2.2.2.1.1 Linearisation of TALEN-encoding mRNA templates-IVT template design 1 56

2.2.2.2 Construction of TALEN-encoding mRNA expression plasmids- IVT template design 2 58
2.2.3 *In vitro* transcription of TALEN-encoding mRNA 63
2.2.3.1 IVT#1: Synthesis of anti-HBV TALEN transcripts using ARCA 63
2.2.3.2 IVT#2: Post-transcriptional capping of in vitro transcribed TALEN transcripts using VCE 64
2.2.3.3 IVT #3: Post-transcriptional capping of in vitro transcribed TALEN transcripts using VCE and cellulose purification 65
2.2.3.4 IV# 4: Co-transcriptional capping of in vitro transcribed TALEN transcripts using CleanCap®AG and cellulose purification 66
2.2.3.5 IVT #5: Co-transcriptional capping of in vitro transcribed TALEN transcripts using CleanCap®AG and cellulose purification- IVT template design 2 67
2.2.4 Immunocytochemistry for HA detection in TALEN-transfected cells 67
2.3 Results 69
2.3.1 Engineering TALEN-encoding mRNA with modified cap-0 and cap-1 structures – IVT template design 1 69
2.3.1.1 Generation of obligate heterodimeric *surface*-targeting TALEN templates 69
2.3.1.2 Successful template linearisation and *in vitro* transcription of ARCA cap-0 anti-HBV transcripts 73
2.3.1.3 Lack of protein expression from ARCA cap-0 transcripts 76
2.3.1.4 *In vitro* transcription of cap-1 anti-HBV transcripts 78
2.3.1.5 Enhanced TALEN expression in liver-derived cells through cellulose purification 80
2.3.2 Engineering TALEN-encoding mRNA with modified cap-1 structures- IVT template design 2 84
2.3.2.1 Generation of modified obligate heterodimeric *core*-and-*surface*-targeting TALEN templates 84
2.3.2.2 *In vitro* transcription of CleanCap® AG-1 anti-HBV transcripts from IVT template design 2 85
2.3.2.3 Robust TALEN expression in liver-derived from modified IVT template design 2 87
2.4 Discussion 89
Chapter 3- Use of TALEN-encoding mRNA to attenuate HBV replication in cell culture 91
3.1 Introduction 91
3.2 Methods 95

3.2.1 Establishing HBV replication in cell culture 95
3.2.1.1 pCH-9/3091 95
3.2.1.2 HBV isolated from HepG2.2.15 95
3.2.1.3 AAV-2 containing HBV genome sequence from subgenotype D3 (AAV-2-D3) 97
3.2.2 Measuring HBsAg levels using enzyme-linked immunosorbent assay (ELISA) 97
3.2.2.1 Assessing HBsAg secretion from Huh7 cells transfected with pCH-9/3091 97
3.2.2.2 Assessing HBsAg secretion from HepG2-hNTCP-C4 cells infected with HBV particles 98
3.2.2.3 Assessing HBsAg secretion from Huh7 cells transduced with AAV-2-D3 98
3.2.3 Cell viability assay 99
3.2.4 Statistical analysis 99
3.3 Results 101
3.3.1 *In vitro* transcribed TALENs from IVT design template 2 mediates enhanced inhibition of HBsAg secretion from liver-derived cells 101
3.3.2 TALENs do not induce cell-mediated toxicity 109
3.4 Discussion 111
Chapter 4- LNP-encapsulated TALEN-encoding mRNA inhibits HBV replication in a transgenic murine model 114
4.1 Introduction 114
4.2 Methods 117
4.2.1 *In vivo* assessment of TALEN-encoding mRNA for targeted inhibition of HBV replication 117
4.2.1.1 Formulating LNP-encapsulated RNA using microfluidics 117
4.2.1.2 RNA quantification and encapsulation efficiency assessment 119
4.2.1.3 Bioluminescence imaging 120
4.2.1.4 ELISA 120
4.2.1.5 Quantification of HBV VPEs 120
4.2.1.6 Assessing HBV gene expression 121
4.2.1.7 Assessing *in vivo* targeted cleavage by Sanger sequencing analysis 122
4.2.1.8 Assessing inflammatory response by cytometric bead array quantification 123
4.2.1.9 Assessing liver toxicity 124
4.2.2 Data analysis 124
4.3 Results 125

4.3.1 Tail vein injections of LNP-encapsulated TALEN-encoding mRNA 125
4.3.1.1 Successful hepatic delivery of LNP-encapsulated mRNA 127
4.3.1.2 TALEN-induced knockdown of HBV replication *in vivo* 129
4.3.1.3 TALENs do not mediate repression of HBV *core* and *surface* transcripts 133
4.3.1.4 Sanger sequencing of target sites 135
4.3.1.5 LNP-encapsulated TALENs demonstrate minimal inflammatory response and absence of liver toxicity 138
4.4 Discussion 141
Chapter 5- Conclusion 145
Chapter 6-Appendix 147
6.1 Standard protocols, buffers and solutions for laboratory use 147
6.1.1 Preparation of $CaCl_2$ chemically competent bacterial cells 147
6.1.2 Denaturing RNA formaldehyde agarose gel (1%) 148
6.1.3 Viral precipitation solution [5 × polyethylene glycol (PEG) 8000] 148
6.1.4 Cellulose chromatography buffer preparation 149
6.2 Mammalian cell culture growth and maintenance 149
6.2.1 Huh7 cells 149
6.2.2 HepG2-hNTCP-C4 cells 150
6.2.3 HepG2.2.15 cells 150
6.2.4 Coating plates with collagen 150
6.3 TALEN DNA binding domain sequences: 152
6.4 Restriction digest confirmation of pT7-Left/Right-TALEN-4×STOP plasmids from IVT template design 2 154
6.5 Anti-HBV TALE sequence validation 159
6.6 Alignment of left and right *Fok*I protein sequences 161
6.7 *In vivo* assessment 162
6.7.1 N/P ratio and LNP sizing 162
6.7.2 LNP effective dose 163
6.7.3 Animal research Ethics clearance certificate 164
6.7.4 Cytometric bead array plot 166
References 167

List of Figures

Figure 1.1: The structure of the hepatitis B virus (HBV) genome. 8
Figure 1.2: The replication cycle of the hepatitis virus (HBV). 11
Figure 1.3: NHEJ or HDR pathways induced after designer nuclease-mediated cleavage. 18
Figure 1.4: Designer nucleases induce double-stranded breaks at target sites. 23
Figure 1.5: Enhanced specificity achieved by obligate heterodimeric Transcription Activator-Like Effector Nucleases (TALENs). 27
Figure 1.6: The structure of anti-HBV obligate heterodimeric TALENs. 28
Figure 1.7: Schematic overview of the IVT process from a DNA template. 31
Figure 1.8: Conventional cap-0 versus anti-reverse cap-0 analogues (ARCAs). 34
Figure 1. 9: The enzymatic conversion from uncapped to cap-0 and cap-1 transcripts using VCEs. 35
Figure 1.10: CleanCap® AG trinucleotide. 37
Figure 1.11: The intracellular delivery of ionisable lipid nanoparticles (iLNPs) to hepatocytes via clathrin-mediated endocytosis. 40

Figure 2.1: TALEN-encoding mRNA with ARCA. 44
Figure 2.2: TALEN-encoding mRNA with vaccinia cap and Ψ. 46
Figure 2.3: TALEN-encoding mRNA with CleanCap® AG and m1Ψ. 48
Figure 2.4: Producing TALEN-encoding mRNA plasmids for *in vitro* transcription- IVT template design 1. 54
Figure 2.5: Linear templates for IVT of TALEN-encoding mRNA -IVT template design 1. 57
Figure 2.6: Producing modified vector for *in vitro* transcription- IVT template design 2. 59
Figure 2.7: Producing TALEN-encoding mRNA plasmids for *in vitro* transcription- IVT template design 2. 61
Figure 2.8: Linear templates for IVT of TALEN-encoding mRNA - IVT template design 2. 62
Figure 2.9: Confirmation of pT7-SL/SR-TALEN plasmids. 70
Figure 2.10: Confirmation of left and right *Fok*I domain nucleases in pT7-SL/SR-TALEN plasmids. 72
Figure 2.11: Linearised pT7-SL/SR-TALEN templates. 74

Figure 2.12: Confirmation of *in vitro* transcribed SL/SR TALEN transcripts with ARCA cap-0. 75
Figure 2.13: Absence of TALEN expression from cap-0 transcripts in Huh7 cells..... 77
Figure 2.14: Confirmation of *in vitro* transcribed SL/SR TALEN cap-1 transcripts..... 79
Figure 2.15: Absence of TALEN expression from cap-1 transcripts produced with VCE in Huh7 cells. 81
Figure 2.16: Detecting TALEN expression from cellulose-treated cap-1 transcripts using VCE in Huh7 cells. 82
Figure 2.17: Detecting TALEN expression from cellulose-treated cap-1 transcripts using CleanCap® AG in Huh 7 cells. 83
Figure 2.18: Confirmation of *in vitro* transcribed Core and Surface TALEN transcripts with CleanCap® AG analogues. 86
Figure 2.19: Enhanced TALEN expression from cellulose-treated cap-1 transcripts using CleanCap® AG in Huh 7 cells-IVT template design 2. 88

Figure 3.1: Target sites on HBV cccDNA for obligate heterodimeric cleavage. 94
Figure 3.2: Measuring HBsAg secretion in Huh7 cells transfected with pCH-9/3091-IVT #1 and IVT #2. 102
Figure 3.3: Measuring HBsAg secretion in Huh7 cells transfected with pCH-9/3091- IVT #3 to IVT #5. 104
Figure 3.4: TALEN-mediated reduction of HBsAg secretion in HepG2-hNTCP-C4 cells. 106
Figure 3.5: TALEN-mediated reduction of HBsAg secretion in Huh7 cells transduced with AAV-2-D3. 108
Figure 3.6: Evaluation of TALEN-induced cellular toxicity. 110

Figure 4.1: Experimental Timeline for TALEN-Treated Mice. 126
Figure 4.2: *In vivo* bioluminescence imaging of reporter gene expression in transgenic mice. . 128
Figure 4.3: TALEN-mediated knockdown of HBsAg secretion in transgenic mice. 131
Figure 4.4: TALEN-mediated inhibition of viral replication. 132
Figure 4.5: Core and Surface TALENs have no impact on hepatic HBV mRNA levels. 134
Figure 4.6: Sanger Sequencing alignment fails to demonstrate site-directed mutagenesis. 137

Figure 4.7: LNP-encapsulated TALENs did not illicit significant cytokine induction in transgenic mice. 139
Figure 4.8: Absence of hepatic toxicity in transgenic mice. 140

Figure 6.1: Treating culture plates with collagen enhances HepG2-hNTCP-C4 growth. 151
Figure 6.2: Confirmation of pT7-Left/Right-TALEN plasmids. 155
Figure 6.3: Confirmation of left and right *Fok*I nuclease domains in pT7-CL/SL-TALEN and pT7-CR/SR-TALEN plasmids. 157
Figure 6.4: Linearised pT7-Left/Right-TALEN templates. 158
Figure 6.5: TALE sequences. 160
Figure 6.6: Heterodimeric *Fok*I multiple sequence alignment. 161
Figure 6.7: Cytokine induction in transgenic mice. 166

List of Tables

Table 2.1: Key differences between IVT template designs 1 and 2 51
Table 2.2: Sequence differences between backbones in IVT template design 1 and 2 84

Table 3.1: Primer sequences used to amplify the HBV *preS1* region 96

Table 4.1: Primer sequences used to amplify the HBV *core* and *surface* genes and *mGAPDH* gene 122
Table 4.2: Primer sequences employed to amplify potential TALE binding and cleavage regions for *C* and *S* ORFs. 123

Table 6.1: TALE RVDs for Core TALENs 152
Table 6.2: TALE RVDs for Surface TALENs 153
Table 6.3: Size and zeta potential measurements of RNA-encapsulated LNPs determined by Zetasizer 162
Table 6.4: Assessing effective dose of LNPs using standards of known concentration for the Ribogreen assay 163

List of Abbreviations

AAVs	-	adeno-associated viruses
AAV-2	-	AAV serotype 2
ABEs	-	A-to-G base editors
ALT	-	alanine aminotransferase
APC	-	Allophycocyanin
ApoE	-	serum apolipoprotein E
ARCAs	-	anti-reverse cap analogues
AST	-	aspartate transaminase
BSA	-	serum albumin
Cas9	-	CRISPR associated 9
CBA	-	cytometric Bead Array
CBEs	-	C-to-T base editors
cccDNA	-	covalently closed circular DNA
CL	-	core left
COVID-19	-	coronavirus disease
CR	-	core right
CRISPR	-	clustered regularly interspaced short palindromic repeats
crRNAs	-	CRISPR RNAs
CTD	-	C-terminal domain
DAPI	-	1× 4,6-diamidino-2-phenylindole chloride
DMEM	-	Dulbecco's Modified Eagle's Medium
DMSO	-	dimethyl sulphoxide
DRs	-	direct repeats
DSBs	-	double-stranded breaks
dslDNA	-	double-stranded linear DNA
dsRNA	-	double-stranded RNA
DTT	-	dithiothreitol
E. coli	-	*Escherichia coli*

ecDNA	-	extrachromosomal circular DNA
EDTA	-	ethylenediamine tetraacetic acid
eGFP	-	enhanced green fluorescent protein
ELISA	-	enzyme-linked immunosorbent assay
Enh	-	Enhancer
ER	-	endoplasmic reticulum
FBS	-	foetal bovine serum
FDA	-	Food and Drug Administration
FEN1	-	flap endonuclease 1
FITC	-	fluorescein isothiocyanate
FLuc	-	Firefly luciferase
FVB	-	Friend leukaemia virus B
GMP	-	guanosine monophosphate
GTase	-	guanylyltransferase
HA	-	haemagglutinin
HBcAg	-	hepatitis core antigen
HBeAg	-	hepatitis B e antigen
HBsAg	-	hepatitis B surface antigen
HBV	-	hepatitis B virus
HBx	-	hepatitis B virus X protein
HCC	-	hepatocellular carcinoma
HDI	-	hydrodynamic injection
HDR	-	homology-directed repair
HDV	-	hepatitis D virus
HIV	-	human immunodeficiency virus
Huh7	-	Human hepatoma 7
IFN	-	interferon
IL	-	Interleukin
iLNPs	-	ionisable LNPs
indel	-	insertion and deletion

IVT	-	*in vitro* transcription
kb	-	kilobases
LC-MS	-	liquid chromatography–mass spectrometry
LDLRs	-	low-density lipoprotein receptors
LiCl	-	lithium chloride
LNPs	-	lipid nanoparticles
m1Ψ	-	N1-methylpseudouridine
m7G	-	7-methylguanosine
MCP-1	-	Monocyte Chemoattractant Protein-1
mGAPDH	-	murine glyceraldehydes-3phosphate dehydrogenase
mmol	-	millimoles
MOI	-	multiplicity of infection
MOPS	-	3-(N-morpholino) propanesulphonic acid
MTase	-	methyltransferase
MWM	-	molecular weight marker
N/P	-	nitrogen-to-phosphorus
NAPs	-	Nucleic acid polymers
NAs	-	nucleoside/nucleotide analogues
ng	-	nanograms
NGS	-	next-generation sequencing
NHEJ	-	non-homologous end-joining
NLS	-	nuclear localisation signal
NTCP	-	sodium taurocholate co-transporting polypeptide
NTD	-	N-terminal domain
ORFs	-	overlapping open reading frames
PAM	-	protospacer adjacent motif
PAMPs	-	pathogen-associated molecular patterns
PBS	-	phosphate buffered saline
PE	-	Phycoerythrin
PEG	-	polyethylene glycol

pgRNA	-	pregenomic RNA
PIPES	-	piperazine-N,N′-bis(2-ethanesulphonic acid)
pmol	-	picomoles
Poly I:C	-	polyinosinic:polycytidylic acid
PRRs	-	pattern recognition receptors
qPCR	-	quantitative PCR
rcDNA	-	relaxed circular DNA
RFP	-	red fluorescent protein
RNase H	-	ribonuclease H
rNTPs	-	ribonucleotide triphosphates
ROI	-	region of interest
RT	-	reverse transcriptase
RVDs	-	repeat variable diresidues
S. aureus	-	*Staphylococcus aureus*
S. pyogenes	-	*Streptococcus pyogenes*
SAM	-	S-adenosyl methionine
SEM	-	standard error of the mean
sgRNA	-	small guide RNAs
siRNAs	-	short interfering RNAs
SL	-	surface left
Smc	-	structural maintenance of chromosomes
SAHPRA	-	South African Health Products Regulatory Authority
SR	-	surface right
SVPs	-	subviral particles
TALENs	-	transcription activator-like effector nucleases
TLR	-	toll-like receptor
TNF	-	Tumour necrosis factor
TP	-	terminal protein
TPase	-	triphosphatase
tracrRNAs	-	*trans*-activating crRNAs

TRITC	-	tetramethyl rhodamine
UTR	-	untranslated region
VCEs	-	vaccinia capping enzymes
VPE/ml	-	viral particle equivalents per millilitre
VPEs	-	viral particle equivalents
WGS	-	whole-genome sequencing
WHO	-	World Health Organization
WHO-UNICEF	-	WHO- United Nations Children's Fund
ZFNs	-	zinc finger nucleases
α	-	Alpha
β	-	Beta
µl	-	microlitre
µM	-	micromolar
Ψ	-	pseudouridine

Chapter 1- Hepatitis B Virus: Understanding disease mechanisms, evaluating existing therapies and exploring novel treatments

1.1 Epidemiology and modes of transmission

The hepatitis B virus (HBV) targets hepatocytes and causes hepatitis B. The first recognised marker of infection was discovered by Baruch Blumberg and colleagues in 1965 (1). This marker, once known as the "Australia antigen," is now referred to as the hepatitis B surface antigen (HBsAg). This discovery increased attention to the medical implications of HBV, prompting research into viral epidemiology and infection. By 1982, a vaccine had been developed against HBV (2). However, despite vaccination efforts, infections continue to rise globally, with approximately 296 million chronic carriers worldwide and an estimated 1.9 million in South Africa alone (3–5). HBV remains a significant global health concern, as chronic infection can progress to cirrhosis and hepatocellular carcinoma (HCC), conditions that are responsible for 1.1 million deaths annually (3).

Following Blumberg's discovery, Okamoto and colleagues proposed categorising HBV into four genotypes based on sequence differences, initially identifying genotypes A-D (6). Over time, research has identified a total of ten genotypes (A-J), with some further classified as sub-genotypes (7–9). Genotypes demonstrate geographic distribution, with the highest infection rates observed in sub-Saharan Africa and Asia (3). Genotypes are distinguished by at least 8% sequence variability and between 4-8% variability between sub-genotypes (6,10). HBV's reverse transcriptase enzyme lacks proofreading ability, resulting in a high mutation rate, leading to frequent nucleotide substitutions and ultimately contributing to genotype diversity among circulating viruses (11,12). From the eight distinct genotypes labelled A through H, only five genotypes (A, B, C, D, and F)

have undergone further classification into sub-genotypes (13,14). The identification of genotypes has provided valuable insight into clinical response and treatment efficacy (15). The impact of chronicity has been noted to differ across various HBV genotypes (16).

The routes of transmission between Asia and Africa, the regions most severely impacted, differ greatly. Perinatal transmission occurs predominantly in Asian populations. Mother-to-child transmission stands as a prevalent source of chronic HBV infection. Factors contributing to chronic infection from MTCT of HBV include HBV DNA levels over 2×10^5 IU/ml, positivity for hepatitis B e antigen (HBeAg), failure of the placental barrier (as HBeAg can cross the placenta), and the underdeveloped immune systems of infants. (17,18). In the absence of preventative measures, over 90% of infants will contract the infection and progress to chronic status (19).

In Africa, children younger than 5 are susceptible to horizontal transmission because of close interactions with infected individuals either from the same household or from infected children from other homes (20,21). Horizontal transmission poses a high risk of chronic infection when it affects young children (22). Despite horizontal transmission being more prevalent among children, recent findings highlight the importance of perinatal transmission during childbirth in Africa (reviewed in (23)). The World Health Organization (WHO) advocates for administering the HBV birth dose vaccine, yet its adoption in South Africa and many other African countries has been lagging. This slow implementation is attributed not only to epidemiological factors but also to logistical challenges, such as ensuring vaccine access to all newborns, particularly those not born in medical facilities (reviewed in (24)).

HBV is transmitted parenterally and can remain stable on environmental surfaces at 37 °C for over three weeks (25). The virus is detected at relatively low concentrations in saliva, semen and vaginal fluids with no detection through faecal-oral transmission (26). The other commonest modes of

transmission occur with contaminated syringes, especially amongst drug users, haemodialysis, tattooing, ear piercings and sexual contact (27). Furthermore, HBV is approximately 100 times more infectious than human immunodeficiency virus (HIV) (28). HBV is present in much higher concentrations in the blood and is more stable outside the human body than HIV.

Individuals living with HIV face an elevated risk of acquiring HIV-HBV co-infection as both viruses share common modes of transmission (29). As of now, around 37 million individuals have been diagnosed with HIV-1 infection globally (30). Of this number, at least 7.4% of the global population experience co-infection with HIV and chronic HBV (30). Most of these cases, around 70%, are found in sub-Saharan Africa. The progression of HBV infection is worsened by the immunodeficiency caused by HIV. This exacerbation leads to heightened HBV replication and reduced rates of HBeAg seroconversion, thereby hastening the progression of cirrhosis and HCC (31). In comparison to individuals infected solely with HBV, the progression of chronicity is five times faster, and mortality is twice as high in cases of HIV-HBV coinfection (32).

HBV has the potential to induce either acute or chronic infection. Mild symptoms such as nausea, fatigue, and vomiting are common, while more severe cases may exhibit jaundice during acute infections (33). Acute infection generally persists between 2-3 months but has been shown to last up to six months (33). However, individuals are clinically diagnosed with chronic infection if HBsAg remains detectable for a period exceeding six months (26).

Chronic infection occurs when the immune system is ineffective in clearing infection. Hence infections are almost always chronic in the case of immunocompromised individuals or children younger than 1 year (reviewed in (34)). Although the immune system in young children is generally naïve, chronically infected adults tend to have the most severe and progressive liver

damage where up to 25% of patients will die from cirrhosis with a large number of cases requiring liver transplantation (reviewed in (34)).

Chronic infection can increase the risk of developing HCC, which is the most common type of liver cancer and the fourth leading cause of cancer-related deaths worldwide (35,36). This highlights the need for new and effective treatments to eliminate both the infection and the disease, making it a global concern.

1.2 Structural and replicative mechanisms of HBV

HBV is an enveloped DNA virus that is formed by reverse transcription of an RNA intermediate called pregenomic RNA (pgRNA), resulting in relaxed circular DNA (rcDNA) that is approximately 3.2 kilobases (kb) long (37). The rcDNA structure consists of a complete minus strand and an incomplete plus strand (**Figure 1.1**). Viral entities may exist in two forms either as infectious particles, known as Dane particles, or non-infectious subviral particles (SVPs) (38,39). Dane particles consist of HBsAg-embedded lipid membranes surrounding an internal icosahedral nucleocapsid. The nucleocapsid is comprised of the hepatitis core antigen (HBcAg), the viral genome, and viral polymerase (38).

The genetic material encodes four overlapping open reading frames (ORFs): *precore*/*core* (*C*), *polymerase* (*P*), *surface* (*S*), and *X* ORFs **(Figure 1.1)** (34). The complete minus strand DNA, complementary to pgRNA, possesses a terminal redundancy of 10 nucleotides, whereas the incomplete positive strand varies in length, with its 3' terminus concluding several nucleotides upstream of strand completion. An RNA oligonucleotide is covalently attached to the 5' end of the plus strand and the viral reverse transcriptase (RT) aids in its complete synthesis (40). Within the

nucleus, host cellular machinery repairs rcDNA to generate covalently closed circular DNA (cccDNA), serving as the template for viral gene transcription (41).

The *precore* and *core* regions constitute the *C* ORF (42). Within the *C* gene, two in-frame start codons facilitate translation (43). Similarly, in the *S* gene, this translation process results in structurally related yet functionally disparate proteins. Transcription originating upstream of *C* generates both pgRNA and *precore* RNA and translation from the *C* start site of pgRNA generates HBcAg, which assembles into the viral capsids (44).

The translation of *precore* RNA from its starting site leads to the production of precore protein (44). The N-terminal residues of precore contain a secretion signal, initiating its transfer into the lumen of the endoplasmic reticulum (ER), where it undergoes cleavage of the signal sequence by a host cell signal peptidase. Following this, precore undergoes proteolytic processing to form HBeAg (45). HBeAg serves as an indicator of active replication (46). Although the precise function of HBeAg remains incompletely understood, it is theorised to contribute to immune tolerance by perpetuating persistent infection (47).

The core protein comprises an N-terminal domain (NTD), spanning the initial 149 residues, involved in capsid assembly, and the C-terminal domain (CTD), which is not required for capsid assembly but pivotal for packaging pgRNA into nucleocapsids capable of replication (48,49). HBcAg proteins rapidly form dimers, acting as the fundamental units for capsid assembly, resulting in two morphological capsid isomers of icosahedral structure (50). These capsids encapsulate viral pgRNA bound to polymerase. Additionally, the CTD harbours several nuclear localisation signals (NLSs) potentially essential for mediating the translocation of nucleocapsids into the nucleus (51).

The *P* ORF encodes the viral polymerase, which comprises four domains, with three of these domains extensively researched as the terminal protein (TP), polymerase/ RT, and ribonuclease H (RNase H) domains (52). The TP domain comprises a key tyrosine residue that is important for the initiation of the DNA minus strand synthesis (53). The polymerase/RT domain can function as an RNA-dependent DNA polymerase to form the minus strand from pgRNA and as a DNA-dependent DNA polymerase to initiate synthesis of the plus strand from the minus strand (52). After reverse transcription, the RNase H domain degrades pgRNA to promote the initiation of plus-strand synthesis.

The *S* ORF consists of three segments: *PreS1*, *PreS2*, and *S*, each containing an AUG start codon. (34). *PreS1* mRNA translates into large (L) HBsAg, comprising *PreS1*, *PreS2*, and *S* domains. Translation from the first AUG in *PreS2* mRNA yields middle (M) HBsAg, containing PreS2 and S domains whereas translation from the second AUG in *PreS2* mRNA results in small (S) HBsAg, containing only the S domain (54). HBsAgs contain modifications that facilitate the attachment of the virus to hepatocytes. The L, M and S domains can either present as glycosylated or non-glycosylated isomers (55). This is because N-linked glycosylation is found constitutively at Asn-4 on the M HBsAg and at Asn-146 on the L, M and S domains. However, approximately 50% of these molecules remain unglycosylated at the 146 sites (55). The L domain features a myristic acid at the N-terminus, crucial for hepatocyte attachment and viral entry (56,57). Removal of the N-terminal myristoylated domain abrogates infection (58).

The *X* ORF encodes the hepatitis B virus X protein (HBx) (59). HBx is pivotal in HBV infection and is associated with hepatocarcinogenesis (60). While most reverse transcription products yield rcDNA, virions containing double-stranded linear DNA (dslDNA) can also arise (61). Upon infection with dslDNA, instead of converting to cccDNA, the HBV genome has a propensity to

integrate into the host genome at locations where double-stranded breaks (DSBs) occur, thereby rendering dslDNA replication-deficient. A recent study revealed truncated HBx in HCC, suggesting that HBx truncation might lead to the loss of its antiproliferative effects, potentially contributing to HCC (62). Importantly, HBx induces destabilisation of the structural maintenance of chromosomes (Smc) 5/6 complex, a known suppressor of expression from episomal HBV DNA (63).

The HBV genome contains additional elements that regulate HBV transcription. These elements include four promoters located at the *C*, *PreS1*, *PreS2*, and *X* sites (64). All transcriptional regulatory elements overlap with the protein-coding sequences, thereby ensuring tight control over the genome (65). The genome also has two direct repeats (DRs), namely DR1 at the 5' end and DR2 at the 3' end of the minus strand, which prime the plus strand DNA (66). Other elements include Enhancer I (EnhI), which is upstream of the *X* promoter, and Enhancer II (EnhII), which is upstream of the *precore* promoter (67). In addition to regulating *X* transcription, EnhI plays a crucial role in global HBV transcription and activation of early transcripts. Meanwhile, EnhII is responsible for the activation of late transcripts (67). Research conducted on HBV-transgenic mice lacking EnhI demonstrated a hindrance in virion production (68).

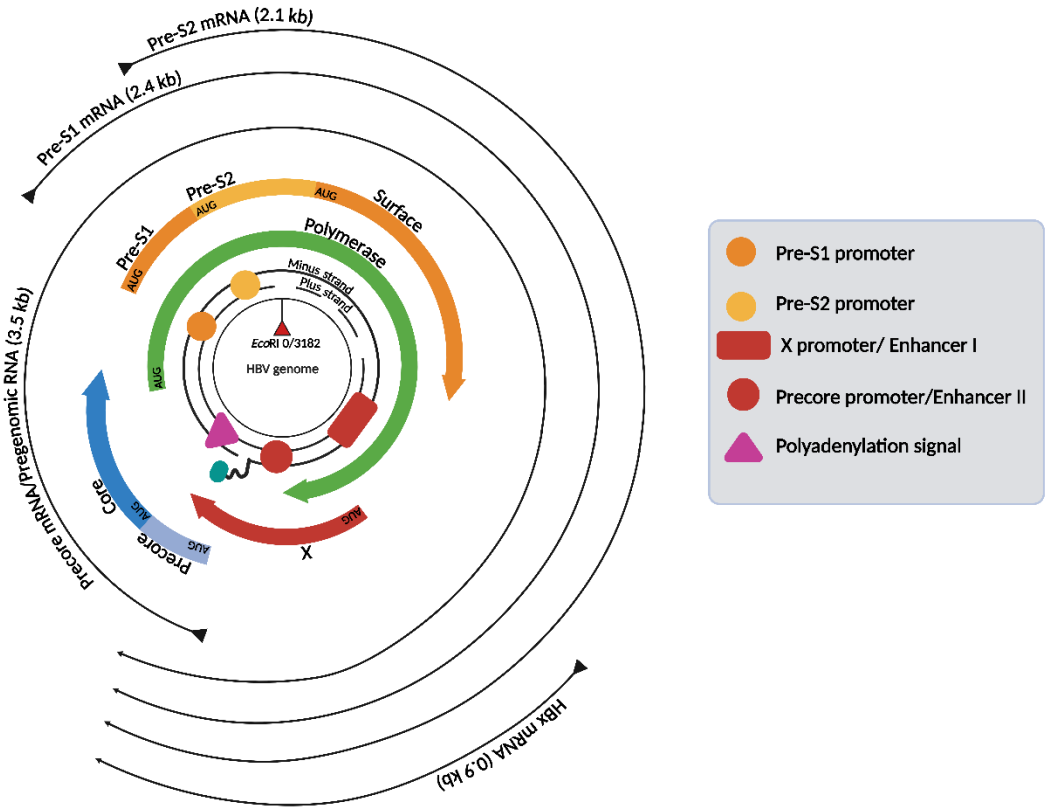


Figure 1.1: The structure of the hepatitis B virus (HBV) genome.

Centrally positioned at the inner most circle is the relaxed circular DNA (rcDNA). The rcDNA consists of a partially double-stranded plus strand and a complete minus strand. The genomic organisation is defined by sequential nucleotide coordinates, starting from the *Eco*RI site. Spanning approximately 3.2 kilobases (kb), the genome comprises four open reading frames (ORFs) designated as *Precore*/*Core*, *Polymerase*, *Surface* and *X*. Enhancer I is located immediately upstream of the *X* promoter, while enhancer II is situated upstream of the *precore* promoter. Additionally, within the *core* ORF, a polyadenylation signal is found on the plus strand. The outermost arrows represent the four major viral transcripts: PreS1, PreS2, X, and the greater-than-genome length pregenomic RNA (pgRNA) (Figure adapted from (69) and generated with Biorender.com).

HBV replication and infection initiate with viral particles clustering on hepatocyte surfaces through glycosaminoglycan-mediated interaction **(Figure 1.2)**. This clustering is pivotal for entry, facilitated by the interaction between myristoylated L HBsAg on virions and the sodium taurocholate co-transporting polypeptide (NTCP) embedded in hepatocyte surfaces (70). Additionally, the "a-determinant" in the S protein is essential for infection, aiding virus attachment to cells by binding to heparan sulphate proteoglycans on cell surfaces (71). Neutralising antibodies target the a-determinant, which includes a site for attaching sugar molecules (N-glycosylation site at N146), functional in only half of the envelope proteins (55). Having both sugar-coated and sugar-free forms of the N146 site serves two purposes: the sugar-free form is necessary for infectivity, while the sugar-coated form helps shield the a-determinant from neutralising antibodies, allowing HBV to escape immune detection and be released from cells (55).

Host factors assist with viral attachment as well as virion uptake into hepatocytes (72,73). Once bound, the virus is irreversibly attached to the hepatocyte (74). There is an incomplete understanding of viral disassembly. However, *in vitro* studies have shown that the mechanism by which the nucleocapsid reaches the nuclear envelope involves endocytosis coupled with microtubule-mediated transport (75,76). Upon cellular entry, the nucleocapsid translocates into the nucleus, where it undergoes disassembly to release the rcDNA genome. Following this, the capsid disassembles, triggering the repair process of the viral genome to generate cccDNA (77).

Wei and Ploss conducted a study delineating the process of rcDNA to cccDNA conversion in a cell-free system (78). This process comprises five critical biochemical steps, primarily dependent on host machinery. Initially, tyrosyl-DNA phosphodiesterase 2 facilitates the separation of the polymerase from the minus strand by breaking the tyrosyl-DNA phosphodiester bond between polymerase and rcDNA (79). Subsequently, primer release from the plus strand is coordinated by

proliferating cell nuclear antigen, flap endonuclease 1 (FEN1), and replication factor C. FEN1 removes redundant sequences from the minus strand by targeting the flap structure at the 5' end (80). DNA polymerase δ repairs the positive strand, and finally, both strands are connected by DNA ligase 1 and topoisomerases I and II (81).

cccDNA is utilised as a template for transcribing pgRNA, *precore* mRNA, and sub-genomic mRNAs (41). The viral transcripts undergo polyadenylation from a shared polyadenylation signal and are capped at their 5' ends (82). The pgRNA synthesis starts five nucleotides downstream from the *precore* initiation codon, serving as a template for reverse transcription and translating viral polymerase and HBV core proteins (reviewed in (52)). Additionally, the longer *precore* mRNA directs the synthesis of the precore protein, while sub-genomic RNAs guide the translation of surface (L, M, and S HBsAg) and X proteins.

Following translation, the assembly of virions commences with the binding of the viral polymerase to pgRNA, thereby initiating encapsidation and leading to the formation of the nucleocapsid (83). Subsequently, pgRNA acts as the framework for the formation of the minus strand DNA through reverse transcription. The intricate reverse transcription process employed by HBV has been previously described (52,83). Crucially, the minus strand provides the template for the formation of plus strand DNA, which ultimately contributes to the generation of rcDNA. The nucleocapsid undergoes budding into the ER, acquiring a lipid bilayer with pre-embedded surface proteins, facilitating the formation of the mature virion, which is released into the extracellular environment. Alternatively, the mature nucleocapsid may be directed back to the nucleus for the generation of cccDNA (84).

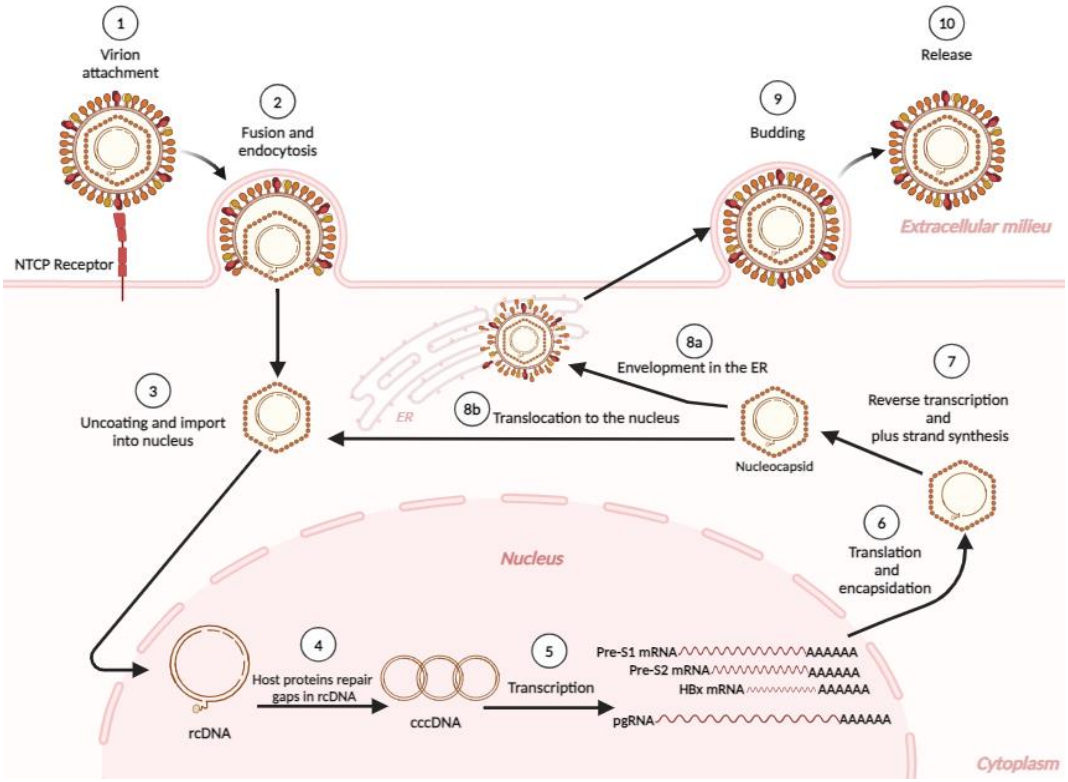


Figure 1.2: The replication cycle of the hepatitis virus (HBV).

1. Virion adheres to the cell surface via glycosaminoglycan-mediated clustering of viral particles on hepatocytes, where surface proteins recognise and bind sodium taurocholate co-transporting polypeptide (NTCP) receptor. **2.** Once attached, cellular mechanisms initiate endocytosis, facilitating the internalisation of the virus into the host cell **(3.)** where the nucleocapsid translocates to the nucleus and disassembles to release the relaxed circular DNA (rcDNA) into the nucleus. **4.** Host cellular machinery engages in the repair of rcDNA, converting it into covalently closed circular DNA (cccDNA). **5.** The cccDNA serves as a template for the transcription of viral RNA. **6.** Within the cytoplasm, viral RNAs undergo translation, yielding viral proteins. The viral polymerase then binds to the pregenomic RNA (pgRNA), initiating encapsidation to form the nucleocapsid. **7.** The pgRNA undergoes reverse transcription, leading to the synthesis of minus and plus strands, thereby forming rcDNA. **8a.** Newly synthesised capsids may either acquire viral HBsAg-embedded envelopes within the endoplasmic reticulum (ER) or **(8b.)** capsids can re-enter the nucleus, contributing to the generation of additional cccDNA. **9.** Capsids that undergo envelopment in the ER are subsequently released from the cell via exocytosis. **10.** Released virions enter the extracellular space, where they can infect neighbouring cells (Figure adapted from (78) and created with Biorender.com).

1.3 Persisting cccDNA: A focus on longevity

Understanding the functions of cccDNA in HBV persistence, including its formation, transcriptional regulation, yield, and intracellular stability, is crucial for devising strategies to eliminate cccDNA. Initially, technical constraints impeded research into cccDNA persistence. This challenge stemmed mainly from the complexities associated with acquiring liver biopsy specimens, an invasive procedure, compounded by the absence of quantitative techniques capable of providing both sensitive and specific measurements of cccDNA.

Quantifying cccDNA is challenging for two main reasons, (i) It exists in low copy numbers, and (ii) replicative intermediates like dslDNA and rcDNA share identical sequences with cccDNA, complicating accurate measurement (85,86). However, recent advancements have introduced a variety of methods, such as PCR quantification and the evaluation of replication markers such as serum HBV RNAs and HBcAg, demonstrating promising outcomes in the identification of cccDNA persistence (87,88).

Below are key factors contributing to the persistence of cccDNA. As mentioned earlier, after infection DNA-containing nucleocapsids can recycle to the nucleus. cccDNA is protected from cytoplasmic nucleases within the nucleus and relies on cellular machinery for maintenance (**Figure 1.2**) (78). Another crucial mechanism involves a negative feedback loop within host cells. Upon sufficient cccDNA synthesis, L surface protein directs new nucleocapsids away from nuclear entry. Instead, it promotes their envelopment and secretion outside the cell, aiding with infecting more hepatocytes. (89).

Epigenetic regulation also plays a role in cccDNA persistence. Within the nucleus, cccDNA interacts with histone and non-histone proteins, forming a minichromosome resembling host

chromatin (79). As with host chromatin, cccDNA transcription is subject to the influence of various transcription factors, signalling factors as well as chromatin-modifying enzymes (90).

Transcriptional regulation is vital for controlling cccDNA transcription and persistence. Without HBx, cccDNA may quickly become silenced, whereas HBx promotes an active transcriptional state (91). Christoph Seeger's study further highlighted the significance of HBx in cccDNA function (92). Seeger generated extrachromosomal circular DNA (ecDNA) containing inactive HBx and enhanced green fluorescent protein (eGFP) to emulate cccDNA. The Smc 5/6 complex inhibited eGFP expression, however HBx expression reversed the transcriptional silencing of ecDNA.

Additionally, HBV has evolved mechanisms to escape host immunity, potentially facilitating cccDNA persistence. Chronic HBV infection has been linked to notable decreases in dendritic cell function and impairment of the innate immune response (93). As previously mentioned, HBsAg can suppress host immune responses by the inhibition of antigen presentation (55). HBeAg has also been associated with immune suppression by modulating cytokine production (94).

To achieve a cure for HBV infection, it is essential to develop therapeutic strategies capable of effectively eliminating or permanently inactivating cccDNA. These approaches focus either on directly targeting cccDNA for degradation and inactivation or on modifying host cellular processes to inhibit its transcriptional activity. Eliminating cccDNA has the potential to prevent viral reactivation and enable sustained suppression of HBV, possibly resulting in a functional cure characterised by undetectable virus levels in the body. Therefore, advancing curative strategies that specifically target cccDNA is essential for achieving HBV eradication and reducing the global burden of chronic hepatitis B. One such advancement involves the use of designer nucleases that target cccDNA, inducing permanent mutations and thereby inactivating cccDNA.

1.4 Existing strategies to combat HBV infection

HBV vaccination is the primary method for preventing infection. Taiwan demonstrated remarkable vaccination success, reporting on seroprevalence of HBsAg plummeting from 9.8% in 1984 to 0.5% in 2004, coinciding with a vaccination rate of 97% among the population (2). Importantly, the incidence of HCC in children also declined significantly after vaccination implementation (95). The current vaccine consists of recombinant HBsAg, given in three doses, and demonstrates effectiveness in over 90% of individuals (96). According to WHO- United Nations Children's Fund (WHO-UNICEF) estimates from 2018, the coverage of birth-dose vaccines stands at 76.1% in South Africa (97). Despite developing adequate vaccine regimens, they remain ineffective against already infected populations or non-responders.

Two primary categories of medications have received approval from the U.S. Food and Drug Administration (FDA) for the treatment of chronic HBV infection (98). The initial category comprises nucleoside/nucleotide analogues (NAs), which primarily target the viral HBV polymerase. As elucidated earlier, the viral polymerase assumes a pivotal role in viral replication. NAs are the preferred treatment for chronic HBV patients as these drugs are administered daily by oral consumption. Despite reduced inhibition of viral replication, NAs are ineffective against existing pools of cccDNA and cccDNA in newly infected cells. Consequently, patients must maintain lifelong treatment, which carries adverse effects including the emergence of drug-resistant viral mutations (99–101).

The second class consists of conventional and pegylated interferon-α (IFN-α) immunomodulatory agents (102). IFN-α has two main functions, it targets the virus and the host immune system (102). The exact mechanism by which IFN-α targets the virus remains unclear. However, IFN-α inhibits viral replication by impeding the formation of core particles and degrading pgRNA (103,104).

Recently IFN-α has been reported to directly target cccDNA with the help of the APOBEC3 family cytidine deaminase 3A (102). Moreover, IFN-α suppresses HBV transcription through epigenetic modulation of cccDNA (105). IFN-α activates the innate as well as the adaptive immune response (102). Although IFN-α targets cccDNA directly, its success is largely influenced by the severity of chronic HBV infection. Furthermore, IFN-α is inadvisable in HBV carriers with cirrhosis, as a majority of patients (70-80%) do not exhibit a treatment response which necessitates lifelong NA therapy (106).

Additional therapeutic approaches involve the use of Bulevirtide formerly known as Myrcludex (107,108). Since its discovery as the HBV viral-entry receptor, NTCP has emerged as a compelling treatment focal point. Bulevirtide is a lipopeptide derivative of the L HBsAg. As mentioned, the L HBsAg plays a vital role in viral attachment and Bulevirtide therefore competes with the naturally occurring L HBsAg to bind to the NTCP, thus reducing viral attachment, entry and importantly replication. Bulevirtide is now commercially accessible in Europe under the brand name Hepcludex® for combating hepatitis D virus (HDV) (109). However, it is still under evaluation for HBV infection (clinicaltrails.gov NCT03852719).

Additional novel therapeutic approaches include short interfering RNAs (siRNAs) and toll-like receptor (TLR) inhibitors. siRNAs typically comprising 21 to 23 nucleotides, function by post-transcriptional gene silencing mechanisms (110). In the clinical trial NCT02604212, siRNA ARC-520 exhibited a moderate decrease in HBsAg levels (111), while siRNA ARC-521 (NCT027975220) demonstrated a substantial reduction in surface antigen. However, both trials were discontinued because of the adverse effects of the formulation. A newer siRNA, VIR-2218, is presently under evaluation in the trial NCT03672188, although official data has not yet been published.

Innate immunity, the primary line of defence, relies on cytoplasmic pattern recognition receptors (PRRs). These receptors interact with pathogen-associated molecular patterns (PAMPs), initiating the production of pro-inflammatory markers such as TLRs (112,113). The phase two clinical trial for TLR 7 inhibitor GS-9620 (NCT0216047) demonstrated good tolerability but did not result in significant HBsAg loss (114). TLR 8 inhibitor GS-9688 is currently undergoing phase two trials (NCT03491553), showing mild side effects and effectiveness in only 4% of patients (115).

Nucleic acid polymers (NAPs) are a class of antiviral compounds with broad-spectrum activity against various enveloped viruses (reviewed in (116)). Their effectiveness is not dependent on specific nucleic acid sequences but rather on their interaction with exposed hydrophobic surfaces, particularly amphipathic α-helices (117). Recent attention has focused on NAPs for treating chronic HBV and HDV, spurred by successful phase II trials of clinical NAP compounds such as REP 2055, REP 2139, and REP 2165 (118,119). These trials have demonstrated rapid loss of HBsAg and seroconversion, accompanied by therapeutic transaminase flares at high rates.

Taken together the available treatment options are only mildly effective against HBV, particularly in the case of chronic infection. Complete viral elimination and cccDNA degradation are yet to be achieved. Therefore, novel approaches against cccDNA are highly sought after.

1.5 Recent advances in treating HBV infection with designer nucleases

Current therapies and candidate drugs can suppress HBV replication but have limited success in eliminating cccDNA reservoirs. Consequently, researchers have turned to exploring the effectiveness of gene editing technologies against HBV. These technologies employ designer nucleases, which can be customised to target specific sequences. Therefore, designer nucleases have garnered considerable attention in the gene therapy domain in recent years. Several designer nucleases have been tested for studying complex diseases and reducing disease burden. Designer nucleases were initially evaluated in induced pluripotent cells (iPCs), human embryonic cells (hESCs) and organisms commonly used in research, such as zebrafish and mice (120–122).

Previous efforts by designer nucleases have aimed to inactivate cccDNA to inhibit viral replication (123–125). In principle, these designer nucleases induce mutations by creating double-strand breaks (DSBs) at specific sites (**Figure 1.3**) (126). DSBs occur naturally and frequently in eukaryotes (127), with homology-directed repair (HDR) and non-homologous end-joining (NHEJ) as the primary error-repair mechanisms (reviewed in (128)). The need for a homologous template is the rate-limiting factor in HDR, resulting in NHEJ occurring more swiftly and frequently than HDR (129). Although designer nuclease-directed HDR shows promise for gene correction, its low incidence limits effectiveness. To improve efficiency, donor sequences with flanking DNA segments matching nuclease binding sites are used, promoting HDR at the targeted genomic locus (130). HDR can introduce precise DNA sequences or correct gene mutations. Consequently, the NHEJ pathway is harnessed in the case of HBV, where repeated cleavage results in insertion and deletion (indel) mutations. Indels effectively incapacitate cccDNA, particularly within HBV which is rigorously regulated.

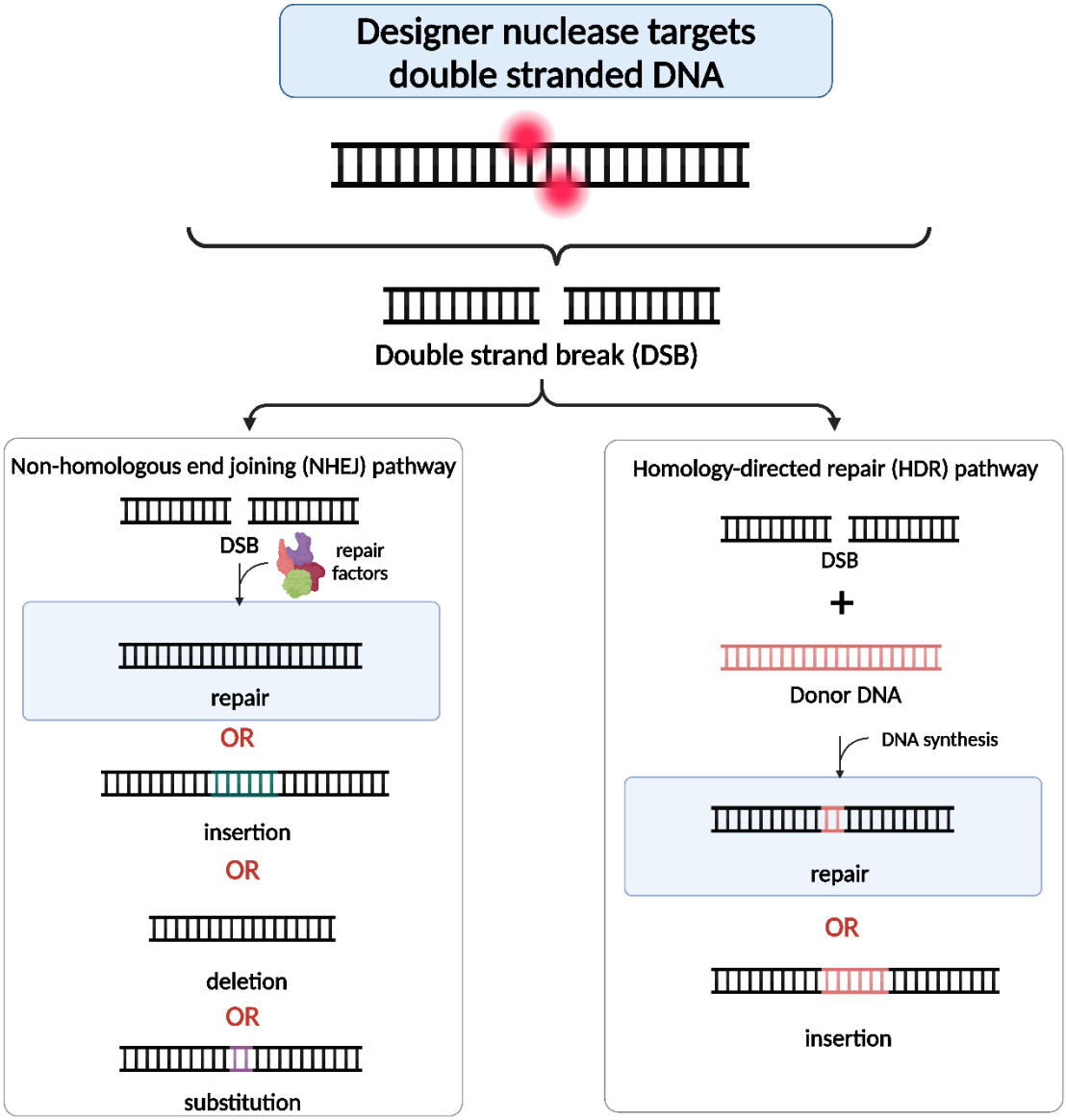


Figure 1.3: NHEJ or HDR pathways induced after designer nuclease-mediated cleavage.

Nuclease-mediated targeting initiates DNA target site cleavage, resulting in a double-strand break (DSB). Traditionally, this DSB undergoes repair via Non-Homologous End Joining (NHEJ) or Homology Directed Repair (HDR). Activation of NHEJ recruits DSB repair factors to the site, leading to the rejoining of DNA strands or causing mutagenic changes such as insertions, deletions, or substitutions. Conversely, introducing a donor sequence triggers the HDR pathway, facilitating gene repair or insertion at the DSB site. Equipped with homologous arms, the donor sequence functions as a blueprint for repair (Figure adapted from (131) and created with Biorender.com).

Designer nucleases employed for targeting HBV cccDNA include zinc finger nucleases (ZFNs), RNA-guided nucleases [i.e. the clustered regularly interspaced short palindromic repeats (CRISPR)/CRISPR-associated 9 (Cas9) system] and transcription activator-like effector nucleases (TALENs) **(Figure 1.4)**. ZFNs were pioneers in gene editing technology, initially developed and tested in model organisms (132). Early studies investigating ZFs demonstrated their ability to bind to target DNA and modulate gene expression selectively (133). In their natural state, ZFs are structured with Cys2-His2 folds. They have short β-sheets holding two cysteine residues and an α-helix containing two histidine residues, all held together by a zinc ion (133,134). Each fold is therefore referred to as a zinc finger. The α-helix of each finger binds to three nucleotides in the major groove of double-stranded DNA (135).

Typically, ZFNs are engineered to contain 3 ZFs which are capable of binding to 9 nucleotides **(Figure 1.4)**. One significant limitation in ZFN design is that the α-helix of one finger affects the orientation of the α-helix side chains in the neighbouring finger (136). This ultimately impacts the DNA binding efficiencies of the ZF peptide. Attaching the nuclease domain of the sequence-independent *Fok*I type IIS restriction enzyme to the ZFs creates the complete ZFN (132). To induce DSBs in DNA, ZFNs must operate as dimers. Each monomer is precisely engineered to bind to distinct nucleotides flanking the target site. When they dimerise, the monomers come together on opposing sides of the DNA, resulting in DSBs (137).

Two pivotal applications of ZFNs against HBV were documented. Cradick et al. showcased a 29% reduction in pgRNA (138). Following this, Weber and colleagues conducted a separate study, revealing that a set of ZFNs targeting *P* and *C* genes induced cytotoxic effects (124). Because of its design constraints, this nuclease system is infrequently employed, especially in HBV targeting applications.

The most recent addition to gene editing technologies is the CRISPR-Cas9 system. Initially identified in archaea and eubacteria, CRISPR-Cas serves as an immune mechanism against invading bacteriophages (139,140). Within its natural environment the invading DNA integrates into the CRISPR locus and undergoes processing into small RNA sequences termed CRISPR RNAs (crRNAs). During gene editing, the crRNA combines with *trans*-activating crRNAs (tracrRNAs), leading to the formation of small guide RNAs (sgRNA) crucial for DNA binding **(Figure 1.4)** (141). The sgRNA interacts with Cas proteins, primarily Cas9, to assemble the complete CRISPR-Cas system. The prevalent nucleases employed are Type II Cas9 sourced from *Streptococcus pyogenes* (*S. pyogenes*) or *Staphylococcus aureus* (*S. aureus*) (142,143). Successful targeted cleavage merely requires the presence of a protospacer adjacent motif (PAM) sequence **(Figure 1.4)** (144). Positioned upstream from the target sequence, the PAM sequence is identified by CRISPR-Cas, which then binds to the target sequence, initiating the intended mutagenic outcomes.

The use of CRISPR-Cas9 systems has raised concerns because of the commensal prevalence of *S. pyogenes* and *S. aureus*. Recent research has unveiled the existence of pre-existing humoral and cell-mediated immunity against the Cas9 protein in human serum (145,146). Owing to its simplicity in design, extensive research has been conducted on the application of CRISPR-Cas9 against HBV, as detailed in a recent review (147). Notably, a study utilising these RNA-guided nucleases in an HBV mouse model containing cccDNA demonstrated the impact of CRISPR on cccDNA in murine HBV replication for the first time (148). However, Martinez et al demonstrated that dual gRNAs led to the emergence of new HBV DNA variants that retained transcriptional activity (149) and in a separate investigation, Fu and team revealed only a 5% targeted mutagenesis in cccDNA (150).

As with ZFNs, TALENs consist of a customisable DNA-binding motif linked to the nuclease domain of *Fok*I. Initially identified in the *Xanthomonas* genus of bacteria, which infects plants, TALEs bind to DNA in crop plants, functioning as transcription factors that modify gene expression in their hosts (151,152). Naturally occurring TALEs contain varying numbers of tandem repeats, ranging from 1.5 to 33.5 (153). Numerous methodologies have been proposed and extensively discussed in the literature for creating custom TALE arrays capable of binding specific DNA sequences (154–156). A minor limitation when constructing TALEs is the requirement for the target sequence to begin with a thymine base to enhance TALE-DNA interaction (157). However, this challenge can be overcome by creating TALENs with diverse spacer sequence lengths to ensure that the target sequence starts with thymine (158).

In gene editing applications, TALEs typically consist of 17.5 or 18.5 tandem repeats, each containing 34 highly conserved amino acids (153). The C-terminal repeat, often shorter, is termed a "half repeat." **(Figure 1.4)** (159). Within these amino acids, positions 12 and 13 are crucial for recognising and binding to individual nucleotides, earning them the designation of repeat variable diresidues (RVDs) (160). The RVD code was recently deciphered which allowed for the design of specific DNA binding arrays (159). Amino acids NI, HD, NN, and NG specifically bind to the nucleotides A, C, G, and T, respectively. However, there is some redundancy in this binding, as NN can also attach to A. To enhance the specificity of this code, researchers investigated alternatives and discovered that substituting NN with NH or NK resulted in a more precise binding to G (161). TALENs combine custom-designed TALEs with a *Fok*I nuclease domain for precise site-specific cleavage. As with ZFNs, the *Fok*I endonuclease functions only as a dimer to cut both strands of duplex DNA. Consequently, TALENs are engineered as two separate monomers, termed left and right monomers, which converge on opposite strands of the target DNA to induce DSBs

(Figure 1.4). In contrast to ZFNs, the mutual influence of adjacent monomers within the DNA binding domains of TALEs does not impact their respective interactions with the target site.

Numerous investigations have reported the application of ZFNs and CRISPR-Cas9 in cccDNA targeting. Nonetheless, these genetically modified nucleases are often associated with increased off-target cleavage and reduced target efficiencies compared to TALENs (124,150). Recent advancements in mitigating off-target effects related to the CRISPR-Cas system have shown progress through the introduction of base editors. Engineered by combining deactivated Cas nucleases with deaminases, these tools induce specific mutations through deamination reactions without inducing double-stranded breaks (162). They are categorised into two main types: C-to-T base editors (CBEs), which convert cytosine to thymine, and A-to-G base editors (ABEs), which convert adenine to guanine (162). Yang et al. demonstrated successful point mutations of cccDNA *in vitro* using a CBE base editor (163).

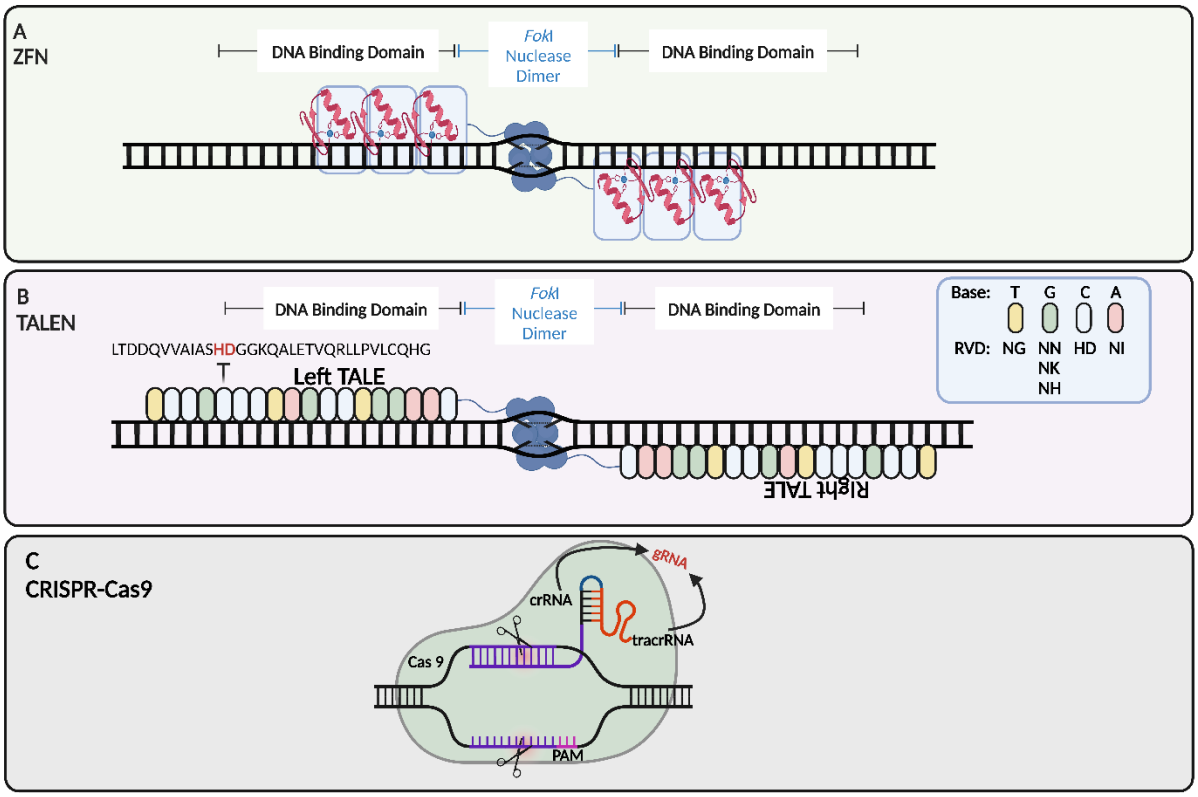


Figure 1.4: Designer nucleases induce double-stranded breaks at target sites.

A. Zinc Finger Nucleases (ZFNs) consist of a DNA binding domain comprising a repeat of three zinc finger motifs (ZFs), each recognising and binding to three nucleotides on each strand of DNA. These ZFs are tethered to the *Fok*I nuclease domain, enabling double-stranded cleavage. **B.** Transcription Activator-Like Effector Nucleases (TALENs) typically contain 17.5 tandem repeats of Transcription Activator-Like Effectors (TALEs) that recognise and bind to target DNA sequences through their repeat-variable di-residues (RVDs). The degenerate RVD code is depicted in the upper right corner. Each repeat consists of 34 amino acids, with positions 12 and 13 crucial for recognising a single nucleotide, where 'HD' recognises cytosine (C). TALEs are linked to *Fok*I nuclease domains, facilitating double-stranded cleavage. **C.** The Clustered Regularly Interspaced Short Palindromic Repeats (CRISPR)-associated protein 9 (Cas9) system utilises a guide RNA (gRNA) complex formed by the fusion of trans-activating CRISPR RNA (tracrRNA) and CRISPR RNA (crRNA). This complex directs Cas9 to the target DNA sequence for cleavage. Additionally, a Protospacer Adjacent Motif (PAM) sequence is essential for Cas9 recognition and guides Cas9 to induce double-stranded breaks (DSBs) at the designated target site (Figure created with Biorender.com).

1.6 Employing and modifying TALENs targeted against HBV

Following the discovery of *Xanthomonas* TALEs and their intrinsic DNA binding properties, research has focussed on enhancing array propagation for efficient TALE assembly. Unlike ZFNs, which require specific context-dependent subunits for DNA binding (136), TALE arrays can be readily assembled using modular cloning techniques, eliminating the need for context-dependent selection.

The primary method for creating TALEs involves Golden Gate cloning alongside a pre-assembled TALE module plasmid library (155,164). Each TALE-encoding DNA module contains a unique sequence encoding RVDs, flanked by type IIS restriction sites. When cleaved, these sites produce specific 5' overhangs that allow ligation with complementary overhangs from other TALE modules, enabling simultaneous cut-ligation reactions without reconstituting the recognition site (165).

Using the Golden Gate approach, Morbitzer and colleagues developed a TALE repeat assembly protocol using a pre-assembled TALE-encoding DNA module library and a two-step cut-ligation approach to produce sequence-specific TALENs (154). The first generation of anti-HBV TALENs was produced using the modular cloning TALE repeat assembly kit combined with *Fok*I nuclease vectors (123). Each TALEN subunit was designed to target specific 19 bp DNA sequences, preceded by a thymine and separated by a 13 bp spacer region to optimise nuclease activity. Bloom and colleagues demonstrated the effective use of these TALENs against HBV targeting the *C*, *P*, and *S* genes (123). In cell culture models, they observed moderate cccDNA targeting, while in mice hydrodynamically injected with an HBV plasmid, 90% reduction in HBsAg was observed. Chen and colleagues also showed similar efficacy with anti-HBV TALENs, noting predicted interactions with target sites and minimal toxicity in cellular and animal models (166).

However, to make this gene editing technology more clinically applicable, enhancing the specificity of TALENs is crucial. TALENs with wildtype *Fok*I nuclease domains may cause unintended off-target effects as a result of potential cleavage by homodimers (two of the same monomers binding non-specifically on opposite DNA strands) **(Figure 1.5)** (167). To address this, Miller and collaborators focussed on developing *Fok*I variants with enhanced specificity for site-directed cleavage (168). They introduced substitutions Q486E and I499A in the left monomer, and E490K and I538V in the right monomer, resulting in the creation of obligate heterodimeric nucleases **(Figure 1.5)**. These modifications prevent homodimer pairing and encourage heterodimer pairing, thus mitigating off-target consequences.

Subsequent developments led to the generation of obligate heterodimeric TALENs by replacing the *Fok*I nuclease domains with variants allowing only for obligate heterodimeric cleavage (**Figure 1.6**) (169). A haemagglutinin (HA) tag and a NLS were incorporated at the N-terminal of each TALEN to assess protein expression. A recent investigation by our team focussed on employing these obligate heterodimeric TALENs for targeting the *S* and *C* genes (169). Obligate heterodimeric TALENs proved equally proficient in targeting and inhibiting viral replication compared to those reported previously. Moreover, they demonstrated enhanced target specificity. This was corroborated by scrutinising mutations occurring at a predicted off-target locus situated in the intronic region of the *phenylalanine hydroxylase* gene. Notably, obligate heterodimeric TALENs induced fewer mutations at this locus than their wildtype counterparts, highlighting the significance of precise targeting.

While the literature has undoubtedly shown the effectiveness of TALENs against HBV, this was typically achieved using plasmid DNA for subsequent TALEN expression, which is not suitable for clinical translation. Moreover, prolonged translation from a DNA template is not optimal when

employing designer nucleases, because the extended expression can increase off-target cleavage. In this study, mRNA encoded the obligate heterodimeric TALENs rather than DNA to pursue a more clinically applicable approach

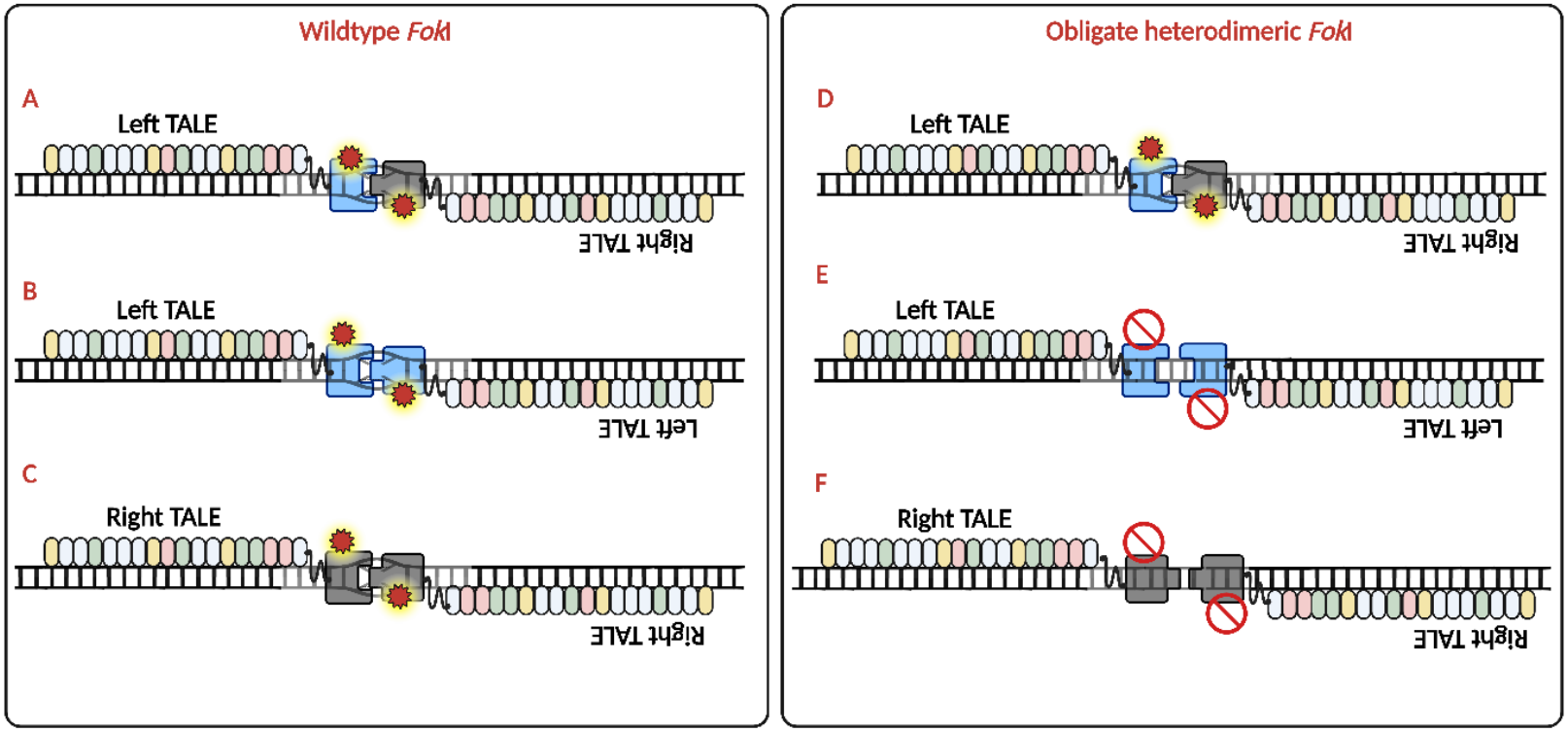


Figure 1.5: Enhanced specificity achieved by obligate heterodimeric Transcription Activator-Like Effector Nucleases (TALENs).

A-C Depict wildtype *Fok*I nuclease domains, with **A.** representing heterodimeric cleavage while **B.** and **C.** represent off-target homodimeric binding leading to cleavage. **D-F.** Represent obligate heterodimeric *Fok*I nuclease domains with substitutions Q486E and I499A in the left monomer, and E490K and I538V in the right monomer. **D.** Illustrates heteromeric cleavage facilitated by electrostatic interactions. Conversely, **E.** and **F.** illustrate homodimerisation, which fails to induce cleavage owing to the presence of two identical monomers resulting in electrostatic repulsion (Figure created with Biorender.com)

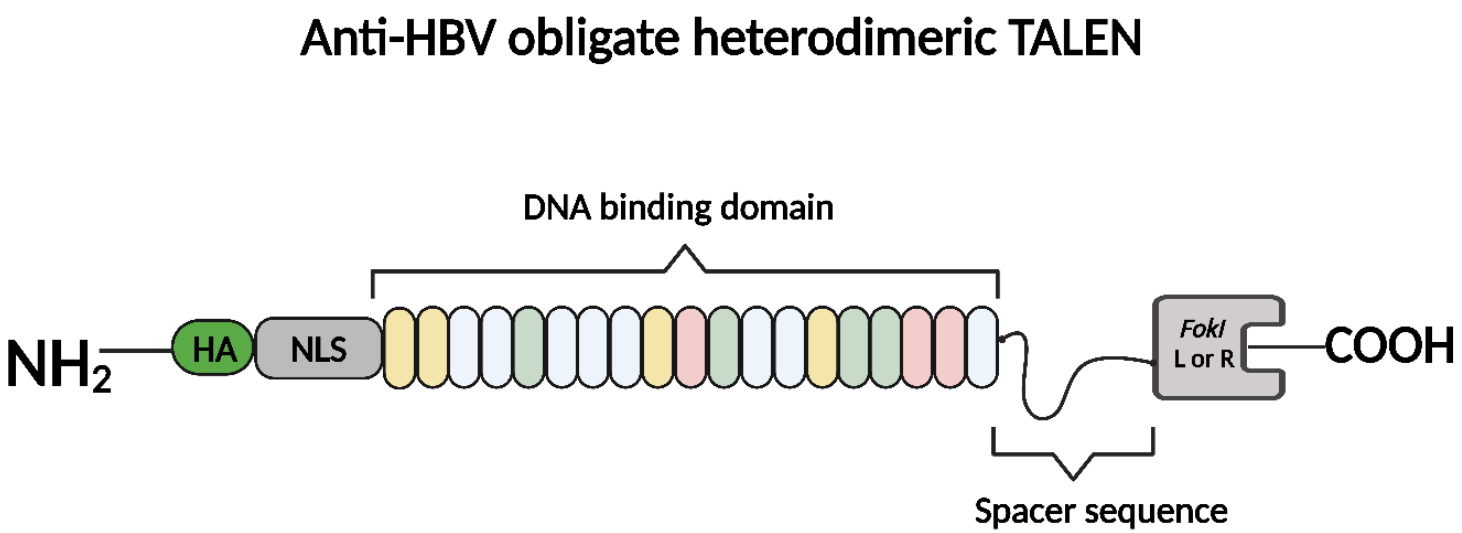


Figure 1.6: The structure of anti-HBV obligate heterodimeric TALENs.

The HA and NLS are found at the N-terminal (NH_2) while the *Fok*I left (L) or right (R) variant is found at the C-terminal (COOH) of the TALE. DNA binding repeat domains consist of 19 TALE modules.

1.7 TALEN-encoding mRNA as an anti-HBV therapeutic

Malone and colleagues were among the first to successfully demonstrate the delivery and expression of mRNA to cells (170). They produced mRNA encoding a reporter gene which was administered to cells using lipid nanoparticles (LNPs). Shortly after reporting this study, Wolff and colleagues pioneered the therapeutic potential of mRNA, reporting functional protein expression in the quadriceps muscle of mice (171). Regrettably, the use of mRNA was impeded by various complications. These challenges included issues with stability and immunogenicity, which prompted the prioritisation of DNA platforms (172). Only recent advancements in mRNA immune alterations, purification, and delivery techniques, have propelled mRNA to the cutting edge of scientific inquiry.

Several important factors such as large-scale manufacturing, defined dose regulation and lack of genome integration are crucial requirements for clinical translation. mRNA boasts several advantages over DNA to achieve clinical translation. These factors encompass the scalability of mRNA production through *in vitro* transcription (IVT) and the formulation process occurring in an environment devoid of cells, thereby reducing uncertainties associated with biological manufacturing. Moreover, after delivery mRNA remains localised within the cytoplasm, mitigating the potential for recombination and genotoxicity, while the therapeutic effect is transient, allowing for improved dosage management. mRNA therefore provides superior therapeutically relevant prerequisites that can be harnessed by TALENs in treating chronic HBV infections. The following sections provide an overview of IVT techniques for mRNA production that can be applied to generate effective TALEN-encoded mRNA.

Key requirements for successful IVT include a DNA template featuring a bacteriophage T7 promoter sequence, followed by sequences encoding a 5’ untranslated region (UTR), an ORF with

an integrated stop codon, a 3' UTR, and ending with a poly(A) tract (**Figure 1.7**) (173). Additionally, IVT also requires components such as a 5' cap structure (7-methylguanosine, m7G), bacteriophage RNA polymerase, ribonucleotide triphosphates (rNTP), and a buffer containing dithiothreitol (DTT), spermidine, and Mg^{2+} ions (174). Plasmid design should also include a suitable restriction cleavage site downstream of the poly(A) tract to aid in linearisation at a defined site (173). mRNA is synthesised from a linear template, where RNA polymerase specific to the encoded promoter initiates IVT.

The 5' cap is coupled to the initial nucleotide of mRNA through a 5'-5' triphosphate bond **(Figure 1.7)** (175). This cap fulfils three primary roles: safeguarding mRNA from exonuclease degradation, facilitating translation initiation, as well as shielding mRNA from immune clearance (176). The eukaryotic initiation factor 4E identifies and attaches to the 5' cap, enabling ribosome assembly on the mRNA for translation initiation (177). The 5' and 3' UTRs encompass specific regulatory sequences crucial for governing translation efficiency and mRNA stability (178,179). Investigations into UTRs from the *α*- and *β-globin* genes have revealed their potential to improve the translation and durability of engineered mRNA as mRNA from these genes are naturally translated at high rates (180). The poly(A) tract slows down the degradation of the mRNA transcript at the 3' end and also works synergistically with the 5' cap in regulating translation efficiency by binding to polyadenosyl-binding proteins (181).

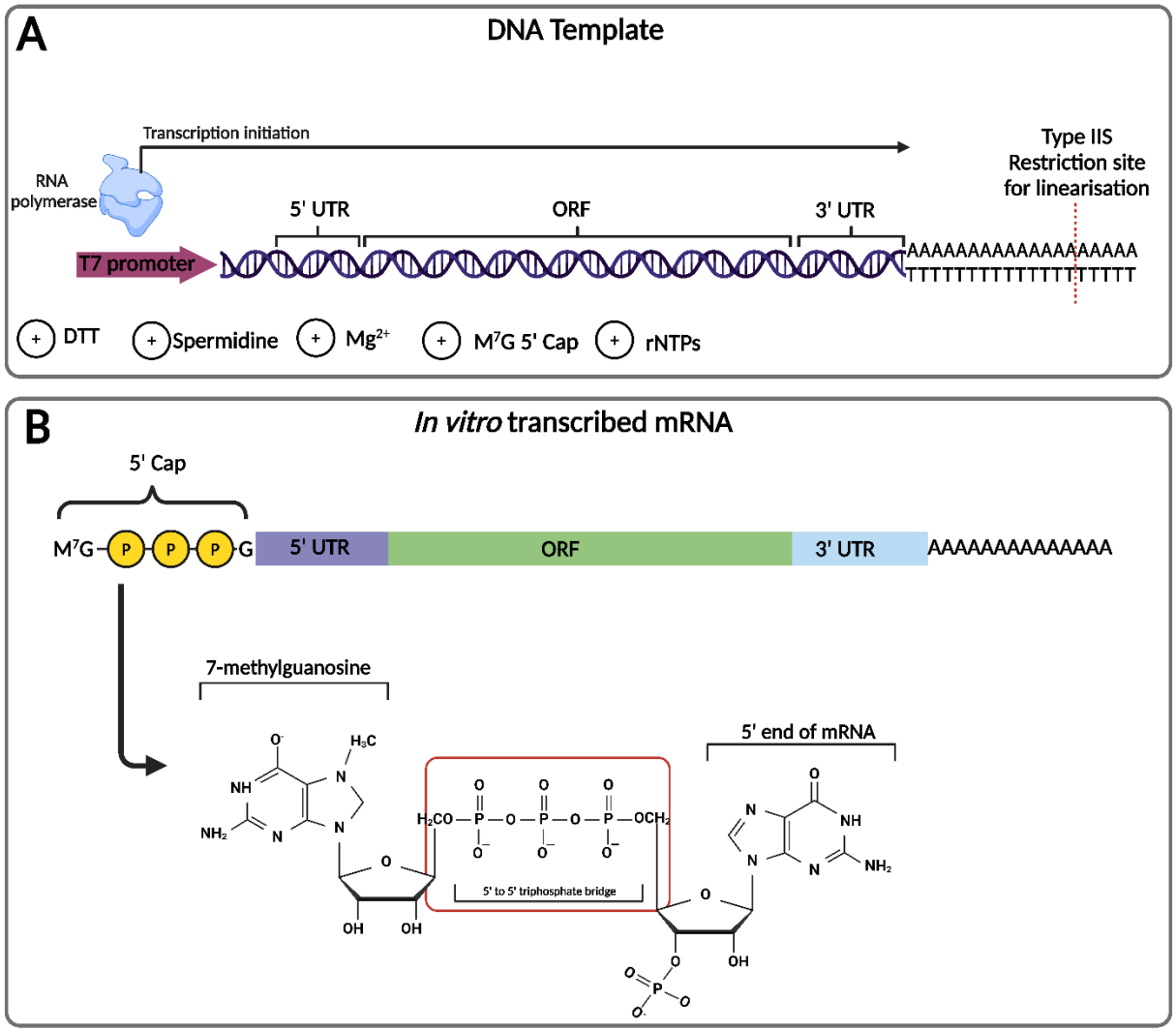


Figure 1.7: Schematic overview of the IVT process from a DNA template.

A. DNA template consists of five essential *cis* elements crucial for IVT: a promoter sequence, 5' and 3' UTRs, and a Poly(A) sequence. Additionally, the reaction includes components such as DTT, spermidine, Mg^{2+}, M^7G cap analogue and rNTPs. A unique restriction site downstream of the poly(A) sequence is required for the linearisation of the DNA template. The T7 RNA polymerase is responsible for binding to the T7 promoter and initiating the transcription process. **B.** Resulting mRNA contains a 5' cap linked to the RNA through a 5' to 5' triphosphate bridge (highlighted in red) (Figure created with Biorender.com).

Synthetically produced 5’ caps are crucial for incorporating into engineered transcripts. Without efficient capping, transcripts are vulnerable to degradation and cannot proceed to translation. The leading commercially available 5’ cap analogues include anti-reverse cap analogues (ARCAs) and CleanCap® derivatives. Alternatively, a 5’ cap can be incorporated into transcripts enzymatically using the capping enzymes from the Vaccinia virus.

In the mid-1990s, Pasquinelli and his team discovered that bacteriophage polymerases could initiate transcription using the 3'-OH group of the m7G moiety (cap-0), rather than the 3'-OH group of the neighbouring nucleotide, leading to the integration of reverse caps (Gpppm7GpN) (182). This reverse orientation negatively impacts translational efficiency, prompting efforts by Stepinski and colleagues to develop ARCAs by modifying the m7G moiety (**Figure 1.8**) (183). ARCAs show exclusive incorporation in the correct orientation and demonstrate at least double the translation efficiency of conventional cap-0 structures.

Viruses have evolved to produce 5' cap structures that enhance translation efficiency and evade host immune defences (reviewed in (184)). The vaccinia virus, a poxvirus prototype, has a highly effective and well-studied RNA capping enzyme consisting of a D1 subunit (185–187) (**Figure 1.9**). The D1 subunit includes three enzymes namely RNA triphosphatase (TPase) which removes the 5’ γ-phosphate, RNA guanylyltransferase (GTase) that adds a guanosine monophosphate (GMP) to the diphosphate 5’ terminus, and guanine-N7 methyltransferase (MTase) that methylates the N7 position of the guanosine cap to generate the cap-0 structure (reviewed in (184)). To form transcripts with cap-1 structures, 2’-O methylation is added by 2’-O methyltransferase (2’-O MTase), which helps the RNA evade recognition by pattern recognition receptors (188). Both MTase and 2’-OTase use S-adenosyl methionine (SAM) as a methyl donor (189). The recent

commercial availability of vaccinia capping enzymes (VCEs) (174) enables near-complete efficiency in producing cap-0 or cap-1 transcripts added in the correct orientation (190).

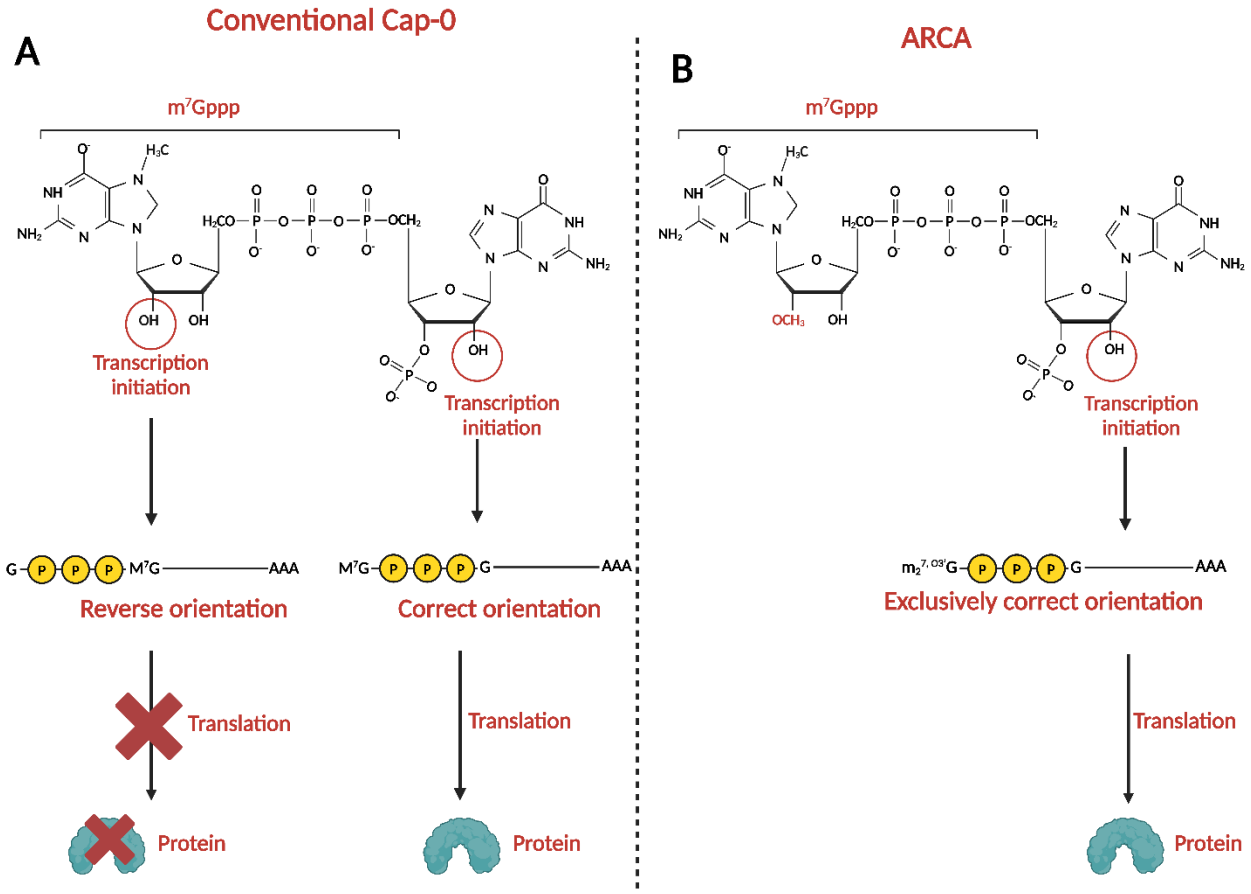


Figure 1.8: Conventional cap-0 versus anti-reverse cap-0 analogues (ARCAs).

A. In the conventional cap-0 structure, bacteriophage polymerases can initiate transcription from either the 3'-OH group of the m7Gppp, leading to reversed capped analogues unsuitable for translation, or from the 3'-OH group of the initial nucleotide, resulting in capped analogues positioned correctly for translation. **B.** Conversely, the ARCA structure is formed by substituting the 3'-OH group of the m7Gppp with an -OCH3 group. This generates capped structures that are favourably oriented for translation (Figure created with Biorender.com).

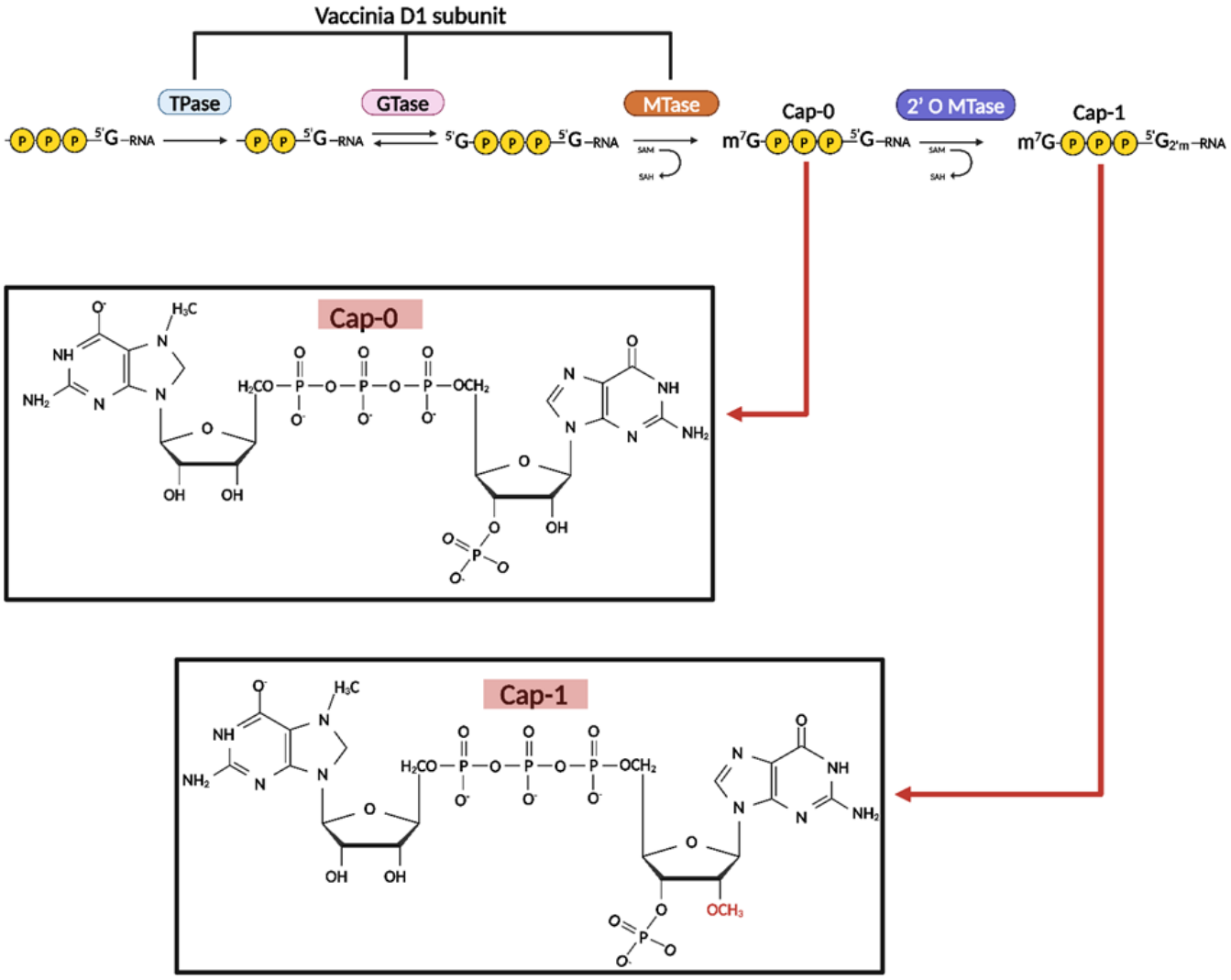


Figure 1. 9: The enzymatic conversion from uncapped to cap-0 and cap-1 transcripts using VCEs.

Cap-0 formation results from a sequence of three enzymatic processes. Initially, triphosphatase (TPase) removes the 5' terminal γ-phosphate from the first nucleotide, depicted as G-ppp. Following this, guanylyltransferase (GTase) adds a guanosine monophosphate (GMP) generating 5'Gppp-5'G (triphosphate linkage). In the next step, guanine-N7 methyltransferase (MTase) transfers a methyl group from S-adenosyl methionine (SAM) to the N7 amine group of the guanosine cap, culminating in the creation of cap-0 structures. The generation of cap-1 requires another enzymatic step executed by the 2'O methyltransferase (2' O MTase), which moves a methyl group from SAM to the +1 ribonucleotide at the 2'O position of the ribose of the starting nucleotide (Figure created with Biorender.com).

Previously, cap-1 synthesis relied on post-transcriptional enzymatic methods. Now, TriLink BioTechnologies' patented CleanCap® technology enables cap-1 production through co-transcriptional capping (173). In this study, CleanCap® AG was used. This method employs a trinucleotide comprising the m7Gppp moiety, 2'O methylated ribose attached to ATP (+1) and G (+2). CleanCap® AG competes with GTP maintaining high GTP concentrations without reducing mRNA yield. CleanCap analogues bind to the +1 and +2 positions of the T7 promoter sequence, requiring careful template design (**Figure 1.10**).

In summary, the key elements involved in engineering mRNA-encoded transcripts hold vast potential for the field of gene therapy. A comprehensive review indicates that mRNA-based therapy applies to numerous diseases unresponsive to existing treatments, including infectious diseases, cardiovascular conditions, and cancer (191). Notably, mRNA-based vaccines have proven effective in controlling the transmission of recent coronavirus disease (COVID-19) (reviewed in (192)**)**. Furthermore, mRNA synthesised through IVT has recently demonstrated efficacy in expressing TALENs for therapeutic purposes (193–195).

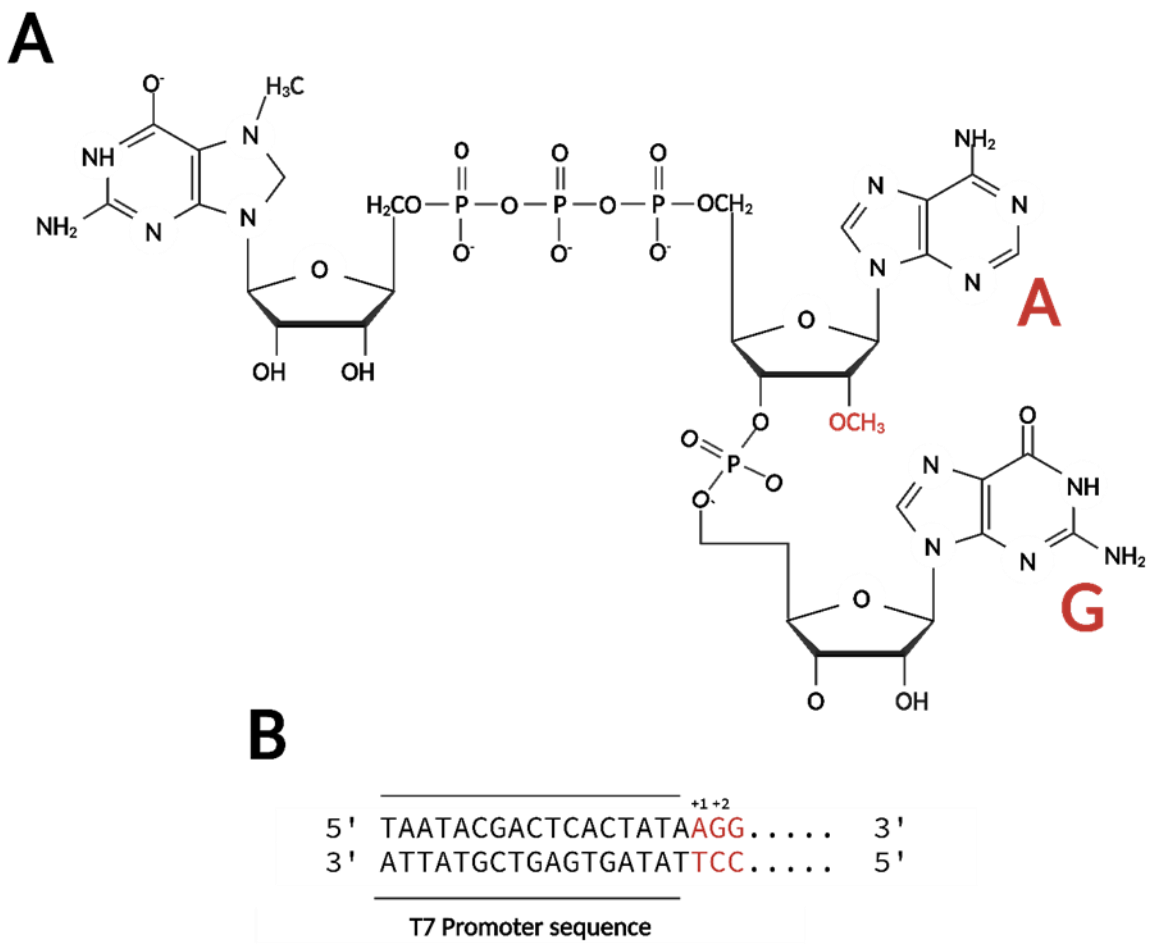


Figure 1.10: CleanCap® AG trinucleotide.

A. An illustration of the CleanCap® AG trinucleotide shows the m7Gppp cap succeeded by ATP featuring an -OCH3 group at the 2' position of the ribose. This results in the formation of the cap-1 structure in transcripts. G is found at the +2 position. **B.** The T7 promoter sequence, essential for initiating transcription with CleanCap® AG, is emphasised in red at the +1 and +2 sites (Figure created with Biorender.com).

1.8 Encapsulating TALEN-encoding mRNA within lipid nanoparticles

The transportation of naked nucleic acids for therapeutic purposes faces several limitations, such as susceptibility to degradation by intra- and extracellular enzymes, and difficulty crossing the plasma membrane as a result of their large size and negative charge (196). Establishing a reliable and efficient delivery system is vital to preserve mRNA integrity during its transit to the target tissue, thereby facilitating TALEN-mediated therapeutic effect in the case of HBV infection.

Lipid-based systems were first characterised over six decades ago (197,198), and about three decades later, a liposomal formulation for chemotherapy was approved in the USA. Since then, the FDA has approved multiple LNP formulations for mRNA delivery (reviewed in (199)). LNPs usually consist of four main components: a permanently cationic/ionisable lipid, a helper lipid (phospholipid), cholesterol and a PEGylated lipid **(Figure 1.11)** (reviewed in (200)). The positively charged ionisable lipid interacts with negatively charged RNA molecules, aiding their escape from endosomes. (201). Phospholipids assist in RNA release in the cytoplasm after endosomal escape while maintaining LNP structural integrity (202). Cholesterol increases membrane rigidity, and PEGylated lipids enhance stability by reducing serum protein adsorption and LNP aggregation (177,203).

LNPs include either single-layer or double-layer vesicles containing a core that is either electron-dense or aqueous. Specifically engineered ionisable LNPs (iLNPs) are commonly used for delivering mRNA to hepatocytes (204), which is advantageous for therapeutic strategies aimed at combating HBV infection, given the virus' predominant hepatocyte targeting. Furthermore, iLNPs utilise their inherent tropism to evade immune activation following intravenous administration.

iLNPs exhibit a positive charge in low pH conditions but remain neutral under physiological pH levels (200). Low-density lipoprotein receptors (LDLRs) on the basal-lateral membrane of hepatocytes are crucial for the uptake of lipid nanoparticles **(Figure 1.11)** (205). In neutral conditions, serum apolipoprotein E (ApoE) binds to LNPs, facilitating their transport to hepatocytes and internalisation through LDLRs, thereby initiating clathrin-mediated endocytosis (204). Upon cellular uptake and entry into endosomal compartments, iLNPs encounter an acidic environment, causing the ionisable lipid to protonate and switch their charge to positive. This change enables interaction with the negatively charged endosomal membrane, leading to membrane destabilisation, pore formation, or rupture. This process enables encapsulated mRNA to escape into the cytoplasm, where it can be translated by ribosomes into protein (206). Notably, iLNPs have been employed in the formulation of the Pfizer/BioNTech and Moderna COVID-19 SARS-CoV-2 vaccines (207,208).

During recent advancements, separate studies showcased the utilisation of LNPs for delivering mRNA-encoding CRISPR-Cas9 (209) or mRNA-encoding CBE to mice (210), aiming to target HBV. Following intravenous tail vein injections, LNPs achieved systemic distribution. The liver, which filters a large portion of blood, is an ideal target because of its high blood flow and fenestrated endothelium, which prohibits particles larger than 150 nm from passing through. This highlights the importance of small LNPs for facilitating passive accumulation and uptake. Efficient delivery of gene editing tools was observed in murine models, along with a notable decrease in HBsAg levels. Importantly, the LNPs did not exhibit immunostimulatory effects, and there were no indications of liver toxicity.

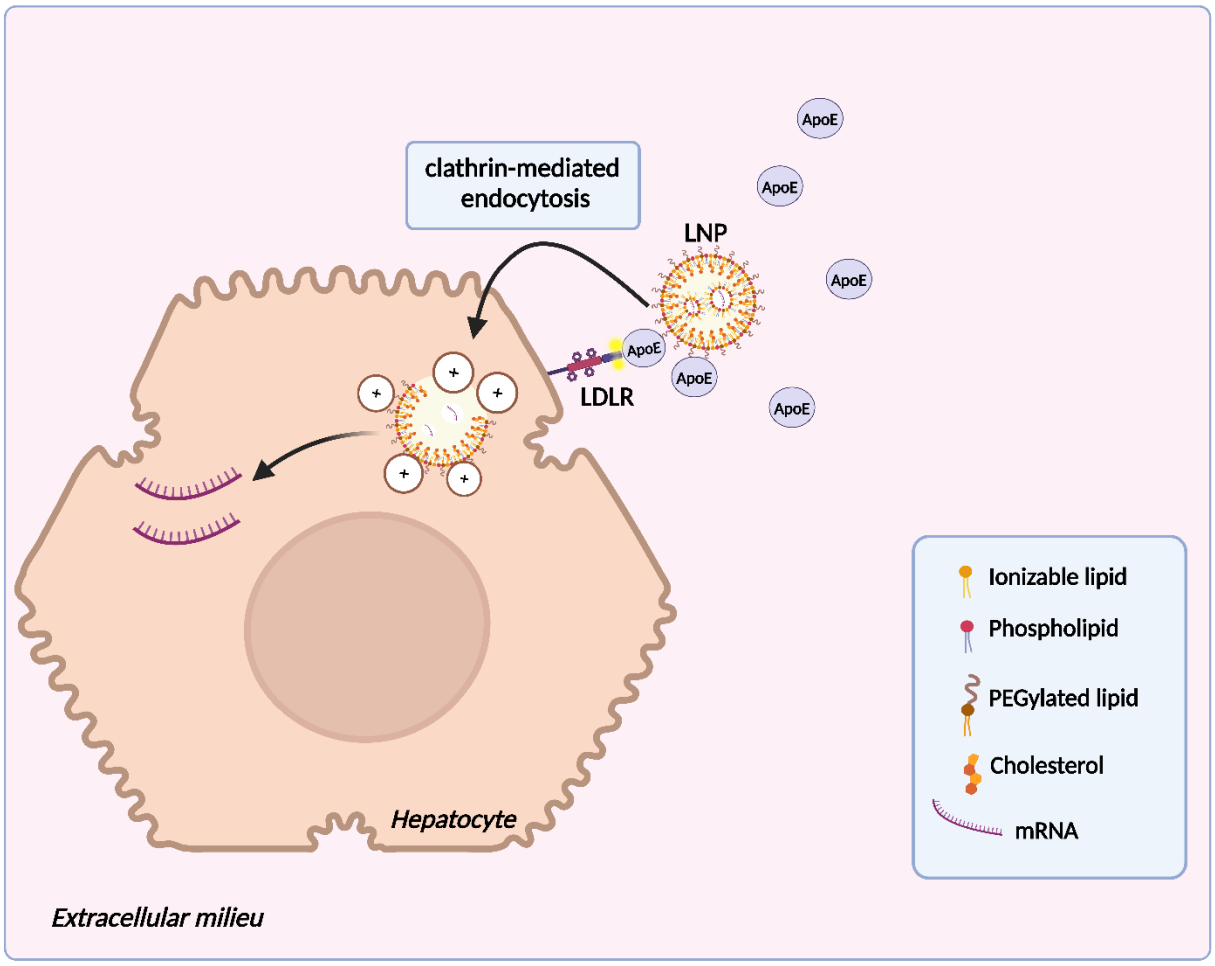


Figure 1.11: The intracellular delivery of ionisable lipid nanoparticles (iLNPs) to hepatocytes via clathrin-mediated endocytosis.

In the extracellular environment, serum apolipoprotein E (APOE) is capable of binding to ionisable lipid nanoparticles (iLNPs). Once bound, APOE facilitates the targeting of iLNPs to the low-density lipoprotein receptor (LDLR) situated on the surface of hepatocytes. Additional lipid components aid in the process of clathrin-mediated endocytosis. Upon internalisation, iLNPs exhibit a positive charge, thereby promoting the release of mRNA payloads (Figure created with Biorender.com).

1.9 Project aims

This thesis builds on previous research demonstrating that plasmids encoding obligate heterodimeric TALENs can enhance the specificity of cccDNA cleavage (169). This project aimed to preclinically validate a novel HBV therapeutic approach targeting the *S* and *C* ORFs, utilising pre-existing obligate heterodimeric TALEN DNA sequences as templates for *in vitro* transcription (IVT) of TALEN-encoding mRNAs.

Plasmids were subsequently generated for mRNA transcription, and IVT reactions with various 5' cap analogues were tested to produce functional TALEN-encoding mRNAs. These TALEN transcripts were then evaluated for their anti-HBV potency in cell culture. Additionally, formulations in iLNPs were prepared for delivering TALEN transcripts *in vivo*. This study marks the first investigation into the anti-HBV efficacy of TALEN-encoding mRNA. The findings indicate that this mRNA-centric approach could overcome the limitations of existing HBV treatments, offering a promising new therapeutic strategy and laying the groundwork for future clinical applications. This represents a significant advancement in HBV therapy and the broader field of mRNA-based gene editing.

Chapter 2- Designing anti-HBV TALEN-encoding mRNA and evaluating TALEN expression in cultured mammalian cells

2.1 Introduction

The design and development of anti-HBV TALEN-encoding mRNAs were explored, followed by an evaluation of their expression in cultured mammalian cells. Building on previous research that highlighted the enhanced specificity of obligate heterodimeric TALENs for cccDNA cleavage, the objective was to create and test a novel therapeutic approach targeting the *C* and *S* ORFs of HBV. TALEN-encoding mRNA offers several advantages over their DNA counterparts, particularly for therapeutic applications. mRNA delivery allows for controlled expression levels, simplified manufacturing, and regulatory processes, making it a safer, more efficient, and controllable tool for gene editing therapies. Given that this is the first time anti-HBV TALEN-encoding mRNAs are being tested, it was crucial to first assess their expression in cell culture before proceeding to functional tests.

Careful optimisation of transcription, capping, and purification methods is essential for the development of effective and stable TALEN-encoding mRNAs, with capping being especially important because of its role in translation and mRNA protection. The 5' cap structure is crucial for mRNA stability and translation efficiency, which are necessary for producing high-quality therapeutic transcripts. Various methods for these processes are systematically described below. The rationale for exploring different capping mechanisms in the design and development of anti-HBV TALEN-encoding mRNAs is rooted in the need to enhance mRNA stability and translation efficiency. Testing a range of capping methods, including co-transcriptional and post-transcriptional approaches with different cap analogues, was undertaken to identify the most

effective strategies for producing translatable products. Additionally, considerations for two different designs of IVT templates are discussed, emphasising their impact on the efficiency and quality of TALEN-encoding mRNA production.

Using ARCA capabilities, the anti-HBV TALENs were transcribed *in vitro* from IVT template design 1, which includes all essential components described in Figure 1.7. ARCA enabled co-transcriptional capping of the mRNAs during the transcription process. (**Figure 2.1**). ARCA cap-0 structures remain susceptible to triggering an IFN response (211). One significant drawback of engineered cap-0 structures is the competition between the cap analogue and GTP nucleotide for incorporation into synthetic mRNA (reviewed in (184)). Consequently, following IVT, a portion of the mRNA retains an uncapped state with a 5' triphosphate, potentially triggering an immune response. Recent studies have highlighted that 2′O methylation of the +1 nucleotide in eukaryotic mRNA, which produces cap-1 transcripts, is essential for the innate immune system to differentiate between foreign and self RNA (reviewed in (212,213)). Therefore, alternative approaches were explored to incorporate cap-1 structures into TALEN transcripts and generate functional TALENs.

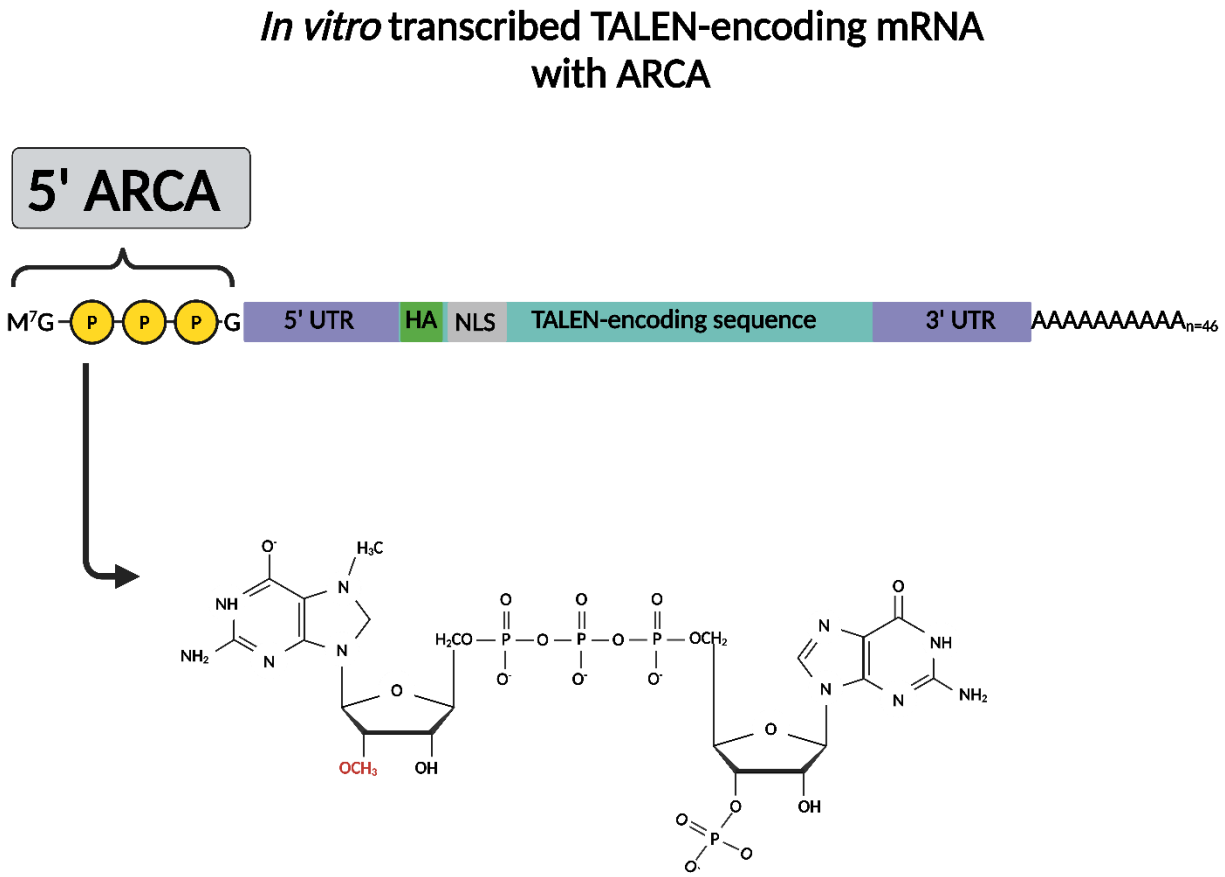


Figure 2.1: TALEN-encoding mRNA with ARCA.

TALEN-encoding mRNA was produced by *in vitro* transcription (IVT) from linearised DNA templates. The resulting transcripts were capped at the 5' end with ARCA through co-transcriptional mechanisms, generating transcripts that are favourable for translation (Figure created with Biorender.com).

Cap-1 structures, combined with modified nucleotides like pseudouridine (Ψ) and N1-methylpseudouridine (m1Ψ), enhance translation and reduce innate immune detection (214,215). Consequently, anti-HBV TALENs bearing cap-1 transcripts were produced from IVT template design 1 using VCEs, with uridine substituted with Ψ to mitigate immune response, allowing successful translation without immune complications (**Figure 2.2**).

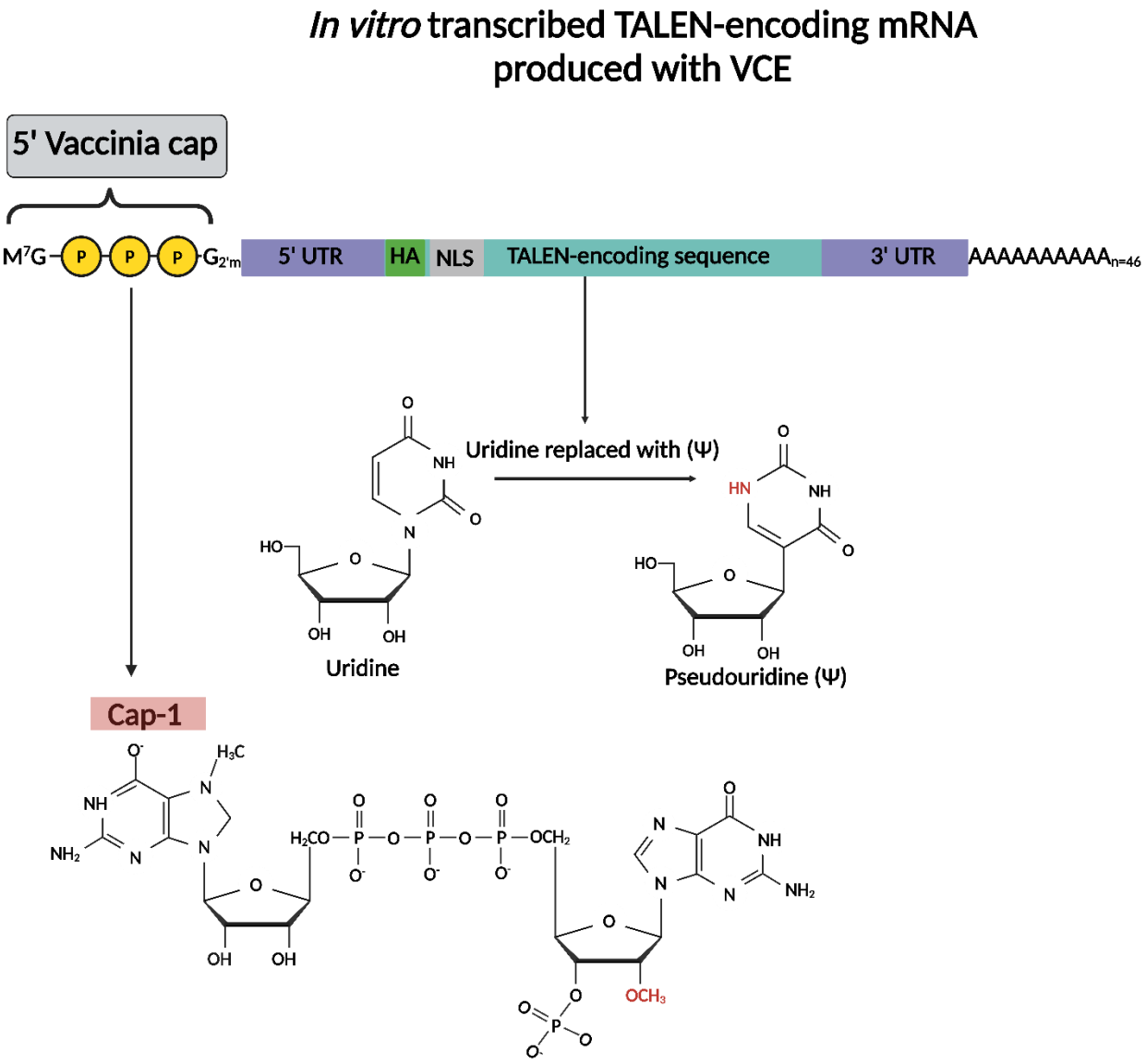


Figure 2.2: TALEN-encoding mRNA with vaccinia cap and Ψ.

TALEN-encoding mRNA was produced by *in vitro* transcription (IVT) from linearised DNA templates. The resulting transcripts were capped post-transcriptionally at the 5' end with VCE to generate cap-1 transcripts. Pseudouridine (Ψ) was incorporated in place of uridine during the IVT reaction to produce less immunogenic transcripts (Figure created with Biorender.com).

Literature demonstrates that transcripts created with VCEs often produce functional proteins, though the IVT process can inadvertently produce double-stranded RNA (dsRNA) by-products (216). To address this issue and improve TALEN expression, additional steps were taken, including the use of cellulose purification to remove dsRNA contaminants (217). To streamline the process and eliminate the need for post-transcriptional capping, CleanCap® AG was used to produce TALEN transcripts from IVT template design 1, which involved substituting uridine with Ψ, followed by cellulose purification. Notably, the template included a single stop codon, and recent studies have demonstrated that Ψ increases mRNA stop codon readthrough in eukaryotic cells, causing ribosomes to translate into the 3' UTR and possibly the poly(A) tail, leading to "nonstop" decay, which affects mRNA integrity and protein functionality (218,219).

To prevent readthrough errors, a redesigned DNA template incorporated four stop codons. Additionally, this template included 5' and 3' UTRs from the *β-globin* gene and an extended poly(A) tract, all of which are known to enhance transcript stability and protein functionality. TALEN mRNA was generated from this newly designed IVT template 2 using CleanCap® AG technology, which involved substituting uridine with m1Ψ and subjecting the transcripts to cellulose purification. (**Figure 2.3**).

Exploration of TALEN-encoding mRNA synthesis and expression underscores the importance of optimising IVT conditions with cap-0 and cap-1 techniques. Key aspects of this process included the use of synthetic uridine substitutes, modifications to DNA templates, and the application of purification protocols to produce functional TALEN proteins.

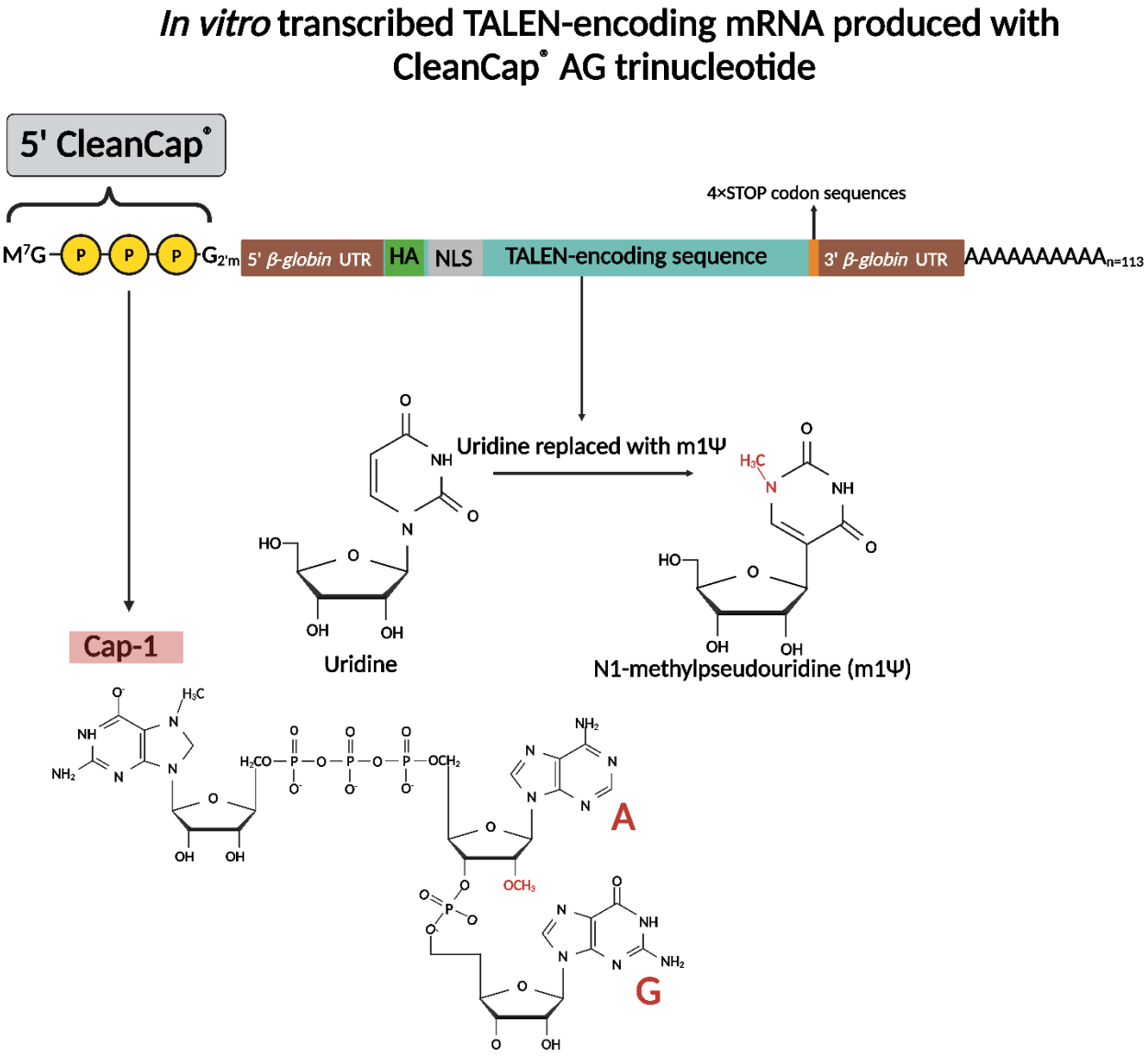


Figure 2.3: TALEN-encoding mRNA with CleanCap® AG and m1Ψ.

TALEN-encoding mRNA was produced from modified DNA templates. CleanCap® AG was incorporated to generate cap-1 transcripts and uridine was replaced with m1Ψ (Figure created with Biorender.com).

Chapter 2

2.2 Methods

2.2.1 Reporter transcripts

2.2.1.1 pT7-eGFP

The pT7-eGFP plasmid was constructed by inserting a sequence encoding eGFP between the 5' and 3' UTRs within a pT7-mRNA-backbone cassette. It was then linearised using *Bpi*I, as explained in section 2.2.2.1.1, to prepare the transcription template. IVT was subsequently performed, detailed in sections 2.2.3.1 to 2.2.3.5, to produce eGFP transcripts. These transcripts were used to evaluate transfection efficiencies and served as a mock control for transcripts IVT #1-4 (see 2.2.3.1-2.2.3.4).

2.2.1.2 pT7-mCherry

The pT7-mCherry plasmid was constructed similarly to pT7-eGFP. A sequence encoding mCherry, a red fluorescent protein (RFP), was integrated between the 5' and 3' UTRs within a pT7-mRNA-backbone-P2A cassette. Subsequent linearisation and IVT reactions are described below (2.2.2.1.1, 2.2.3.1-2.2.3.5). mCherry transcripts similarly to eGFP served dual function to evaluate transfection efficiency as well as serve as a mock control for transcripts IVT #5 (2.2.3.5).

2.2.2 Generation of two distinct plasmid templates for IVT

IVT template design 1 included all necessary elements to produce TALEN transcripts (**see Figure 1.7**). This template contained the obligate heterodimeric sequences targeting the *surface* (*S*) gene of HBV. However, recent research indicates that a single stop codon may be insufficient during *in vitro* production, as modified nucleotides like Ψ can cause transcription to extend into the 3' UTR, resulting in ineffective transcripts (218,219). Template design 2 was developed to address potential

readthrough errors and incorporate additional modifications to enhance translation efficiency. This template contained the obligate heterodimeric sequences targeting the (*S*) and *core* (*C*) genes of HBV. The main distinction between these templates is that the second template included UTRs from the *β-globin* gene, known to improve translation efficiency. It also featured additional stop codons immediately after the *Fok*I sequence and an extended poly(A) tail of 113 bases. Alongside template redesign, various IVT conditions were optimised (see methods below) to ensure the production of functional TALEN-encoding mRNA. Table 2.1 below summarises the key differences between these two template designs.

Table 2.1: Key differences between IVT template designs 1 and 2

	Plasmid nomenclature	**Essential plasmid components described from 5' →3' direction**
IVT Template Design 1	pT7-SL-TALEN pT7-SR-TALEN	○ 5' UTR ○ HA epitope ○ NLS embedded in the surface left (SL) or surface right (SR) TALE ○ Left or right *Fok*I nuclease domain sequence ○ TAA single stop codon ○ 3' UTR ○ poly(A) tract, n=46
IVT Template Design 2	pT7-CL-TALEN-4×STOP pT7-CR-TALEN-4×STOP pT7-SL-TALEN-4×STOP pT7-SR-TALEN-4×STOP	○ 5' UTR from *β-globin* ○ HA epitope ○ NLS embedded in the core left (CL), core right (CR), SL or SR TALE ○ Left or right *Fok*I nuclease domain sequence ○ TGA-TAA-TGA-TAG codons (4×STOP) ○ 3' UTR from *β-globin* ○ poly(A) tract, n=113

2.2.2.1 Construction of TALEN-encoding mRNA expression plasmids- IVT template design 1

The first cloning strategy employed a DNA template comprising a T7 promoter sequence, followed by a GC-rich 5' UTR, the TALEN-encoding sequence, a 3' UTR, and a poly(A) tail. Additionally, an HA tag and NLS were incorporated directly upstream of the TALEN-encoding sequence. Plasmids were constructed to serve as templates for *in vitro* transcription of obligate heterodimeric TALEN sequences targeting the *S* gene of HBV. The sequences encoding the TALENs were excised from previously generated pCMV-SL/SR-TALEN constructs (169). TALEs were derived from the TALE protein *avrBs4* scaffold and the subsequent RVDs are outlined in **Appendix 6.3** (220). The pT7-mRNA-backbone plasmid was employed as the expression vector to generate the final TALEN-encoding mRNA expression plasmids namely pT7-SL-TALEN and pT7-SR-TALEN.

The pCMV-SL/SR-TALEN constructs were subjected to two separate restriction digestions to remove the TALE-encoding (SL or SR) and *Fok*I-encoding (left or right) sequences **(Figure 2.4)**. First, 1 µg of the pCMV-SL/SR-TALEN constructs were digested using *Xba*I and *Bam*HI to remove the TALE-encoding sequence. In a second reaction, 1 µg of the same construct was digested with *Bam*HI and *Apa*I to excise the *Fok*I-encoding sequence. Additionally, 1 µg of the pT7-mRNA-backbone (mRNA expression vector) was digested using *Xba*I and *Apa*I. Each reaction, prepared with appropriate buffers and water according to the manufacturer's protocols (New England Biolabs, NJ, USA), was incubated at 37 °C for two hours.

The digested products were separated on a 1% agarose gel containing 0.3 µg/ml of ethidium bromide (Thermo Fisher Scientific, CA, USA) and visualised using the Omega Fluor™ Gel Documentation System (Aplegen, CA, USA). Bands corresponding to TALE (2346 bp), *Fok*I left

(Q486E and I499A, 601 bp) or right variant (E490K and I538V, 601 bp), and pT7-mRNA-backbone (3737 bp) were excised and purified with the QIAquick Gel Extraction kit following the manufacturer's protocol (Qiagen, Hilden, Germany). Given that the entire TALEN sequence (2947 bp) is close in size to the backbone (3737 bp), a three-way ligation with two inserts was performed to avoid complications during ligation. The purity and concentration of the recovered DNA were assessed using the NanoPhotometer® Spectrophotometer (Implen Inc., CA, USA).

The TALE- and *Fok*I-encoding sequences were used as insert fragments and ligated into the pT7-mRNA-backbone plasmid to generate the final pT7-SL/SR-TALEN expression plasmids, named pT7-SL-TALEN and pT7-SR-TALEN **(Figure 2.4)**. Ligation was performed overnight at 14 °C, following the manufacturer's protocol (Thermo Fisher Scientific, CA, USA).

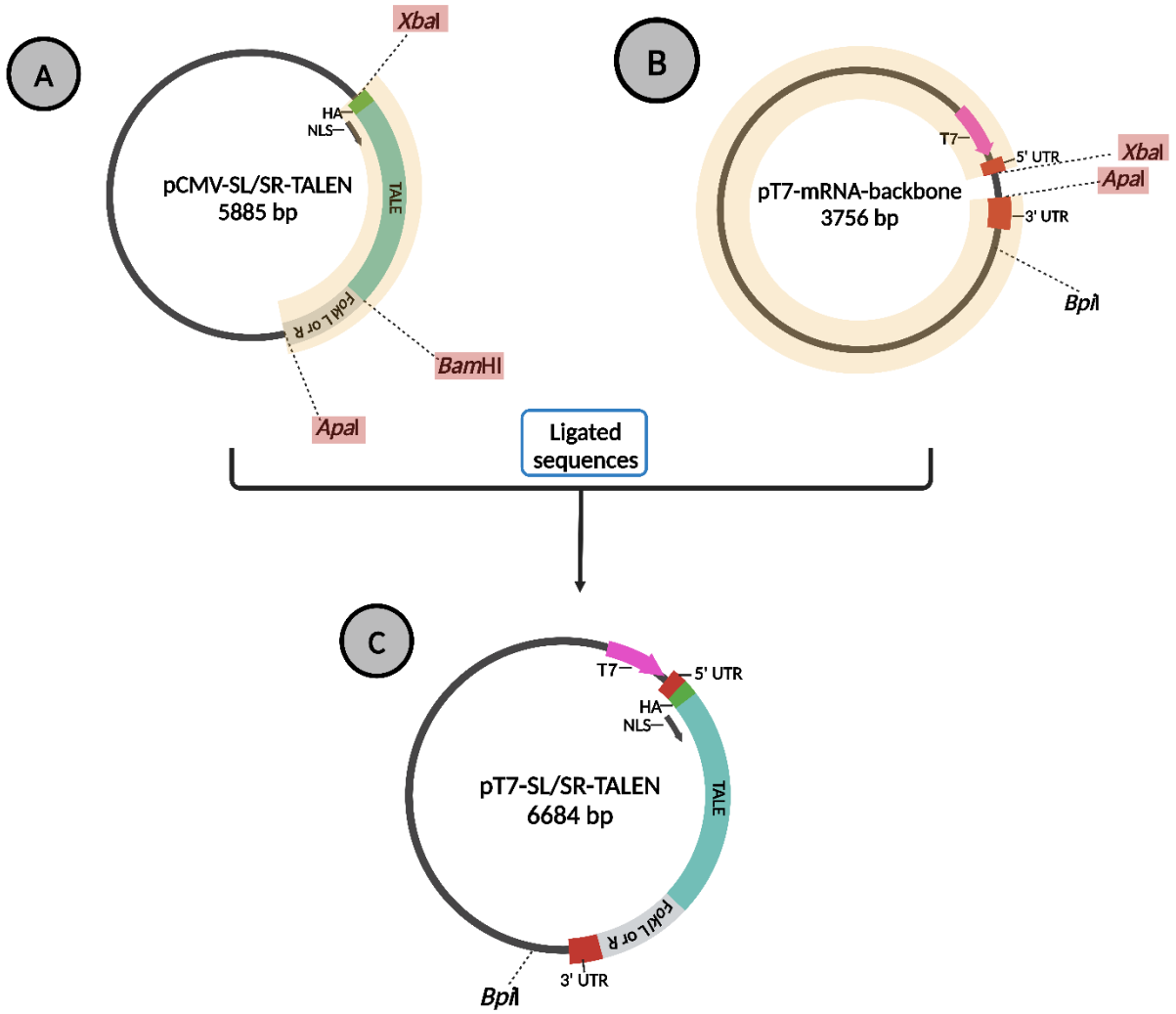


Figure 2.4: Producing TALEN-encoding mRNA plasmids for *in vitro* transcription- IVT template design 1.

A. TALEN mRNA expressing plasmids were generated by cleaving TALEN-encoding plasmids (pCMV-SL/SR-TALEN) using *Xba*I and *Bam*HI to excise the TALE portion (either SL or SR) and *Bam*HI and *Apa*I to excise either the *Fok*I left or right nuclease domain. **B.** pT7-mRNA-backbone contains sequences for T7 bacteriophage promoter, 5' and 3'UTRs and a poly(A) tract. The pT7-mRNA-backbone plasmid was cleaved with *Xba*I and *Apa*I. **C.** The TALE (either for SL or SR) and *Fok*I sequences were inserted into the pT7-mRNA-backbone vector to produce pT7-SL/SR-TALEN plasmids containing the *Bpi*I site (Figure created with Biorender.com).

After ligation, 10 µl aliquots from each ligation reaction were employed to transform 100 µl of XL10-Gold® Ultracompetent *Escherichia coli* (*E. coli*) cells (Agilent Technologies, CA, USA) (**Appendix 6.1.1**). The transformations were incubated on ice for 20 minutes followed by the application of the conventional heat-shock method. The transformed cells were plated on agar containing ampicillin and subsequently incubated overnight at 37 °C. Single colonies were selected from the overnight transformation, cultured in 10 ml of Luria Bertani medium and subsequently, incubated overnight at 37 °C in a shaking incubator. Plasmid DNA extraction and purification were performed using Econospin™ All-in-One Mini Spin Columns (Epoch Life Science, TX, USA) following the manufacturer's protocol.

Clones were screened using *Xba*I and *Apa*I to confirm the successful integration of the TALEN-encoding sequence into the pT7-mRNA-backbone expression vector. Furthermore, screening with *Nae*I was performed to distinguish between the left and right *Fok*I domain sequences. Positive clones were subsequently prepared in bulk using the Qiagen Plasmid Maxi Kit (Qiagen, Hilden, Germany) according to the manufacturer's instructions.

2.2.2.1.1 Linearisation of TALEN-encoding mRNA templates-IVT template design 1

The final pT7-SL-TALEN and pT7-SR-TALEN plasmids contained a type IIS *Bpi*I restriction site located immediately downstream of the poly(A) tract, which is essential for template linearisation. Both plasmids were digested overnight using *Bpi*I to linearise the templates **(Figure 2.5)**. For the digestion, 35 µg of both pT7-SL-TALEN and pT7-SR-TALEN plasmids were mixed with 3 U of *Bpi*I, 20 µl of a 10× rCutSmart Buffer (New England Biolabs, NJ, USA), and water to a final volume of 200 µl. The reactions were then incubated overnight at 37 °C. After overnight linearisation, gel analysis was performed on an aliquot (~1 µl) to confirm complete template linearisation. Subsequently, template DNA was precipitated by adding 0.1 volumes of 3 M sodium acetate (~20 µl) and 2.5 volumes of 100% ethanol (~500 µl) to each reaction. The mixture was then incubated at -20 °C for a minimum of 30 minutes. Following incubation, the DNA was centrifuged at 14,000 ×g at 4 °C in a benchtop centrifuge for 30 minutes. The supernatant was cautiously removed, and the DNA pellet was washed with 1 ml of 70% ethanol. After another centrifugation step, the ethanol was gently removed, and the DNA pellet was suspended in water for storage.

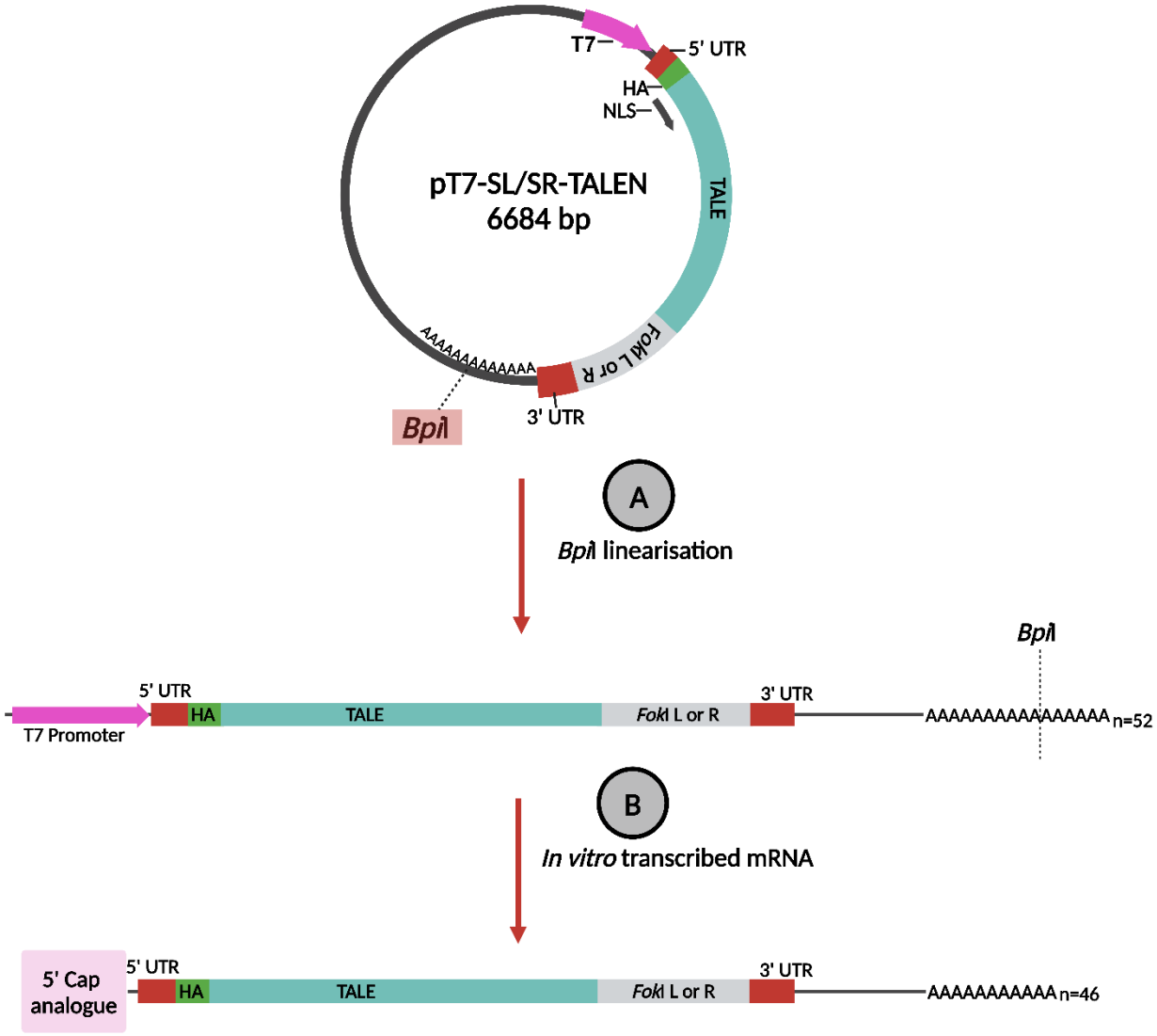


Figure 2.5: Linear templates for IVT of TALEN-encoding mRNA -IVT template design 1.

A. The pT7-SL/SR-TALEN plasmids were linearised with *Bpi*I. **B.** The T7 RNA polymerase initiates transcription at the T7 promoter sequence to produce *in vitro* transcribed mRNA expressing TALENs (Figure created with Biorender.com).

2.2.2.2 Construction of TALEN-encoding mRNA expression plasmids- IVT template design 2

Plasmids were constructed to serve as templates for *in vitro* transcription of obligate heterodimeric TALEN sequences targeting the *C* and *S* genes of HBV. The sequences encoding the TALENs were excised from previously generated pCMV-Left/Right-TALEN constructs (169). To create the final TALEN-encoding mRNA expression plasmids, a modified pT7-mRNA-mod-backbone and pUC57-mini-GenScript (GenScript Biotech, NJ, USA) plasmid were employed.

The pUC57-mini-GenScript included *Esp*3I and *Apa*I sites necessary for downstream sub-cloning of TALEN sequences, additionally, this plasmid also contained repeat stop codon sequences necessary for enhancing transcription. pUC57-mini-GenScript was digested using *Nde*I and *Bsa*I and the pT7-mRNA-mod-backbone was digested with *Nde*I and *Esp*3I. *Bsa*I and *Esp*3I are type IIS restriction enzymes **(Figure 2.6)**. The *Bsa*I site from the pUC57-mini-GenScript and the *Esp*3I site from the pT7-mRNA-mod-backbone were designed to produce compatible overhangs. The sequence from pUC57-mini-GenScript was ligated into pT7-mRNA-mod-backbone to produce the final pT7-mRNA-4×STOP expression vector.

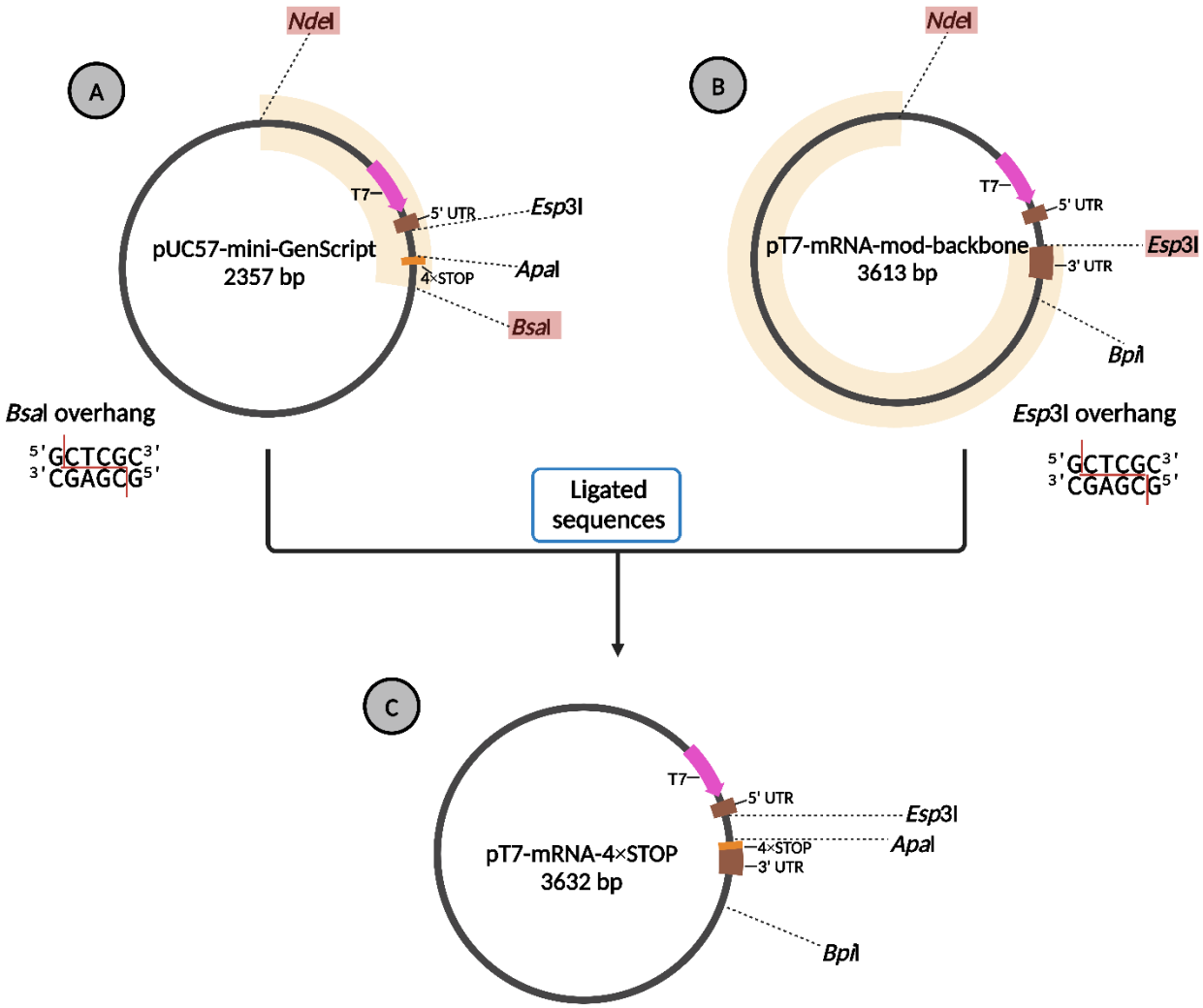


Figure 2.6: Producing modified vector for *in vitro* transcription- IVT template design 2.

A. pUC57-mini-GenScript plasmid contains sequences for T7 bacteriophage promoter, 5' UTR from *β-globin*, 4× stop codon sequences as well as *Esp*3I and *Apa*I recognition sites essential for downstream subcloning. pUC57-mini-GenScript plasmid was digested with *Nde*I and *Bsa*I. **B.** pT7-mRNA-mod-backbone contains the 3'UTR from *β-globin* and a poly(A) tract. The pT7-mRNA-backbone plasmid was cleaved with *Nde*I and *Esp3*I. *Bsa*I and *Esp*3I are type IIS restriction enzymes and in these plasmids are arranged such that digesting the plasmids with these enzymes produces complementary overhangs. **C.** The pUC57-mini-GenScript insert was ligated into the pT7-mRNA-mod-backbone to produce the pT7-mRNA-4×STOP plasmid (Figure created with Biorender.com).

Subsequently, the pCMV-Left/Right-TALEN constructs were digested using *Nco*I and *Xho*I to produce Fragment 1 and *Xho*I and *Apa*I to produce Fragment 2 **(Figure 2.7)**. Since the TALE-encoding sequence contains multiple *Nco*I cleavage sites it was necessary to digest the TALEN construct as two fragments. The pT7-mRNA-4×STOP construct was digested with *Esp*3I and *Apa*I. The *Nco*I site from Fragment 1 and the *Esp3*I site from the pT7-mRNA-4×STOP produce compatible overhangs. All restriction digestions were performed as previously described following the manufacturer's instructions (New England Biolabs, NJ, USA). Therefore, in a three-way ligation, Fragment 1 and Fragment 2 inserts, as well as the pT7-mRNA-4×STOP vector, produced the final 4 pT7-Left/Right-TALEN-4×STOP templates namely, pT7-CL-TALEN-4×STOP, pT7-CR-TALEN-4×STOP, pT7-SL-TALEN-4×STOP, and pT7-SR-TALEN-4×STOP **(Figure 2.7)**.

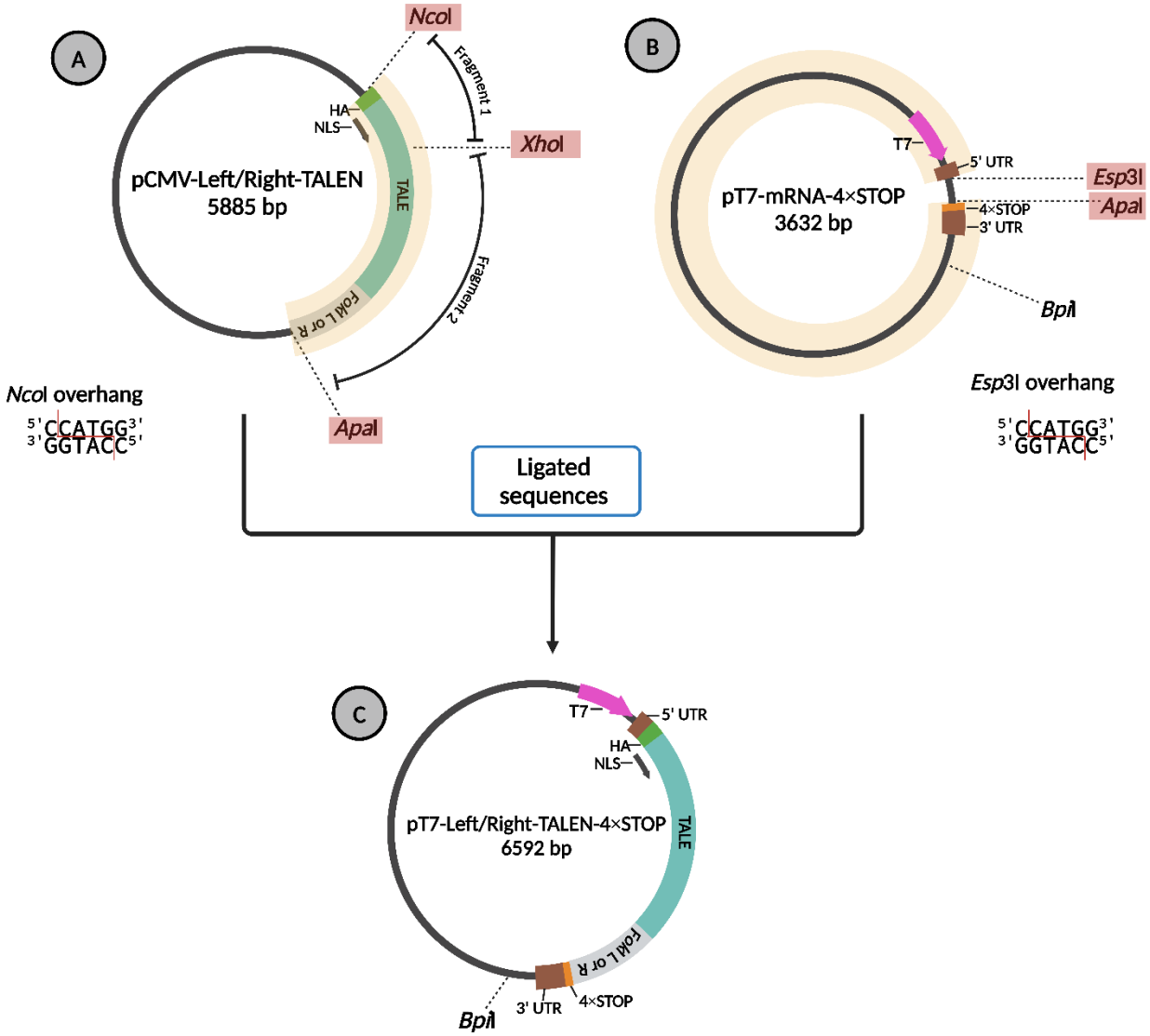


Figure 2.7: Producing TALEN-encoding mRNA plasmids for *in vitro* transcription- IVT template design 2.

A. TALEN mRNA expressing plasmids were generated by cleaving TALEN-encoding plasmids (pCMV-Left/Right-TALEN) using *Nco*I and *Xho*I to excise a portion of TALE sequence (either CL, CR, SL or SR) and *Xho*I and *Apa*I to excise the remaining TALE sequence as well as the *Fok*I left or right nuclease domain. **B.** pT7-mRNA-4×STOP was cleaved with *Esp*3I and *Apa*I**.** *Esp*3I produces overhangs compatible with *Nco*I. **C.** The TALE and *Fok*I sequences were inserted into the pT7-mRNA-4×STOP vector to produce pT7-Left/Right-TALEN-4×STOP containing a *Bpi*I site (Figure created with Biorender.com).

Positive clones were prepared as described in 2.2.2.1 and were subjected to Sanger (automated capillary) sequencing on the ABI 3500XL Sequencer (Inqaba Biotech, PTA, South Africa) to validate TALE and *Fok*I sequence fidelity (**Appendix 6.5-6.6**). Linearisation was carried out as previously described 2.2.2.1.1 **(Figure 2.8)**.

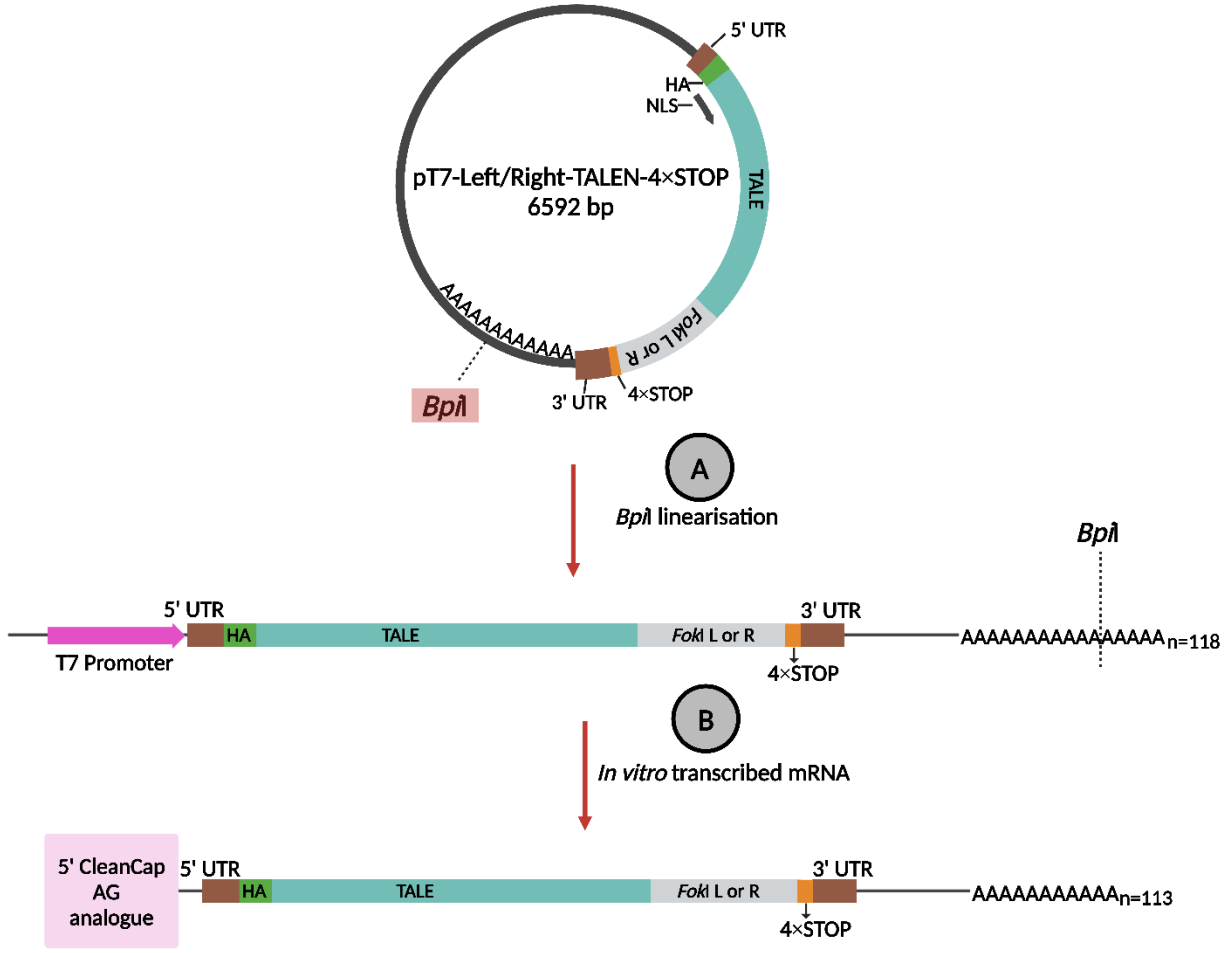


Figure 2.8: Linear templates for IVT of TALEN-encoding mRNA - IVT template design 2.

A. The pT7-Left/Right-TALEN-4×STOP plasmids were linearised with *Bpi*I. **B.** The T7 RNA polymerase initiates transcription at the T7 promoter sequence to produce *in vitro* transcribed mRNA expressing TALENs. The patented CleanCap® AG is also included in the reaction (Figure created with Biorender.com).

2.2.3 *In vitro* transcription of TALEN-encoding mRNA

Different IVT reactions can be used to generate either cap-0 or cap-1 transcripts. In this investigation, three distinct reactions were employed, using templates derived from IVT template design 1 and 2, to synthesise anti-HBV TALEN transcripts. The first IVT reaction incorporated ARCA to yield cap-0 transcripts. The inclusion of ARCA in TALEN transcripts aimed to impede the reverse 5' capping process, ensuring transcripts proficient in translation. Subsequently, the second IVT reaction involved the integration of VCE to produce cap-1 transcripts, thereby mitigating immune responses, particularly crucial for *in vivo* applications. Furthermore, Ψ was incorporated to closely resemble endogenous RNA and attenuate immunostimulation. Finally, cap-1 transcripts were generated using CleanCap® AG and m1Ψ, offering simplified incorporation of 2′-O-methyltransferase (2'O MTase) while maintaining high IVT efficiency, with up to 99% of the template converted into transcripts. The assorted transcripts were evaluated to assess TALEN expression in cell culture.

2.2.3.1 IVT#1: Synthesis of anti-HBV TALEN transcripts using ARCA

To synthesise mRNA transcripts resembling endogenous eukaryotic mRNA, linearised templates from design 1 underwent IVT through a co-transcriptional capping mechanism. The mMESSAGE mMACHINE™ T7 Transcription Kit (Invitrogen, CA, USA) facilitated this process. The addition of an anti-reverse cap analogue (ARCA) during the reaction produced transcripts with an mRNA-like cap at their 5' end.

In a summarised procedure, 5 µg of linearised template DNA was combined with 6 mM each of ATP, CTP and UTP, 1.2 mM of GTP and 4.8 mM of ARCA, 10 µl of 10× reaction buffer, 2 U of T7 enzyme, and nuclease-free water to reach a total volume of 100 µl. This mixture was then

incubated for 2 hours at 37 °C. Following transcription, the RNA was treated with 2 U of DNase I (New England Biolabs, NJ, USA) and 10 µl of 10× DNase I reaction buffer (New England Biolabs, NJ, USA) was added to the reaction to eliminate plasmid DNA, with further incubation at 37°C for 15 minutes. The resulting RNA products were termed SL TALEN and SR TALEN.

To recover the RNA, lithium chloride (LiCl) precipitation was employed. For this step, 50 µl of 7.5 M LiCl (1 mM EDTA, pH 8.0) was added to each reaction, mixed carefully, and then incubated at -20 °C for a minimum of 30 minutes. Subsequently, the RNA was collected by centrifugation at 14,000 ×g for 15 minutes at 4 °C. Following the removal of the supernatant, the pellet was subjected to washing with 1 ml of 70% ethanol to ensure the removal of any remaining unincorporated nucleotides and centrifuged again. The 70% ethanol was carefully decanted, and the RNA was dissolved in nuclease-free water. Lastly, RNA concentration and purity were measured using spectrophotometry, while RNA integrity was assessed using a 1% denaturing formaldehyde gel (**Appendix 6.1.2**).

2.2.3.2 IVT#2: Post-transcriptional capping of in vitro transcribed TALEN transcripts using VCE

First, linearised templates from design 1 were *in vitro* transcribed, followed by post-transcriptional capping. IVT was performed using the TranscriptAid T7 High Yield Transcription Kit (Invitrogen, CA, USA), designed for large-scale RNA synthesis. A mixture of 4 µl of 5× TranscriptAid Reaction Buffer, 1 mM rNTP mix (ATP, CTP, GTP), 1mM of pseudouridine-5'-Triphosphate (Ψ) (TriLink Biotechnologies CA, USA), 1 µg of template DNA, and 2 U of TranscriptAid Enzyme Mix was prepared, reaching a final volume of 20 µl with nuclease-free water. The transcription mix was incubated at 37 °C for 2 hours. Subsequently, RNA was treated with DNase I and recovered using LiCl precipitation as previously described.

To cap the transcripts, the One-Step Cap-1 mRNA synthesis kit, employing VCE and mRNA Cap 2'O MTase enzyme (New England Biolabs, NJ, USA), was used. Ten micrograms of uncapped RNA and nuclease-free water were prepared to a total volume of 14 µl. The RNA was heated at 65° C for 5 minutes and then cooled for 5 minutes on ice. Briefly, 10 U of The VCE together with 4 mM of S-adenosyl methionine (SAM), 10 mM of GTP, 50 U of 2'O MTase and 2 µl of 10× capping buffer was mixed with heat-denatured RNA. The VCE added the m^7G cap structure to the 5' end of the transcript, while the 2'O MTase added a methyl group to the 2'O ribose of the first nucleotide, producing a cap-1 structure.

Capped mRNA transcripts were recovered again following precipitation with LiCl as previously described. Spectrophotometry was used to determine purity and concentration of RNA and 1% denaturing formaldehyde gel was used to assess integrity of the RNA.

2.2.3.3 IVT #3: Post-transcriptional capping of in vitro transcribed TALEN transcripts using VCE and cellulose purification

After IVT using the TranscriptAid T7 High Yield Transcription Kit, transcripts underwent cellulose purification before capping. The cellulose purification procedure was carried out by initially mixing 0.2 g of cellulose with 1 ml of chromatography buffer (**Appendix 6.1.4**). This mixture was then incubated at room temperature while shaking vigorously for 10 minutes. Next, 700 µl of the cellulose slurry was transferred to an ultrafiltration Spin-Column with a 0.45 µM cut-off (Merck, DA, Germany) and centrifuged for one minute at 14,000 × g. The resulting eluate was removed, and the column underwent a washing step with 500 µl of chromatography buffer. After a 5 minute incubation at room temperature with vigorous shaking, the column was once again centrifuged for one minute at 14,000 × g, and the eluate was discarded.

Next, RNA (up to 150 µg) was mixed with 500 µl of chromatography buffer in the column, and the mixture was incubated at room temperature with vigorous shaking for 30 minutes. Following centrifugation, the eluate was transferred to a fresh column preloaded with cellulose and incubated for 30 minutes as previously described. The mixture was then centrifuged for one minute at 14,000 × g. RNA recovery involved adding an equal volume of 2.5M LiCl to the RNA-chromatography buffer mixture, followed by incubation at -20 °C for an hour or ideally overnight, to maximise yields. The RNA pellet was then reconstituted in nuclease-free water following a 30-minute centrifugation at 14,000 × g at a temperature of 4°C.

Following cellulose purification, transcripts were capped as described in 2.2.3.2 and subjected to LiCl precipitation once more as previously described. The purity and concentration of the RNA were also assessed as previously described.

2.2.3.4 IV# 4: Co-transcriptional capping of in vitro transcribed TALEN transcripts using CleanCap®AG and cellulose purification

Given the rising efficiency of CleanCap®AG for single-reaction Cap-1 mRNA production, linearised templates from design 1 were *in vitro* transcribed through a co-transcriptional mechanism. The reaction consisted of 10 µl of a 10× Transcription Buffer, 5 mM of NTP mix (New England Biolabs, NJ, USA) containing ATP, CTP, and GTP, 5 mM of Ψ, 5 µg of template DNA, 4 mM of CleanCap® AG, 0.8 U of T7 RNA high concentration (New England Biolabs, NJ, USA), 1 U of Murine RNAse inhibitor (New England Biolabs, NJ, USA), and 0.002 U of inorganic pyrophosphate (New England Biolabs, NJ, USA), adjusted to a total volume of 100 µl with nuclease-free water. The mixture was incubated at 37 °C for 2 hours.

Subsequently, the RNA was treated with DNase I and recovered using LiCl precipitation as previously described. The transcripts underwent cellulose purification as detailed earlier. The purity and concentration of the RNA were determined as previously described.

2.2.3.5 IVT #5: Co-transcriptional capping of in vitro transcribed TALEN transcripts using CleanCap®AG and cellulose purification- IVT template design 2

The templates from design 2 were utilised for the IVT reaction, following the protocol of IVT# 4 with the substitution of Ψ for 5 mM of m1Ψ. The final RNA products were termed CL TALEN, CR TALEN, SL TALEN and SR TALEN. The subsequent LiCl and cellulose purification steps were conducted as previously described. The purity and concentration of the RNA were assessed as mentioned above.

2.2.4 Immunocytochemistry for HA detection in TALEN-transfected cells

Human hepatoma 7 (Huh7) cells were maintained according to standard procedures (**Appendix 6.2.1**). Huh7 cells were seeded in a 48-well plate at a 70% confluency in 225 µl of medium per well one day before transfection. Transfections were carried out using Lipofectamine™ MessengerMAX™ Transfection Reagent (Invitrogen, CA, USA) following the manufacturer's instructions. Five hundred nanograms of each of the SL, SR TALEN transcripts (IVT#1-4), or CL, CR, SL and SR TALEN transcripts (IVT#5) were added to individual wells. Additionally, in separate wells, 500 ng of eGFP-mRNA (IVT #1-4) or mCherry-mRNA (IVT #5), were added to cells. mCherry was used as an additional control for the final set of transcripts (IVT #5) since the fluorescein isothiocyanate (FITC) filter detects both GFP and HA tag, while mCherry is not detected by the FITC filter, making it an effective negative control. Transfection reactions were performed in experimental triplicates and expression was assessed by immunofluorescence 6 hours

after transfection. Fluorescence was observed using the EVOS® XL Cell Imaging System (Invitrogen, MA, USA) to assess GFP or mCherry expression. After confirming expression, the culture medium was aspirated, and cells were rinsed with 200 µl of 1× phosphate buffered saline (PBS, Thermo Fisher Scientific, CA, USA). Cells were then fixed with 200 µl of pre-chilled methanol at room temperature for 15 minutes. All incubation steps were conducted at room temperature, and PBS washes were included between steps.

Following fixation, cells were treated with 200 µl of 0.1% Triton X (Sigma-Aldrich, MO, USA) for 10 minutes to permeabilise the cells. Triton X was aspirated, and cells were rinsed twice with PBS. Cells were treated with 100 µl of 1% bovine serum albumin (BSA) for blocking (Roche Applied Science, Mannheim, Germany) and placed in a humidity chamber for one hour to prevent drying.

The blocking solution was aspirated, and cells were exposed to 30 µl of mouse anti-HA primary antibody (diluted 1:200 in 1% BSA) for one hour in a humidity chamber. Afterwards, cells were washed twice then treated with 30 µl of goat anti-mouse Alexa Fluor 488 secondary antibody (diluted 1:200 in 1% BSA) for 40 minutes in a humidity chamber. Following two additional washes, cells were stained with 50 µl of 1× 4,6-diamidino-2-phenylindole chloride (DAPI) for 5 minutes. A final wash step was conducted before capturing images of the cells using fluorescence microscopy.

2.3 Results

2.3.1 Engineering TALEN-encoding mRNA with modified cap-0 and cap-1 structures – IVT template design 1

2.3.1.1 Generation of obligate heterodimeric *surface*-targeting TALEN templates

The sequences encoding the obligate heterodimeric TALENs targeted against the *S* ORF of HBV were excised from previously generated pCMV-SL/SR-TALEN plasmids to clone into the pT7-mRNA-backbone expression vector. This vector includes all essential components for downstream IVT: a T7 promoter at the 5' end, followed by TALEN-encoded sequences flanked by a GC-rich 5' UTR and 3' UTR, ending with a poly(A) sequence. The TALEN sequences include the DBDs specifically designed to target the *S* ORF of HBV and left or right *Fok*I nuclease domains for obligate heterodimeric cleavage. Additionally, an HA-encoding sequence and NLS were incorporated at the N terminus of the TALE sequence, which are crucial for detecting protein expression and localising the TALENs to the nucleus for effective targeting.

Initially the complete mRNA-expression templates, namely pT7-SL-TALEN and pT7-SR-TALEN, were digested with *Xba*I and *Apa*I which produced bands at 3737 bp and 2947 bp respectively therefore confirming the entire TALEN-encoding sequence was cloned into the expression vector (**Figure 2.9**). Furthermore, the DNA templates were digested with *Nae*I to selectively distinguish the left and right *Fok*I sequences (**Figure 2.10**). *Nae*I cleaved the left domain sequence once and the right domain sequence twice, producing bands at 4173 and 2511 bp.

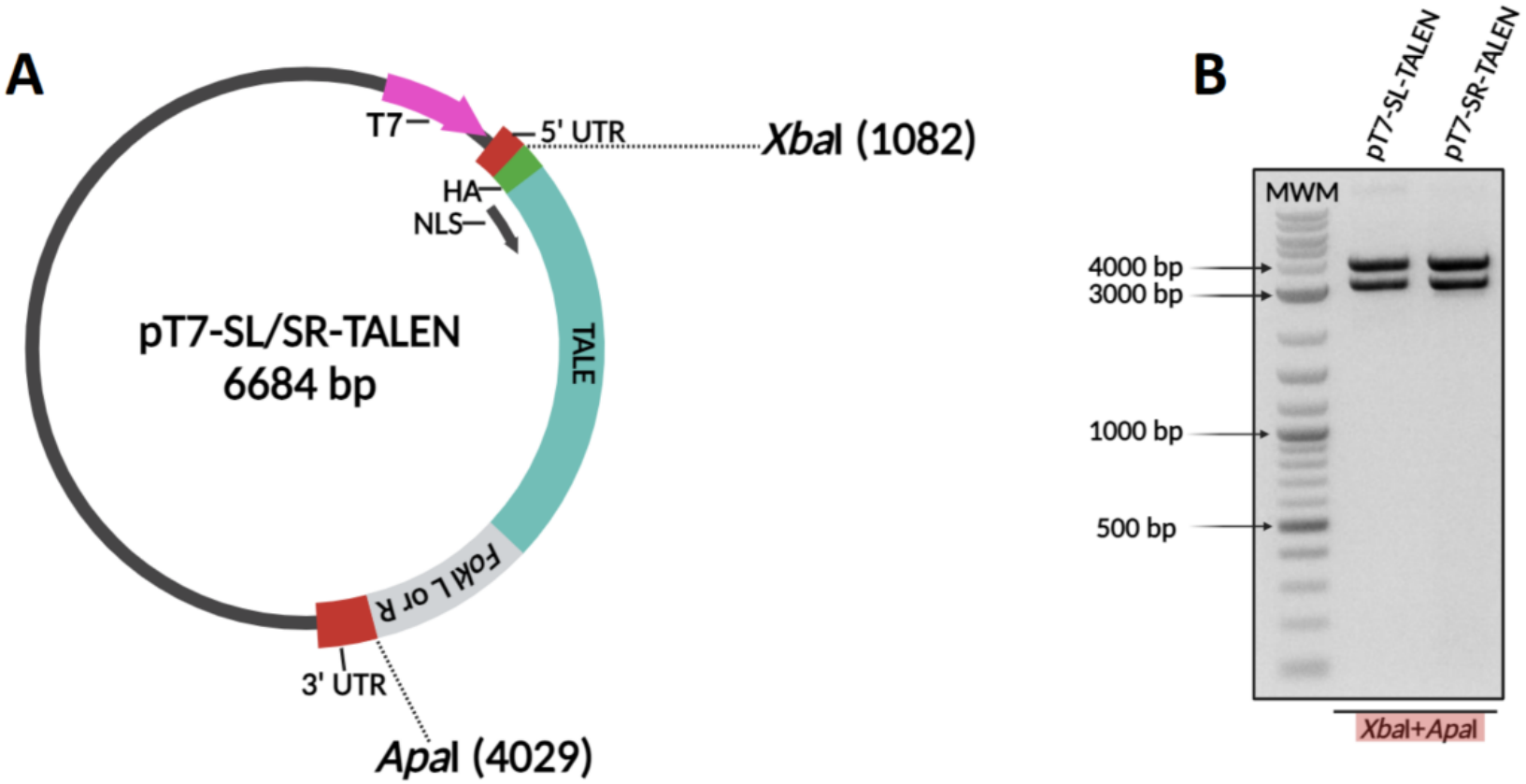
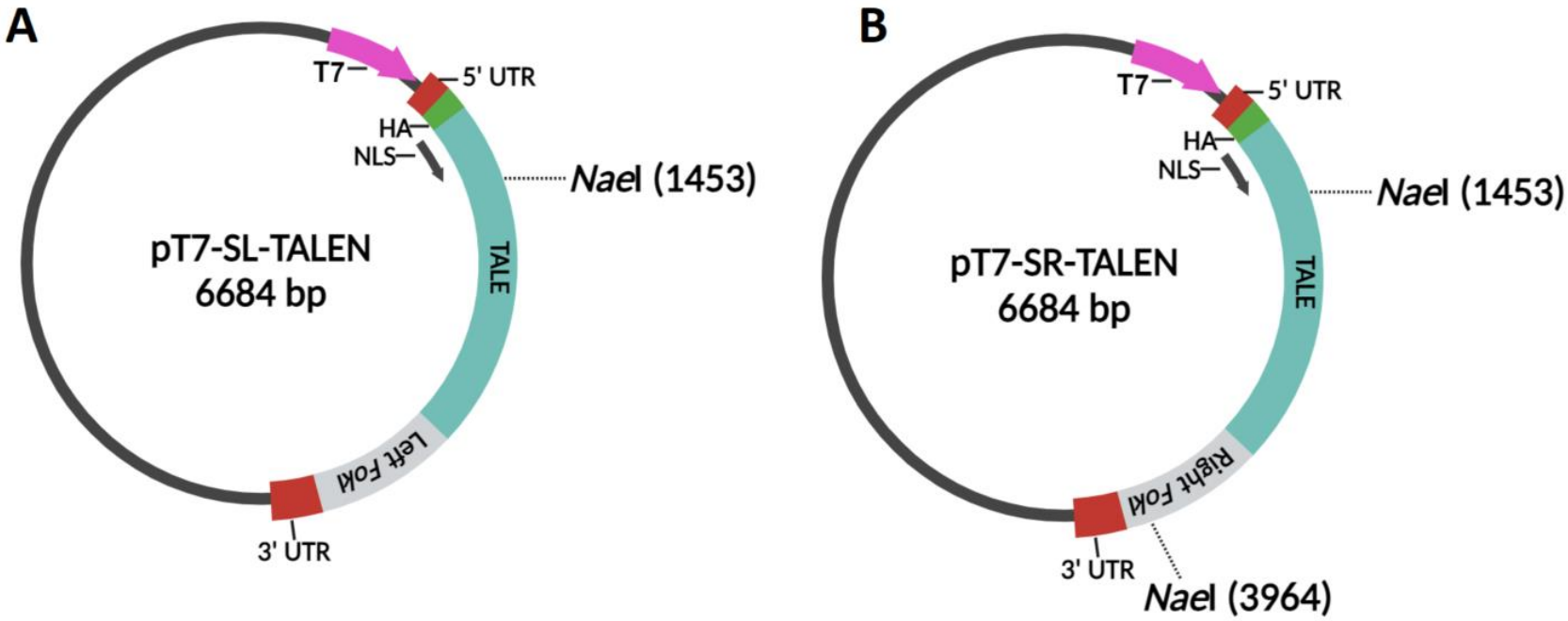


Figure 2.9: Confirmation of pT7-SL/SR-TALEN plasmids.

pT7-SL-TALEN and pT7-SR-TALEN plasmids were produced by inserting previously described TALEN sequences from pCMV-SL/SR-TALEN plasmids into the pT7-mRNA-backbone. **A.** The final pT7-SL/SR-TALEN plasmid map with the selected restriction digest enzymes is depicted. **B.** Agarose gel electrophoresis reveals migration banding patterns for pT7-SL-TALEN and pT7-SR-TALEN with *Xba*I and *Apa*I digesting templates to produce bands at approximately 3737 bp and 2947 bp. (MWM: molecular weight marker, 1 kb Plus DNA Ladder, New England Biolabs, NJ, USA).


A
T7
5' UTR
HA
NLS
NaeI (1453)
pT7-SL-TALEN
6684 bp
TALE
Left FokI
3' UTR
B
T7
5' UTR
HA
NLS
NaeI (1453)
pT7-SR-TALEN
6684 bp
TALE
Right FokI
3' UTR
NaeI (3964)

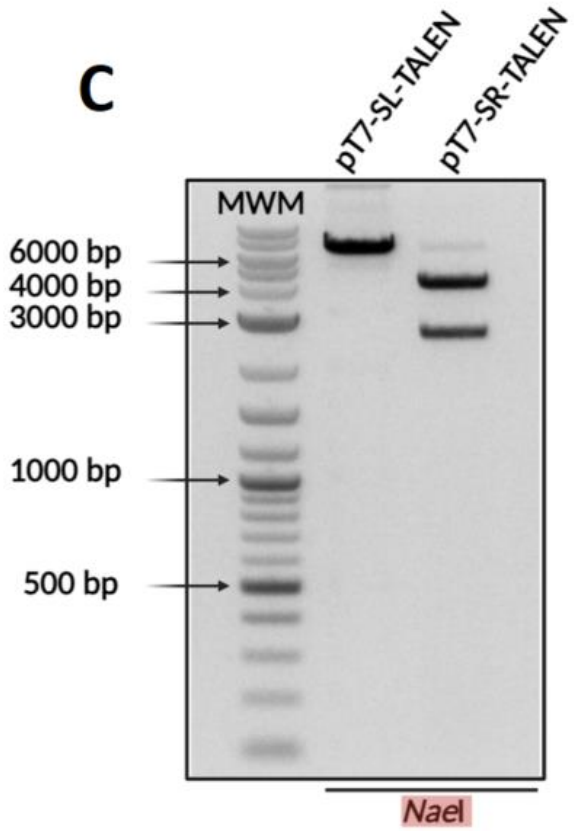


Figure 2.10: Confirmation of left and right *Fok*I domain nucleases in pT7-SL/SR-TALEN plasmids.

To distinguish between left and right nuclease domain sequences of the pT7-SL-TALEN and pT7-SR-TALEN plasmids, *Nae*I restriction digestion was performed. **A.** pT7-SL-TALEN plasmid map with selected *Nae*I restriction site is depicted for the left domain sequence while **B.** pT7-SR-TALEN plasmid map with selected *Nae*I restriction site is depicted for the right domain sequence. **C.** Agarose gel electrophoresis reveals migration banding patterns with *Nae*I digestion producing a single band for pT7-SL-TALEN and two bands at 4173 bp and 2511 bp for pT7-SR-TALEN. (MWM: molecular weight marker, 1 kb Plus DNA Ladder, New England Biolabs, NJ, USA).

2.3.1.2 Successful template linearisation and *in vitro* transcription of ARCA cap-0 anti-HBV transcripts

Each template contained the type IIS *Bpi*I restriction enzyme within the poly(A) tail which yielded complete digestion of all plasmid DNA (**Figure 2.11**). The linearised templates were subsequently *in vitro* transcribed and co-transcriptionally capped with ARCA cap-0 to produce homogeneous intact RNA (SL and SR TALENs) at approximately 3198 bases (IVT#1) **(Figure 2.12)**.

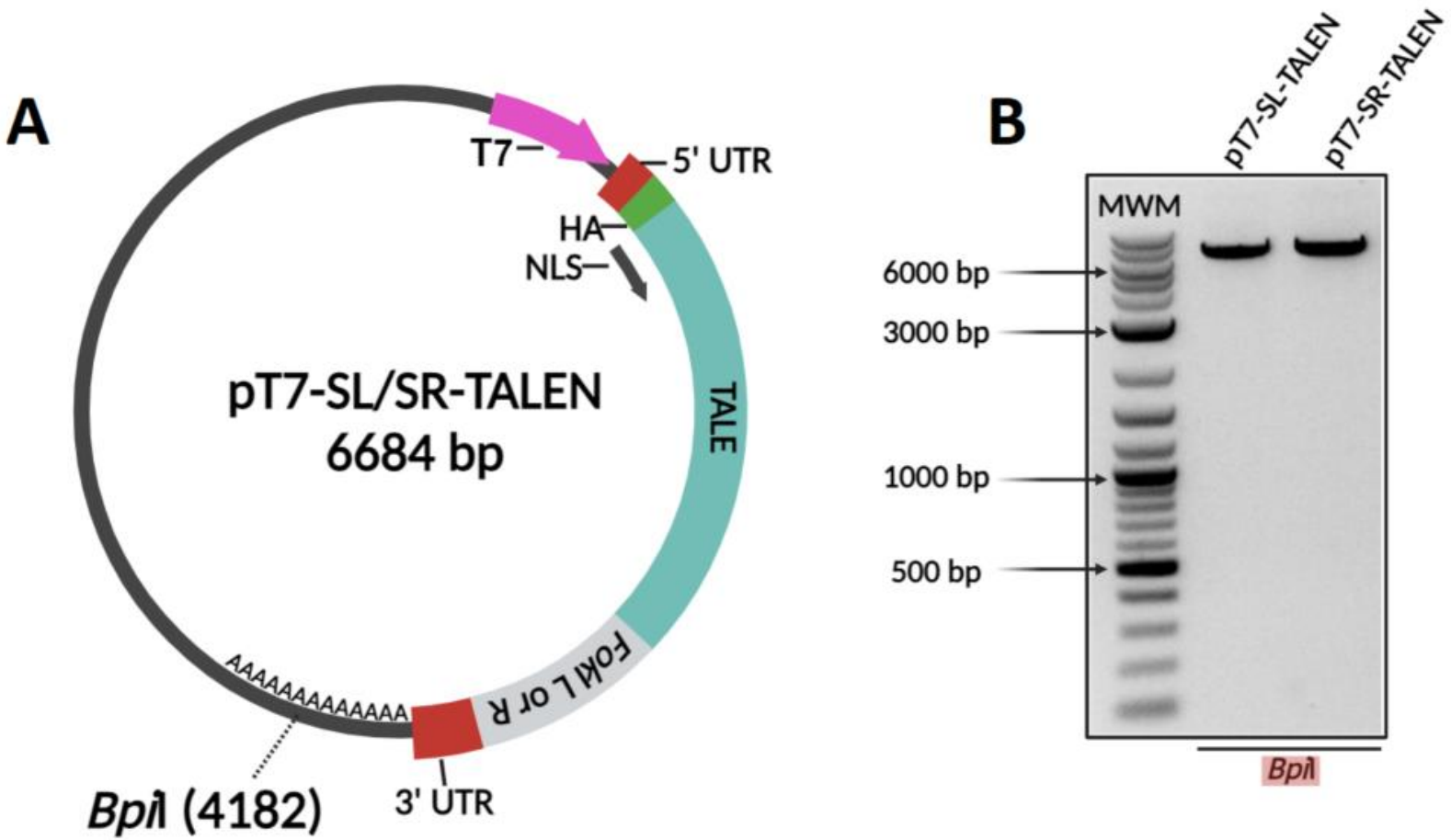


Figure 2.11: Linearised pT7-SL/SR-TALEN templates.

pT7-SL-TALEN and pT7-SR-TALEN were linearised with *Bpi*I, yielding crisp linear bands. **A.** pT7-SL/SR-TALEN plasmid map with the selected *Bpi*I restriction site located within the poly(A) sequence is depicted. **B.** Agarose gel electrophoresis validated the linearisation process (MWM: molecular weight marker, 1 kb Plus DNA Ladder, New England Biolabs, NJ, USA).

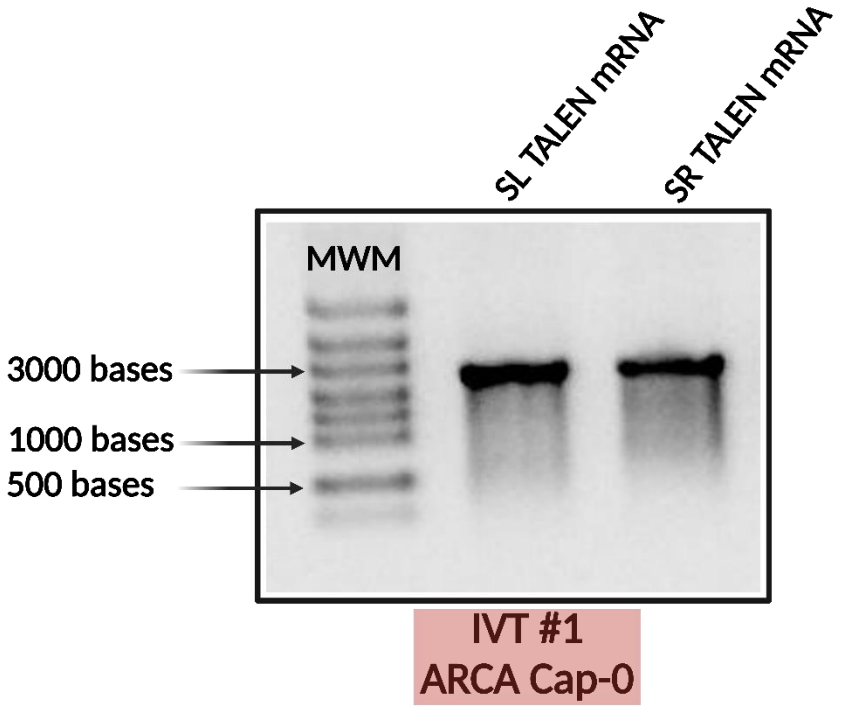


Figure 2.12: Confirmation of *in vitro* transcribed SL/SR TALEN transcripts with ARCA cap-0.

The pT7-SL/SR-TALEN linearised templates were *in vitro* transcribed co-transcriptionally with ARCA cap-0 to produce SL and SR TALEN mRNA. mRNA was resolved on 1% formaldehyde gel. Both transcripts resolved around the predicted 3198 bases. (MWM: molecular weight marker, RiboRuler high range RNA ladder, Thermo Fisher Scientific, CA, USA).

2.3.1.3 Lack of protein expression from ARCA cap-0 transcripts

The TALEN mRNA sequences include an HA epitope in the N-terminal, allowing for their detection in cultured cells. To verify TALEN expression in hepatocyte-derived Huh7 cells from clone 1 experiments, transient transfections were performed using SL or SR TALEN transcripts. GFP transfections were included to assess transfection efficiency, while untransfected cells served as a negative control. Although the GFP protein was expressed well, unexpectedly TALENs did not express in cell culture as expression was comparable to untransfected control (**Figure 2.13**).

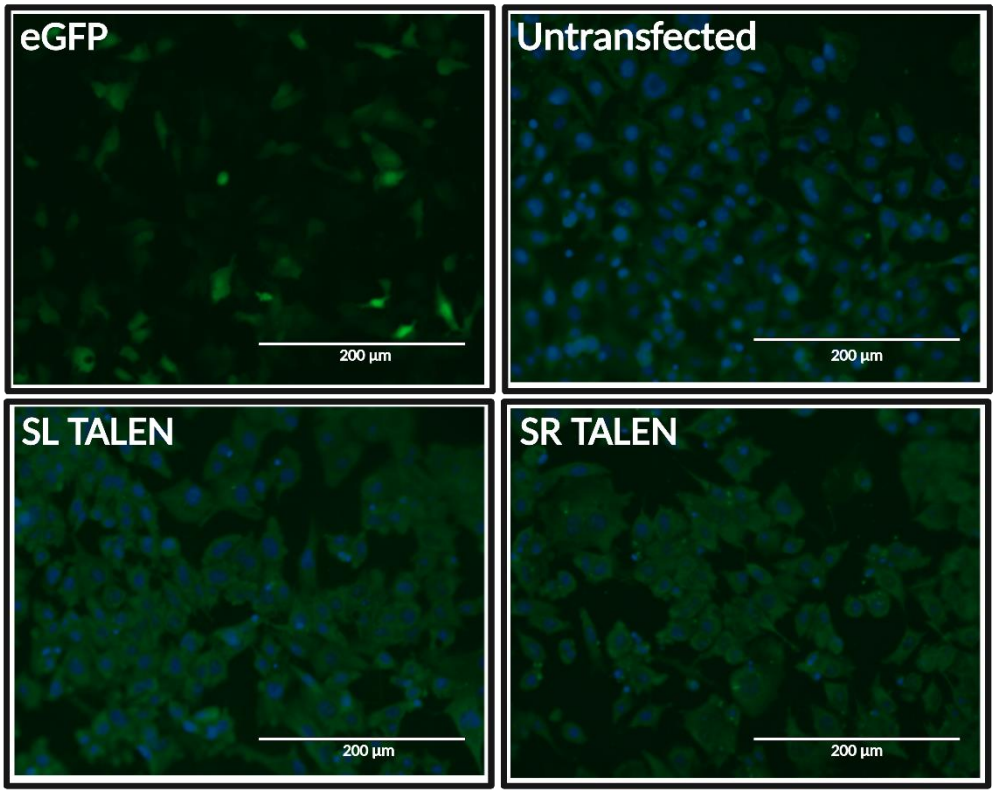


Figure 2.13: Absence of TALEN expression from cap-0 transcripts in Huh7 cells.

Huh7 cells were transiently transfected with SL or SR TALEN transcripts to assess TALEN expression in cultured cells. GFP served as a transfection marker, while untransfected cells acted as the negative control. Immunofluorescence was visualised using microscopy. Cell nuclei were counterstained with DAPI, and images were captured at 20× magnification.

2.3.1.4 *In vitro* transcription of cap-1 anti-HBV transcripts

Given the negative results from ARCA cap-0 transcripts and literature insights, optimised IVT protocols were performed using linearised templates to achieve protein expression in cell culture. Initially, TALEN templates were *in vitro* transcribed, and VCEs were used to generate cap-1 TALEN transcripts, which were further purified by cellulose chromatography. Additionally, templates were *in vitro* transcribed with CleanCap® AG, enabling simultaneous transcription and cap-1 formation. All transcripts were observed at the expected 3198 bases (IVT#2-4) (**Figure 2.14**).

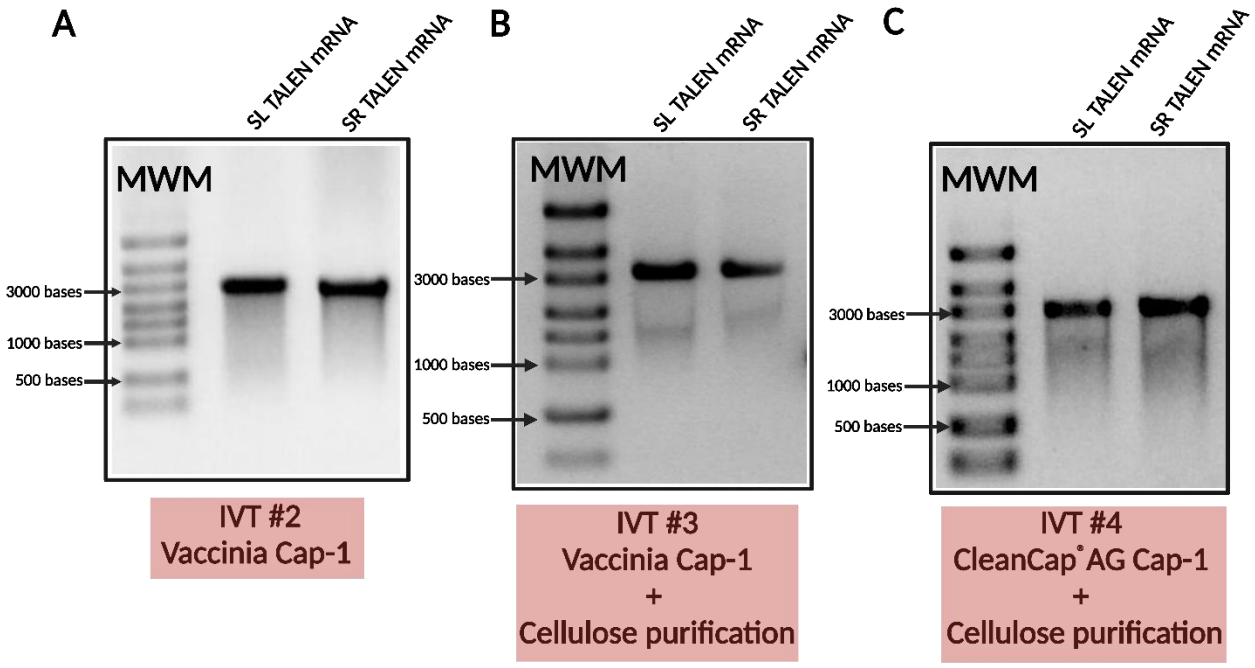


Figure 2.14: Confirmation of *in vitro* transcribed SL/SR TALEN cap-1 transcripts.

In vitro transcription was carried out on the pT7-SL/SR-TALEN linearised templates. **A.** Linearised templates were *in vitro* transcribed and post-transcriptionally capped with vaccinia enzymes to produce cap-1 SL/SR TALEN mRNA. **B.** SL and SR TALEN mRNA produced by VCEs were cellulose purified. **C.** Linearised templates were *in vitro* transcribed and co-transcriptionally capped with CleanCap® AG to produce cap-1 transcripts. mRNA was resolved on 1% formaldehyde gel. All transcripts resolved around the predicted 3198 bases. (MWM: molecular weight marker, RiboRuler high range RNA ladder, Thermo Fisher Scientific, CA, USA).

2.3.1.5 Enhanced TALEN expression in liver-derived cells through cellulose purification

Cap-1 transcripts, like ARCA cap-0 transcripts, were transiently transfected into Huh 7 cells. GFP transfections were included to assess transfection efficiency, with untransfected cells serving as a negative control (**Figures 2.15-2.17**). GFP expression was successfully detected regardless of whether VCEs or CleanCap® AG was used to produce cap-1 transcripts. However, TALEN expression was not observed in VCE-produced transcripts, as they were comparable to the untransfected control (**Figure 2.15**). A potential reason for the lack of TALEN detection could be dsRNA contamination, which may impede translation and stimulate innate immunity. Run-off transcription at the 3′ end of the DNA template can lead to prolonged RNA extension, forming "loop back RNA" or "backward transcribed" RNA which can result in undesired protein products (221,222). Immunogenic dsRNA is an undesired byproduct that is challenging to reduce.

Guy et al. developed a simple method to eliminate dsRNA contaminants using cellulose purification (217). This method was applied to the same vaccinia-produced transcripts, and for the first time, TALEN expression was detected with distinct nuclear localisation (**Figure 2.16**). This indicated that the transcripts were successfully translated in the cytoplasm and transported to the nucleus for their intended purpose. Notably, TALEN expression was even more impressive from CleanCap® AG produced cap-1 transcripts after cellulose purification (**Figure 2.17**).

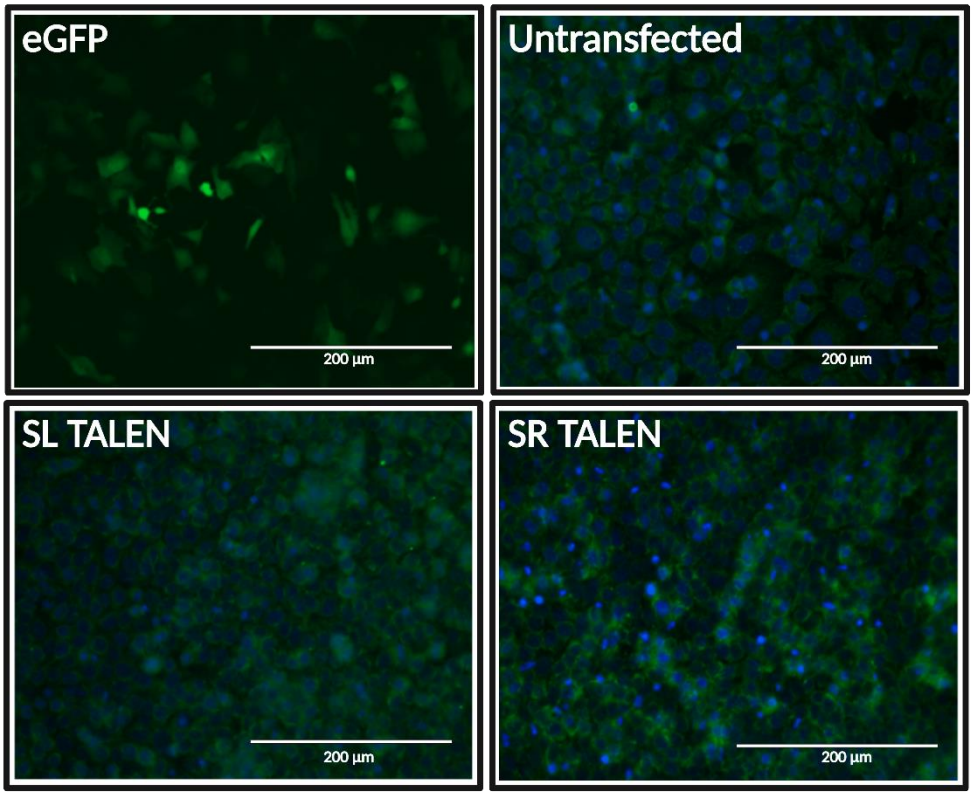


Figure 2.15: Absence of TALEN expression from cap-1 transcripts produced with VCE in Huh7 cells.

Huh7 cells were transiently transfected with SL or SR TALEN monomers produced with VCE to evaluate TALEN expression in cultured cells. GFP was used as a transfection indicator, with untransfected cells serving as the control group. Cell nuclei were stained with DAPI, and images were taken at 20× magnification.

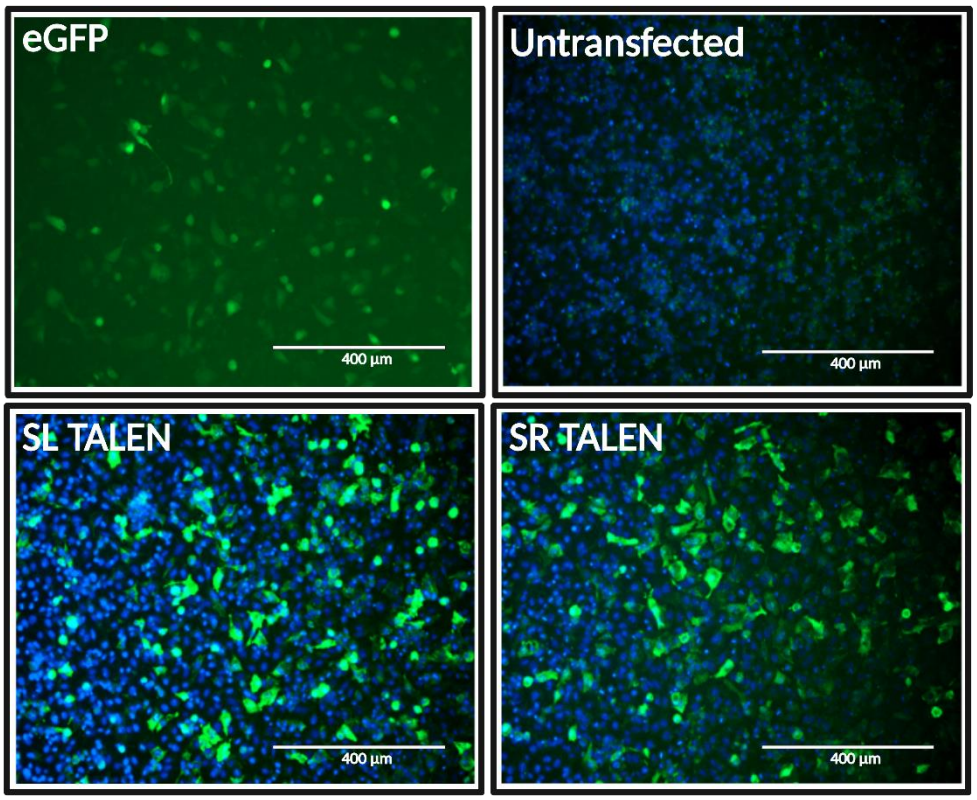


Figure 2.16: Detecting TALEN expression from cellulose-treated cap-1 transcripts using VCE in Huh7 cells.

Huh7 cells were transiently transfected with SL or SR TALEN monomers produced with VCE and further treated with cellulose purification in culture. Efficient GFP expression was detected. Immunofluorescence was detected using microscopy. An anti-HA primary antibody followed by fluorescently labelled secondary antibody was used to detect the HA epitope. The nuclei were stained with DAPI and cells were imaged at 10× magnification.

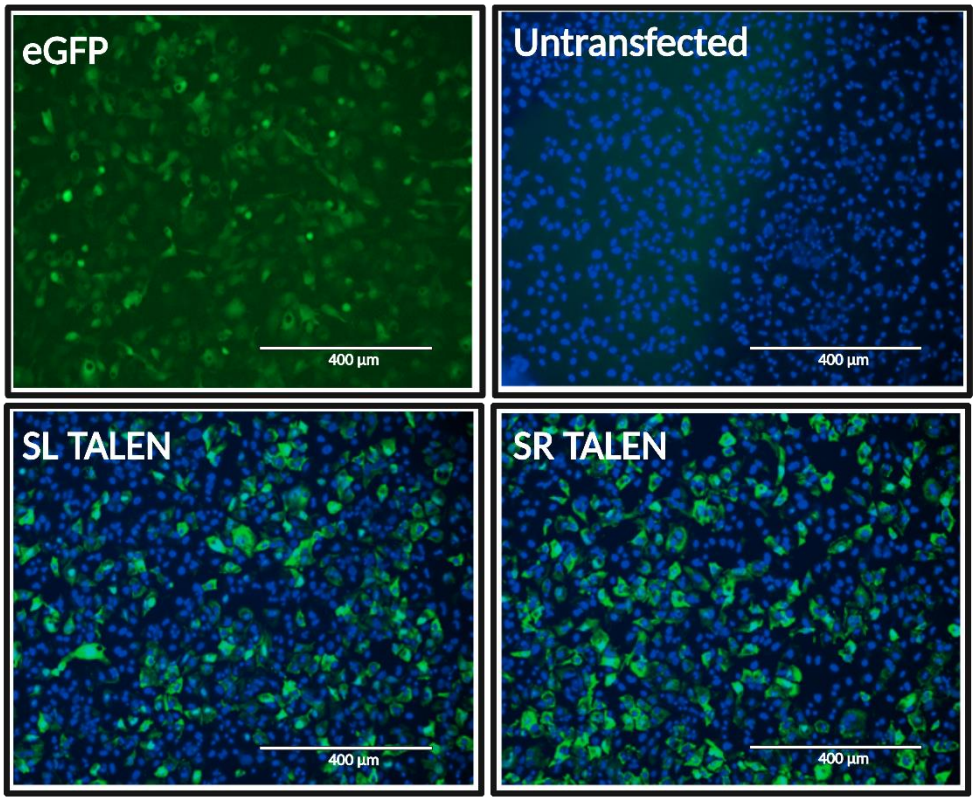


Figure 2.17: Detecting TALEN expression from cellulose-treated cap-1 transcripts using CleanCap® AG in Huh 7 cells.

Huh7 cells were transiently transfected with SL or SR Surface TALEN monomers produced with CleanCap® AG and further treated with cellulose purification. GFP expression was robust, with untransfected cells serving as the control. Enhanced immunodetection of the HA epitope was observed in TALEN treated wells. Immunofluorescence was visualised under microscopy. Cell nuclei were counterstained with DAPI, and images were captured at 10× magnification.

2.3.2 Engineering TALEN-encoding mRNA with modified cap-1 structures- IVT template design 2

2.3.2.1 Generation of modified obligate heterodimeric *core*-and-*surface*-targeting TALEN templates

Sequences encoding heterodimeric TALENs targeting the *C* and *S* ORF of HBV were excised from pCMV-CL/CR/SL/SR-TALEN plasmids and cloned into pT7-Left/Right-TALEN-4×STOP expression vectors. Table 2.2 outlines the main differences between IVT template designs 1 and 2. Design 2 includes enhancements for TALEN expression: (i) mRNA with 5' and 3' UTRs from *β-globin* which are reported to enhance transcript stability by increasing mRNA half-life (180) (ii) the addition of stop codons which prevents transcription through the 3' UTR as well as addressing the issue of inefficient translation termination in the presence of Ψ, and (iii) an extended poly(A) tail which provides added protection against exonuclease degradation.

Table 2.2: Sequence differences between backbones in IVT template design 1 and 2

IVT Template Design 1	IVT Template Design 2
5' UTR (47 bp)	5' *β-globin* UTR (40 bp)
3' UTR (107 bp)	3' *β-globin* UTR (133 bp)
TAA single stop codon	TGA-TAA-TGA-TAG sequences (4×STOP codons)
Poly(A) tract (46 bases)	Poly(A) tract (113 bases)

2.3.2.2 *In vitro* transcription of CleanCap® AG-1 anti-HBV transcripts from IVT template design 2

As with the first IVT template design, design 2 was assessed by restriction digestion, with results detailed in **Appendix 6.4**. This assessment confirmed that the entire TALEN-encoding sequence was cloned into the expression vector, distinguished between left and right TALENs, and evaluated complete template linearisation. In accordance with the plasmid maps and sequencing alignment data (**Appendix 6.4-6.6**), all clones displayed the expected banding patterns. The linearised templates were *in vitro* transcribed and co-transcriptionally capped with CleanCap® AG (IVT #5) to produce homogeneous intact RNA **(Figure 2.18)**.

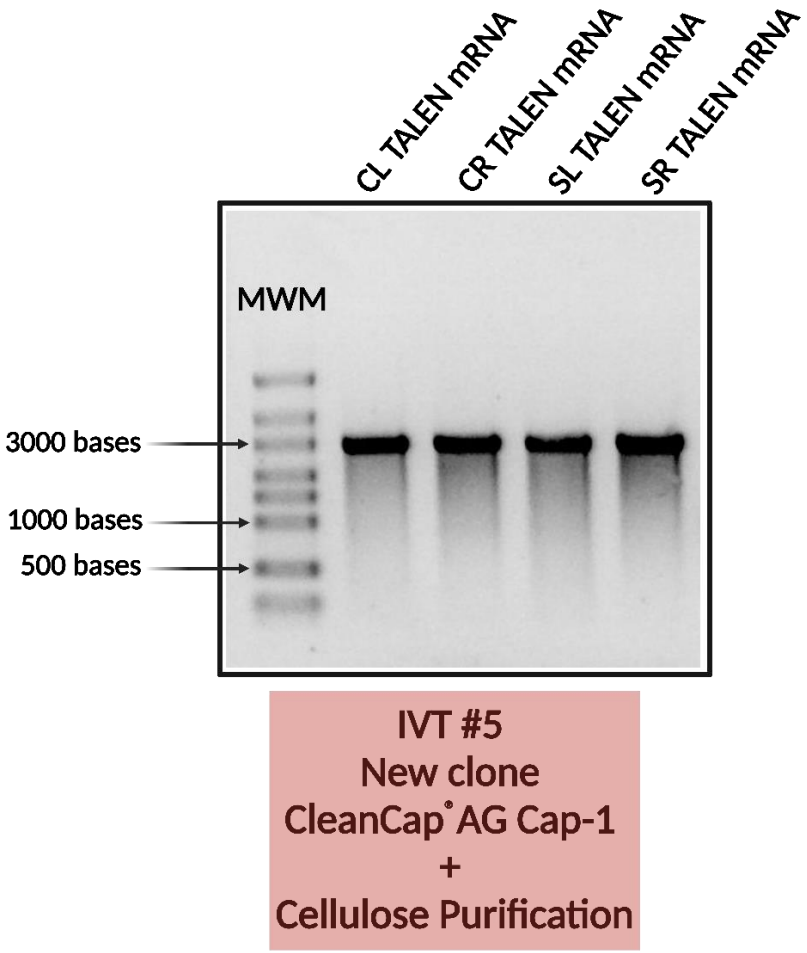


Figure 2.18: Confirmation of *in vitro* transcribed Core and Surface TALEN transcripts with CleanCap® AG analogues.

The pT7-Left/Right-TALEN linearised templates were *in vitro* transcribed with CleanCap® AG and resolved at 3198 bases on 1% formaldehyde gel. (MWM: molecular weight marker, RiboRuler high range RNA ladder, Thermo Fisher Scientific, CA, USA).

2.3.2.3 Robust TALEN expression in liver-derived from modified IVT template design 2

Huh7 cells were transiently transfected with either CL, CR, SL, or SR TALEN transcripts. As a negative control, cells were also transfected with mCherry, which lacks an HA epitope. mCherry was robustly expressed and detected using the tetramethyl rhodamine (TRITC) filter **(Figure 2.19)**. Core and Surface TALEN transcripts were identified in both the nucleus and cytoplasm of transfected cells, indicating efficient expression, translation, and nuclear transport of these proteins. As expected, mCherry did not exhibit a green signal under the FITC filter.

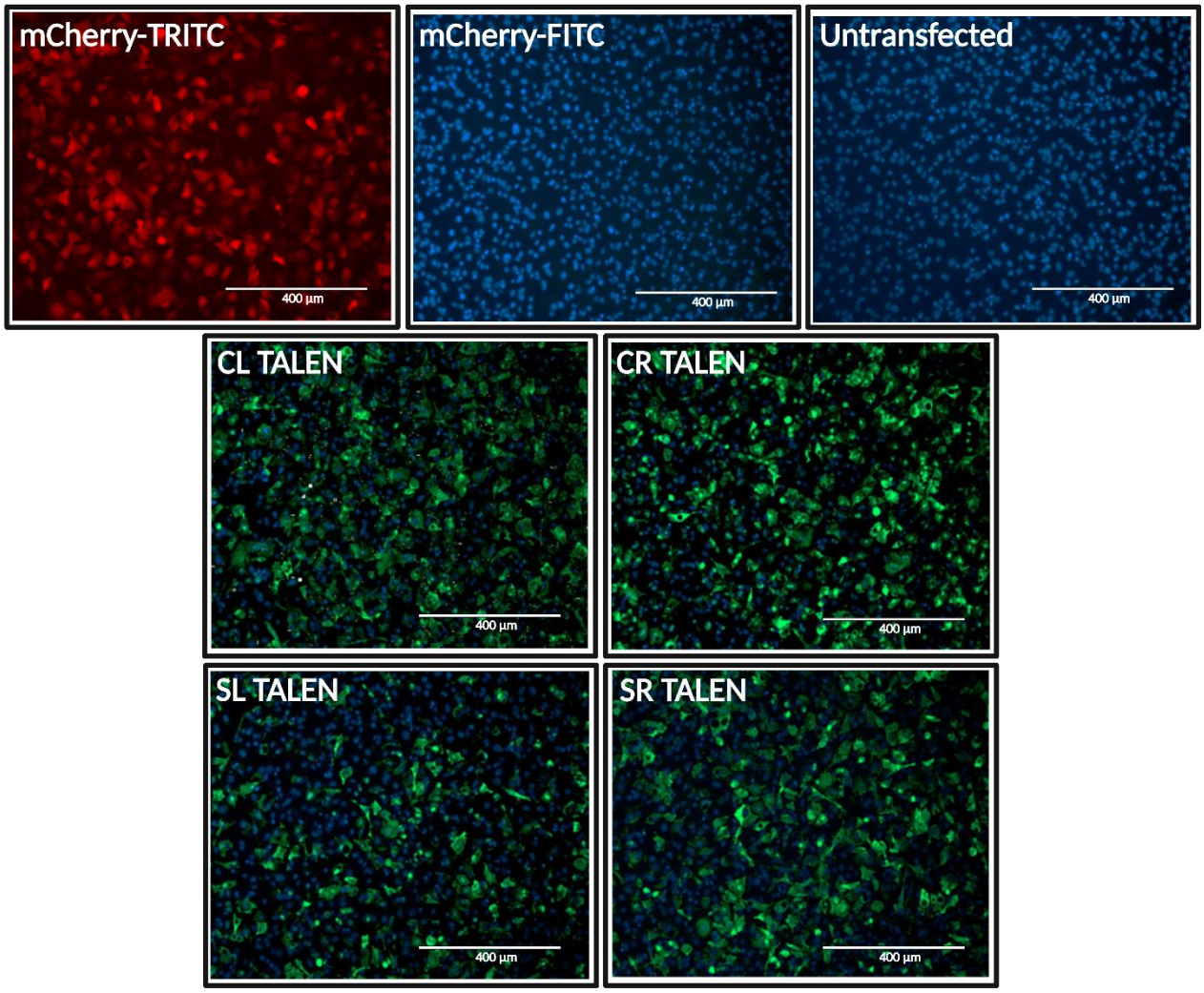


Figure 2.19: Enhanced TALEN expression from cellulose-treated cap-1 transcripts using CleanCap® AG in Huh 7 cells-IVT template design 2.

Huh7 cells were transiently transfected with CL, CR, SL or SR TALEN monomers produced with CleanCap® AG and further treated with cellulose purification. Transfection efficiency was evaluated using mCherry (TRITC), which was also transfected into separate wells as a negative control (mCherry mRNA FITC). Untransfected wells served as an additional negative control. Cell nuclei were counterstained with DAPI, and images were captured at 10× magnification. Only transcripts containing the HA epitope displayed bright green fluorescence.

2.4 Discussion

The design and development of effective mRNA therapeutics for gene editing require meticulous attention to detail, particularly in optimising IVT conditions and capping protocols. The initial experiments in this study focussed on designing IVT templates to produce anti-HBV TALENs targeting *S* ORFs of HBV using IVT template design 1. Various cap analogues, including ARCA, vaccinia capped, and CleanCap® AG were tested to evaluate their influence on TALEN-encoding mRNA expression in cell culture. High yields of TALEN transcripts were generated successfully, confirmed by formaldehyde gel electrophoresis for integrity. However, gel electrophoresis cannot distinguish between capped and uncapped transcripts.

During co-transcriptional capping, competition between cap analogues and GTP can produce uncapped, non-translatable transcripts, which reduce efficiency and trigger immune responses (184). High-throughput methods for distinguishing capped from uncapped transcripts include fluorescent labelling, which often suffers from high background signals (223), and microfluidic capillary gel electrophoresis, which is time-consuming and provides semi-quantitative results (224). Advanced techniques like nanopore sequencing and liquid chromatography–mass spectrometry (LC-MS) are more effective but complex and costly (225–227). Notably, LC-MS has shown that post-transcriptional capping with VCEs is superior to ARCA capping, suggesting that further investigation into capping methods could improve protein production (190).

Unfortunately, ARCA inclusion hindered TALEN translation and impeded expression in cell culture. In contrast, post-transcriptional capping with VCE and Ψ in cap-1 TALEN transcripts facilitated successful expression in the nucleus of cultured cells, but only after cellulose purification. Cellulose-based chromatography, recognised for its affinity for dsRNA, has been reported to enable the selective solution of ssRNA, achieving up to 80% recovery of mRNA (217).

TALEN expression was further enhanced using CleanCap® AG and Ψ after cellulose purification. Modified nucleotides are known to evade immune stimulation, however, Mulroney and colleagues made an intriguing observation between m1Ψ and ribosomal +1 frameshifting (228). Through examination of unmodified and modified Firefly luciferase (FLuc) constructs, they discerned that m1Ψ uniquely induced ribosomal +1 frameshifted peptides. Notably, this frameshifting phenomenon manifested in individuals and mice immunised with the COVID-19 vaccine BNT162b2, resulting in off-target T-cell immune responses to the +1 frameshifted peptide. The occurrence of frameshifting appears to be correlated with mRNA slippery sequences and ribosome stalling during translation mediated by m1Ψ, underscoring the necessity for further investigation into the impact of modified nucleotides on protein synthesis.

Based on literature indicating that Ψ causes erroneous transcription into the 3' UTR, a new template was designed to prevent readthrough errors, resulting in impressive expression in cell culture. Given the complexities of designing mRNA templates and optimising IVT conditions, capping protocols and incorporating modified nucleotides, thorough refinement is crucial for producing functional mRNA transcripts. Our studies indicated that using CleanCap® AG with transcripts generated from custom IVT template design 2 resulted in the highest level of detectable expression compared to transcripts from IVT template design 1. This conclusion is supported by the increased presence of fluorescence from fluorophore-conjugated antibodies to the HA tag. However fluorescence intensity was not quantified and future experiments should incorporate quantification of fluorescence intensity to enhance the robustness of the findings. Building on these findings, subsequent research was aimed at examining the therapeutic potential of these optimised TALEN transcripts.

Chapter 3- Use of TALEN-encoding mRNA to attenuate HBV replication in cell culture

3.1 Introduction

TALEN-encoding mRNA was designed to induce DSBs at predetermined genomic loci within HBV. This phenomenon triggers the cell's inherent DNA repair mechanisms, which may proceed either through NHEJ or HDR pathways (reviewed in (128)). As elucidated previously, the error-prone nature of NHEJ repair facilitates introduction of mutations at the targeted locus after TALEN-mediated cleavage. These mutations can manifest as either indels or nucleotide substitutions. The deliberate induction of such targeted mutagenesis is crucial for gene disruption or the generation of knock-out mutations.

The process of DNA repair following designer nuclease-mediated cleavage is intricate. The efficacy of nuclease cleavage is variable among diverse cell lines, target cells, and donor sequences (229), underscoring a multifaceted interplay of factors yet to be fully elucidated. Putative influences include the cellular milieu surrounding the genomic target DNA. Genomic loci bound by nucleosomes exhibit diminished cleavage efficiency compared to those devoid of nucleosomes (230). Nevertheless, it is promising that several designer nucleases, including TALENs, have demonstrated the ability to disrupt gene expression, especially in cases where NHEJ is the preferred mechanism of repair.

DNA-binding proteins are designed to locate specific target sites amid millions of non-specific sequences, balancing the need for rapid dynamics with stable target binding. This challenge is often referred to as the "speed-stability paradox" (231). This two-state model proposed for DNA-binding proteins encompasses a search and recognition phase (231,232).

ZFs bind DNA during the search phase with one ZF dissociating from the backbone while the remaining fingers bind non-specifically (233,234). Extended non-specific binding can lead to higher off-target effects. Cas9 binding and cleavage are more complex than initially believed. In contrast to DNA-binding proteins, CRISPR-Cas9 relies on RNA-guided DNA hybridisation for target recognition and cleavage. Self-folding stability of gRNAs has recently been shown to hinder Cas9 binding (235,236). Additionally, gRNAs with mismatches can lead to more effective cleavage compared to perfectly matching gRNAs (235). This raises concerns about potential off-target effects, a major topic of discussion in CRISPR technology (150,237,238). Furthermore, gRNAs that target non-canonical PAMs can enhance cleavage efficiency, thereby increasing Cas9's compatibility with various PAM sequences. Therefore, careful consideration must be taken when designing gRNAs to optimise Cas9 binding efficiency and minimise off-target effects.

Unlike other DNA-binding proteins, TALEs lack common motifs such as helix-turn-helix or leucine zippers but excel in quickly locating target sequences without increasing off-target effects. During the search phase, TALEs bind non-specific DNA loosely, thereby minimising strong electrostatic interactions between the DBD and the DNA backbone (239). This loose binding facilitates rapid sliding or hopping along the DNA (239,240). When TALEs attempt to transition to the recognition phase with non-target DNA, they encounter steric and electrostatic clashes that destabilise the complex. However, upon encountering the correct target sequence, TALEs form stable molecular contacts, aligning RVDs for energetically favourable interactions. This mechanism prevents TALEs from becoming trapped at non-target sites and enhances search efficiency. TALEs effectively overcome the search speed-stability paradox, demonstrating superior efficiency in identifying target sequences even within large genomes.

To further enhance TALE targeting, a minimum of three cytosine or guanine nucleotides incorporating RVDs HD and NN are essential for optimal functionality (241). Both HD and NN are deemed 'strong' RVDs, and TALE constructs lacking these RVDs show significantly reduced efficiency. The obligate heterodimeric TALE constructs targeting the *C* and *S* ORF include sufficient HD and NN RVDs (**Appendix 6.5**), enhancing their efficiency in binding to target DNA and inducing DSBs.

The use of engineered TALENs to directly target viruses offers a promising approach for antiviral gene therapy. This strategy is particularly suitable for viruses that establish latent infections, such as HIV and HBV, which are challenging to eradicate with current therapies. However, the high mutagenicity of HIV raises concerns about the emergence of escape mutants following TALEN-induced cleavage. In contrast, HBV has a compact genome structure and initiates replication through an episomal cccDNA reservoir. Given the essential nature of HBV's ORFs, mutations within its genome are likely to exert significant impact on viral fitness. Consequently, the nuclease-mediated cleavage and subsequent NHEJ repair of cccDNA hold the potential to permanently disable the virus. For this reason, obligate heterodimeric TALEN-encoding mRNA was employed to target *C* and *S* ORFs of HBV cccDNA with the aim of inducing DSBs (**Figure 3.1**). To validate TALEN function HBsAg secretion, a crucial marker of replication, was measured in cell culture models after TALEN treatment.

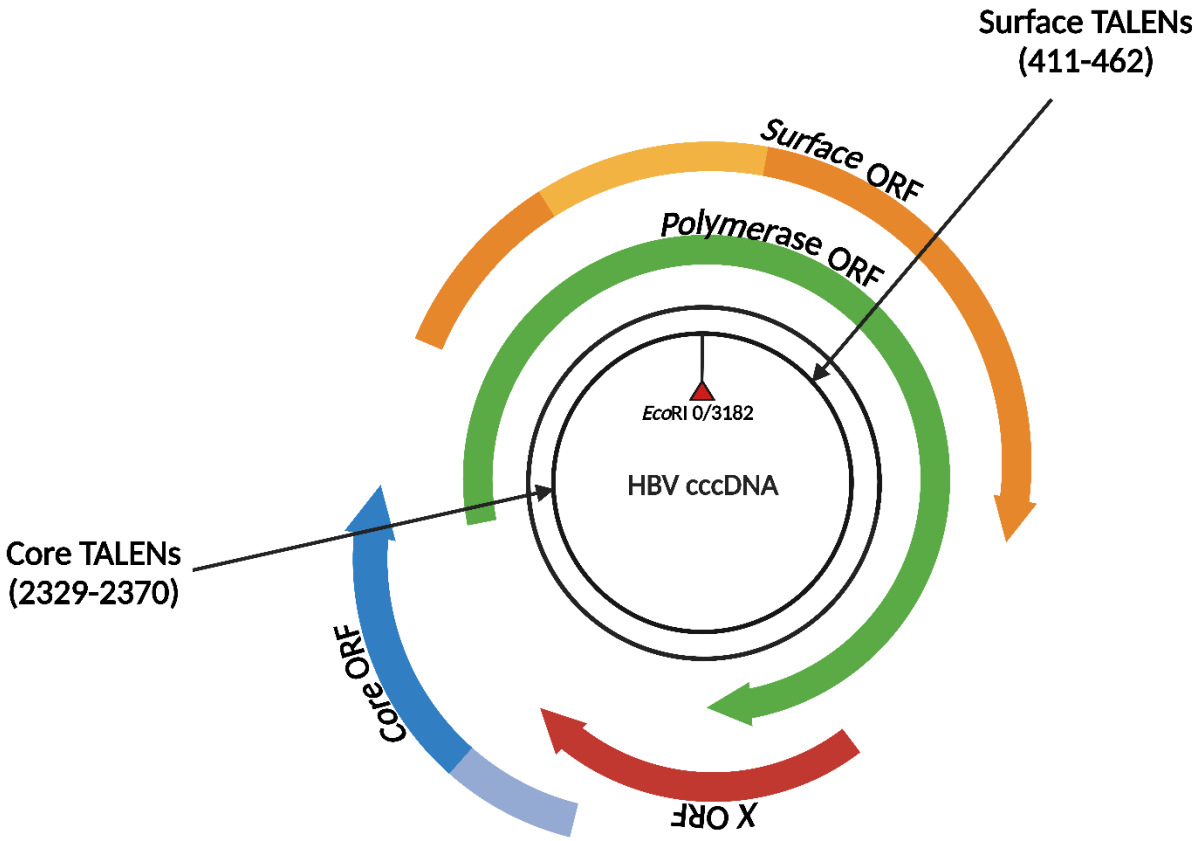


Figure 3.1: Target sites on HBV cccDNA for obligate heterodimeric cleavage.

Two obligate heterodimeric TALENs were generated to target both the *core* and *surface* ORFs of HBV cccDNA. These sites are indicated by arrows. These TALENs also aim at the overlapping *polymerase* ORF (Figure created with Biorender.com).

3.2 Methods

3.2.1 Establishing HBV replication in cell culture

3.2.1.1 pCH-9/3091

Engineered by Nassal and team, the pCH-9/3091 plasmid was developed as a replication-competent construct for HBV (242). This construct harbours a greater-than-genome length HBV sequence based on genotype D, facilitating the transcription of pgRNA. Subsequent reverse transcription of pgRNA initiates the formation of cccDNA. In this investigation, pCH-9/3091 was employed to establish replication in cultured cells.

3.2.1.2 HBV isolated from HepG2.2.15

HepG2-hNTCP-C4 cells were cultured following standard protocols (**Appendix 6.2.2**) and are susceptible to HBV infection owing to their constitutive expression of the human NTCP receptor. HepG2.2.15 cells harbour an integrated HBV sequence and serve as a source of infectious HBV particles. HepG2.2.15 cells were also cultured using standard procedures (**Appendix 6.2.3**). HepG2.2.15 cells were seeded at 50% confluency, and after 9 days, cell culture supernatant was collected and clarified through filtration using 0.22 μm filters. The virus was concentrated by mixing 1 volume of 5 × polyethylene glycol (PEG) 8000 (**Appendix 6.1.3**) with 4 volumes of HepG2.2.15 culture supernatant, followed by overnight incubation at 4 °C and subsequent centrifugation. The resulting pellet was resuspended in medium. Total viral DNA was extracted using the QIAamp® DNA Mini Kit according to the purification protocol for blood and bodily fluids (Qiagen, Hilden, Germany). Following extraction, viral quantification was performed by quantitative PCR (qPCR), with a standard curve generated using ten-fold serial dilutions of pCH-9/3091. The qPCR protocol was arranged using the FastStart Essential DNA Green Master Kit

(Roche Applied Science, Mannheim, Germany) according to the manufacturer's instructions with 10 picomoles (pmol) of each forward and reverse primer (**Table 3.1**), 5 µl of extracted DNA (and pCH-9/3091), and 5.5 µl of distilled water.

Table 3.1: Primer sequences used to amplify the HBV *preS1* region

Primer name	Primer sequence
HBV surface Forward	5'-TGC ACC TGT ATT CCC ATC-3'
HBV surface Reverse	5'-CTG AAA GCC AAA CAG TGG-3'

All qPCR reactions were performed using the Bio-Rad CFX96™ Real Time System (Bio-Rad, CA, USA). For this reaction the following cycling conditions were used: hot start at 95 °C for 10 minutes and 40 cycles of denaturing at 95 °C for 15 seconds, annealing at 57 °C for 15 seconds and elongation at 72 °C for 20 seconds with a single SYBR® Green signal acquisition at this step. Melting curve analysis was carried out immediately after qPCR as follows: DNA was denatured at 95 °C for 10 seconds followed by cooling to 65 °C for 5 minutes and then heating to 95 °C at a ramp rate of 0.5 °C/s with continuous SYBR® Green signal acquisition. To determine the quantity of HBV DNA copies in each sample, serial dilutions of pCH-9/3091 were employed. The plasmid copy number was computed utilising the formula:

$$\text{copy number} = \frac{\text{mass (ng)} \times \text{Avogadro's number}}{\text{length (bp)} \times 1 \times 10^{9} \times 660\ \text{g/mol}}$$

Here, the mass represents the plasmid amount in nanograms (ng), the length denotes the plasmid size in base pairs, 1×10^{9} is the conversion factor to ng and each base pair carries a molecular weight of 660 Daltons. Hepatitis B viral particle equivalents per millilitre (VPE/ml) were extrapolated from the standard curve. The VPE/ml was subsequently used to infect HepG2-hNTCP-C4 cells with a multiplicity of infection (MOI) of 10.

3.2.1.3 AAV-2 containing HBV genome sequence from subgenotype D3 (AAV-2-D3)

Recombinant adeno-associated viruses (AAVs) were utilised to replicate HBV subgenotype D3 *in vitro*. Recombinant AAV serotype 2 (AAV-2) vectors carrying greater-than-genome length sequences of HBV DNA from subgenotype D3 were generated as previously described (243). Transduced liver-derived cultured cells demonstrated the production of HBsAg and HBcAg, along with the generation of all RNA transcripts. Consequently, this model was employed as a convenient replication model to assess HBV expression.

3.2.2 Measuring HBsAg levels using enzyme-linked immunosorbent assay (ELISA)

3.2.2.1 Assessing HBsAg secretion from Huh7 cells transfected with pCH-9/3091

One day before transfection, Huh7 cells were seeded in a 48-well plate at a cell density of 50% with 225 µl of medium per well. Transfection was conducted using Lipofectamine™ 3000 (Invitrogen, CA, USA) to deliver 50 ng of pCH-9/3091 to cells and incubated for one hour. Cells were then transfected with 225 ng of SL and SR TALEN transcripts (IVT #1-4). For transcripts from IVT #5 cells were either transfected with 225 ng of CL and CR, and in separate cells with 225 ng of SL and SR TALEN transcripts using Lipofectamine™ MessengerMAX™ (Invitrogen, CA, USA). In separate wells, cells were transfected with 450 ng of eGFP-mRNA (IVT #1-4) or 450 ng of mCherry-mRNA (IVT #5). All transfections were performed in experimental triplicates according to the manufacturer's instructions and evaluated for HBsAg secretion at 24 and 48 hours after transfection.

HBsAg secretion was determined using ELISA with the Monolisa™ HBs Ag ULTRA kit (Bio-Rad, CA, USA). In brief, 100 µl of culture supernatant was added to a microplate precoated with monoclonal anti-HBsAg antibodies. After adding 50 µl of conjugate solution, the mixture was

incubated for 1.5 hours at 37 °C. The wells were washed five times with 1 × washing solution using the Microplate Washer APW-200 (Hangzhou Allsheng Instruments Co., Ltd, Zhejiang, China), followed by the addition of 100 µl of enzyme development solution. The microplate was then incubated in darkness at room temperature for 30 minutes. After incubation, the reaction was stopped by adding 100 µl of stopping solution to each well. The optical density (OD) of each sample was measured at 490 nm and 655 nm wavelengths using the Multiskan SkyHigh Microplate Spectrophotometer (Thermo Fisher Scientific, CA, USA) after a 4-minute interval. The OD reading at 655 nm was then subtracted from the OD reading at 490 nm.

3.2.2.2 Assessing HBsAg secretion from HepG2-hNTCP-C4 cells infected with HBV particles

HepG2-hNTCP-C4 cells were seeded into 24-well collagen-coated plates (**Appendix 6.2.4**) at a density of 65%. After 24 hours, the cells were treated with DMEM/F12 containing 2% DMSO. Forty-eight hours thereafter, the cells were infected with HBV at an MOI of 10 in a solution comprising 2% DMSO, 4% PEG, and DMEM/F12 up to desired volume. The virus was incubated for 8 hours, followed by three washes with 1 × PBS, and then cells were transfected with 500 ng of each of the CL and CR or SL and SR TALEN transcripts (IVT #5). Additionally, separate wells received 1,000 ng of mCherry-mRNA (IVT #5). All transfections were conducted using Lipofectamine™ MessengerMAX™ in triplicate according to the manufacturer's instructions and evaluated for HBsAg secretion 24 hours after infection, as described in section 3.2.2.1.

3.2.2.3 Assessing HBsAg secretion from Huh7 cells transduced with AAV-2-D3

One day prior to infection, Huh7 cells were seeded in a 24-well plate at a cell density of 50% with 450 µl of medium per well. AAV-2-D3 was then added to the cells at an MOI of 1,000 and incubated for 40 hours. Subsequently, Lipofectamine™ MessengerMAX™ was used to transfect

cells with 500 ng of each of the CL and CR or SL and SR TALEN transcripts (IVT #5). Additionally, separate wells received 1,000 ng of mCherry-mRNA (IVT #5). All transfections were carried out in experimental triplicates following the manufacturer's instructions and evaluated for HBsAg secretion at 48, 72, and 96 hours after infection, as described in section 3.2.2.1.

3.2.3 Cell viability assay

Huh7 and HepG2-hNTCP-C4 cells were seeded into a 96-well plate at a cell density of 50%, with 110 µl of medium per well, 24 hours before transfection. Lipofectamine™ MessengerMAX™ was employed to transfect cells with 100 ng of each of the CL and CR TALEN transcripts or 100 ng of SL and SR TALEN transcripts. mCherry was transfected in separate wells. Additionally, 50% dimethyl sulphoxide (DMSO, Sigma-Aldrich, MO, USA) was used to transfect cells and acted as a positive control. These transfections were conducted in triplicate and evaluated for cell viability 24 hours post-transfection. Subsequently, 20 µl of MTT solution (5 mg/ml dissolved in 1 × PBS, Sigma-Aldrich, MO, USA) was added to each well and incubated at 37 °C for one hour. After incubation, the culture medium was removed, and 200 µl of DMSO was added and resuspended in each well. Following a five-minute incubation period, ODs were measured at 570 nm and 655 nm using an iMARK™ Microplate reader (Bio-Rad, CA, USA). The OD reading at 655 nm was subtracted from the OD reading at 570 nm.

3.2.4 Statistical analysis

All experiments using cultured cells were conducted in biological triplicates. Statistical analysis involved calculating and plotting the mean and standard error of the mean (SEM) for each dataset. To determine statistical significance, a Two-tailed Student's t-test was conducted using GraphPad

Prism 8.0 (GraphPad Software Inc., CA, USA). Groups with a p-value less than 0.05 were deemed significant.

3.3 Results

3.3.1 *In vitro* transcribed TALENs from IVT design template 2 mediates enhanced inhibition of HBsAg secretion from liver-derived cells

Initially, TALEN expression was evaluated in Huh7 cells. Transcripts from IVT #1 and #2 did not express in cell culture. Nevertheless, TALEN functionality was examined by assessing the secretion of HBsAg. Huh7 cells were transiently transfected with the pCH-9/3091 replication-competent plasmid. One hour later, cells were transfected with Surface TALEN transcripts. Huh7 cells transfected with pCH-9/3091 and eGFP mRNA served as the negative control. Transfections were conducted in triplicate, and secreted HBsAg levels were measured 24 and 48 hours after transfection. As anticipated, none of the TALEN transcripts led to a significant reduction in HBsAg compared to their respective control (**Figure 3.2**).

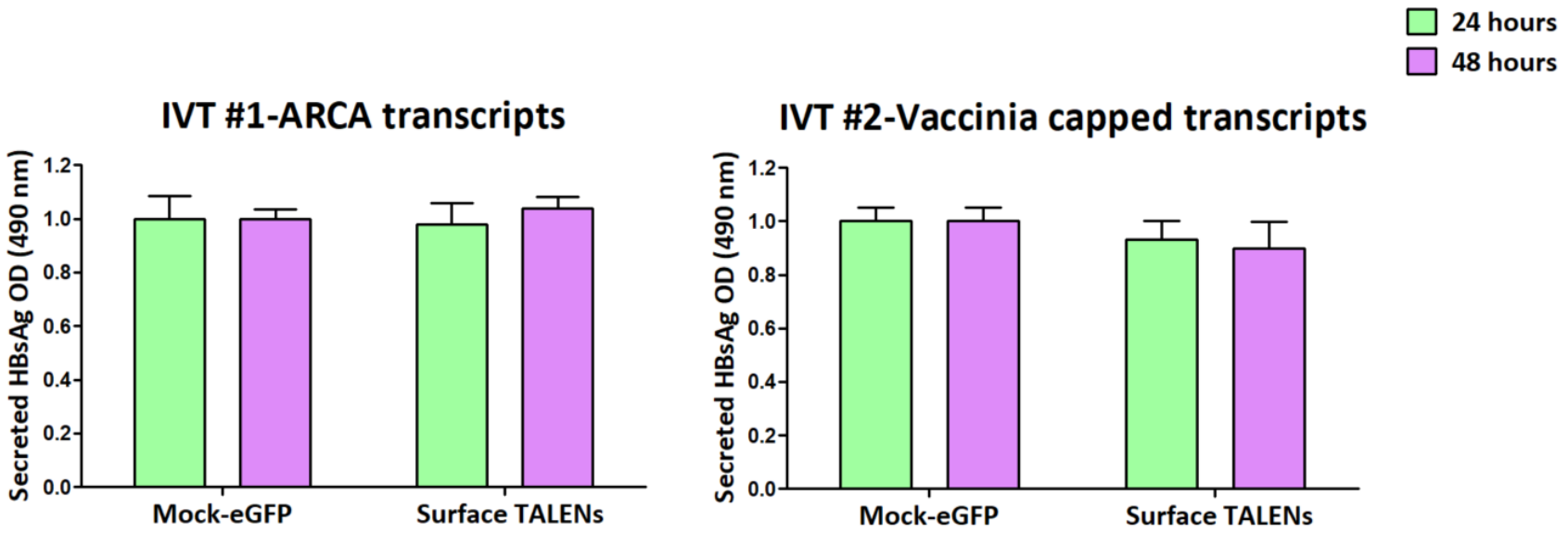


Figure 3.2: Measuring HBsAg secretion in Huh7 cells transfected with pCH-9/3091-IVT #1 and IVT #2.

The levels of secreted HBsAg in the culture media were measured 24 hours and 48 hours after transfection. Huh7 cells were initially transfected with pCH-9/3091 followed by transfection with Surface TALEN transcripts. Mock-treated cells were transfected with eGFP mRNA and pCH-9/3091.

Transcripts from IVT #3 to IVT #5 exhibited efficient TALEN expression. As described above Huh7 cells were transiently transfected with pCH-9/3091 and incubated for one hour, followed by transfection of either Surface TALENs along with eGFP-mRNA from IVT #3 and IVT #4, or the transfection of Core and Surface TALENs, and mCherry-mRNA from IVT #5. Unexpectedly, TALEN transcripts from IVT #3 did not reduce HBsAg levels (**Figure 3.3**). IVT #4 TALEN transcripts demonstrated a 16% reduction in HBsAg levels at the 24-hour mark, which was not sustained by the 48-hour mark (**Figure 3.3**). Conversely, Surface TALEN transcripts from IVT #5 exhibited a significant reduction in HBsAg levels at 62% observed at 24 hours and a sustained reduction of 40% at 48 hours (**Figure 3.3**). The observed increase in HBsAg secretion with transcripts from IVT #5 at 48 hours could be attributed to the persistent replication of HBV from the pCH-9/3091 plasmid, which may not accurately mimic natural HBV infection.

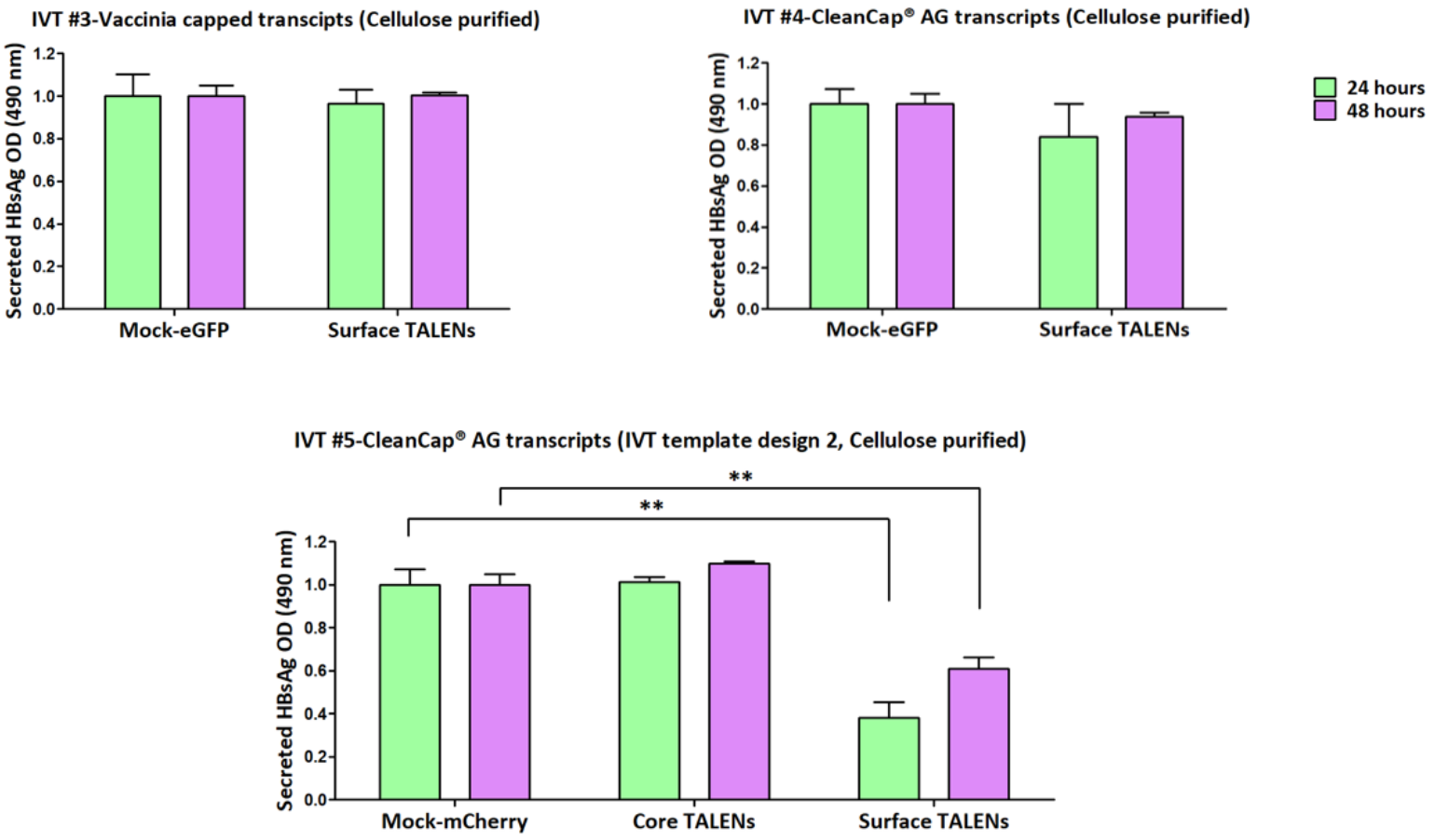


Figure 3.3: Measuring HBsAg secretion in Huh7 cells transfected with pCH-9/3091- IVT #3 to IVT #5.

Secreted HBsAg levels were measured 24 hours and 48 hours after transfection. Huh7 cells were transiently transfected with pCH-9/3091 followed by transfection with Surface TALEN transcripts from IVT #3 and IVT #4 while cells were transfected with Core and Surface TALEN transcripts from IVT #5. Mock-treated cells were transfected with eGFP mRNA and pCH-9/3091 from IVT #3 and IVT #4 and mCherry mRNA and pCH-9/3091 from IVT #5 (**: $p<0.01$).

As a result of the inefficacy of transcripts from IVT #1 to IVT #4 in providing effective anti-HBV therapeutic potential, only transcripts from IVT #5 were utilised in subsequent experiments. To simulate natural infection, HepG2-hNTCP-C4 cells were infected with HBV particles at an MOI of 10. HepG2-hNTCP-C4 cells harbour the well-known NTCP receptor crucial for viral entry (107). Eight hours after infection, cells were transfected with Core and Surface TALEN transcripts from IVT #5, while mCherry-mRNA served as a negative control. Twenty-four hours after infection, both Core and Surface TALENs exhibited a significant reduction in HBsAg levels of 30% and 31% respectively (**Figure 3.4**). The reduction in HBsAg mediated by TALENs is presumed to occur primarily through the targeted disruption of the *S* ORF by Surface TALENs. This implies that the reduction observed with Core TALENs might occur through indirect interference, thereby impeding viral protein expression, as has been observed previously (169).

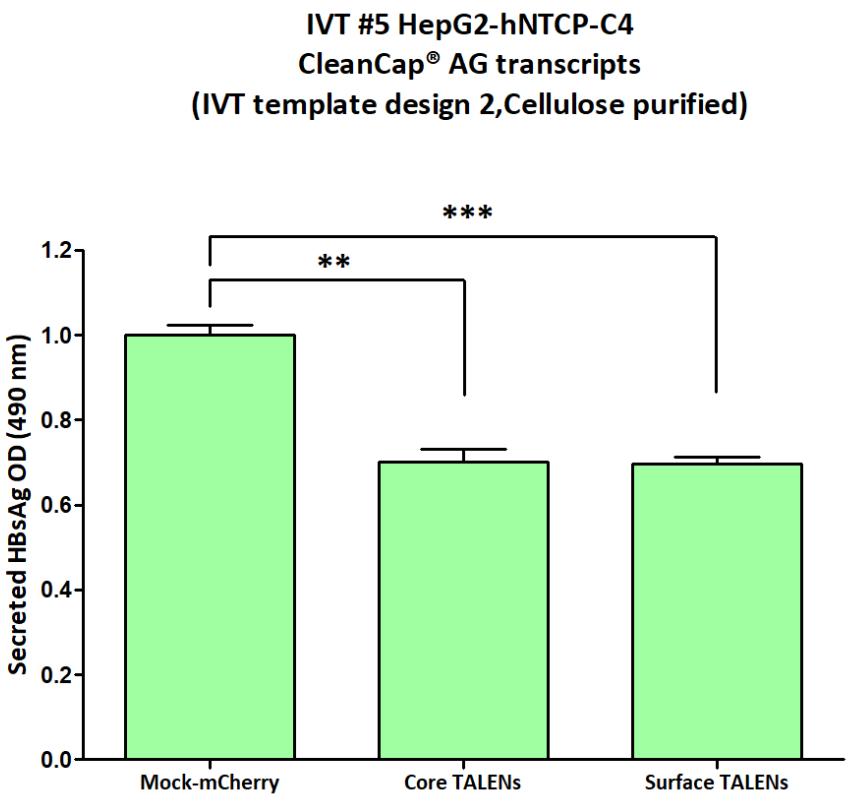


Figure 3.4: TALEN-mediated reduction of HBsAg secretion in HepG2-hNTCP-C4 cells.

Secreted HBsAg were measured 24 hours after infection. HepG2-hNTCP-C4 cells were infected with HBV particles at an MOI of 10. Following an 8-hour incubation, cells were transfected with Core and Surface TALEN transcripts whereas mock-treated cells were transfected with mCherry mRNA (**: $p<0.01$, ***: $p<0.001$).

In a different model of infection, Huh7 cells were transduced with AAV-2-D3 at an MOI of 1,000. Forty hours after infection, cells were transfected with TALEN transcripts from IVT #5 and mCherry-mRNA as a negative control. The secretion of HBsAg was evaluated at 48, 72, and 96 hours after infection (**Figure 3.5**). At 48 hours, both Core and Surface TALENs led to a reduction in HBsAg levels by 31% and 28% respectively. By 72 hours, both Core and Surface TALENs further decreased HBsAg secretion to 41% and 67% respectively. Subsequently, at 96 hours, the reduction mediated by Core TALENs reverted to 31%, whereas Surface TALENs continued to diminish HBsAg levels to 80%. This illustrates the direct impact of Surface TALENs on the *S* ORF.

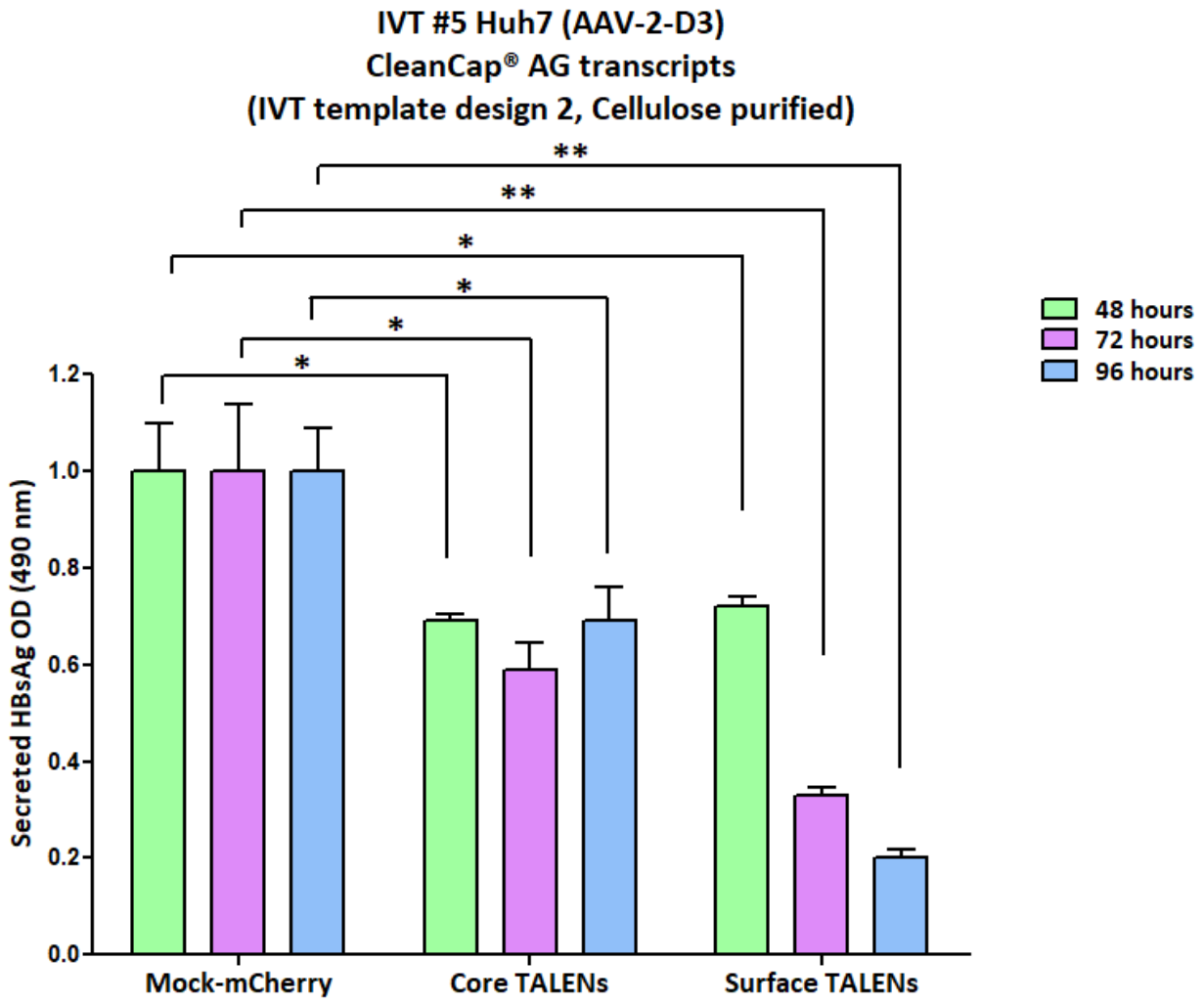


Figure 3.5: TALEN-mediated reduction of HBsAg secretion in Huh7 cells transduced with AAV-2-D3.

Secreted HBsAg was measured at 48, 72 and 96 hours after infection. Huh7 cells were transduced with AAV-2-D3 at an MOI of 1,000. Following a 40-hour incubation cells were transfected with Core and Surface TALEN transcripts and mock-treated cells were transfected with mCherry mRNA (*: $p<0.05$, **: $p<0.01$).

3.3.2 TALENs do not induce cell-mediated toxicity

To assess the potential cytotoxicity caused by nuclease effects, an MTT assay was performed on Huh7 and HepG2-hNTCP-C4 cells transiently transfected with TALENs from IVT #5. The MTT assay relies on the reduction of MTT to formazan, which occurs exclusively in viable cells, serving as an indicator of cell viability. Cells were transiently transfected with Core or Surface TALEN transcripts, and with mCherry-mRNA serving as a negative control. Additionally, cells were exposed to 50% DMSO to serve as a positive control for cell death. Cells were also treated with the transfection agent only to rule out transfection-mediated toxicity. All transfections were compared to untransfected cells. Transfections were conducted in triplicate, and the MTT assay was performed 24 hours after transfection. No significant difference was observed between TALEN-treated cells and mock or untreated controls, indicating comparable cellular activity (**Figure 3.6**). As anticipated, DMSO treatment resulted in substantial cell death. These findings suggest that TALENs do not induce cellular toxicity, and the observed anti-HBV effects mediated by TALENs are likely attributed to TALEN-mediated cleavage rather than cellular toxicity.

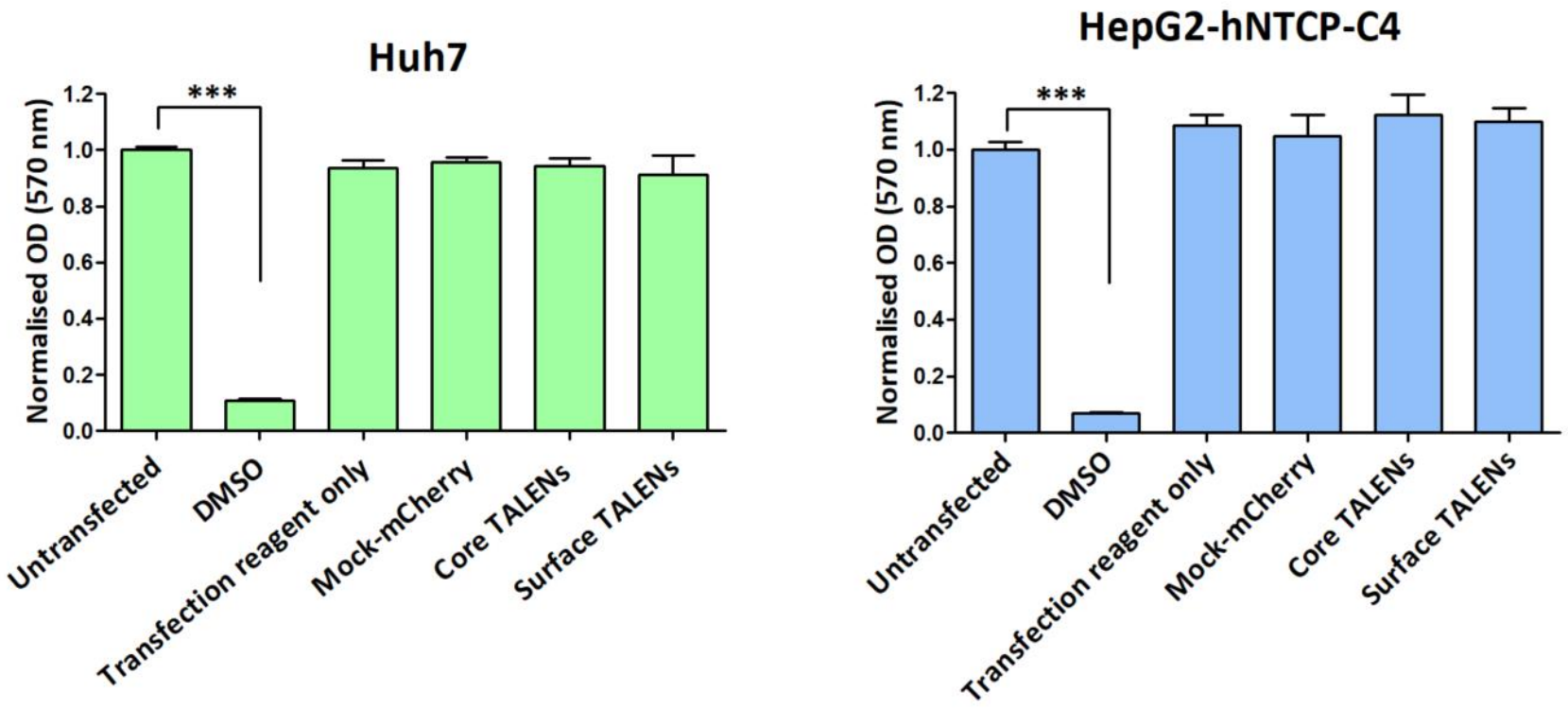


Figure 3.6: Evaluation of TALEN-induced cellular toxicity.

Huh7 and HepG2-hNTCP-C4 cells were transfected with Core and Surface TALEN transcripts and mock-treated cells were treated with mCherry mRNA or transfection reagent lacking transcripts. Cells treated with 50% DMSO served as the positive control. MTT reduction was measured 24 hours after transfection (***: $p<0.001$).

3.4 Discussion

The persistence of exceptionally stable cccDNA presents a significant challenge to achieving complete HBV eradication. Despite various therapeutic approaches aimed at controlling the disease, a definitive cure remains out of reach. However, the advent of designer nucleases has allowed for precise and effective targeting of cccDNA (123,124,150). This study marks the pioneering demonstration of obligate heterodimeric TALEN-encoding mRNA to target HBV cccDNA, offering a novel therapeutic strategy against the virus.

The design of the TALEN mRNA expression backbone was a crucial determinant for generating functional protein. Transcripts that failed to express in cell culture also failed to elicit anti-HBV effects, as evidenced by the unaltered HBsAg levels compared to controls (**Figure 3.2**). Conversely, transcripts subjected to cellulose treatment in IVT #3 and #4 expressed well in cell culture but did not significantly reduce HBsAg levels. Beyond the previously discussed limitations of IVT template 1, another relevant factor is that TALEN expression was assessed just 6 hours post-transfection. RNA degradation at later time points can occur as a result of the shortening of the poly(A) tail, which reduces the mRNA's stability and increases degradation by cellular exonucleases (reviewed in (244)). mRNA degradation is a key regulatory mechanism in gene expression and is often initiated by deadenylation of the 3' poly(A) tail (245,246). This step is essential for mRNA turnover and translational repression when the mRNA is no longer required. The poly(A) tail, averaging about 200 nucleotides in mammals (247) is crucial for mRNA stability and translation. The precise length required for effective transcription and translation is difficult to predict, underscoring the importance of evaluating poly(A) tail lengths for post-transcriptional gene expression control.

The mRNA expression backbone from IVT #5 was further refined by incorporating UTRs from *β-globin* genes to enhance RNA stability. Additionally, a longer poly(A) tract was added, which likely contributed to the augmented functionality. This refinement potentially accounts for the observed 80% decrease in HBsAg secretion in Huh7 cells transduced with AAV-2-D3 targeted by the Surface TALENs, as well as the prolonged efficacy of TALENs by mitigating premature degradation. The reduction in HBsAg concentration by Core TALENs is likely attributed to their targeted effects on the *C* ORF, which inhibits new virion assembly. Additionally, because of HBV's compact genome, Core TALENs also target the *P* ORF. The *P* ORF encodes the viral RT, which is essential for converting pgRNA into cccDNA—a critical step in viral replication. Mutations in the *P* gene can impair this enzyme, reducing or halting viral replication and significantly lowering the viral load. Therefore, the decrease in HBsAg observed with Core TALENs may be an indirect effect resulting from these disruptions.

Previous studies using pCH-9/3091 for anti-HBV assessment, although valuable, do not accurately replicate the dynamics of natural infection, where cells are infected by a virus rather than constitutively expressed plasmids. Consequently, research extended to more suitable infection models, such as HepG2-hNTCP-C4-infected cells and AAV-2-D3-infected cells, to better simulate natural infection. TALENs exhibited a modest reduction in HBsAg in HepG2-hNTCP-C4 cells, while their functionality was notably enhanced in the AAV-2-D3 model. The high infection variability and differentiation requirements of HepG2-hNTCP-C4 cells underscore the importance of the observed modest reduction. While DMSO is commonly used to promote differentiation in HBV cell culture models (248,249), it has toxicity concerns and variable effectiveness. Recent findings show that Huh7.5-NTCP cells can be infected with HBV without DMSO (250). Moreover, ELISA detection of HBsAg after TALEN treatment in these cells remains effective if the specific

epitope bound by the capture antibody is not disrupted by the mutation or if the protein's 3D conformation is preserved. In the AAV-2-D3 model, TALENs achieved a sustained HBsAg decline, demonstrating their efficacy through permanent mutations.

Low cleavage efficiencies and associated cytotoxicity of TALENs have been documented when targeting endogenous genes, as cellular repair mechanisms responding to DSBs lead to genotoxicity and apoptosis. However, TALENs targeting episomal viral replication intermediates are generally less likely to induce similar cytotoxic effects. A major challenge in gene therapy is the unintended cytotoxicity resulting from the introduction of exogenous nucleases. While ZFNs have previously demonstrated cytotoxicity (124), TALENs engineered for enhanced target site specificity have shown reduced toxicity (123,166,169). In line with these observations, TALEN-encoding mRNA did not induce cellular toxicity in our experiments. These findings support the notion of TALENs as non-cytotoxic agents and establishes a foundation for further experimentation in a murine model of HBV replication

Chapter 4- LNP-encapsulated TALEN-encoding mRNA inhibits HBV replication in a transgenic murine model

4.1 Introduction

Designer nucleases have been tested in various HBV cell culture models, demonstrating anti-HBV efficacy. These models are essential for initial screening, optimisation, and safety assessment, serving as a cost-effective and ethical foundation before progressing to *in vivo* testing. *In vivo* models remain crucial for understanding HBV pathogenesis and immune responses, as the liver's unique microenvironment significantly impacts HBV replication and therapeutic efficacy. Comprehensive *in vivo* evaluation is necessary to confirm the safety and effectiveness of treatments, facilitating their advancement in the development pipeline.

The host spectrum of HBV is very narrow, with non-human primates such as chimpanzees and Mauritian cynomolgus macaque monkeys being susceptible to infection (251–253). Other mammalian species like tree shrews (*Tupaia belangeri*) and woodchucks can also be infected (254–258). However, the virus-host dynamics in these systems differ significantly from those in humans (reviewed in (259)). Notably, the chimpanzee is the only known immunocompetent non-human primate model fully susceptible to HBV, capable of mimicking the pathogenesis and disease progression seen in human infections (251,252).

Despite their relevance, the use of these animal models is severely constrained by ethical considerations, procurement difficulties, and high maintenance costs. These challenges create a bottleneck in understanding HBV disease mechanisms and developing effective therapies. Consequently, there is a critical need for more accessible HBV models. Laboratory mouse strains

offer a practical alternative and are invaluable for HBV research owing to their ease of handling, lower costs, and established use in scientific studies (123,166,169,243,260).

HBV transgenic models were first developed between the mid-1980s and early 1990s. These models expressed either individual HBV genes encoding HBsAg (261,262), HBcAg (263), HBeAg (264), and HBx (265), or the complete set of HBV genes capable of producing infectious virions in murine hepatocytes (68). These models have significantly contributed to our understanding of HBV replication, particularly in identifying the oncogenic function of HBx, its role in altering host gene expression, and its eventual link to HCC (265–267). Additionally, HBV transgenic mice have facilitated investigations into the assembly, secretion, immune responses, and functionality of HBV proteins.

The integrated HBV genome includes terminally redundant DNA representing greater-than-genome length sequences enabling efficient viral replication. This includes the synthesis of rcDNA from pgRNA, final assembly, and production of infectious HBV particles indistinguishable from human-derived variants (68). These transgenic mice have been instrumental in evaluating the effects of antiviral drugs such as anti-HBV siRNAs (268,269) and polymerase inhibitors (270–272) that hinder HBV replication.

However, the HBV mouse model is not without complications. A significant limitation is that mice do not naturally recapitulate HBV infection, and cccDNA pools are not established (68). Humanised transgenic models have been developed to overcome this obstacle, involving grafting human hepatocytes into immunodeficient mice (273–276). These models closely approximate human HBV infection and produce cccDNA, but they present challenges like kidney disorders, low breeding efficiency, fatal bleeding, and immunodeficiency, which limit the study of immune

responses (277). High costs and technical difficulties also restrict their use. Despite these obstacles, humanised mice remain valuable for advancing HBV research and developing new therapies.

Recent advancements in human liver organoids offer a promising alternative for modelling HBV infection (278,279). These organoids, derived from healthy donor liver tissue, can be challenged with recombinant virus, HBV-infected patient serum, or by transgenic modification to produce cccDNA. This provides a more relevant system for studying HBV dynamics. Their potential for future research and therapeutic development makes them a compelling area for further investigation.

Previous efforts using hydrodynamic injection (HDI) to administer pCH-9/3091 in non-transgenic mice have efficiently facilitated DNA entry into hepatocytes by generating high pressure to permeabilise capillary endothelium and create pores in hepatocyte membranes (123,169). Standard HDI involves injecting a volume equivalent to 8-10% of the mouse's body weight within 5-8 seconds (280). Despite its effectiveness, HDI is stressful for mice and can cause significant liver damage. Moreover, the delivery of naked DNA has drawbacks, including degradation by intra- and extracellular enzymes and difficulties in crossing the plasma membrane because of its large, negatively charged sequences.

To mitigate these constraints, this study aimed to improve the delivery of anti-HBV TALENs by expressing them as mRNA encapsulated within cationic lipids for transfer into a non-humanised transgenic model (281). Although this model may not fully replicate cccDNA, it remains valuable for studying HBV replication. This work explores the delivery of TALEN-encoding mRNA targeting both the integrated HBV genome and rcDNA in murine hepatocytes. It also evaluates the efficacy of TALENs in inhibiting HBV replication *in vivo*.

4.2 Methods

4.2.1 *In vivo* assessment of TALEN-encoding mRNA for targeted inhibition of HBV replication

The TALEN-mediated suppression of viral replication was evaluated in the Friend leukaemia virus B (FVB) HBV transgenic mouse model (281). While these mice are typically susceptible to FVB infection, they were not infected with FVB for this study. Mice, weighing between 20 and 30 g, received injections into their tail veins. Transcripts from IVT #5 were used in murine experiments. All procedures adhered to protocols approved by the University of the Witwatersrand Animal Research Ethics Committee (**Appendix 6.7.3**). The mice were divided into three groups, (i) firefly luciferase/mCherry (FLuc/mCherry) "no TALEN" mock group (n=4), (ii) Core TALEN group (n=8), and (iii) Surface TALEN group (n=8). Each injection comprised 40 µg of mRNA in a total volume of 150 µl.

4.2.1.1 Formulating LNP-encapsulated RNA using microfluidics

LNPs were prepared using the NanoAssemblr® Ignite™ (Precision NanoSystems, Canada) with NxGen cartridges for microfluidic mixing. Initially, lipids were dissolved in ethanol and mixed at a final percent molar ratio of 50:10:38.5:1.5 for SM-102:DSPC:Cholesterol:DMG-PEG2000 (282). Fluc/mCherry and TALEN-encoding mRNAs were subsequently diluted in sodium acetate (6.25 mM, pH 5). The diluted lipids and mRNA were loaded into individual syringes and then connected to the NxGen cartridge in the NanoAssemblr Ignite machine. The solvent and aqueous phases were combined concurrently to produce LNPs encapsulating mRNA. The solvent phase, containing lipids, and the aqueous phase, containing mRNA, were introduced into the mixing system at a flow rate ratio of 3:1. The total flow rate for the combined phases was maintained at

12 ml/min. This approach ensured the precise mixing of lipids and mRNA, facilitating the formation of LNPs with optimal encapsulation efficiency.

LNPs were generated with a nitrogen-to-phosphorus (N/P) ratio of 6:1 (**Appendix 6.7.1**). The N/P was determined by dividing the moles of RNA by the desired ratio (e.g., for a 6:1 N/P, divide by 6) to ascertain the required moles of ionisable cationic lipid. Subsequently, the weight of the ionisable cationic lipid component was calculated. The final LNP formulation was diluted approximately 40-fold with 1 × PBS (pH 7.4) and concentrated using Amicon® Ultra-15 Centrifugal filters (100 kDa MWCO; Sigma-Aldrich, MO, USA). Centrifugation was performed in a swing bucket rotor at 1,000 × g for 10-15 minutes, with membrane washing between steps until the desired final volume was achieved. LNPs were finally filter sterilised using Acrodisc® Supor® membrane syringe filters (Pall Corporation, NY, USA).

For size and zeta potential measurements, LNPs were diluted 200-fold in nuclease-free water. Size measurements were performed using a clear rectangular cuvette in the ZetaSizer ZS Xplorer (Malvern Panalytical Ltd, UK) under default conditions (n=3 technical replicates). Zeta potential was measured in a cuvette with gold-plated electrodes using a 1 ml syringe in the ZetaSizer, also under default conditions (n=3 technical replicates). In summary, LNP formulations containing 20 µg each of left and right mRNA TALEN monomers (either Core TALENs or Surface TALENs) were administered in mice. A separate group received LNPs with 20 µg each of FLuc mRNA and mCherry mRNA as a mock control.

4.2.1.2 RNA quantification and encapsulation efficiency assessment

To determine the effective dose (concentration of encapsulated mRNA) and encapsulation efficiency (% of mRNA encapsulated by LNPs in the sample) the Quant-iT RiboGreen RNA Kit (Thermo Fisher Scientific, MA, USA) was employed. This assay measures unencapsulated RNA in the absence of a detergent, and total RNA following LNP lysis with Triton X-100. The assay was set up as described in the PNI Ribogreen® Assay Protocol (Precision NanoSystems, Canada). Briefly in a black 96-well plate (Thermo Fisher Scientific, MA, USA) 15 µl of the mRNA-LNP sample was diluted in 250 µl of 1× TE buffer, pH 7.5. A background with Triton X-100 was included to eliminate interference. Fifty microlitres of the diluted samples were further diluted in 50 µl of either TE buffer (pH 7.5) or Triton buffer (2% Triton X-100 in TE buffer). This process was duplicated. A standard curve was prepared using RNA of known concentrations (**Appendix 6.7.2**), incorporating Triton buffer to neutralise background interference from Triton X-100, thereby ensuring accurate quantification of total RNA in the sample after LNP lysis. The samples were then incubated at 37 °C for 10 minutes to lyse LNPs in the presence of Triton X-100 detergent. Ribogreen reagent (100 µl of a 1:100 dilution) was added to each well. Fluorescence was measured using the GloMax® Explorer (Promega, WI, USA) at excitations of 500-550 nm. Encapsulation efficiencies and effective mRNA concentrations were calculated using the following equations, where total RNA (µg/ml) was determined using the standard curve:

$$\text{Encapsulation Efficiency (\%)} = 1 - \left(\frac{\text{Fluorescence Value of RNA LNPs in the Absence of Lysis}}{\text{Fluorescence Value of RNA LNPs Lysed with Triton Buffer}}\right) \times 100$$

Effective Concentration (µg/ml) = Total RNA Concentration (µg/ml) × Encapsulation Efficiency (%)

4.2.1.3 Bioluminescence imaging

Mice were injected into their tail veins with LNPs encapsulating 20 µg each of FLuc mRNA and mCherry mRNA on day 0. To confirm effective delivery of LNPs, bioluminescence imaging was performed at 6 and 24 hours after injection using an IVIS Kinetic In Vivo Optical Imaging System (Perkin Elmer Inc., MA, USA). Briefly, mice were intraperitoneally administered 150 mg/kg of a 15 mg/ml D-luciferin solution (Perkin Elmer Inc., MA, USA) at 6 hours and again at 24 hours before imaging and placed in an induction chamber. Five percent isoflurane was used to anesthetise the mice, which were then transferred to the imaging chamber with an anaesthetic mask delivering 2% isoflurane. After imaging, the mice were returned to their cages. The region of interest (ROI) for each mouse was determined using Aura Imaging Software, and liver-specific luminescence was mapped based on luciferase radiance measurements (p/sec/cm²/sr).

4.2.1.4 ELISA

ELISAs were conducted on serum samples collected on days 1, 8, and 15 to assess HBsAg knockdown. Serum was diluted at a 1:4 ratio with saline, with 100 µl of the diluted sample used for the assay. The ELISA procedure was performed as detailed in Section **3.2.2**.

4.2.1.5 Quantification of HBV VPEs

Real-time qPCR was employed to quantify the number of VPEs in serum samples collected on day 15, which were diluted 1:8 with saline. Total DNA was extracted using the QIAamp DNA Mini Kit according to the manufacturer's instructions. The extracted DNA served as the template for qPCR analysis, with a standard curve generated from ten-fold serial dilutions of pCH-9/3091. The qPCR was conducted under the same cycling conditions as detailed in Section **3.2.1.2**.

4.2.1.6 Assessing HBV gene expression

To assess HBV gene expression total RNA was extracted from 100 mg of mouse liver. Liver sections were homogenised in 1 ml of TRIzol® Reagent (Thermo Fisher Scientific, CA, USA) and incubated at room temperature for 5 minutes. RNA was extracted following standard procedures. Briefly, the homogenates were centrifuged at 10,000 × g for 10 minutes at 4 °C to isolate the aqueous phase containing RNA. RNA was then precipitated with isopropanol, washed with ethanol, and resuspended in nuclease-free water. RNA purity and concentration were measured spectrophotometrically. Reverse transcription qPCR was performed using the Luna® Universal One-Step RT-qPCR Kit (New England Biolabs, NJ, USA). RNA was reverse transcribed to cDNA and subsequently quantified in the same reaction as follows: 1 µg of RNA, 1 µl 20 × Luna WarmStart® RT Enzyme Mix, 10 µl of Luna Universal One-Step Reaction Mix (2×), 0.4 µm forward and reverse primers for core, surface and murine *glyceraldehydes-3-phosphate dehydrogenase* (m*GAPDH*) (**Table 4.1)** and nuclease-free water up to 20 µl was mixed. The cycling conditions were as follows: reverse transcription to cDNA at 55 °C for 10 minutes, initial denaturing at 95 °C for 1 minute followed by 40 cycles of denaturing at 95 °C for 10 seconds, and elongation at 60 °C for 30 seconds, with a single SYBR® Green signal acquisition at this step. Lastly, the melting curve analysis was performed by denaturing DNA at 95 °C for 10 seconds, cooled to 65 °C for 5 minutes and then heated to 95 °C at a ramp rate of 0.5 °C/s with continuous SYBR® Green signal acquisition.

HBV surface mRNA and pgRNA were quantified relative to m*GAPDH* mRNA. HBV gene expression was normalised to m*GAPDH* expression, with relative amounts determined from Ct values.

Table 4.1: Primer sequences used to amplify the HBV *core* and *surface* genes and *mGAPDH* gene

Primer name	Primer sequence
HBV Core Forward	5'-ACC ACC AAA TGC CCC TAT-3'
HBV Core Reverse	5'-TTC TGC GAG CG GCG A-3'
mGAPDH Foward	5'-TTC ACC ACC ATG GAG AAG G-3'
mGAPDH Reverse	5'-GGC TGG ACT GTG GTC ATG A-3'

4.2.1.7 Assessing *in vivo* targeted cleavage by Sanger sequencing analysis

To evaluate targeted cleavage in murine samples, 25 mg of liver tissue was dissected, homogenised, and stored in 80 µL of PBS. Total DNA was extracted using the QIAamp DNA Mini Kit following the tissue protocol. PCR was used to amplify sequences of approximately 260 base pairs upstream and downstream of the target sites for the Core and Surface TALENs, with sequences from FLuc/mCherry treatment serving as a negative control. PCR was conducted as follows, 12.5 µL of 2× Master Mix (Taq DNA Polymerase Master Mix RED Kit, Ampliqon, Copenhagen, Denmark), 10 pmol of each forward and reverse primer (**Table 4.2**), 5 µl of extracted DNA, and 5.5 µl of distilled water. The subsequent amplification was performed using the Bio-Rad T100™ Thermal Cycler, employing the following cycling parameters: initial denaturation at 95 °C for 15 seconds, annealing at 60 °C for 15 seconds, extension at 72 °C for 15 seconds, final elongation at 72 °C for 5 minutes, followed by cooling to 4 °C. PCR products were resolved on a 1.5% agarose gel, purified using the QIAquick® Gel Extraction Kit according to the manufacturer's instructions, and eluted in 30 µL of distilled water. The purity and concentration of the DNA were then determined using spectrophotometry.

Table 4.2: Primer sequences employed to amplify potential TALE binding and cleavage regions for *C* and *S* ORFs.

Primer name	Primer sequence
Core Forward	5'-GAA CTA ATG ACT CTA GCT ACC T-3'
Core Reverse	5'-CCT ACA AAC TGT TCA CAT TT-3'
Surface Foward	5'-CCT AGG ACC CCT TCT CGT GT-3'
Surface Reverse	5'-ACT GAG CCA GGA GAA ACG GG-3'

The PCR amplicons were subjected to Sanger (automated capillary) sequencing on the ABI 3500XL Sequencer (Inqaba Biotech, PTA, South Africa). The resulting sequences were then aligned by Inqaba using QIAGEN CLC Main Workbench, utilising its assembly and alignment tools.

4.2.1.8 Assessing inflammatory response by cytometric bead array quantification

To evaluate whether LNP-encapsulated TALENs induced an inflammatory response, serum samples from mice were harvested. Mice were divided into five groups, each receiving a tail vein injection of either 100 µg polyinosinic:polycytidylic acid (Poly I:C, a synthetic dsRNA immune stimulant), 150 µl saline, 40 µg mCherry/FLuc, 40 µg Core TALENs, or 40 µg Surface TALENs. Each group comprised three mice, which were euthanised 6 hours after injection to harvest serum. Cytokine levels were measured using the Cytometric Bead Array (CBA) Mouse Kit (BD BioSciences, CA, USA), assessing six cytokines namely, interleukin (IL)-6, IL-12p70, Tumour necrosis factor (TNF), Interferon-gamma (IFN-γ), Monocyte Chemoattractant Protein-1 (MCP-1), and IL-10. The assay was performed in a 96-well V-bottom plate (Thermo Fisher Scientific, MA, USA). Lyophilised standards were reconstituted in 2 ml of assay diluent and incubated at room

temperature for 15 minutes, followed by serial dilutions. Bead populations corresponding to one cytokine were vortexed for 30 seconds and combined. Each sample required 10 µl of the combined six bead populations. Fifty microlitres of the bead mix were added to each well, followed by 50 µl of standards and 50 µl of undiluted serum samples. Subsequently, 50 µl of mouse inflammation phycoerythrin (PE) Detection Reagent were added. The plate was sealed, covered with foil, and placed on a plate shaker at 120 × g for 5 minutes before incubating at room temperature for 2 hours. After incubation, the plate was centrifuged at 200 × g for 5 minutes, and the supernatant was discarded by plate inversion. Excess supernatant was carefully aspirated. Each well was washed with 120 µl of wash buffer to resuspend the beads. The plate was covered and shaken as before. Acquisition was performed using the BD Accuri™ C6 flow cytometer (BD BioSciences, CA, USA), and the data was quantified using BD® CBA Analysis Software.

4.2.1.9 Assessing liver toxicity

Serum collected on day 15 was diluted at a ratio of 1:4 in PBS, and the activities of alanine aminotransferase (ALT) and aspartate aminotransferase (AST), both indicative of hepatotoxicity, were assessed. Analysis was conducted at the National Health Laboratory Services (NHLS) at the Charlotte Maxeke Academic Hospital (Johannesburg, South Africa) using an automated photometric analyser, the Advia 1800 Chemistry System (Siemens Healthineers, Erlangen, Germany).

4.2.2 Data analysis

All *in vivo* experiments were performed in triplicate. Relative light units, ALT, and AST analyses were plotted for individual mice. Statistical analysis, including the mean and standard error of the mean (SEM) were calculated as previously described in **3.2.4**.

4.3 Results

4.3.1 Tail vein injections of LNP-encapsulated TALEN-encoding mRNA

Core and Surface TALENs showed effective anti-HBV activity in cell culture models, leading to their selection for *in vivo* evaluation. TALEN-encoding mRNAs were encapsulated in iLNPs, which were characterised for size and charge before being injected into HBV transgenic mice (**Appendix 6.7.2**). For the experimental groups, the injection solutions contained equal amounts of left and right TALEN mRNA for both Core or Surface TALENs. Control groups received FLuc/mCherry mRNA. FLuc served as a reporter to assess hepatic delivery efficiency. The study spanned 15 days (**Figure 4.1**). Mice were injected on day 0 and blood samples were collected on days 1, 8, and 15 to evaluate anti-HBV effects and potential liver-induced toxicity. Liver samples were harvested on day 15 to assess HBV gene suppression and TALEN-mediated cleavage.

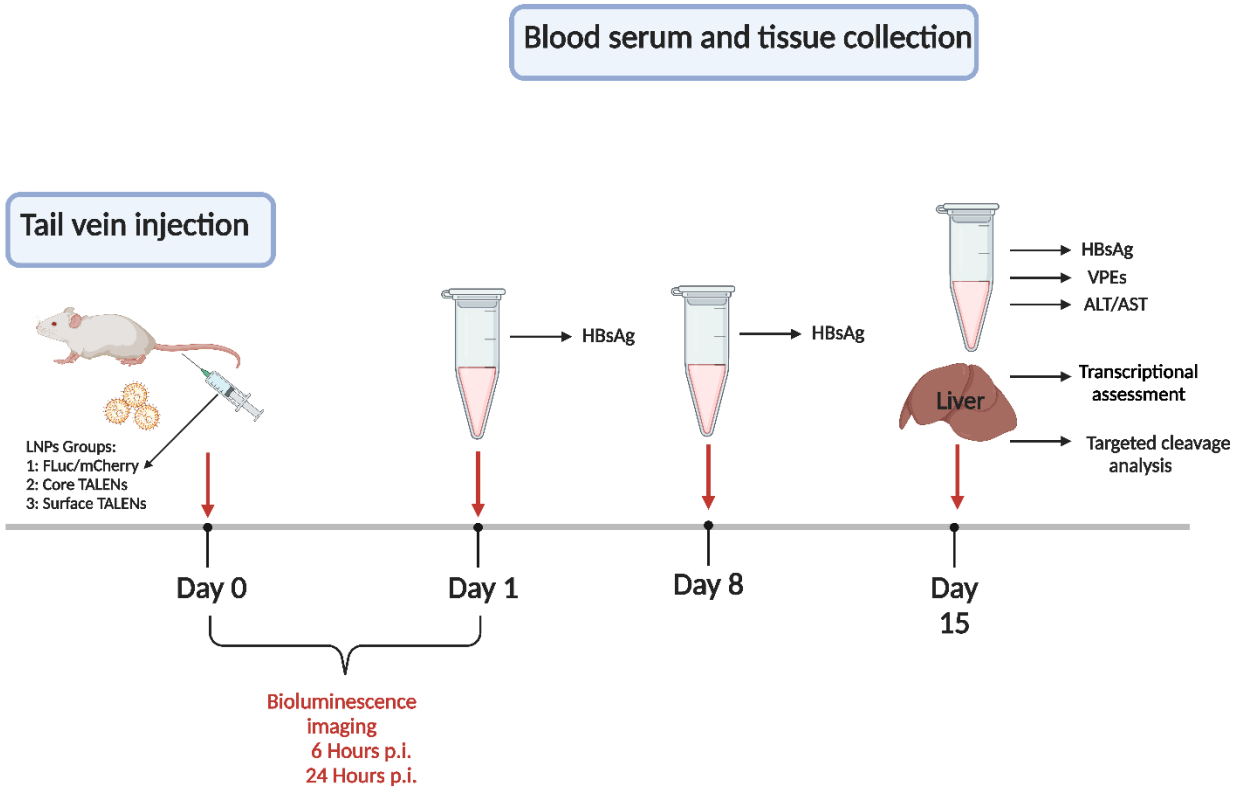


Figure 4.1: Experimental Timeline for TALEN-Treated Mice.

Mice were divided into three groups: FLuc/mCherry, Core TALENs and Surface TALENs. Bioluminescence imaging was performed on the FLuc/mCherry group at 6- and 24-hours post-injection. Blood samples were collected on days 1 and 8 to assess HBsAg levels and day 15 to assess HBsAg levels, VPEs and liver toxicity. On day 15, the mice were euthanised, and their livers were harvested to test HBV gene expression and targeted cleavage.

4.3.1.1 Successful hepatic delivery of LNP-encapsulated mRNA

To confirm the efficient delivery of LNP-encapsulated mRNA to the liver in the mouse model, bioluminescence imaging was performed at 6 and 24 hours after injection. LNP delivery efficiencies were assessed by measuring luciferase radiance, expressed as emitted relative light units, in each region of interest (ROI) (**Figure 4.2**). Bioluminescence was detected exclusively in the livers by 6 hours after injection and persisted at 24 hours with consistent mean luciferase radiance across the group. The successful hepatic delivery and expression of FLuc mRNA indicate that the LNPs are highly effective in delivering mRNA with tropism to hepatocytes. LNPs were shown to effectively protect mRNA from degradation, ensuring the stability and integrity of the mRNA during delivery. The use of ionisable lipids likely enhanced delivery efficiency by improving endosomal escape of encapsulated mRNA, ensuring it reaches the cytoplasm for translation. Efficient delivery is crucial for TALENs to reach liver target cells and effectively cleave the HBV genome.

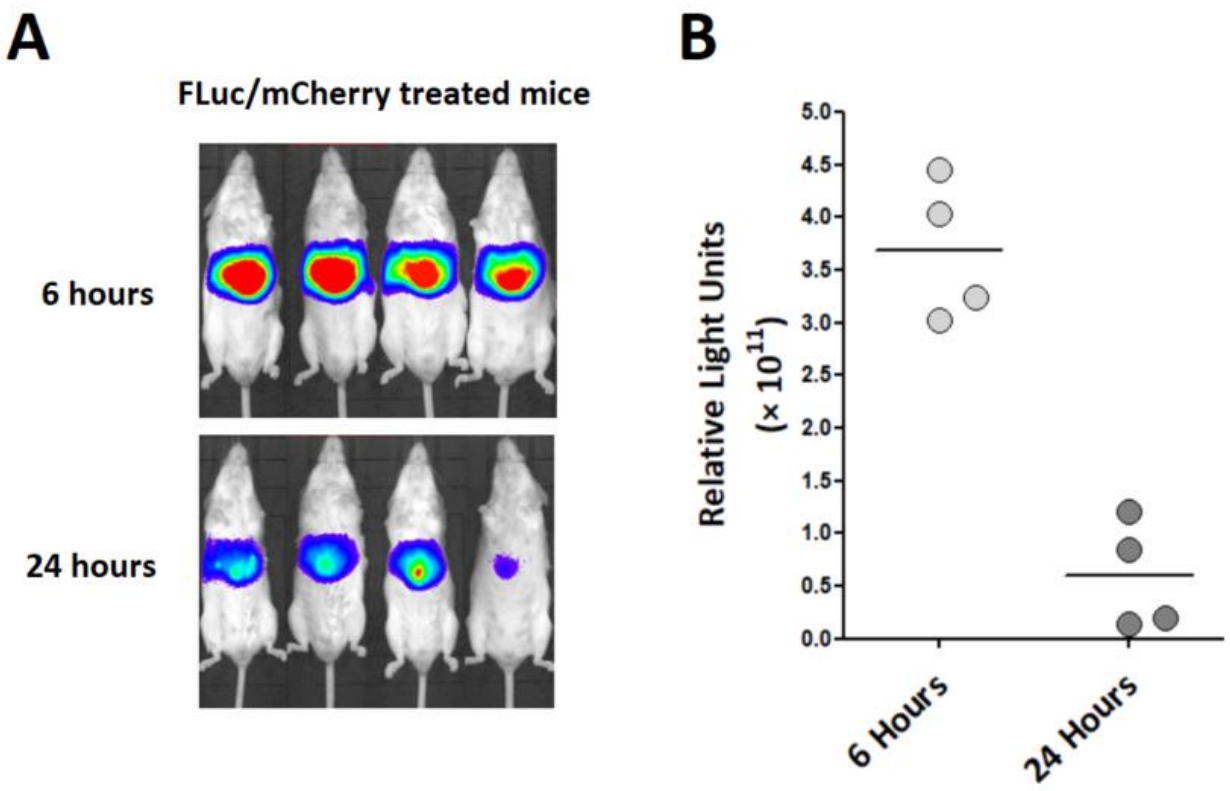


Figure 4.2: *In vivo* bioluminescence imaging of reporter gene expression in transgenic mice.

Mice were injected with LNPs containing FLuc and mCherry as a mock-treated group. Live imaging of firefly luciferase expression (bioluminescence) was performed on mice at two time points. Liver-specific delivery was detected in all mice. The relative light units emitted from the livers of injected mice were calculated, showing equivalent delivery efficiencies between mice. Data from individual mice is shown.

4.3.1.2 TALEN-induced knockdown of HBV replication *in vivo*

To evaluate TALEN-mediated inhibition of HBsAg secretion, transgenic mice were used. HBsAg levels in mock-treated mice were compared to their baseline secretion levels, while HBsAg levels in TALEN-treated mice were assessed relative to their own baseline levels. Core TALENs significantly reduced HBsAg levels by 49%, 63%, and 44% on days 1, 8, and 15, respectively (**Figure 4.3**). Surface TALENs also reduced HBsAg by 60%, 63%, and 43% on days 1, 8, and 15, respectively. In contrast, the mock-treated mice did not exhibit significant HBsAg knockdown at any time point, although a 25% decrease was observed on day 8. By day 15, HBsAg secretion levels in the mock-treated group had returned to baseline. Notably, Core and Surface TALEN-treated mice demonstrated the most substantial HBsAg reduction on day 8. HBsAg secretion in transgenic mice exhibited variability, which may account for the general decrease observed across all groups on this day. Despite an increase in HBsAg levels by day 15 relative to day 8, significant knockdown remained evident for TALEN-treated mice. Collectively, Core and Surface TALENs exhibited substantial inhibition of HBsAg secretion in transgenic mice which persisted through day 15, underscoring the therapeutic potential of these TALENs against HBV replication. Although Core TALENs were not expected to impact HBsAg levels directly, their observed effect may be indirect, as previously noted in cell culture (**Figures 3.4 and 3.5**).

To evaluate the direct impact of TALENs on HBV virion secretion, circulating viral particle equivalents (VPEs) were measured in serum samples collected on day 15 post-injection. Total DNA was extracted from these samples, and rcDNA was quantified using real-time qPCR. Both Core and Surface TALEN-treated mice demonstrated a remarkable >99% reduction in circulating VPEs compared to mock-treated mice (**Figure 4.4**). Core TALENs target the *core* ORF, inducing mutations that produce non-functional core proteins. These defective proteins cannot encapsidate

pgRNA, disrupting capsid assembly and thus preventing the formation of new virions. It is important to note that most circulating HBsAg is found in SVPs rather than virions. Therefore, the observed reduction in HBsAg secretion in Core TALEN-treated mice is likely an indirect effect. While Core TALENs primarily disrupt virion formation, this disruption may also reduce overall HBV replication, indirectly affecting SVP production and leading to the decrease in HBsAg levels. In contrast, Surface TALENs target the *surface* ORF, leading to a significant reduction in HBsAg, a crucial component for virion assembly. These findings indicate that both Core and Surface TALENs significantly inhibit hepatitis B virion secretion by disrupting key viral proteins necessary for virion production. This confirms the efficacy of TALENs as a therapeutic strategy to reduce HBV virion production and inactivate viral replication.

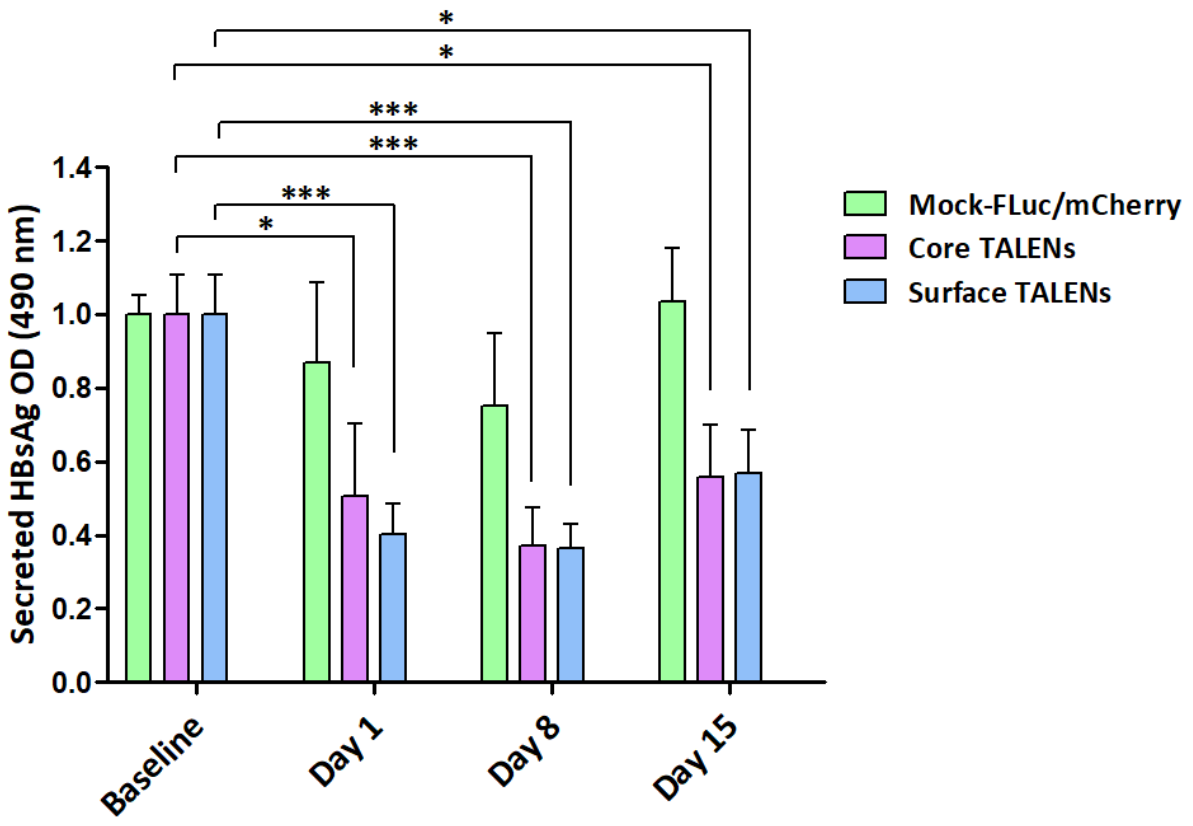


Figure 4.3: TALEN-mediated knockdown of HBsAg secretion in transgenic mice.

LNP-encapsulated Fluc/mCherry-encoding and TALEN-encoding mRNA were administered to HBV transgenic mice by tail vein injection. HBsAg secretion was measured from mice serum on day 1, 8 and 15 after injection. Data obtained from this assay were averaged and normalised to respective baseline ODs for each group. Error bars are indicative of the normalised SEM where n=4 (Mock), n=8 (Core TALEN-treated mice) and n=8 (Surface TALEN-treated mice) (**: $p<0.01$; ***: $p<0.001$).

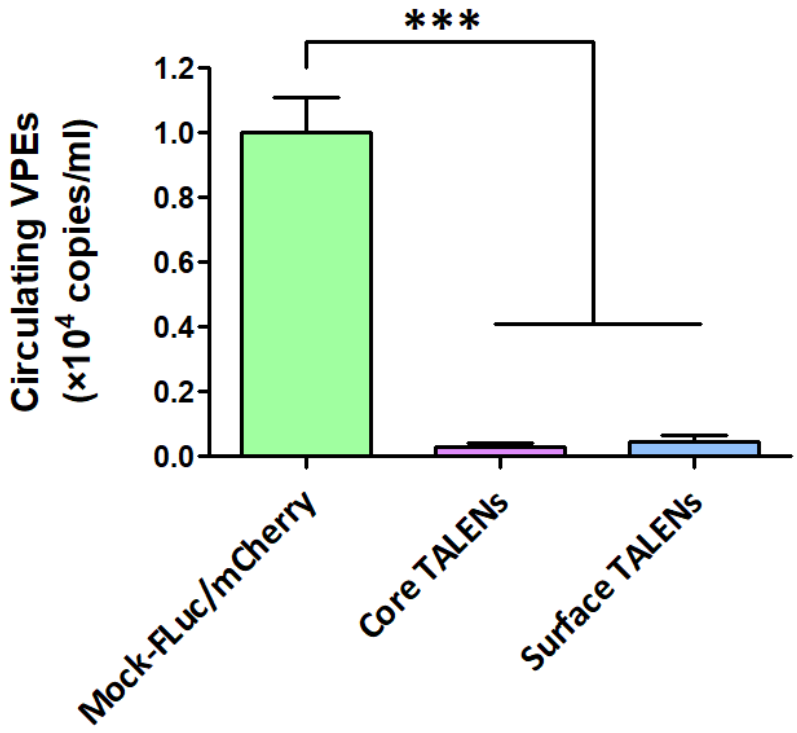


Figure 4.4: TALEN-mediated inhibition of viral replication.

rcDNA was quantified using real-time qPCR to measure circulating VPEs in serum samples from mice serum on day 15 after injection. Error bars are indicative of the normalised SEM where n=4 (Mock), n=8 (Core TALEN-treated mice) and n=8 (Surface TALEN-treated mice) (***: $p<0.001$).

4.3.1.3 TALENs do not mediate repression of HBV *core* and *surface* transcripts

To evaluate the impact of TALENs on HBV gene expression, RNA was extracted from liver samples of TALEN-treated mice and converted to cDNA. qPCR was performed to measure levels of *pgRNA* and HBV *surface* mRNA, with results normalised to *mGAPDH* expression. As expected, mice treated with Core and Surface TALENs did not affect HBV mRNA levels (**Figure 4.5**). This indicates that these TALENs are not inhibiting the transcription of HBV DNA. Instead, they induce mutations at the target sites, leading to truncated or aberrant protein production.

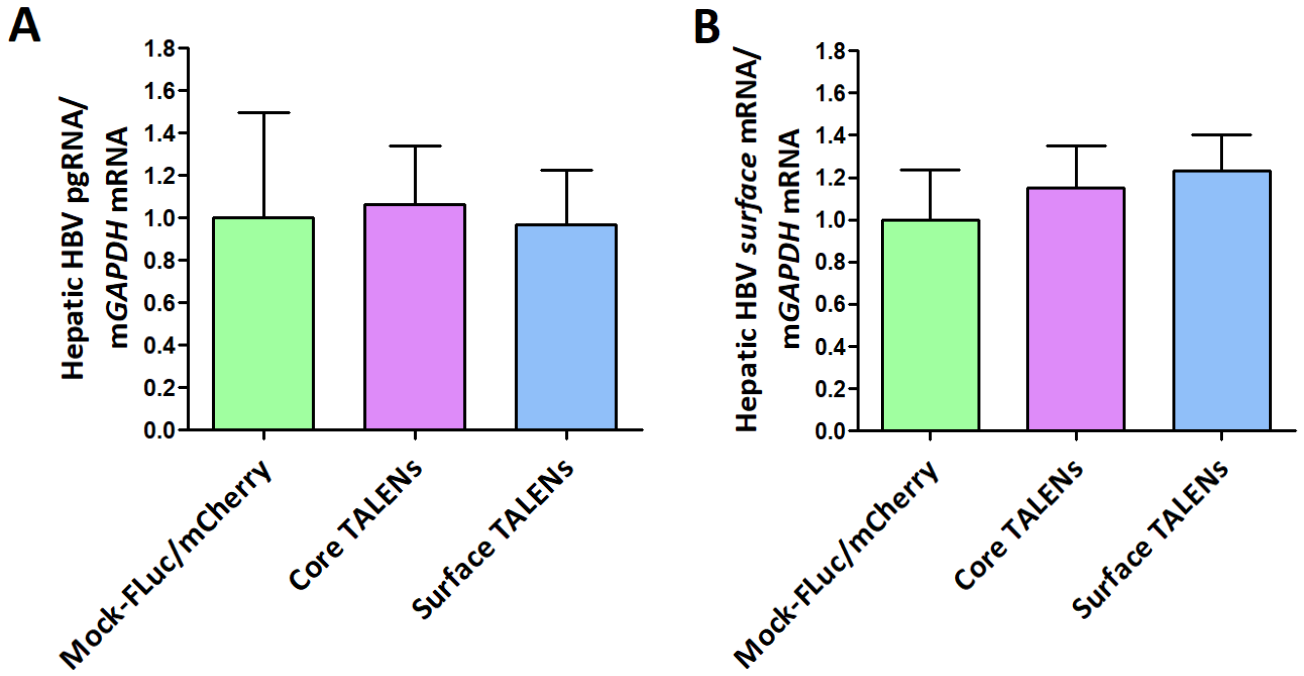
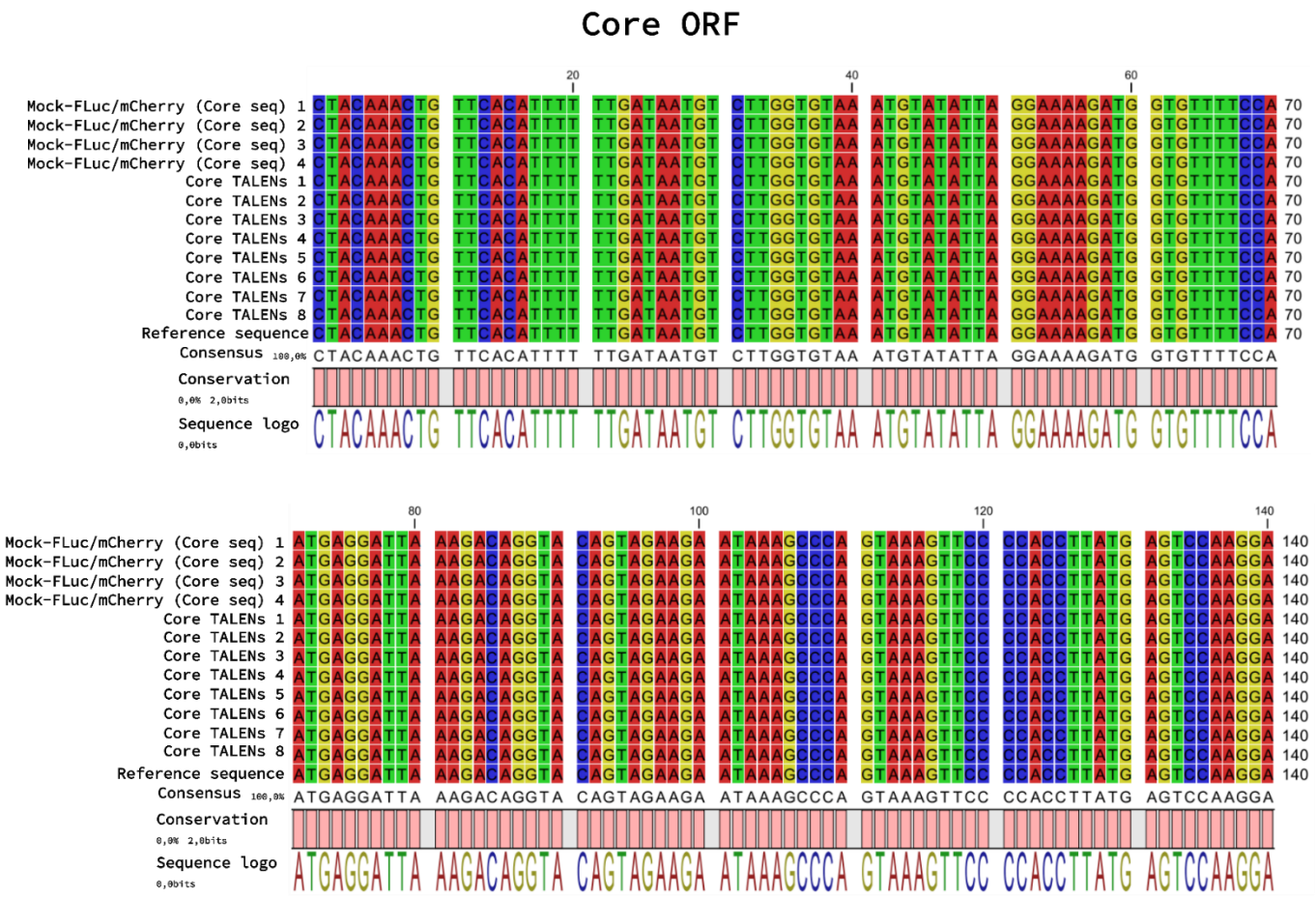


Figure 4.5: Core and Surface TALENs have no impact on hepatic HBV mRNA levels.

To measure HBV gene expression in TALEN-treated mice, HBV mRNA levels were measured from murine liver samples on day 15 post injection. **A.** pgRNA and **B.** *surface* mRNA levels were measured by qPCR and relativised to m*GAPDH* mRNA levels. Means were calculated and normalised to the mock group. Error bars are indicative of the normalised SEM where n=4 (Mock), n=8 (Core TALEN-treated mice) and n=8 (Surface TALEN-treated mice).

4.3.1.4 Sanger sequencing of target sites

To confirm that TALENs caused targeted disruption within the HBV genome, DNA was extracted from liver samples collected on day 15 post-injection. The specific target sites of the TALENs were amplified by PCR to assess whether the intended gene editing had occurred. The resulting PCR amplicons were then analysed using Sanger sequencing to identify possible INDELs that would indicate successful disruption of the target sites. Amplicons were carefully examined using QIAGEN CLC Main Workbench to detect deviations from the expected reference sequence, which would manifest as INDELs. However, despite thorough analysis, no evidence of targeted disruption was observed in the liver samples of the mice treated with TALENs and suggests that mutated sequences were not amplified (**Figure 4.6**). PCR amplification can introduce bias, favouring certain sequences over others. If the mutated sequences were less efficiently amplified because of this bias, they may have been underrepresented in the final PCR product, leading to an apparent lack of INDELs. Further investigation is warranted for the detection of INDELs.


Core ORF
Mock-FLuc/mCherry (Core seq) 1
Mock-FLuc/mCherry (Core seq) 2
Mock-FLuc/mCherry (Core seq) 3
Mock-FLuc/mCherry (Core seq) 4
Core TALENs 1
Core TALENs 2
Core TALENs 3
Core TALENs 4
Core TALENs 5
Core TALENs 6
Core TALENs 7
Core TALENs 8
Reference sequence
Consensus
Conservation
Sequence logo
CTACAAACTG TTCACATTTT TTGATAATGT CTTGGTGTAA ATGTATATTA GGAAAAGATG GTGTTTTCCA
ATGAGGATTA AAGACAGGTA CAGTAGAAGA ATAAAGCCCA GTAAAGTTCC CCACCTTATG AGTCCAAGGA

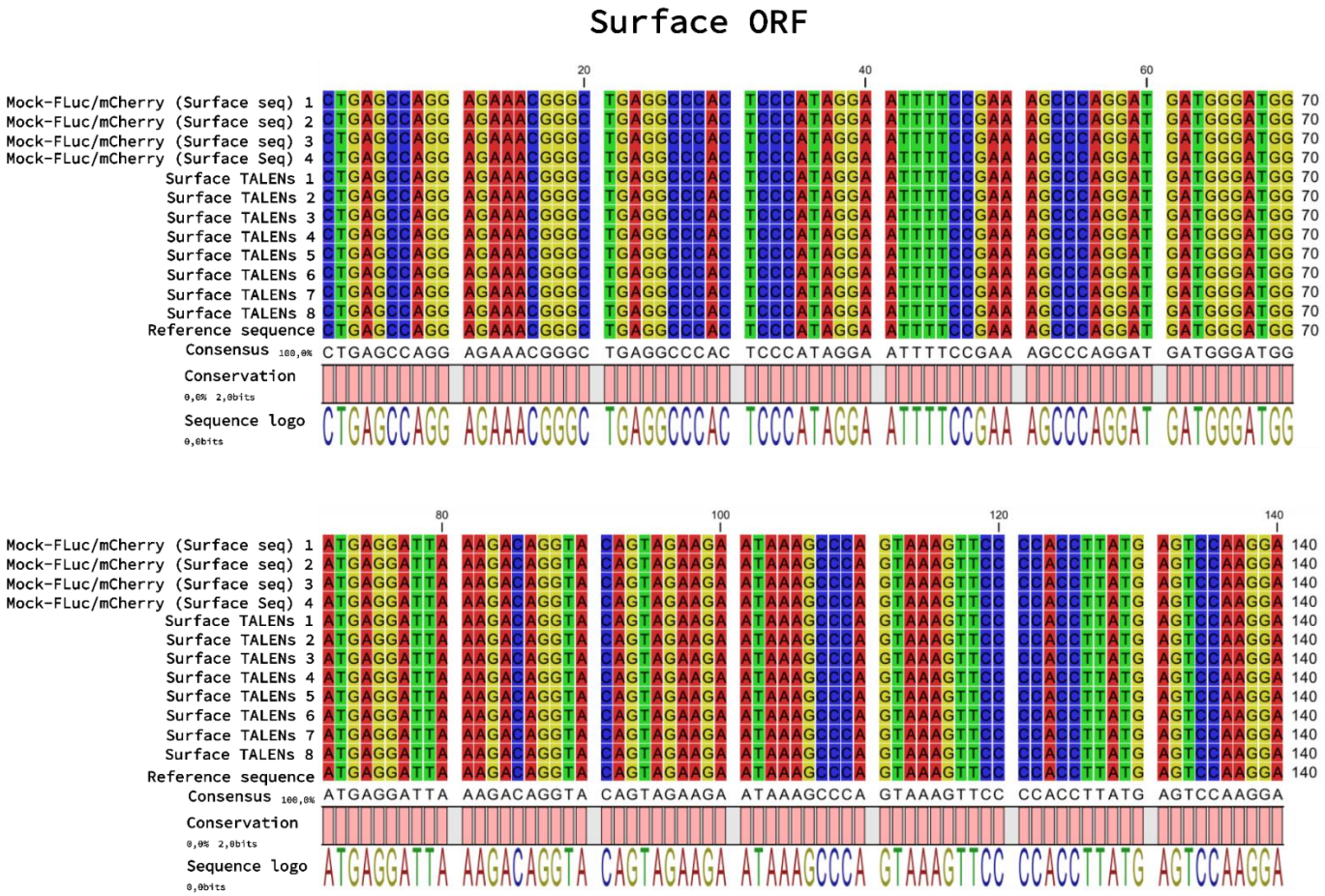


Figure 4.6: Sanger Sequencing alignment fails to demonstrate site-directed mutagenesis.

Intrahepatic HBV-encoding DNA was extracted from liver samples, amplified by PCR, and analysed using Sanger sequencing. Representative sequences (1-140 bases) from the Core ORF (top) and Surface ORF (bottom) were aligned with the reference sequence. No differences were observed between the reference sequence and sequences derived from mice treated with TALENs.

4.3.1.5 LNP-encapsulated TALENs demonstrate minimal inflammatory response and absence of liver toxicity

The administration of TALENs *in vivo* carries the potential risk of cytotoxicity resulting from unintended DSBs. To assess the safety of TALENs, secreted pro-inflammatory cytokines and liver enzymes were measured as indicators of toxicity. The concentration of IL-12p70, IFN-γ, TNF, MCP-1, IL-10, and IL-6 were evaluated 6 hours post-administration of either LNP-encapsulated FLuc/mCherry or LNP-encapsulated TALENs using the CBA assay (**Figure 4.7**). Saline was used as the negative control while Poly I:C served as the positive control. As expected, Poly I:C significantly increased the concentrations of TNF, MCP-1, and IL-6, and caused a substantial but non-significant increase in IL-10 compared to saline. Unexpectedly Poly I:C resulted in lower concentrations of IL-12p70 and IFN-γ than saline. While LNP-encapsulated TALENs resulted in elevated levels of IL-12p70, IFN-γ, IL-6, and MCP-1 compared to saline, these increases were not statistically significant. The notable rise in MCP-1 is expected, given its key role as one of the earliest and most abundantly expressed chemokines during inflammatory responses (283,284), its elevation in treated mice is unsurprising. However, LNP-encapsulated FLuc/mCherry triggered significant increases in IFN-γ, TNF, MCP-1, and IL-6 compared to saline which is likely attributable to the LNPs themselves rather than the mRNA, as LNP-encapsulated TALENs did not significantly elevate any measured cytokines.

On day 15, serum was collected, and ALT and AST levels—markers of liver damage—were found to be comparable between mock and TALEN-treated mice, remaining within normal thresholds. This suggests that TALENs did not cause significant liver toxicity (**Figure 4.8**).

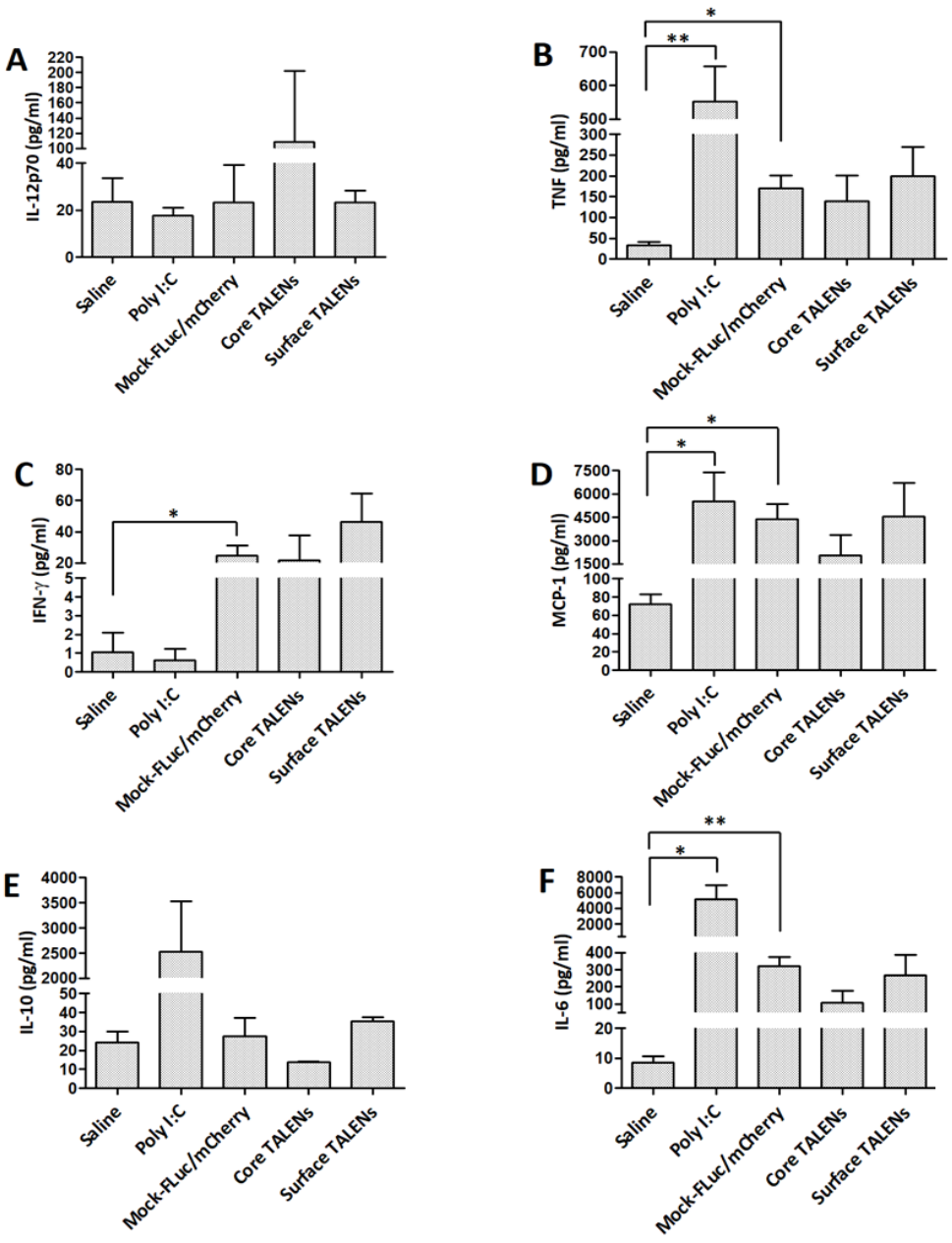


Figure 4.7: LNP-encapsulated TALENs did not illicit significant cytokine induction in transgenic mice.

Serum cytokine levels **A.** IL-12p70, **B.** IFN-γ, **C.** TNF, **D.** MCP-1, **E.** IL-10, and **F.** IL-6 were measured 6 hours after injection. Saline served as the negative control. Data are presented as averages with error bars representing the standard error of the mean (SEM) calculated from three mice per group (*: $p<0.05$, **: $p<0.01$).

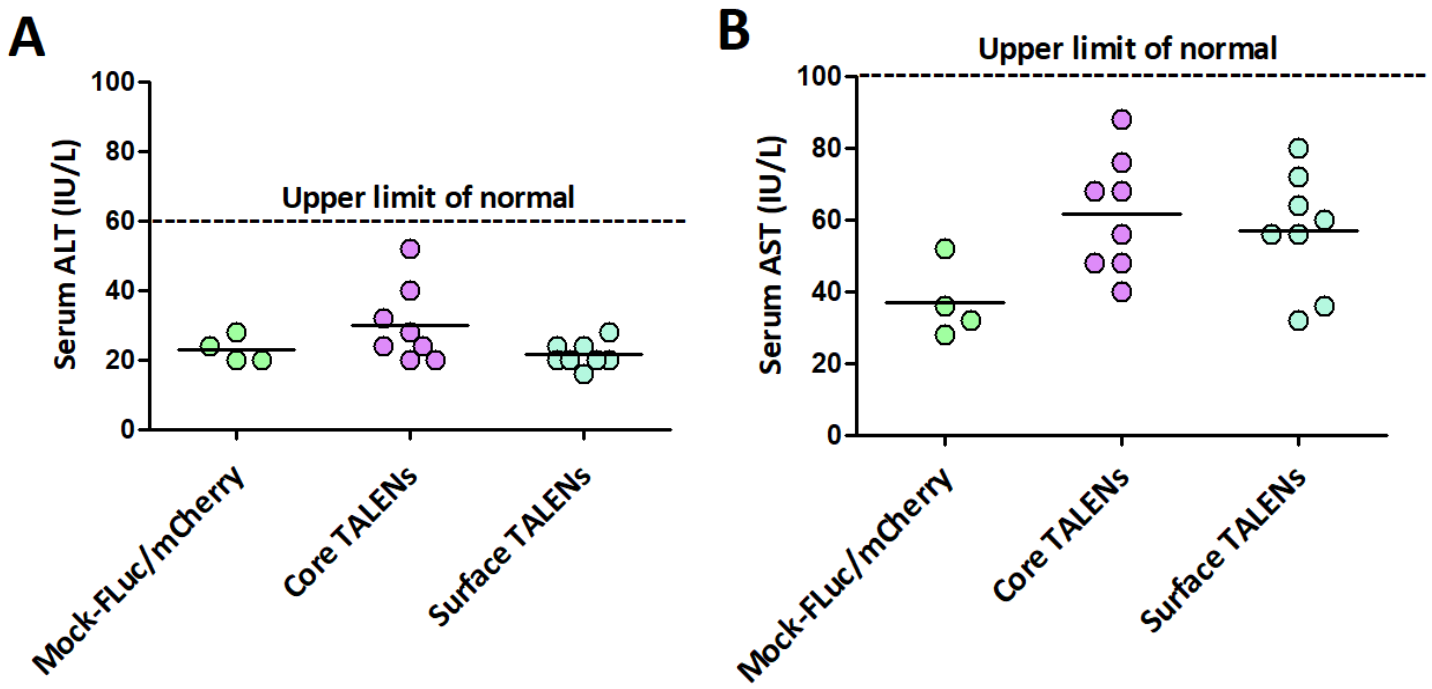


Figure 4.8: Absence of hepatic toxicity in transgenic mice.

A. Serum alanine transaminase (ALT) and **B.** aspartate aminotransferase (AST) activity was measured in mock and TALEN-treated mice 15 days after injection. Markers of hepatotoxicity were not elevated. Data of serum samples from individual mice are shown. Horizontal bars depict mean values.

4.4 Discussion

The use of animal models is pivotal for validating and refining therapeutic strategies before transitioning to human clinical trials. In this study, LNP-encapsulated TALEN-encoding mRNA was administered via tail vein injections in HBV transgenic mice. The engineered obligate heterodimeric TALENs, specifically designed to target the *C* and *S* ORFs of HBV, resulted in significant reductions in HBsAg levels and circulating VPEs.

The observed reduction in HBsAg levels after TALEN treatment did not match the nearly 100% reduction in VPEs, which may be attributed to several factors. HBsAg detection includes both infectious and non-infectious SVPs, with SVPs potentially obscuring reductions in viral replication. The antigen response may lag actual viral suppression, and the rates of HBsAg release and clearance might not immediately reflect changes in viral load. Variability in assay sensitivity and measurement techniques also plays a role; for instance, qPCR for measuring VPEs provides a more quantitative measure compared to the semi-quantitative ELISA used for measuring HBsAg secretion. Despite this, a major reduction in VPEs indicates a significant decrease in the number of infectious particles, which directly affects the potential for virus transmission and persistence.

To directly evaluate the influence of targeted mutagenesis on viral gene expression, intrahepatic HBV mRNA levels were quantified using reverse transcription qPCR. TALENs, which induce disruptive mutations in target sequences, typically do not affect transcription unless they specifically target promoter or enhancer regions. Previous studies showed that ZFPs targeting the enhancer region regulating core and small surface protein expression also unexpectedly reduced levels of large surface proteins (285). Similarly, another study reported suppression of HBsAg secretion by a TALEN targeting the *P* ORF of HBV, suggesting transcriptional interference as a mechanism (123). However, the Core TALENs used in this study do not target transcriptional

regulation domains, indicating that the observed reduction in HBsAg is caused by another mechanism. Despite not being designed to target surface proteins, Core TALEN treatment resulted in a significant reduction in HBsAg in mice, consistent with previous studies where TALENs targeting the *C* ORF led to similar reductions in HBsAg (123,169). Moreover, the significant decrease in VPEs induced by Core TALENs likely contributes to the reduced HBsAg levels, as Core TALENs impede new virion assembly, a pivotal process for the self-assembly of capsid structure.

A key challenge in gene therapy is avoiding cytotoxicity from exogenous nucleic acids. LNPs were formulated with SM-102, a lipid with hepatotropic properties, to ensure targeted delivery of TALENs to hepatocytes. SM-102 enables LNPs to preferentially accumulate in the liver, enhancing the precision of TALEN delivery and reducing off-target effects in other organs. This liver-specific targeting improves the overall safety profile of the treatment.

Previous studies have demonstrated that TALENs typically exhibit low cytotoxicity (123,166,169). This study represents the first investigation into the immune response to LNP-encapsulated TALEN-encoding mRNA, which did not significantly increase the concentrations of any measured cytokines. The lack of a significant immune response may be attributed to mRNA modifications, such as the incorporation of the Cap-1 structure with CleanCap® AG and the modified nucleotide m1Ψ, which enhance translation and help the RNA evade immune detection.

Although SM-102 is effective in delivering mRNA within LNP formulations, it has been associated with potential proinflammatory responses through mechanisms such as immune activation, cellular stress, and inflammasome activation (reviewed in (286)). LNPs containing FLuc/mCherry mRNA caused significant increases in levels of IFN-γ, TNF, MCP-1, and IL-6. This inflammatory response may stem from the adjuvant-like effects of LNPs with SM-102, which can trigger mild

inflammation upon recognition by the immune system. Although this feature is beneficial for vaccines, it may be less suitable for gene therapy, where minimising immune activation is crucial. Evidence from preclinical (287) and clinical studies (288) indicates that while SM-102 facilitates mRNA delivery effectively, it also contributes to transient inflammatory responses. Continued research and careful evaluation of these inflammatory effects are crucial for optimising the safety and efficacy of LNP-based therapeutics and vaccines. Strategies to reduce the immunogenicity of in-house cationic lipids in LNP formulations include optimising lipid composition, modifying surface chemistry, refining lipid structure, incorporating immunosuppressive agents, ensuring manufacturing purity, and conducting comprehensive immunogenicity testing. These approaches will enhance the safety profile and therapeutic effectiveness of mRNA-based treatments. ALT and AST levels, markers of liver function, showed no significant increase in TALEN-treated samples, indicating minimal cytotoxicity and off-target effects. These results support the potential of TALENs as a gene therapy tool with a favourable safety profile, further studies with larger sample sizes are needed to confirm these findings and optimise LNP formulations.

Sanger sequencing, while cost-effective and relatively straightforward for analysing targeted sequences, is limited in its ability to detect low-frequency mutations or small INDELs. Low-frequency variants, such as INDELs introduced by TALENs, may go undetected due to the generation of consensus sequences that reflect only the most prevalent sequences, thereby masking rare mutations critical for gene editing. This can occur if the consensus sequences do not capture these minor variations. To mitigate PCR bias, using methods like digital droplet PCR or next-generation sequencing (NGS) can provide a more accurate representation of sequence variations. Platforms such as Illumina MiSeq or Ion Torrent offer high coverage and can identify rare variants among wild-type sequences. Additionally, reanalysing raw sequencing data without consensus

sequence generation may help identify low-frequency INDELs. Investigating HBV transcript expression through single-cell RNA sequencing could determine if TALENs impact only a subset of cells, providing insight into whether the absence of observed INDELs results from incomplete genome disruption. Finally, sampling at multiple time points post-injection can elucidate the kinetics of TALEN activity and potential delayed effects. Despite the reduction in HBsAg and VPE levels suggesting a biological effect from TALENs, this may not solely stem from detectable INDEL formation. This underscores the necessity for advanced methods to capture the full range of TALEN-induced modifications. Utilising targeted NGS with high coverage could yield deeper insights into these genetic changes and confirm low-frequency mutations that might influence observed outcomes.

The observed reduction in HBsAg levels lasted up to 15 days after a single TALEN dose. A key benefit of using mRNA is its short half-life, which is advantageous for TALEN delivery. The transient expression of TALENs enables the induction of permanent mutations while minimising off-target effects that can arise from prolonged exposure to designer nucleases. In contrast, DNA-based delivery can result in prolonged-expression and increased off-target effects. Recent improvements in mRNA technology, including cap and nucleotide modifications, support its continued use in therapeutic applications. This foundational research provides a critical framework for translation into the clinical application of TALENs in the management of HBV infection.

Chapter 5- Conclusion

This study highlights the potential of TALENs as a promising therapeutic strategy for chronic HBV infection. Current antiviral therapies are ineffective in achieving a cure because of the persistence of cccDNA in infected hepatocytes, which serves as a reservoir for viral replication. Designer nucleases address this challenge by targeting conserved regions of the HBV genome, disrupting cccDNA and significantly reducing viral load.

In this study, obligate heterodimeric TALEN-encoding mRNA was developed and used to transfect liver-derived cells, resulting in significant reductions in HBsAg levels across various cell culture models, with no cytotoxic effects observed. The enhanced efficacy observed with TALENs featuring the CleanCap® AG analogue and modified nucleotide m1Ψ underscores the importance of optimising mRNA design for therapeutic use. Additionally, the administration of LNP-encapsulated TALEN mRNA in a transgenic murine model of HBV replication led to significant reductions in viral markers without inducing liver toxicity or inflammatory response, confirming the safety and efficacy of this approach.

Despite these promising findings, further research is required to fully realise the clinical potential of TALENs. Future investigations should prioritise the following:

- Examining cccDNA in more relevant models: The transgenic murine model used in this study offered valuable insights into TALEN efficacy and demonstrated TALEN-mediated disruption of integrated HBV sequences. However, to better validate these findings, models that more accurately replicate human cccDNA dynamics, such as human liver organoids, should be explored. This is crucial for understanding interactions observed in patients with HBV-related HCC.

- Optimising mRNA production and delivery: Advancing the production of Good Manufacturing Practice (GMP)-grade mRNA and refining LNP delivery systems to reduce immunogenicity will be crucial for transitioning TALENs from research to clinical practice.
- Translation to clinical trials: Advancing TALEN-based therapies to clinical trials in South Africa involves several key steps. Initial preclinical validation ensures the safety and efficacy of TALEN treatment, with NGS recommended to assess both on-target and potential off-target effects. Key steps include obtaining regulatory approval from the South African Health Products Regulatory Authority (SAHPRA) by submitting comprehensive preclinical data and clinical trial designs. GMP-grade manufacturing of TALEN-encoding mRNA is essential, with facilities such as Afrigen Biologics & Vaccines providing this capability. The trial protocol must receive ethical approval from the South African Medical Research Council and local ethics committees. Recruitment and trial execution should adhere to local standards, ensuring participant safety. Data analysis and reporting are followed by submitting a New Drug Application to SAHPRA for market approval. Finally, post-marketing surveillance will then monitor the therapy's long-term safety and efficacy, ensuring it meets regulatory, ethical, and healthcare standards.

In conclusion, this study demonstrated that TALEN-encoding mRNA targeting the *core* and *surface* ORFs effectively inactivated hepatitis B viral replication in cell culture models. Furthermore, these TALENs disrupted viral protein production and inhibited replication in a stringent transgenic murine model of HBV replication, with no significant hepatotoxicity observed. This research represents a pioneering demonstration of TALEN efficacy when delivered as mRNA, offering a promising approach for treating chronic HBV infection.

Chapter 6-Appendix

6.1 Standard protocols, buffers and solutions for laboratory use

6.1.1 Preparation of $CaCl_2$ chemically competent bacterial cells

Materials:

- XL10-Gold® Ultracompetent *Escherichia coli* (*E. coli*) cells (Agilent Technologies, CA, USA)
- Luria Bertani medium: The medium was prepared by dissolving 10 g of Tryptone (Oxoid Ltd, Hampshire, England), 5 g of Yeast Extract (Oxoid Ltd, Hampshire, England), and 5 g of sodium chloride in one litre of distilled water. It was then autoclaved at 121 °C and 1 kg/cm² for 20 minutes. After autoclaving, the medium was stored at room temperature.
- Transformation buffer: Transformation buffer was made by adding 100 millimoles (mmol) of $CaCl_2.2H_2O$ (Sigma-Aldrich, MO, USA), 10 mmol of piperazine-N,N′-bis(2-ethanesulphonic acid) (PIPES) (Sigma-Aldrich, MO, USA), and 15 ml of glycerol into 100 ml of distilled water (pH 7) and autoclaved as above. The buffer was stored at -20 °C.

Protocol: Ten millilitres of Luria Bertani medium was inoculated with 20 µl of *E. coli* and incubated overnight at 37 °C in a shaking incubator. After incubation, the bacterial culture was transferred to 150 ml of fresh Luria Bertani medium and further incubated at 37 °C for 4 hours with shaking. Subsequently, the bacterial culture was centrifuged at 2,000 × g for 25 minutes at 4 °C. The supernatant was then removed, and the pellet was resuspended in 1 ml of transformation buffer. The volume was adjusted to 35 ml with transformation buffer, and the mixture was incubated on ice for 30 minutes. After incubation, the mixture was centrifuged for 10 minutes at 1,000 × g at 4 °C. The supernatant was discarded, and the pellet was reconstituted in a final volume

of 2 ml of transformation buffer. Chemically competent bacteria were aliquoted into 100 µl working stocks and stored at -80 °C.

6.1.2 Denaturing RNA formaldehyde agarose gel (1%)

Materials:

- 10 × 3-(N-morpholino) propanesulphonic acid (MOPS) buffer: MOPS buffer was made by adding 0.2 moles of MOPS (Sigma-Aldrich, MO, USA), 50 mmol sodium acetate, and 10 mmol ethylenediamine tetraacetic acid (EDTA) into one litre of distilled water. The pH of this solution was adjusted to 7 and autoclaved as described above.
- 32% Formaldehyde solution

Protocol: One gram of agarose powder was added to 72 ml of distilled water and heated in a microwave until the agarose dissolved completely. Once melted, the agarose solution was cooled to 60 °C. Following this, 10 ml of 10 × MOPS Buffer was added, followed immediately by 18 ml of 32% formaldehyde solution. The resulting liquid gel was poured into a casting tray and allowed to solidify at room temperature. RNA samples were then heat-denatured at 95 °C for 5 minutes and loaded into the gel. The gel, placed in a casting chamber with 1 × MOPS buffer, was set to run at 80 V for 40 minutes.

6.1.3 Viral precipitation solution [5 × polyethylene glycol (PEG) 8000]

- 5 × PEG was made by adding 250 g of PEG 8000 (Sigma-Aldrich, MO, USA), 57.5 g of sodium chloride and distilled water up to 500 ml. The solution was sterilised by autoclaving and stored at 37 °C.

6.1.4 Cellulose chromatography buffer preparation

- Chromatography buffer: Buffer was made by adding 10 mmol of HEPES (pH 7.2), 0.1 mmol of EDTA, 125 mmol of sodium chloride and 80 ml of 16% (v/v) ethanol up to 500 ml of autoclaved distilled water.

6.2 Mammalian cell culture growth and maintenance

6.2.1 Huh7 cells

Human hepatoma (Huh7) cells were cultured in Nunc™ EasYFlask™ 75 cm^2 cell culture flasks (Thermo Fisher Scientific, CA, USA) using low-glucose (1 g/L) Gibco™ Dulbecco's Modified Eagle's Medium (DMEM) (Thermo Fisher Scientific, CA, USA). The medium was supplemented with 10% heat-inactivated foetal bovine serum (FBS) (Sigma-Aldrich, MO, USA), penicillin (100 U/ml), and streptomycin (100 µg/ml). Cells were incubated at 37 °C in a 5% CO_2 atmosphere and subcultured when they reached 90-100% confluence. For cell subculturing, the cells were rinsed with 5 ml of saline containing 0.01% EDTA and then incubated at 37 °C for 10 minutes in 10 ml of the same saline solution. Following the saline treatment, the cells were exposed to 3 ml of 1× TrypLE™ Express (Thermo Fisher Scientific, CA, USA) for 3 minutes to facilitate detachment of adherent cells, with gentle agitation used to aid in the process. TrypLE™ Express functions by breaking peptide bonds at the C-terminal sides of lysine and arginine residues, serving as an effective substitute for trypsin. After detachment, an equal volume of fresh low-glucose medium was added to deactivate the TrypLE™ Express. The cells were gently resuspended and transferred to a sterile tube for centrifugation at 200 × g for 3 minutes. Following centrifugation, the supernatant was discarded, and the cell pellet was resuspended in 15 ml of fresh medium. These

cells were subsequently cultured in tissue culture dishes and maintained under the same conditions until the next passage.

6.2.2 HepG2-hNTCP-C4 cells

HepG2-hNTCP-C4 cells obtained from the National Institute of Infectious Diseases (Tokyo, Japan) (248) were cultured in 75 cm^2 flasks using DMEM/F12 with GlutaMAX™ (Thermo Fisher Scientific, CA, USA). The medium was supplemented with 10% FBS, penicillin (200 U/ml), streptomycin (200 µg/ml), 10 mM HEPES, 50 mM hydrocortisone, insulin (5µg/ml) and G418 (400 µg/ml). Cells were incubated and subcultured as described in 5.1.4.1.

6.2.3 HepG2.2.15 cells

HepG2.2.15 cells were cultured in 75 cm^2 flasks using normal glucose DMEM (Thermo Fisher Scientific, CA, USA) supplemented with 10% FBS, penicillin (100 U/ml) and streptomycin (100 µg/ml). Cells were incubated and subcultured as described in 5.1.4.1.

6.2.4 Coating plates with collagen

In a 24-well plate, 10 µg/ml of Collagen I from rat tail (Thermo Fisher Scientific, CA, USA) was diluted in 20 mM acetic acid. Approximately 250 µl of the collagen solution was added to each well and incubated at room temperature in a Laminar Flow hood for at least 1 hour. The solution was aspirated and the wells were rinsed 3 times with 1 × PBS to remove the acid. Plates were then immediately used for downstream applications. An example of cells at 30% confluency is demonstrated below (**Figure 6.1**).

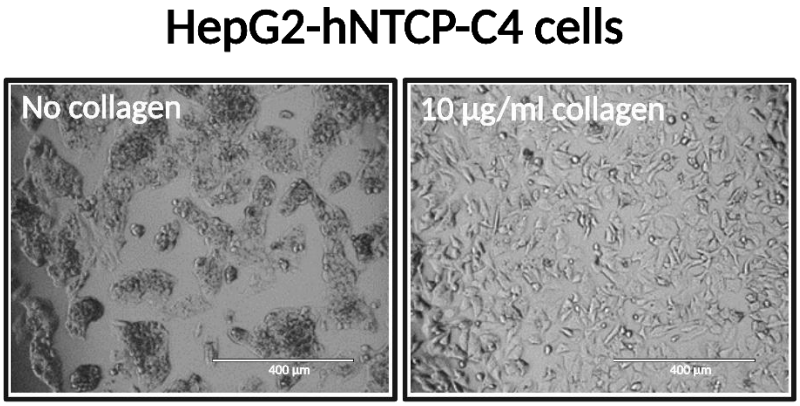


Figure 6.1: Treating culture plates with collagen enhances HepG2-hNTCP-C4 growth.

Cells grown in the absence of collagen form clumps with sparse growth, whereas cells treated with collagen form a monolayer.

6.3 TALEN DNA binding domain sequences:

Table 6.1: TALE RVDs for Core TALENs

Core TALEs (from 2319-2370 bp relative to the HBV genome)			
Left TALE DBD sequence	**DNA base**	**Right TALE DBD sequence**	**DNA base**
LTPDQVVAIAS**NI**GGKQALETVQRLLPVLCQAHG	A	LTPDQVVAIAS**NI**GGKQALETVQRLLPVLCQAHG	A
LIPQQVVAIAS**NG**GGKQALETVQRLLPVLCQDHG	T	LTPEQVVAIAS**NN**GGKQALETVQRLLPVLCQAHG	G
LTPEQVVAIAS**HD**GGKQALETVQALLPVLCQAHG	C	LTPEQVVAIAS**NN**GGKQALETVQRLLPVLCQAHG	G
LTPDQVVAIAS**NI**GGKQALETVQRLLPVLCQAHG	A	LTPEQVVAIAS**NN**GGKQALETVQRLLPVLCQAHG	G
LTPDQVVAIAS**NI**GGKQALETVQRLLPVLCQAHG	A	LTPEQVVAIAS**NN**GGKQALETVQRLLPVLCQAHG	G
LTPEQVVAIAS**HD**GGKQALETVQALLPVLCQAHG	C	LTPDQVVAIAS**NI**GGKQALETVQRLLPVLCQAHG	A
LTPDQVVAIAS**NI**GGKQALETVQRLLPVLCQAHG	A	LTPEQVVAIAS**HD**GGKQALETVQALLPVLCQAHG	C
LTPEQVVAIAS**HD**GGKQALETVQALLPVLCQAHG	C	LTPEQVVAIAS**HD**GGKQALETVQALLPVLCQAHG	C
LIPQQVVAIAS**NG**GGKQALETVQRLLPVLCQDHG	T	LIPQQVVAIAS**NG**GGKQALETVQRLLPVLCQDHG	T
LIPQQVVAIAS**NG**GGKQALETVQRLLPVLCQDHG	T	LTPEQVVAIAS**NN**GGKQALETVQRLLPVLCQAHG	G
LTPEQVVAIAS**HD**GGKQALETVQALLPVLCQAHG	C	LTPEQVVAIAS**HD**GGKQALETVQALLPVLCQAHG	C
LTPEQVVAIAS**HD**GGKQALETVQALLPVLCQAHG	C	LTPEQVVAIAS**HD**GGKQALETVQALLPVLCQAHG	C
LTPEQVVAIAS**NN**GGKQALETVQRLLPVLCQAHG	G	LIPQQVVAIAS**NG**GGKQALETVQRLLPVLCQDHG	T
LTPEQVVAIAS**NN**GGKQALETVQRLLPVLCQAHG	G	LTPEQVVAIAS**NN**GGKQALETVQRLLPVLCQAHG	G
LTPDQVVAIAS**NI**GGKQALETVQRLLPVLCQAHG	A	LTPEQVVAIAS**NN**GGKQALETVQRLLPVLCQAHG	G
LTPEQVVAIAS**NN**GGKQALETVQRLLPVLCQAHG	G	LIPQQVVAIAS**NG**GGKQALETVQRLLPVLCQDHG	T
LTPDQVVAIAS**NI**GGKQALETVQRLLPVLCQAHG	A	LTPEQVVAIAS**HD**GGKQALETVQALLPVLCQAHG	C
LTPEQVVAIAS**HD**GGKQALETVQALLPVLCQAHG	C	LTPEQVVAIAS**NN**GGKQALETVQRLLPVLCQAHG	G

Table 6.2: TALE RVDs for Surface TALENs

Surface TALEs (from 411-462 bp relative to the HBV genome)			
Left TALE DBD sequence	**DNA base**	**Right TALE DBD sequence**	**DNA base**
LTPEQVVAIAS**HD**GGKQALETVQALLPVLCQAHG	C	LTPDQVVAIAS**NI**GGKQALETVQRLLPVLCQAHG	A
LIPQQVVAIAS**HD**GGKQALETVQRLLPVLCQDHG	C	LTPEQVVAIAS**HD**GGKQALETVQRLLPVLCQAHG	C
LTPEQVVAIAS**NG**GGKQALETVQALLPVLCQAHG	T	LTPEQVVAIAS**HD**GGKQALETVQRLLPVLCQAHG	C
LTPDQVVAIAS**NK**GGKQALETVQRLLPVLCQAHG	G	LTPEQVVAIAS**NG**GGKQALETVQRLLPVLCQAHG	T
LTPDQVVAIAS**HD**GGKQALETVQRLLPVLCQAHG	C	LTPEQVVAIAS**NG**GGKQALETVQRLLPVLCQAHG	T
LTPEQVVAIAS**NG**GGKQALETVQALLPVLCQAHG	T	LTPDQVVAIAS**NK**GGKQALETVQRLLPVLCQAHG	G
LTPDQVVAIAS**NK**GGKQALETVQRLLPVLCQAHG	G	LTPEQVVAIAS**NI**GGKQALETVQALLPVLCQAHG	A
LTPEQVVAIAS**HD**GGKQALETVQALLPVLCQAHG	C	LTPEQVVAIAS**NG**GGKQALETVQALLPVLCQAHG	T
LIPQQVVAIAS**NG**GGKQALETVQRLLPVLCQDHG	T	LIPQQVVAIAS**NI**GGKQALETVQRLLPVLCQDHG	A
LIPQQVVAIAS**NI**GGKQALETVQRLLPVLCQDHG	A	LTPEQVVAIAS**NK**GGKQALETVQRLLPVLCQAHG	G
LTPEQVVAIAS**NG**GGKQALETVQALLPVLCQAHG	T	LTPEQVVAIAS**NG**GGKQALETVQALLPVLCQAHG	T
LTPEQVVAIAS**NK**GGKQALETVQALLPVLCQAHG	G	LTPEQVVAIAS**HD**GGKQALETVQALLPVLCQAHG	C
LTPEQVVAIAS**HD**GGKQALETVQRLLPVLCQAHG	C	LIPQQVVAIAS**HD**GGKQALETVQRLLPVLCQDHG	C
LTPEQVVAIAS**HD**GGKQALETVQRLLPVLCQAHG	C	LTPEQVVAIAS**NI**GGKQALETVQRLLPVLCQAHG	A
LTPDQVVAIAS**NG**GGKQALETVQRLLPVLCQAHG	T	LTPEQVVAIAS**NK**GGKQALETVQRLLPVLCQAHG	G
LTPEQVVAIAS**HD**GGKQALETVQRLLPVLCQAHG	C	LIPQQVVAIAS**NI**GGKQALETVQRLLPVLCQDHG	A
LTPDQVVAIAS**NI**GGKQALETVQRLLPVLCQAHG	A	LTPEQVVAIAS**NI**GGKQALETVQALLPVLCQAHG	A
LTPEQVVAIAS**NG**GGKQALETVQALLPVLCQAHG	T	LTPEQVVAIAS**NK**GGKQALETVQRLLPVLCQAHG	G

6.4 Restriction digest confirmation of pT7-Left/Right-TALEN-4×STOP plasmids from IVT template design 2

Final templates from IVT template design 2 were pT7-CL-TALEN-4×STOP, pT7-CR-TALEN-4×STOP, pT7-SL-TALEN-4×STOP and pT7-SR-TALEN-4×STOP. These templates were digested with *Xba*I and *Apa*I to confirm TALEN sequences (**Figure 6.2**). Furthermore, the templates were digested with *Nae*I to selectively distinguish the left and right *Fok*I sequences. *Nae*I cleaved the left domain sequence twice producing bands at 5079 bp and 1513 bp. *Nae*I cleaved the right domain sequence thrice yielding bands at 2568, 2511, and 1513 bp where the 2568 and 2511 bp bands are similar in size and appear as a thick single band (**Figure 6.3**). Finally, templates were linearised with *Bpi*I (**Figure 6.4**).

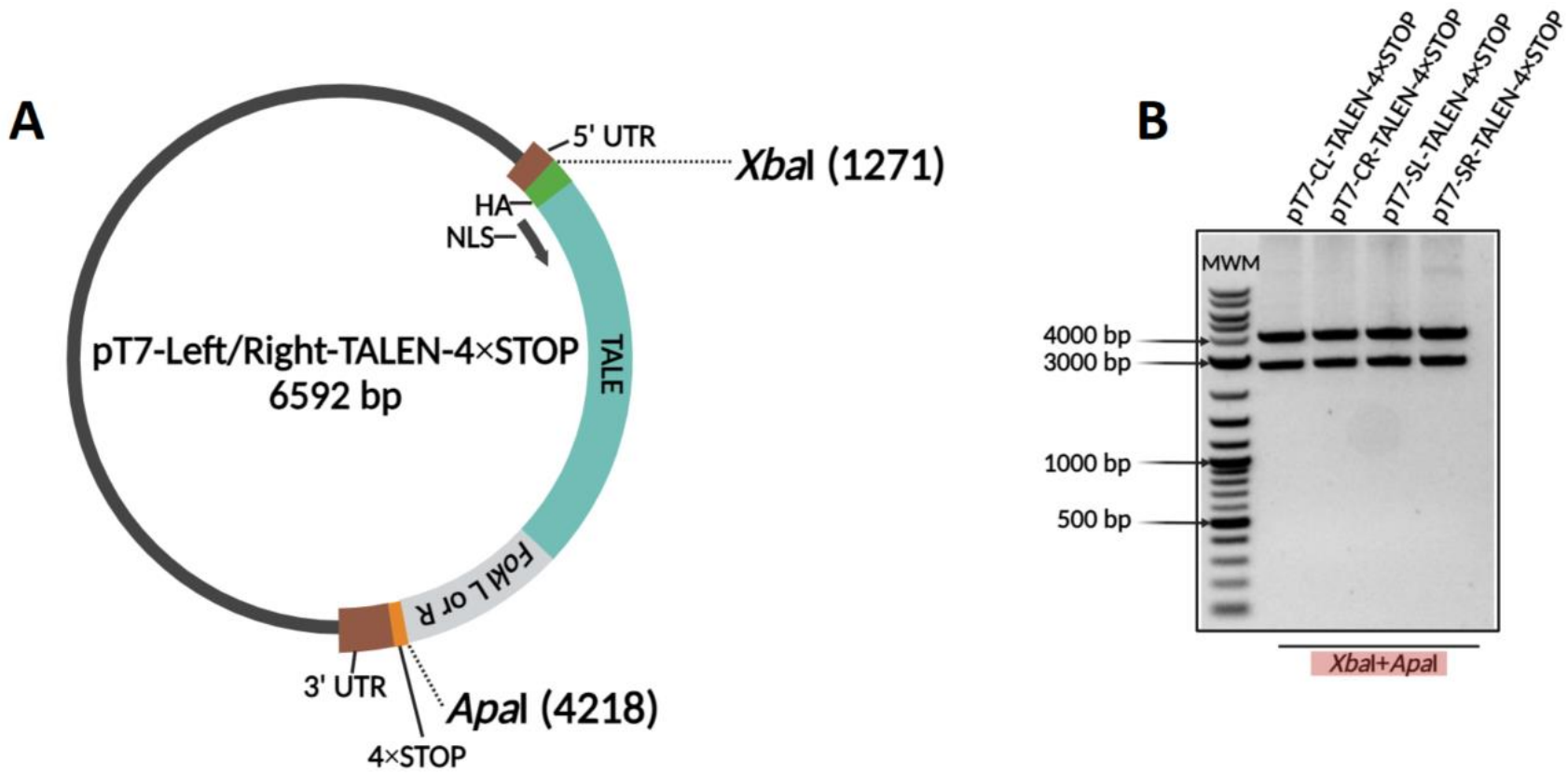
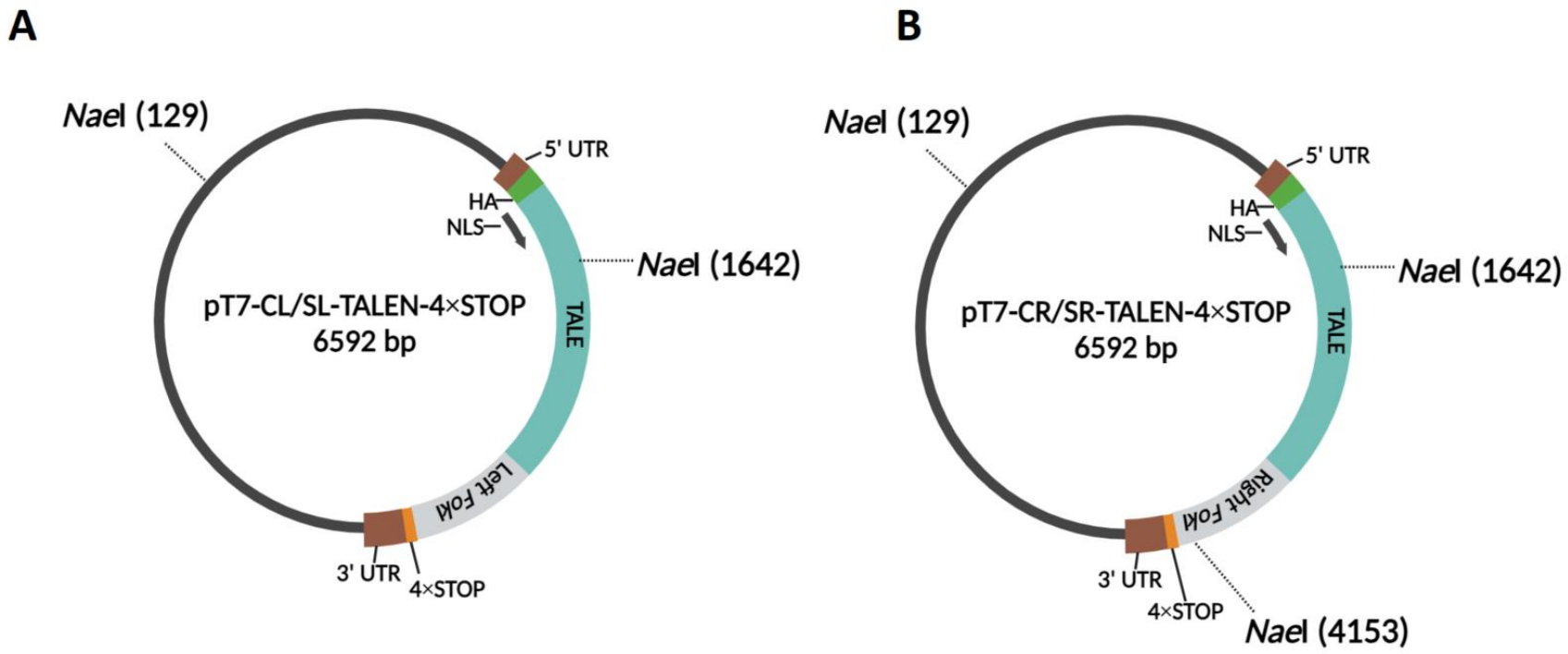


Figure 6.2: Confirmation of pT7-Left/Right-TALEN plasmids.

pT7-Left/Right-TALEN plasmids were produced by inserting previously existing TALEN sequences from pCMV-Left/Right-TALEN plasmids into a modified pT7-mRNA-4×STOP plasmid. **A.** The final pT7-Left/Right-TALEN-4×STOP plasmid map with the selected enzyme digestion sites is depicted. **B.** Agarose gel electrophoresis reveals migration banding patterns for all TALEN plasmids with *Xba*I and *Apa*I producing bands at approximately 3645 bp and 2947 bp. (MWM: molecular weight marker, 1 kb Plus DNA Ladder, New England Biolabs, NJ, USA).


A
NaeI (129)
5' UTR
HA
NLS
NaeI (1642)
pT7-CL/SL-TALEN-4×STOP
6592 bp
TALE
Left FokI
3' UTR
4×STOP
B
NaeI (129)
5' UTR
HA
NLS
NaeI (1642)
pT7-CR/SR-TALEN-4×STOP
6592 bp
TALE
Right FokI
3' UTR
4×STOP
NaeI (4153)

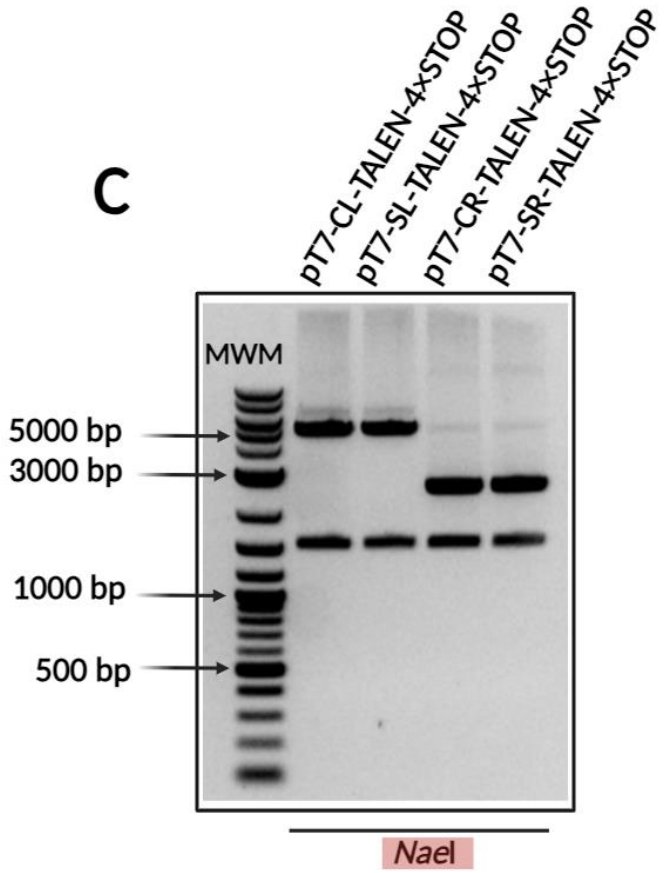


Figure 6.3: Confirmation of left and right *Fok*I nuclease domains in pT7-CL/SL-TALEN and pT7-CR/SR-TALEN plasmids.

To differentiate between left and right nuclease domain sequences of the pT7-CL/SL-TALEN and pT7-CR/SR-TALEN plasmids, *Nae*I restriction digestion was performed. **A.** pT7-CL/SL-TALEN plasmid map with selected *Nae*I restriction sites is depicted for the left domain sequence while **B.** pT7-CR/SR-TALEN plasmid map with selected *Nae*I restriction sites is depicted for the right domain sequence. **C.** Agarose gel electrophoresis reveals migration banding patterns with *Nae*I digestion producing bands at 5079 bp and 1513 bp for pT7-CL/SL-TALEN and three bands at 2568, 2511, and 1513 bp for pT7-SR-TALEN. (MWM: molecular weight marker, 1 kb Plus DNA Ladder, New England Biolabs, NJ, USA).

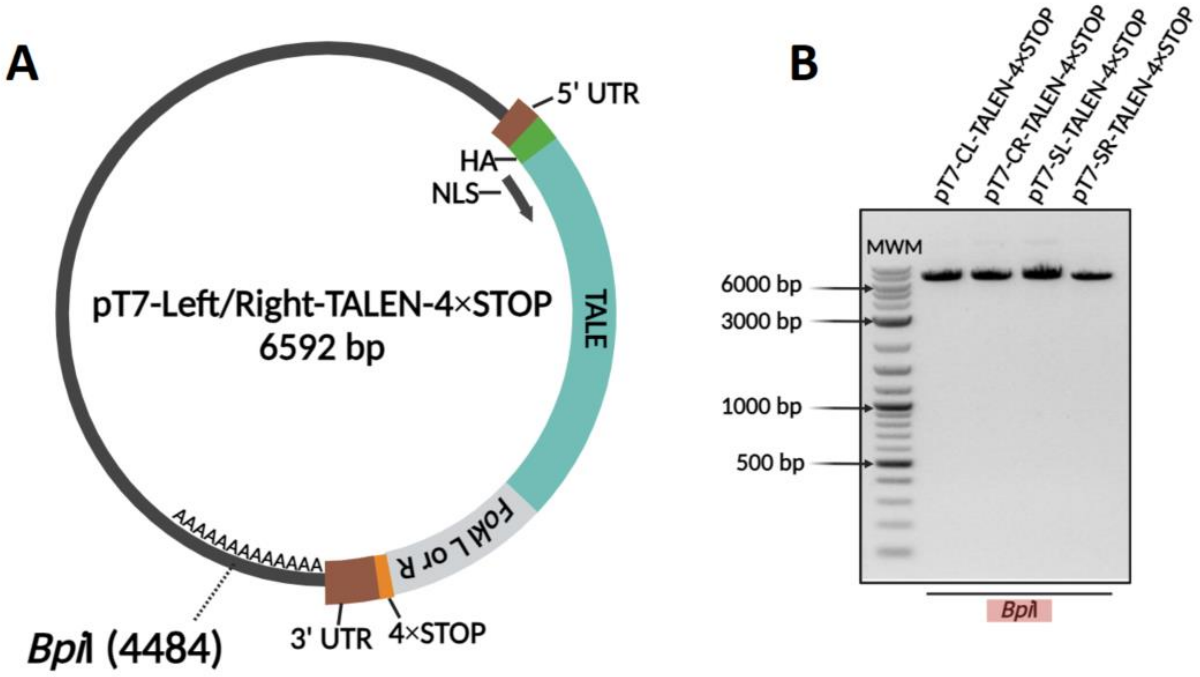


Figure 6.4: Linearised pT7-Left/Right-TALEN templates.

pT7-Left/Right-TALEN plasmids were linearised with *Bpi*I, resulting in linear bands. **A.** pT7-Left/Right-TALEN plasmid map with the selected *Bpi*I restriction site is depicted. **B.** Agarose gel electrophoresis validated the linearisation process (MWM: molecular weight marker, 1 kb Plus DNA Ladder, New England Biolabs, NJ, USA).

6.5 Anti-HBV TALE sequence validation

Core left TALE



Core right TALE





[1]Figure 6.5: TALE sequences.

Presented are the TALE sequences validated through Sanger (standard capillary) sequencing from the pT7-CL-TALEN-4×STOP, pT7-CR-TALEN-4×STOP, pT7-SL-TALEN-4×STOP and pT7-SR-TALEN-4×STOP plasmids. The HA and NLS sequences are boxed in red and the first few RVDs are highlighted in red.

[1] TALE sequences were also validated for Template 1 and resulted in the same sequencing pattern

6.6 Alignment of left and right *Fok*I protein sequences

```
Reference       GSQLVKSELEEKKSELRHKLKYVPHEYIELIEIARNSTQDRILEMKVMEFFMKVYGYRGK
CL FokI         GSQLVKSELEEKKSELRHKLKYVPHEYIELIEIARNSTQDRILEMKVMEFFMKVYGYRGK
SL FokI         GSQLVKSELEEKKSELRHKLKYVPHEYIELIEIARNSTQDRILEMKVMEFFMKVYGYRGK

                ************************************************************

Reference       HLGGSRKPDGAIYTVGSPIDYGVIVDTKAYSGGYNLPIGQADEMQRYVEENQTRNKHINP
CL FokI         HLGGSRKPDGAIYTVGSPIDYGVIVDTKAYSGGYNLPIGQADEMERYVEENQTRNKHANP
SL FokI         HLGGSRKPDGAIYTVGSPIDYGVIVDTKAYSGGYNLPIGQADEMERYVEENQTRNKHANP

                ************************************************************

Reference       NEWWKVYPSSVTEFKFLFVSGHFKGNYKAQLTRLNHITNCNGAVLSVEELLIGGEMIKAG
CL FokI         NEWWKVYPSSVTEFKFLFVSGHFKGNYKAQLTRLNHITNCNGAVLSVEELLIGGEMIKAG
SL FokI         NEWWKVYPSSVTEFKFLFVSGHFKGNYKAQLTRLNHITNCNGAVLSVEELLIGGEMIKAG

                ************************************************************

Reference       TLTLEEVRRKFNNGEINF*GP
CL FokI         TLTLEEVRRKFNNGEINF*GP
SL FokI         TLTLEEVRRKFNNGEINF*GP

                ********************


Reference       GSQLVKSELEEKKSELRHKLKYVPHEYIELIEIARNSTQDRILEMKVMEFFMKVYGYRGK
CR FokI         GSQLVKSELEEKKSELRHKLKYVPHEYIELIEIARNSTQDRILEMKVMEFFMKVYGYRGK
SR FokI         GSQLVKSELEEKKSELRHKLKYVPHEYIELIEIARNSTQDRILEMKVMEFFMKVYGYRGK

                ************************************************************

Reference       HLGGSRKPDGAIYTVGSPIDYGVIVDTKAYSGGYNLPIGQADEMQRYVEENQTRNKHINP
CR FokI         HLGGSRKPDGAIYTVGSPIDYGVIVDTKAYSGGYNLPIGQADEMQRYVKENQTRNKHINP
SR FokI         HLGGSRKPDGAIYTVGSPIDYGVIVDTKAYSGGYNLPIGQADEMQRYVKENQTRNKHINP

                ************************************************************

Reference       NEWWKVYPSSVTEFKFLFVSGHFKGNYKAQLTRLNHITNCNGAVLSVEELLIGGEMIKAG
CR FokI         NEWWKVYPSSVTEFKFLFVSGHFKGNYKAQLTRLNHVTNCNGAVLSVEELLIGGEMIKAG
SR FokI         NEWWKVYPSSVTEFKFLFVSGHFKGNYKAQLTRLNHVTNCNGAVLSVEELLIGGEMIKAG

                ************************************************************

Reference       TLTLEEVRRKFNNGEINF*GP
CR FokI         TLTLEEVRRKFNNGEINF*GP
SR FokI         TLTLEEVRRKFNNGEINF*GP
                ********************
```

[2]Figure 6.6: Heterodimeric *Fok*I multiple sequence alignment.

The aligned *Fok*I amino acid sequences from the plasmids pT7-CL-TALEN-4×STOP, pT7-CR-TALEN-4×STOP, pT7-SL-TALEN-4×STOP, and pT7-SR-TALEN-4×STOP is shown alongside the reference wildtype *Fok*I left or right domain sequences. Mutations Q486E and I499A in the left domain are highlighted in green, while mutations E490K and I538V in the right domain are highlighted in yellow.

*Fok*I sequences were also validated for Template 1 and resulted in the same sequence alignment.

6.7 *In vivo* assessment

6.7.1 N/P ratio and LNP sizing

A key parameter in LNP formulation for RNA delivery is the N/P ratio, which measures the ratio of amino lipid nitrogen in the cationic lipid to the phosphate groups in the RNA. Higher N/P ratios enhance RNA encapsulation efficiency by increasing the interaction between cationic lipids and RNA, resulting in more potent and stable LNPs. Previous studies demonstrated effective LNPs with an N/P ratio of 6 using SM-102 (289,290), prompting the adoption of this ratio in our formulations. The table below depicts the size and zeta potential of the generated LNPs.

Table 6.3: Size and zeta potential measurements of RNA-encapsulated LNPs determined by Zetasizer

LNP	Size (nm)	Polydispersity index[3]	Zeta potential (mV)[4]
FLuc	88.3	0.1048	+8.103
mCherry	66.57	0.03811	-1.665
Core Left TALEN	72.77	0.08846	+7.904
Core Right TALEN	73.02	0.08989	+8.812
Surface Left TALEN	78.18	0.1108	+6.038
Surface Right TALEN	71.82	0.05677	+7.46

[3] The polydispersity index assesses the consistency of particle size distribution, ranging from 0.0 (indicating perfect uniformity) to 1.0 (representing high polydispersity with multiple-size populations). Generally, values of 0.3 or lower are deemed acceptable for lipid-based nanoparticle materials (reviewed in (291)).
[4] Nanoparticles exhibiting a zeta potential within the range of -10 to +10 mV are regarded as approximately neutral (292).

6.7.2 LNP effective dose

RNA stock (20 µg/ml RNA), 1 × TE Buffer, and Triton Buffer (2% Triton-X 100 in TE) were set up listed as below (**Table 6.4**) and added to a 96-well plate in duplicate. The fluorescence values obtained from the Ribogreen assay were averaged and plotted to determine the slope and intercept of the standard cure. The resulting standard curve was used to calculate the effective dose for RNA-encapsulated LNPs.

Table 6.4: Assessing effective dose of LNPs using standards of known concentration for the Ribogreen assay

Final RNA (µg/ml)	RNA stock (µl)	TE buffer volume (µl)	Triton Buffer (µl)	Vol/well (µl)
2.5	25	25	50	100
1	10	40	50	100
0.5	5	45	50	100
0.25	2.5	47.5	50	100
0.1	1	49	50	100

6.7.3 Animal research Ethics clearance certificate

ANIMALS RESEARCH ETHICS COMMITTEE (AREC)

UNIVERSITY OF THE WITWATERSRAND JOHANNESBURG

STRICTLY CONFIDENTIAL

CLEARANCE CERTIFICATE NUMBER: AREC23-08-009C

APPLICANT: Ms T Smith
School: Pathology; Department: Molecular Medicine and Haematology; Location: Wits Research Animal Facility

PROJECT TITLE: Inactivation of hepatitis B virus (HBV) using obligate heterodimeric Transcription Activator-Like Effector Nucleases (TALENs) expressed as mRNA-containing lipoplexes delivered by tail vein injection into FVB HBV transgenic mice
Category: ; Species and Numbers involved: 36X, either sex, 3-5 weeks , approximately 20g, Friend leukaemia virus B (FVB) HBV transgenic mice, mouse

Approval is hereby given for the use of animals for the research project named above and described in the application reviewed by a quorate meeting of the AREC held on 31 October 2023. This approval remains valid until 10 January 2026 and is conditional to the following (if blank there are no special conditions):

Condition 1	Condition 2	Condition 3	Condition 4
The breeding of HBV transgenic mice is no longer authorised and AGTRU will use the remaining mice at WRAF	Retro-orbital bleeding as a non-terminal procedure is not authorised.		

All material changes to the approved research must be reported to the AREC before they are implemented. Failure to do so will invalidate this clearance certificate.

An annual progress report must be provided to the AREC.

The use of these animals is subject to AREC guidelines on the use and care of laboratory animals, is limited to the procedures described in the application and is subject to additional conditions listed below:

I, the Chair of the AREC (or my designated representative) am satisfied that the proposed research is ethical as judged by local law, international standards and University policy.

Signed: _____ _____ Date: __12/01/2024_____

(Chairperson of the AREC)

CC: Student supervisor: Prof P Arbuthnot
Acting Director Wits Research Animal Facility (WRAF): Sr Amelia Rammekwa

ANIMALS RESEARCH ETHICS COMMITTEE (AREC)

UNIVERSITY OF THE WITWATERSRAND, JOHANNESBURG

I am satisfied that the persons listed in this application are competent to perform the procedures described in the application, in the context of Section 23 (1) (c) of the veterinary and Para-veterinary Professions Act (19 of 1982).

Signed: ___ Date: _12 January 2024__

(Registered Veterinarian)

6.7.4 Cytometric bead array plot

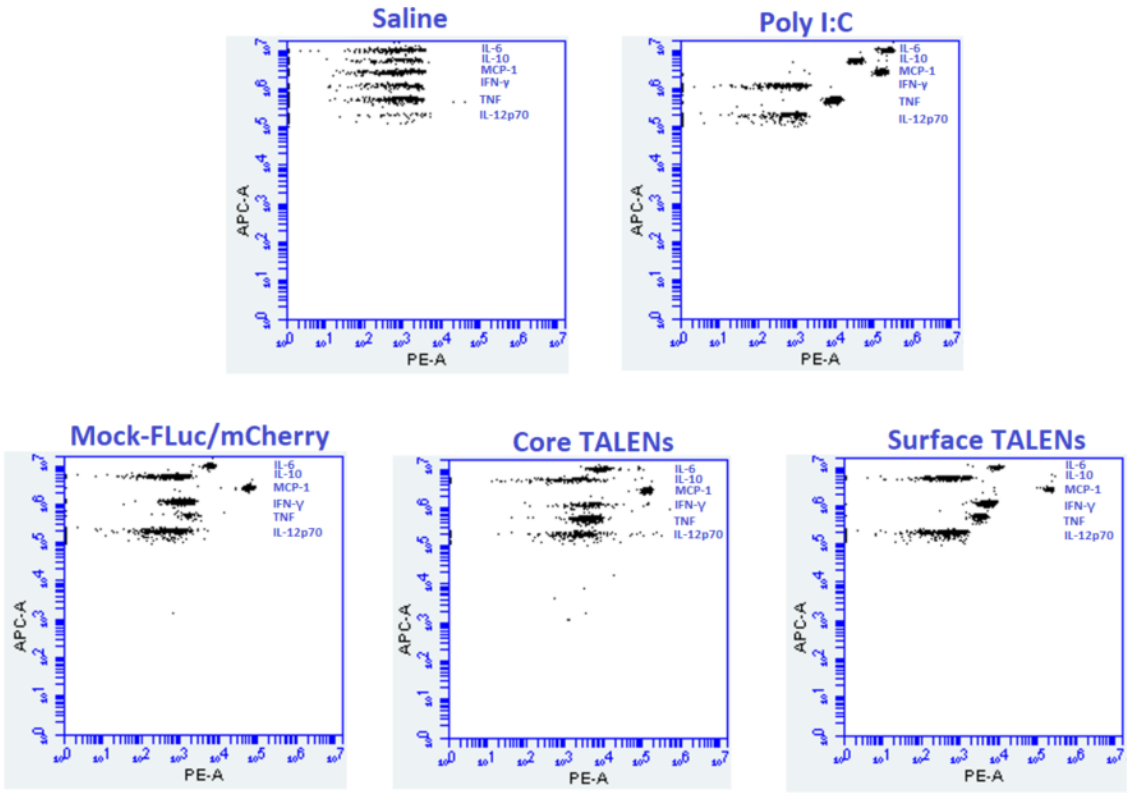


Figure 6.7: Cytokine induction in transgenic mice.

Serum was collected 6 hours after LNP administration and measured for IL-12p70, IFN-γ, TNF, MCP-1, IL-10 and IL-6 induction. Representative dot blots demonstrate cytokine induction for the different experimental groups. Poly I:C and saline served as positive and negative controls, respectively. APC-A: Allophycocyanin, PE-A: Phycoerythrin.

References

1. Blumberg BS. A ‘New’ Antigen in Leukemia Sera. JAMA. 1965;191(7):541.

2. Chen DS. A Mass Vaccination Program in Taiwan Against Hepatitis B Virus Infection in Infants of Hepatitis B Surface Antigen—Carrier Mothers. JAMA. 1987;257(19):2597.

3. World Health Organization (WHO). Hepatitis B, Key facts. [Internet]. 2024 [cited 2024 Apr 10]. Available from: http://www.who.int/news-room/fact-sheets/detail/hepatitis-b.

4. Alberts CJ, Clifford GM, Georges D, Negro F, Lesi OA, Hutin YJF, et al. Worldwide prevalence of hepatitis B virus and hepatitis C virus among patients with cirrhosis at country, region, and global levels: a systematic review. Lancet Gastroenterol Hepatol. 2022;7(8):724–35.

5. Maepa MB, Ely A, Kramvis A, Bloom K, Naidoo K, Simani OE, et al. Hepatitis B Virus Research in South Africa. Viruses. 2022;14(9):1939.

6. Okamoto H, Tsuda F, Sakugawa H, Sastrosoewignjo RI, Imai M, Miyakawa Y, et al. Typing Hepatitis B Virus by Homology in Nucleotide Sequence: Comparison of Surface Antigen Subtypes. J Gen Mol Virol. 1988;69(10):2575–83.

7. Kramvis A, Kew MC. Epidemiology of hepatitis B virus in Africa, its genotypes and clinical associations of genotypes. Hepatology. 2007;37(s1).

8. Sunbul M. Hepatitis B virus genotypes: Global distribution and clinical importance. WJG. 2014;20(18):5427.

9. Croagh CM. Genotypes and viral variants in chronic hepatitis B: A review of epidemiology and clinical relevance. WJH. 2015;7(3):289.

10. Norder H, Couroucé AM, Magnius LO. Complete Genomes, Phylogenetic Relatedness, and Structural Proteins of Six Strains of the Hepatitis B Virus, Four of Which Represent Two New Genotypes. Virology. 1994;198(2):489–503.

11. Girones R, Miller RH. Mutation rate of the hepadnavirus genome. Virology. 1989;170(2):595–7.

12. Nowak MA, Bonhoeffer S, Hill AM, Boehme R, Thomas HC, McDade H. Viral dynamics in hepatitis B virus infection. Proc Natl Acad Sci USA. 1996;93(9):4398–402.

13. Cooksley WGE. Do we need to determine viral genotype in treating chronic hepatitis B? J Viral Hepat. 2010;17(9):601–10.

14. Shi W, Zhang Z, Ling C, Zheng W, Zhu C, Carr MJ, et al. Hepatitis B virus subgenotyping: history, effects of recombination, misclassifications, and corrections. Infect Genet Evol. 2013;16:355–61.

15. Lin S, Liu C, Shang H, Chen H, Yang B, Chen J, et al. HBV serum markers of 49164 patients and their relationships to HBV genotype in Fujian province of China. J Clin Lab Anal. 2013;27(2):130–6.

16. Yang F, Yin Y, Wang F, Zhang L, Wang Y, Sun S. An Altered Pattern of Liver Apolipoprotein A-I Isoforms Is Implicated in Male Chronic Hepatitis B Progression. J Proteome Res. 2010;9(1):134–43.

17. Milich DR, Jones JE, Hughes JL, Price J, Raney AK, McLachlan A. Is a function of the secreted hepatitis B e antigen to induce immunologic tolerance in utero? Proc Natl Acad Sci USA. 1990;87(17):6599–603.

18. Tian Y, Kuo C fu, Akbari O, Ou J hsiung J. Maternal-Derived Hepatitis B Virus e Antigen Alters Macrophage Function in Offspring to Drive Viral Persistence after Vertical Transmission. Immunity. 2016;44(5):1204–14.

19. Yi P, Chen R, Huang Y, Zhou RR, Fan XG. Management of mother-to-child transmission of hepatitis B virus: Propositions and challenges. J Clin Virol. 2016;77:32–9.

20. Mendy ME, Welzel T, Lesi OA, Hainaut P, Hall AJ, Kuniholm MH, et al. Hepatitis B viral load and risk for liver cirrhosis and hepatocellular carcinoma in The Gambia, West Africa. J Viral Hepat. 2010;17(2):115–22.

21. Spearman CW, Afihene M, Ally R, Apica B, Awuku Y, Cunha L, et al. Hepatitis B in sub-Saharan Africa: strategies to achieve the 2030 elimination targets. Lancet Gastroenterol Hepatol. 2017;2(12):900–9.

22. Alexopoulou A, Baltayiannis G, Jammeh S, Waters J, Dourakis SP, Karayiannis P. Hepatitis B Surface Antigen Variant with Multiple Mutations in the *a* Determinant in an Agammaglobulinemic Patient. J Clin Microbiol. 2004;42(6):2861–5.

23. Dionne-Odom J, Njei B, Tita ATN. Elimination of Vertical Transmission of Hepatitis B in Africa: A Review of Available Tools and New Opportunities. Clin Ther. 2018;40(8):1255–67.

24. Kramvis A. Challenges for hepatitis B virus cure in resource-limited settings in sub-Saharan Africa. Curr Opin HIV AIDS. 2020;15(3):185–92.

25. Than TT, Jo E, Todt D, Nguyen PH, Steinmann J, Steinmann E, et al. High Environmental Stability of Hepatitis B Virus and Inactivation Requirements for Chemical Biocides. Int J Infect Dis. 2019;219(7):1044–8.

26. Kwon SY, Lee CH. Epidemiology and prevention of hepatitis B virus infection. Korean J Hepatol. 2011;17(2):87.

27. Alter MJ, Margolis HS. The Emergence of Hepatitis B as a Sexually Transmitted Disease. Med Clin North Am. 1990;74(6):1529–41.

28. Negero A, Sisay Z, Medhin G. Prevalence of Hepatitis B surface antigen (HBsAg) among visitors of Shashemene General Hospital voluntary counseling and testing center. BMC Res Notes. 2011;4:35.

29. Sayan M, Özgüler M, Sarıgül Yıldırım F, Yıldırmak T, Gündüz A, Dokuzoğuz B, et al. Molecular Identification of HIV-1 in the Presence of Hepatitis B Virus and Hepatitis C Virus Co-infections. Balkan Med J. 2020;37(3):125–30.

30. World Health Organization (WHO). The Global Health Observatory. HIV. Global situation and trends. [Internet]. 2022 [cited 2024 Apr 8]. Available from: http://https://www.who.int/data/gho/data/themes/hiv-aids.

31. Datta S, Roychoudhury S, Ghosh A, Dasgupta D, Ghosh A, Chakraborty B, et al. Distinct Distribution Pattern of Hepatitis B Virus Genotype C and D in Liver Tissue and Serum of Dual Genotype Infected Liver Cirrhosis and Hepatocellular Carcinoma Patients. Ray R, editor. PLoS ONE. 2014;9(7):e102573.

32. Chun HM, Roediger MP, Hullsiek KH, Thio CL, Agan BK, Bradley WP, et al. Hepatitis B Virus Coinfection Negatively Impacts HIV Outcomes in HIV Seroconverters. J Infect Dis. 2012;205(2):185–93.

33. Kappus MR, Sterling RK. Extrahepatic manifestations of acute hepatitis B virus infection. Gastroenterol Hepatol (N Y). 2013;9(2):123–6.

34. Seeger C, Mason WS. Hepatitis B virus biology. Microbiol Mol Biol Rev. 2000;64(1):51–68.

35. Xie Y. Hepatitis B Virus-Associated Hepatocellular Carcinoma. In: Infectious Agents Associated Cancers: Epidemiology and Molecular Biology. 2017. p. 11–21.

36. Yang JD, Hainaut P, Gores GJ, Amadou A, Plymoth A, Roberts LR. A global view of hepatocellular carcinoma: trends, risk, prevention and management. Nat Rev Gastroenterol Hepatol. 2019;16(10):589–604.

37. Rieger A, Nassal M. Specific hepatitis B virus minus-strand DNA synthesis requires only the 5' encapsidation signal and the 3'-proximal direct repeat DR1. J Virol. 1996;70(1):585–9.

38. Dane DS, Cameron CH, Briggs M. Virus-like Particles in Serum of Patients with Australia-Antigen-Associated Hepatitis. The Lancet. 1970;295(7649):695–8.

39. Hruska JF, Clayton DA, Rubenstein JL, Robinson WS. Structure of hepatitis B Dane particle DNA before and after the Dane particle DNA polymerase reaction. J Virol. 1977;21(2):666–72.

40. Wang GH, Seeger C. The reverse transcriptase of hepatitis B virus acts as a protein primer for viral DNA synthesis. Cell. 1992;71(4):663–70.

41. Beck J, Nassal, Michael M. Hepatitis B virus replication. WJG. 2007;13(1):48.

42. Jean-Jean O, Levrero M, Hans W, Perricaudet M, Rossignol JM. Expression mechanism of the hepatitis B virus (HBV) C gene and biosynthesis of HBe antigen. Virology. 1989;170(1):99–106.

43. Liang TJ. Hepatitis B: The virus and disease. Hepatology. 2009;49(S5):S13–21.

44. Datta S, Chatterjee S, Veer V, Chakravarty R. Molecular Biology of the Hepatitis B Virus for Clinicians. J Clin Exp Hepatol. 2012;2(4):353–65.

45. Ito K, Kim KH, Lok ASF, Tong S. Characterization of Genotype-Specific Carboxyl-Terminal Cleavage Sites of Hepatitis B Virus e Antigen Precursor and Identification of Furin as the Candidate Enzyme. J Virol. 2009;83(8):3507–17.

46. Milich D. Exploring the biological basis of hepatitis B e antigen in hepatitis B virus infection. Hepatology. 2003;38(5):1075–86.

47. Alexopoulou A, Karayiannis P. HBeAg negative variants and their role in the natural history of chronic hepatitis B virus infection. World J Gastroenterol. 2014;20(24):7644–52.

48. Gallina A, Bonelli F, Zentilin L, Rindi G, Muttini M, Milanesi G. A recombinant hepatitis B core antigen polypeptide with the protamine-like domain deleted self-assembles into capsid particles but fails to bind nucleic acids. J Virol. 1989;63(11):4645–52.

49. Hatton T, Zhou S, Standring DN. RNA- and DNA-binding activities in hepatitis B virus capsid protein: a model for their roles in viral replication. J Virol. 1992;66(9):5232–41.

50. Wynne SA, Crowther RA, Leslie AGW. The Crystal Structure of the Human Hepatitis B Virus Capsid. Molecular Cell. 1999;3(6):771–80.

51. Liao W, Ou JH. Phosphorylation and nuclear localization of the hepatitis B virus core protein: significance of serine in the three repeated SPRRR motifs. J Virol. 1995;69(2):1025–9.

52. Nassal M. Hepatitis B viruses: Reverse transcription a different way. Virus Research. 2008;134(1–2):235–49.

53. Clark DN, Hu J. Unveiling the roles of HBV polymerase for new antiviral strategies. Future Virol. 2015;10(3):283–95.

54. Schulze A, Schieck A, Ni Y, Mier W, Urban S. Fine Mapping of Pre-S Sequence Requirements for Hepatitis B Virus Large Envelope Protein-Mediated Receptor Interaction. J Virol. 2010;84(4):1989–2000.

55. Julithe R, Abou-Jaoudé G, Sureau C. Modification of the hepatitis B virus envelope protein glycosylation pattern interferes with secretion of viral particles, infectivity, and susceptibility to neutralizing antibodies. J Virol. 2014;88(16):9049–59.

56. Lepère-Douard C, Trotard M, Le Seyec J, Gripon P. The first transmembrane domain of the hepatitis B virus large envelope protein is crucial for infectivity. J Virol. 2009;83(22):11819–29.

57. Dandri M, Locarnini S. New insight in the pathobiology of hepatitis B virus infection. Gut. 2012;61(Suppl 1):6–17.

58. Blanchet M, Sureau C. Infectivity determinants of the hepatitis B virus pre-S domain are confined to the N-terminal 75 amino acid residues. J Virol. 2007;81(11):5841–9.

59. Zoulim F, Saputelli J, Seeger C. Woodchuck hepatitis virus X protein is required for viral infection in vivo. J Virol. 1994;68(3):2026–30.

60. Doria M, Klein N, Lucito R, Schneider RJ. The hepatitis B virus HBx protein is a dual specificity cytoplasmic activator of Ras and nuclear activator of transcription factors. EMBO J. 1995;14(19):4747–57.

61. Martinez MG, Smekalova E, Combe E, Gregoire F, Zoulim F, Testoni B. Gene Editing Technologies to Target HBV cccDNA. Viruses. 2022;14(12):2654.

62. Tu T, Zhang H, Urban S. Hepatitis B Virus DNA Integration: In Vitro Models for Investigating Viral Pathogenesis and Persistence. Viruses. 2021;13(2):180.

63. Decorsière A, Mueller H, Van Breugel PC, Abdul F, Gerossier L, Beran RK, et al. Hepatitis B virus X protein identifies the Smc5/6 complex as a host restriction factor. Nature. 2016;531(7594):386–9.

64. Quarleri J. Core promoter: a critical region where the hepatitis B virus makes decisions. World J Gastroenterol. 2014;20(2):425–35.

65. Zheng Y, Li J, Ou J hsiung. Regulation of hepatitis B virus core promoter by transcription factors HNF1 and HNF4 and the viral X protein. J Virol. 2004;78(13):6908–14.

66. Habig JW, Loeb DD. Sequence identity of the direct repeats, DR1 and DR2, contributes to the discrimination between primer translocation and in situ priming during replication of the duck hepatitis B virus. J Mol Biol. 2006;364(1):32–43.

67. Doitsh G, Shaul Y. Enhancer I predominance in hepatitis B virus gene expression. Mol Cell Biol. 2004;24(4):1799–808.

68. Guidotti LG, Matzke B, Schaller H, Chisari FV. High-level hepatitis B virus replication in transgenic mice. J Virol. 1995;69(10):6158–69.

69. Seeger C, Mason WS. Molecular biology of hepatitis B virus infection. Virology. 2015;479–480:672–86.

70. Yan H, Zhong G, Xu G, He W, Jing Z, Gao Z, et al. Sodium taurocholate cotransporting polypeptide is a functional receptor for human hepatitis B and D virus. eLife. 2012;1:e00049.

71. Sureau C, Salisse J. A conformational heparan sulfate binding site essential to infectivity overlaps with the conserved hepatitis B virus A-determinant. Hepatology. 2013;57(3):985–94.

72. Glebe D. Viral and cellular determinants involved in hepadnaviral entry. WJG. 2007;13(1):22.

73. Rehman Z, Fahim A, Sadia H. Deciphering the mystery of hepatitis B virus receptors: A historical perspective. VirusDis. 2015;26(3):97–104.

74. Dandri M, Petersen J. Mechanism of Hepatitis B Virus Persistence in Hepatocytes and Its Carcinogenic Potential. Clin Infect Dis. 2016;62 Suppl 4(4):281–8.

75. Macovei A, Radulescu C, Lazar C, Petrescu S, Durantel D, Dwek RA, et al. Hepatitis B Virus Requires Intact Caveolin-1 Function for Productive Infection in HepaRG Cells. J Virol. 2010;84(1):243–53.

76. Urban S, Schulze A, Dandri M, Petersen J. The replication cycle of hepatitis B virus. J Hepatol. 2010;52(2):282–4.

77. Kann M. Intracellular transport of hepatitis B virus. WJG. 2007;13(1):39.

78. Wei L, Ploss A. Core components of DNA lagging strand synthesis machinery are essential for hepatitis B virus cccDNA formation. Nat Microbiol. 2020;5(5):715–26.

79. Königer C, Wingert I, Marsmann M, Rösler C, Beck J, Nassal M. Involvement of the host DNA-repair enzyme TDP2 in formation of the covalently closed circular DNA persistence reservoir of hepatitis B viruses. Proc Natl Acad Sci USA. 2014;111(40).

80. Kitamura K, Que L, Shimadu M, Koura M, Ishihara Y, Wakae K, et al. Flap endonuclease 1 is involved in cccDNA formation in the hepatitis B virus. Siddiqui A, editor. PLoS Pathog. 2018;14(6):e1007124.

81. Sheraz M, Cheng J, Tang L, Chang J, Guo JT. Cellular DNA Topoisomerases Are Required for the Synthesis of Hepatitis B Virus Covalently Closed Circular DNA. James Ou JH, editor. J Virol. 2019;93(11):e02230-18.

82. Schreiner S, Nassal M. A Role for the Host DNA Damage Response in Hepatitis B Virus cccDNA Formation—and Beyond? Viruses. 2017;9(5):125.

83. Hu J, Boyer M. Hepatitis B virus reverse transcriptase and epsilon RNA sequences required for specific interaction in vitro. J Virol. 2006;80(5):2141–50.

84. Mhamdi M, Funk A, Hohenberg H, Will H, Sirma H. Assembly and budding of a hepatitis B virus is mediated by a novel type of intracellular vesicles. Hepatology. 2007;46(1):95–106.

85. Nassal M. HBV cccDNA: viral persistence reservoir and key obstacle for a cure of chronic hepatitis B. Gut. 2015;64(12):1972–84.

86. Qu B, Ni Y, Lempp FA, Vondran FWR, Urban S. T5 Exonuclease Hydrolysis of Hepatitis B Virus Replicative Intermediates Allows Reliable Quantification and Fast Drug Efficacy Testing of Covalently Closed Circular DNA by PCR. Ou JHJ, editor. J Virol. 2018;92(23):e01117-18.

87. Zhang YY, Zhang BH, Theele D, Litwin S, Toll E, Summers J. Single-cell analysis of covalently closed circular DNA copy numbers in a hepadnavirus-infected liver. Proc Natl Acad Sci USA. 2003;100(21):12372–7.

88. Li X, Zhao J, Yuan Q, Xia N. Detection of HBV Covalently Closed Circular DNA. Viruses. 2017;9(6):139.

89. Lenhoff RJ, Summers J. Coordinate regulation of replication and virus assembly by the large envelope protein of an avian hepadnavirus. J Virol. 1994;68(7):4565–71.

90. Levrero M, Pollicino T, Petersen J, Belloni L, Raimondo G, Dandri M. Control of cccDNA function in hepatitis B virus infection. J Hepatol. 2009;51(3):581–92.

91. Lucifora J, Arzberger S, Durantel D, Belloni L, Strubin M, Levrero M, et al. Hepatitis B virus X protein is essential to initiate and maintain virus replication after infection. J Hepatol. 2011;55(5):996–1003.

92. Seeger C. A CRISPR-based system to investigate HBV cccDNA biology. Ou JHJ, editor. J Virol. 2023;97(10):e01185-23.

93. Van Der Molen RG, Sprengers D, Binda RS, De Jong EC, Niesters HGM, Kusters JG, et al. Functional impairment of myeloid and plasmacytoid dendritic cells of patients with chronic hepatitis B. Hepatology. 2004;40(3):738–46.

94. Wang W, Bian H, Li F, Li X, Zhang D, Sun S, et al. HBeAg induces the expression of macrophage miR-155 to accelerate liver injury via promoting production of inflammatory cytokines. Cell Mol Life Sci. 2018;75(14):2627–41.

95. Chang MH, Chen CJ, Lai MS, Hsu HM, Wu TC, Kong MS, et al. Universal hepatitis B vaccination in Taiwan and the incidence of hepatocellular carcinoma in children. Taiwan Childhood Hepatoma Study Group. N Engl J Med. 1997;336(26):1855–9.

96. Liao S su, Li R cheng, Li H, Yang J ye, Zeng X jia, Gong J, et al. Long-term efficacy of plasma-derived hepatitis B vaccine: a 15-year follow-up study among Chinese children. Vaccine. 1999;17(20–21):2661–6.

97. World Health Organization (WHO). WHO UNICEF estimates time series for South Africa [Internet]. 2018. Available from: https://apps.who.int/immunization_monitoring/globalsummary/estimates?c=ZAF.

98. Fung J, Lai CL, Seto WK, Yuen MF. Nucleoside/nucleotide analogues in the treatment of chronic hepatitis B. J Antimicrob Chemother. 2011;66(12):2715–25.

99. Gane EJ, Wang Y, Liaw YF, Hou J, Thongsawat S, Wan M, et al. Efficacy and safety of prolonged 3-year telbivudine treatment in patients with chronic hepatitis B: Long-term telbivudine in CHB patients. Liver Int. 2011;31(5):676–84.

100. Schildgen O, Sirma H, Funk A, Olotu C, Wend UC, Hartmann H, et al. Variant of Hepatitis B Virus with Primary Resistance to Adefovir. N Engl J Med. 2006;354(17):1807–12.

101. Yuen MF, Seto WK, Chow DHF, Tsui K, Wong DKH, Ngai VWS, et al. Long-term lamivudine therapy reduces the risk of long-term complications of chronic hepatitis B infection even in patients without advanced disease. Antivir Ther. 2007;12(8):1295–303.

102. Brunetto MR, Bonino F. Interferon Therapy of Chronic Hepatitis B. Intervirology. 2014;57(3–4):163–70.

103. Wieland SF, Guidotti LG, Chisari FV. Intrahepatic Induction of Alpha/Beta Interferon Eliminates Viral RNA-Containing Capsids in Hepatitis B Virus Transgenic Mice. J Virol. 2000;74(9):4165–73.

104. Xu C, Guo H, Pan XB, Mao R, Yu W, Xu X, et al. Interferons Accelerate Decay of Replication-Competent Nucleocapsids of Hepatitis B Virus. J Virol. 2010;84(18):9332–40.

105. Belloni L, Allweiss L, Guerrieri F, Pediconi N, Volz T, Pollicino T, et al. IFN-α inhibits HBV transcription and replication in cell culture and in humanized mice by targeting the epigenetic regulation of the nuclear cccDNA minichromosome. J Clin Invest. 2012;122(2):529–37.

106. Iannazzo S, Coco B, Brunetto MR, Rossetti F, Caputo A, Latour A, et al. Individualized Treatment of Hbeag-Negative Chronic Hepatitis B Using Pegylated Interferon-α2A as First-Line and Week-12 HBV Dna/Hbsag Stopping Rule: A Cost-Effectiveness Analysis. Antivir Ther. 2013;18(4):1–11.

107. Nakabori T, Hikita H, Murai K, Nozaki Y, Kai Y, Makino Y, et al. Sodium taurocholate cotransporting polypeptide inhibition efficiently blocks hepatitis B virus spread in mice with a humanized liver. Sci Rep. 2016;6(1):27782.

108. Cheng D, Han B, Zhang W, Wu W. Clinical effects of NTCP-inhibitor myrcludex B. J Viral Hepat. 2021;28(6):852–8.

109. Liu H, Zakrzewicz D, Nosol K, Irobalieva RN, Mukherjee S, Bang-Sørensen R, et al. Structure of antiviral drug bulevirtide bound to hepatitis B and D virus receptor protein NTCP. Nat Commun. 2024;15(1):2476.

110. Zamore PD, Tuschl T, Sharp PA, Bartel DP. RNAi: double-stranded RNA directs the ATP-dependent cleavage of mRNA at 21 to 23 nucleotide intervals. Cell. 2000;101(1):25–33.

111. Yuen M, Schiefke I, Yoon J, Ahn SH, Heo J, Kim JH, et al. RNA Interference Therapy With ARC-520 Results in Prolonged Hepatitis B Surface Antigen Response in Patients With Chronic Hepatitis B Infection. Hepatology. 2020;72(1):19–31.

112. Akira S, Uematsu S, Takeuchi O. Pathogen Recognition and Innate Immunity. Cell. 2006;124(4):783–801.

113. Suslov A, Wieland S, Menne S. Modulators of innate immunity as novel therapeutics for treatment of chronic hepatitis B. Curr Opin Microbiol. 2018;30:9–17.

114. Janssen HLA, Brunetto MR, Kim YJ, Ferrari C, Massetto B, Nguyen AH, et al. Safety, efficacy and pharmacodynamics of vesatolimod (GS-9620) in virally suppressed patients with chronic hepatitis B. J Hepatol. 2018;68(3):431–40.

115. Mackman RL, Mish M, Chin G, Perry JK, Appleby T, Aktoudianakis V, et al. Discovery of GS-9688 (Selgantolimod) as a Potent and Selective Oral Toll-Like Receptor 8 Agonist for the Treatment of Chronic Hepatitis B. J Med Chem. 2020;63(18):10188–203.

116. Vaillant A. Nucleic acid polymers: Broad spectrum antiviral activity, antiviral mechanisms and optimization for the treatment of hepatitis B and hepatitis D infection. Antiviral Res. 2016;133:32–40.

117. Al-Mahtab M, Bazinet M, Vaillant A. Safety and Efficacy of Nucleic Acid Polymers in Monotherapy and Combined with Immunotherapy in Treatment-Naive Bangladeshi Patients with HBeAg+ Chronic Hepatitis B Infection. PLoS One. 2016;11(6):e0156667.

118. Bazinet M, Pântea V, Placinta G, Moscalu I, Cebotarescu V, Cojuhari L, et al. Safety and Efficacy of 48 Weeks REP 2139 or REP 2165, Tenofovir Disoproxil, and Pegylated Interferon Alfa-2a in Patients With Chronic HBV Infection Naïve to Nucleos(t)ide Therapy. Gastroenterology. 2020;158(8):2180–94.

119. Bazinet M, Pântea V, Cebotarescu V, Cojuhari L, Jimbei P, Anderson M, et al. Persistent Control of Hepatitis B Virus and Hepatitis Delta Virus Infection Following REP 2139-Ca and Pegylated Interferon Therapy in Chronic Hepatitis B Virus/Hepatitis Delta Virus Coinfection. Hepatol Commun. 2021;5(2):189–202.

120. Hockemeyer D, Soldner F, Beard C, Gao Q, Mitalipova M, DeKelver RC, et al. Efficient targeting of expressed and silent genes in human ESCs and iPSCs using zinc-finger nucleases. Nat Biotechnol. 2009;27(9):851–7.

121. Merkert S, Martin U. Targeted genome engineering using designer nucleases: State of the art and practical guidance for application in human pluripotent stem cells. Stem Cell Res. 2016;16(2):377–86.

122. Weeks DP, Spalding MH, Yang B. Use of designer nucleases for targeted gene and genome editing in plants. Plant Biotechnol J. 2016;14(2):483–95.

123. Bloom K, Ely A, Mussolino C, Cathomen T, Arbuthnot P. Inactivation of Hepatitis B Virus Replication in Cultured Cells and In Vivo with Engineered Transcription Activator-Like Effector Nucleases. Mol Ther. 2013;21(10):1889–97.

124. Weber ND, Stone D, Sedlak RH, De Silva Feelixge HS, Roychoudhury P, Schiffer JT, et al. AAV-mediated delivery of zinc finger nucleases targeting hepatitis B virus inhibits active replication. PLoS One. 2014;9(5):e97579.

125. Kennedy EM, Bassit LC, Mueller H, Kornepati AVR, Bogerd HP, Nie T, et al. Suppression of hepatitis B virus DNA accumulation in chronically infected cells using a bacterial CRISPR/Cas RNA-guided DNA endonuclease. Virology. 2015;476:196–205.

126. Lee J, Chung J, Kim HM, Kim D, Kim H. Designed nucleases for targeted genome editing. Plant Biotechnol J. 2016;14(2):448–62.

127. Jackson SP. Sensing and repairing DNA double-strand breaks. Carcinogenesis. 2002;23(5):687–96.

128. Lieber MR. The mechanism of double-strand DNA break repair by the nonhomologous DNA end-joining pathway. Annu Rev Biochem. 2010;79:181–211.

129. Mao Z, Bozzella M, Seluanov A, Gorbunova V. Comparison of nonhomologous end joining and homologous recombination in human cells. DNA Repair. 2008;7(10):1765–71.

130. Urnov FD, Miller JC, Lee YL, Beausejour CM, Rock JM, Augustus S, et al. Highly efficient endogenous human gene correction using designed zinc-finger nucleases. Nature. 2005;435(7042):646–51.

131. Hussain A, Ding X, Alariqi M, Manghwar H, Hui F, Li Y, et al. Herbicide Resistance: Another Hot Agronomic Trait for Plant Genome Editing. Plants. 2021;10(4):621.

132. Kim YG, Cha J, Chandrasegaran S. Hybrid restriction enzymes: zinc finger fusions to Fok I cleavage domain. Proc Natl Acad Sci U S A. 1996;93(3):1156–60.

133. Miller J, McLachlan AD, Klug A. Repetitive zinc-binding domains in the protein transcription factor IIIA from Xenopus oocytes. The EMBO Journal. 1985;4(6):1609–14.

134. Klug A. The Discovery of Zinc Fingers and Their Applications in Gene Regulation and Genome Manipulation. Annu Rev Biochem. 2010;79(1):213–31.

135. Händel EM, Alwin S, Cathomen T. Expanding or Restricting the Target Site Repertoire of Zinc-finger Nucleases: The Inter-domain Linker as a Major Determinant of Target Site Selectivity. Mol Ther. 2009;17(1):104–11.

136. Cornu TI, Thibodeau-Beganny S, Guhl E, Alwin S, Eichtinger M, Joung J, et al. DNA-binding Specificity Is a Major Determinant of the Activity and Toxicity of Zinc-finger Nucleases. Mol Ther. 2008;16(2):352–8.

137. Bitinaite J, Wah DA, Aggarwal AK, Schildkraut I. FokI dimerization is required for DNA cleavage. Proc Natl Acad Sci USA. 1998;95(18):10570–5.

138. Cradick TJ, Keck K, Bradshaw S, Jamieson AC, McCaffrey AP. Zinc-finger Nucleases as a Novel Therapeutic Strategy for Targeting Hepatitis B Virus DNAs. Mol Ther. 2010;18(5):947–54.

139. Horvath P, Barrangou R. CRISPR/Cas, the Immune System of Bacteria and Archaea. Science. 2010;327(5962):167–70.

140. Jinek M, Chylinski K, Fonfara I, Hauer M, Doudna JA, Charpentier E. A Programmable Dual-RNA–Guided DNA Endonuclease in Adaptive Bacterial Immunity. Science. 2012;337(6096):816–21.

141. Wu X, Kriz AJ, Sharp PA. Target specificity of the CRISPR-Cas9 system. Quant Biol. 2014;2(2):59–70.

142. Marraffini LA. The CRISPR-Cas system of Streptococcus pyogenes: function and applications. In: Ferretti JJ, Stevens DL, Fischetti VA, editors. Streptococcus pyogenes: Basic Biology to Clinical Manifestations [Internet]. Oklahoma City (OK): University of Oklahoma Health Sciences Center; 2016 [cited 2024 Apr 10]. Available from: http://www.ncbi.nlm.nih.gov/books/NBK355562/

143. Yourik P, Fuchs RT, Mabuchi M, Curcuru JL, Robb GB. Staphylococcus aureus Cas9 is a multiple-turnover enzyme. RNA. 2019;25(1):35–44.

144. Sander JD, Joung JK. CRISPR-Cas systems for editing, regulating and targeting genomes. Nat Biotechnol. 2014;32(4):347–55.

145. Charlesworth CT, Deshpande PS, Dever DP, Camarena J, Lemgart VT, Cromer MK, et al. Identification of preexisting adaptive immunity to Cas9 proteins in humans. Nat Med. 2019;25(2):249–54.

146. Gough V, Gersbach CA. Immunity to Cas9 as an Obstacle to Persistent Genome Editing. Mol Ther. 2020;28(6):1389–91.

147. Yang YC, Yang HC. Recent Progress and Future Prospective in HBV Cure by CRISPR/Cas. Viruses. 2021;14(1):4.

148. Dong C, Qu L, Wang H, Wei L, Dong Y, Xiong S. Targeting hepatitis B virus cccDNA by CRISPR/Cas9 nuclease efficiently inhibits viral replication. Antiviral Res. 2015;118:110–7.

149. Martinez MG, Combe E, Inchauspe A, Mangeot PE, Delberghe E, Chapus F, et al. CRISPR-Cas9 Targeting of Hepatitis B Virus Covalently Closed Circular DNA Generates Transcriptionally Active Episomal Variants. MBio. 2022;13(2):e02888-21.

150. Fu Y, Foden JA, Khayter C, Maeder ML, Reyon D, Joung JK, et al. High-frequency off-target mutagenesis induced by CRISPR-Cas nucleases in human cells. Nat Biotechnol. 2013;31(9):822–6.

151. Fujikawa T, Ishihara H, Leach JE, Tsuyumu S. Suppression of Defense Response in Plants by the avrBs3/pthA Gene Family of Xanthomonas spp. MPMI. 2006;19(3):342–9.

152. Wright DA, Li T, Yang B, Spalding MH. TALEN-mediated genome editing: prospects and perspectives. Biochem J. 2014;462(1):15–24.

153. Moscou MJ, Bogdanove AJ. A Simple Cipher Governs DNA Recognition by TAL Effectors. Science. 2009;326(5959):1501–1501.

154. Morbitzer R, Elsaesser J, Hausner J, Lahaye T. Assembly of custom TALE-type DNA binding domains by modular cloning. Nucleic Acids Res. 2011;39(13):5790–9.

155. Cermak T, Doyle EL, Christian M, Wang L, Zhang Y, Schmidt C, et al. Efficient design and assembly of custom TALEN and other TAL effector-based constructs for DNA targeting. Nucleic Acids Res. 2011;39(12):e82–e82.

156. Reyon D, Tsai SQ, Khayter C, Foden JA, Sander JD, Joung JK. FLASH assembly of TALENs for high-throughput genome editing. Nat Biotechnol. 2012;30(5):460–5.

157. Rogers JM, Barrera LA, Reyon D, Sander JD, Kellis M, Keith Joung J, et al. Context influences on TALE–DNA binding revealed by quantitative profiling. Nat Commun. 2015;6(1):7440.

158. Booher NJ, Bogdanove AJ. Tools for TAL effector design and target prediction. Methods. 2014;69(2):121–7.

159. Boch J, Scholze H, Schornack S, Landgraf A, Hahn S, Kay S, et al. Breaking the Code of DNA Binding Specificity of TAL-Type III Effectors. Science. 2009;326(5959):1509–12.

160. Jankele R, Svoboda P. TAL effectors: tools for DNA Targeting. Brief Funct Genomics. 2014;13(5):409–19.

161. Cong L, Zhou R, Kuo YC, Cunniff M, Zhang F. Comprehensive interrogation of natural TALE DNA-binding modules and transcriptional repressor domains. Nat Commun. 2012;3:968.

162. Gaudelli NM, Komor AC, Rees HA, Packer MS, Badran AH, Bryson DI, et al. Programmable base editing of A•T to G•C in genomic DNA without DNA cleavage. Nature. 2017;551(7681):464–71.

163. Yang YC, Chen YH, Kao JH, Ching C, Liu IJ, Wang CC, et al. Permanent Inactivation of HBV Genomes by CRISPR/Cas9-Mediated Non-cleavage Base Editing. Mol Ther Nucleic Acids. 2020;20:480–90.

164. Zhang F, Cong L, Lodato S, Kosuri S, Church GM, Arlotta P. Efficient construction of sequence-specific TAL effectors for modulating mammalian transcription. Nat Biotechnol. 2011;29(2):149–53.

165. Engler C, Kandzia R, Marillonnet S. A one pot, one step, precision cloning method with high throughput capability. PLoS One. 2008;3(11):e3647.

166. Chen J, Zhang W, Lin J, Wang F, Wu M, Chen C, et al. An Efficient Antiviral Strategy for Targeting Hepatitis B Virus Genome Using Transcription Activator-Like Effector Nucleases. Mol Ther. 2014;22(2):303–11.

167. Grau J, Boch J, Posch S. TALENoffer: genome-wide TALEN off-target prediction. Bioinformatics. 2013;29(22):2931–2.

168. Miller JC, Holmes MC, Wang J, Guschin DY, Lee YL, Rupniewski I, et al. An improved zinc-finger nuclease architecture for highly specific genome editing. Nat Biotechnol. 2007;25(7):778–85.

169. Smith T, Singh P, Chmielewski KO, Bloom K, Cathomen T, Arbuthnot P, et al. Improved Specificity and Safety of Anti-Hepatitis B Virus TALENs Using Obligate Heterodimeric FokI Nuclease Domains. Viruses. 2021;13(7):1344.

170. Malone RW, Felgner PL, Verma IM. Cationic liposome-mediated RNA transfection. Proc Natl Acad Sci USA. 1989;86(16):6077–81.

171. Wolff JA, Malone RW, Williams P, Chong W, Acsadi G, Jani A, et al. Direct Gene Transfer into Mouse Muscle in Vivo. Science. 1990;247(4949):1465–8.

172. Weissman D, Karikó K. mRNA: Fulfilling the Promise of Gene Therapy. Mol Ther. 2015;23(9):1416–7.

173. Henderson JM, Ujita A, Hill E, Yousif-Rosales S, Smith C, Ko N, et al. Cap 1 Messenger RNA Synthesis with Co-transcriptional CleanCap®Analog by In Vitro Transcription. Curr Protoc. 2021;1(2):e39.

174. Fuchs AL, Neu A, Sprangers R. A general method for rapid and cost-efficient large-scale production of 5′ capped RNA. RNA. 2016;22(9):1454–66.

175. Li Y, Kiledjian M. Regulation of mRNA decapping. WIREs RNA. 2010;1(2):253–65.

176. Cowling VH. Regulation of mRNA cap methylation. Biochem J. 2010;425(2):295–302.

177. Lindqvist L, Imataka H, Pelletier J. Cap-dependent eukaryotic initiation factor-mRNA interactions probed by cross-linking. RNA. 2008;14(5):960–9.

178. Suknuntha K, Tao L, Brok-Volchanskaya V, D'Souza SS, Kumar A, Slukvin I. Optimization of Synthetic mRNA for Highly Efficient Translation and its Application in the Generation of Endothelial and Hematopoietic Cells from Human and Primate Pluripotent Stem Cells. Stem Cell Rev and Rep. 2018;14(4):525–34.

179. Asrani KH, Farelli JD, Stahley MR, Miller RL, Cheng CJ, Subramanian RR, et al. Optimization of mRNA untranslated regions for improved expression of therapeutic mRNA. RNA Biol. 2018;1–7.

180. Adibzadeh S, Fardaei M, Takhshid MA, Miri MR, Rafiei Dehbidi G, Farhadi A, et al. Enhancing Stability of Destabilized Green Fluorescent Protein Using Chimeric mRNA Containing Human Beta-Globin 5' and 3' Untranslated Regions. Avicenna J Med Biotechnol. 2019;11(1):112–7.

181. Goss DJ, Kleiman FE. Poly(A) binding proteins: are they all created equal? WIREs RNA. 2013;4(2):167–79.

182. Pasquinelli AE, Dahlberg JE, Lund E. Reverse 5' caps in RNAs made in vitro by phage RNA polymerases. RNA. 1995;1(9):957–67.

183. Stepinski J, Waddell C, Stolarski R, Darzynkiewicz E, Rhoads RE. Synthesis and properties of mRNAs containing the novel 'anti-reverse' cap analogs 7-methyl(3'-O-methyl)GpppG and 7-methyl (3'-deoxy)GpppG. RNA. 2001;7(10):1486–95.

184. Ramanathan A, Robb GB, Chan SH. mRNA capping: biological functions and applications. Nucleic Acids Res. 2016;44(16):7511–26.

185. Higman MA, Christen LA, Niles EG. The mRNA (guanine-7-)methyltransferase domain of the vaccinia virus mRNA capping enzyme. Expression in Escherichia coli and structural and kinetic comparison to the intact capping enzyme. J Biol Chem. 1994;269(21):14974–81.

186. Mao X, Shuman S. Intrinsic RNA (guanine-7) methyltransferase activity of the vaccinia virus capping enzyme D1 subunit is stimulated by the D12 subunit. Identification of amino acid residues in the D1 protein required for subunit association and methyl group transfer. J Biol Chem. 1994;269(39):24472–9.

187. Schwer B, Shuman S. Genetic analysis of poxvirus mRNA cap methyltransferase: suppression of conditional mutations in the stimulatory D12 subunit by second-site mutations in the catalytic D1 subunit. Virology. 2006;352(1):145–56.

188. Habjan M, Hubel P, Lacerda L, Benda C, Holze C, Eberl CH, et al. Sequestration by IFIT1 Impairs Translation of 2′O-unmethylated Capped RNA. Diamond MS, editor. PLoS Pathog. 2013;9(10):e1003663.

189. Byszewska M, Śmietański M, Purta E, Bujnicki JM. RNA methyltransferases involved in 5' cap biosynthesis. RNA Biol. 2014;11(12):1597–607.

190. Beverly M, Dell A, Parmar P, Houghton L. Label-free analysis of mRNA capping efficiency using RNase H probes and LC-MS. Anal Bioanal Chem. 2016;408(18):5021–30.

191. Qin S, Tang X, Chen Y, Chen K, Fan N, Xiao W, et al. mRNA-based therapeutics: powerful and versatile tools to combat diseases. Sig Transduct Target Ther. 2022;7(1):166.

192. Chaudhary N, Weissman D, Whitehead KA. mRNA vaccines for infectious diseases: principles, delivery and clinical translation. Nat Rev Drug Discov. 2021;20(11):817–38.

193. Nanjidsuren T, Park CW, Sim BW, Kim SU, Chang KT, Kang MH, et al. GRK5-Knockout Mice Generated by TALEN-Mediated Gene Targeting. Anim Biotechnol. 2016;27(4):223–30.

194. Lux CT, Pattabhi S, Berger M, Nourigat C, Flowers DA, Negre O, et al. TALEN-Mediated Gene Editing of HBG in Human Hematopoietic Stem Cells Leads to Therapeutic Fetal Hemoglobin Induction. Mol ther, Methods clin dev. 2019;12:175–83.

195. Mock U, Machowicz R, Hauber I, Horn S, Abramowski P, Berdien B, et al. mRNA transfection of a novel TAL effector nuclease (TALEN) facilitates efficient knockout of HIV co-receptor CCR5. Nucleic Acids Res. 2015;43(11):5560–71.

196. Schreier H. The new frontier: gene and oligonucleotide therapy. Pharm Acta Helv. 1994;68(3):145–59.

197. Bangham AD, Horne RW. Negative staining of phospholipids and their structural modification by surface-active agents as observed in the electron microscope. J Mol Biol. 1964;8(5):660-IN10.

198. Bangham AD, Standish MM, Watkins JC. Diffusion of univalent ions across the lamellae of swollen phospholipids. J Mol Biol. 1965;13(1):238-IN27.

199. Bulbake U, Doppalapudi S, Kommineni N, Khan W. Liposomal Formulations in Clinical Use: An Updated Review. Pharmaceutics. 2017;9(4):12.

200. Hou X, Zaks T, Langer R, Dong Y. Lipid nanoparticles for mRNA delivery. Nat Rev Mater. 2021;7(1):65–65.

201. Kulkarni JA, Witzigmann D, Leung J, Tam YYC, Cullis PR. On the role of helper lipids in lipid nanoparticle formulations of siRNA. Nanoscale. 2019;11(45):21733–9.

202. Heyes J, Palmer L, Bremner K, MacLachlan I. Cationic lipid saturation influences intracellular delivery of encapsulated nucleic acids. J Control Release. 2005;107(2):276–87.

203. Kulkarni JA, Cullis PR, Van Der Meel R. Lipid Nanoparticles Enabling Gene Therapies: From Concepts to Clinical Utility. Nucleic Acid Ther. 2018;28(3):146–57.

204. Kim M, Jeong M, Hur S, Cho Y, Park J, Jung H, et al. Engineered ionizable lipid nanoparticles for targeted delivery of RNA therapeutics into different types of cells in the liver. Sci Adv. 2021;7(9):eabf4398.

205. Go GW, Mani A. Low-density lipoprotein receptor (LDLR) family orchestrates cholesterol homeostasis. Yale J Biol Med. 2012;85(1):19–28.

206. Akinc A, Querbes W, De S, Qin J, Frank-Kamenetsky M, Jayaprakash KN, et al. Targeted Delivery of RNAi Therapeutics With Endogenous and Exogenous Ligand-Based Mechanisms. Mol Ther. 2010;18(7):1357–64.

207. Baden LR, El Sahly HM, Essink B, Kotloff K, Frey S, Novak R, et al. Efficacy and Safety of the mRNA-1273 SARS-CoV-2 Vaccine. N Engl J Med. 2021;384(5):403–16.

208. Polack FP, Thomas SJ, Kitchin N, Absalon J, Gurtman A, Lockhart S, et al. Safety and Efficacy of the BNT162b2 mRNA Covid-19 Vaccine. N Engl J Med. 2020;383(27):2603–15.

209. Jiang C, Mei M, Li B, Zhu X, Zu W, Tian Y, et al. A non-viral CRISPR/Cas9 delivery system for therapeutically targeting HBV DNA and pcsk9 in vivo. Cell Res. 2017;27(3):440–3.

210. Smekalova EM, Martinez MG, Combe E, Kumar A, Dejene S, Leboeuf D, et al. Cytosine base editing inhibits hepatitis B virus replication and reduces HBsAg expression in vitro and in vivo. Mol Ther Nucleic Acids. 2024;35(1):102112.

211. Schuberth-Wagner C, Ludwig J, Bruder AK, Herzner AM, Zillinger T, Goldeck M, et al. A Conserved Histidine in the RNA Sensor RIG-I Controls Immune Tolerance to N1-2’O-Methylated Self RNA. Immunity. 2015;43(1):41–51.

212. Ghosh A, Lima CD. Enzymology of RNA cap synthesis. Wiley Interdiscip Rev RNA. 2010;1(1):152–72.

213. Decroly E, Ferron F, Lescar J, Canard B. Conventional and unconventional mechanisms for capping viral mRNA. Nat Rev Microbiol. 2012;10(1):51–65.

214. Karikó K, Buckstein M, Ni H, Weissman D. Suppression of RNA recognition by Toll-like receptors: the impact of nucleoside modification and the evolutionary origin of RNA. Immunity. 2005;23(2):165–75.

215. Karikó K, Muramatsu H, Welsh FA, Ludwig J, Kato H, Akira S, et al. Incorporation of pseudouridine into mRNA yields superior nonimmunogenic vector with increased translational capacity and biological stability. Mol Ther. 2008;16(11):1833–40.

216. Ziegenhals T, Frieling R, Wolf P, Göbel K, Koch S, Lohmann M, et al. Formation of dsRNA by-products during in vitro transcription can be reduced by using low steady-state levels of UTP. Front Mol Biosci. 2023;10:1291045.

217. Baiersdörfer M, Boros G, Muramatsu H, Mahiny A, Vlatkovic I, Sahin U, et al. A Facile Method for the Removal of dsRNA Contaminant from In Vitro-Transcribed mRNA. Mol Ther Nucleic Acids. 2019;15:26–35.

218. Eyler DE, Franco MK, Batool Z, Wu MZ, Dubuke ML, Dobosz-Bartoszek M, et al. Pseudouridinylation of mRNA coding sequences alters translation. Proc Natl Acad Sci U S A. 2019;116(46):23068–74.

219. Arribere JA, Cenik ES, Jain N, Hess GT, Lee CH, Bassik MC, et al. Translation readthrough mitigation. Nature. 2016;534(7609):719–23.

220. Mussolino C, Morbitzer R, Lütge F, Dannemann N, Lahaye T, Cathomen T. A novel TALE nuclease scaffold enables high genome editing activity in combination with low toxicity. Nucleic Acids Res. 2011;39(21):9283–93.

221. Triana-Alonso FJ, Dabrowski M, Wadzack J, Nierhaus KH. Self-coded 3'-extension of run-off transcripts produces aberrant products during in vitro transcription with T7 RNA polymerase. J Biol Chem. 1995;270(11):6298–307.

222. Gholamalipour Y, Karunanayake Mudiyanselage A, Martin CT. 3' end additions by T7 RNA polymerase are RNA self-templated, distributive and diverse in character-RNA-Seq analyses. Nucleic Acids Res. 2018;46(18):9253–63.

223. Gunawardana D, Domashevskiy AV, Gayler KR, Goss DJ. Efficient preparation and properties of mRNAs containing a fluorescent cap analog: Anthraniloyl-m(7)GpppG. Translation (Austin). 2015;3(1):e988538.

224. Sun Y, Lu ZX, Miller M, Perroud T, Tong Y. Application of microfluidic chip electrophoresis for high-throughput nucleic acid fluorescence fragment analysis assays. NAR Genom Bioinform. 2023;5(1):lqad011.

225. Garalde DR, Snell EA, Jachimowicz D, Sipos B, Lloyd JH, Bruce M, et al. Highly parallel direct RNA sequencing on an array of nanopores. Nat Methods. 2018;15(3):201–6.

226. Wang Y, Zhang S, Jia W, Fan P, Wang L, Li X, et al. Identification of nucleoside monophosphates and their epigenetic modifications using an engineered nanopore. Nat Nanotechnol. 2022;17(9):976–83.

227. Inagaki M, Abe N, Li Z, Nakashima Y, Acharyya S, Ogawa K, et al. Cap analogs with a hydrophobic photocleavable tag enable facile purification of fully capped mRNA with various cap structures. Nat Commun. 2023;14(1):2657.

228. Mulroney TE, Pöyry T, Yam-Puc JC, Rust M, Harvey RF, Kalmar L, et al. N1-methylpseudouridylation of mRNA causes +1 ribosomal frameshifting. Nature. 2024;625(7993):189–94.

229. Hockemeyer D, Wang H, Kiani S, Lai CS, Gao Q, Cassady JP, et al. Genetic engineering of human pluripotent cells using TALE nucleases. Nat Biotechnol. 2011;29(8):731–4.

230. Yarrington RM, Verma S, Schwartz S, Trautman JK, Carroll D. Nucleosomes inhibit target cleavage by CRISPR-Cas9 in vivo. Proc Natl Acad Sci U S A. 2018;115(38):9351–8.

231. Slutsky M, Mirny LA. Kinetics of Protein-DNA Interaction: Facilitated Target Location in Sequence-Dependent Potential. Biophys J. 2004;87(6):4021–35.

232. Bauer M, Metzler R. Generalized facilitated diffusion model for DNA-binding proteins with search and recognition states. Biophys J. 2012;102(10):2321–30.

233. Iwahara J, Levy Y. Speed-stability paradox in DNA-scanning by zinc-finger proteins. Transcription. 2013;4(2):58–61.

234. Zandarashvili L, Esadze A, Vuzman D, Kemme CA, Levy Y, Iwahara J. Balancing between affinity and speed in target DNA search by zinc-finger proteins via modulation of dynamic conformational ensemble. Proc Natl Acad Sci U S A. 2015;112(37):E5142-5149.

235. Corsi GI, Qu K, Alkan F, Pan X, Luo Y, Gorodkin J. CRISPR/Cas9 gRNA activity depends on free energy changes and on the target PAM context. Nat Commun. 2022;13(1):3006.

236. Zhdanova PV, Lomzov AA, Prokhorova DV, Stepanov GA, Chernonosov AA, Koval VV. Thermodynamic Swings: How Ideal Complex of Cas9-RNA/DNA Forms. Int J Mol Sci. 2022;23(16):8891.

237. Richter MF, Zhao KT, Eton E, Lapinaite A, Newby GA, Thuronyi BW, et al. Phage-assisted evolution of an adenine base editor with improved Cas domain compatibility and activity. Nat Biotechnol. 2020;38(7):883–91.

238. Pacesa M, Lin CH, Cléry A, Saha A, Arantes PR, Bargsten K, et al. Structural basis for Cas9 off-target activity. Cell. 2022;185(22):4067-4081.e21.

239. Cuculis L, Abil Z, Zhao H, Schroeder CM. Direct observation of TALE protein dynamics reveals a two-state search mechanism. Nat Commun. 2015;6(1):7277.

240. Cuculis L, Abil Z, Zhao H, Schroeder CM. TALE proteins search DNA using a rotationally decoupled mechanism. Nat Chem Biol. 2016;12(10):831–7.

241. Streubel J, Blücher C, Landgraf A, Boch J. TAL effector RVD specificities and efficiencies. Nat Biotechnol. 2012;30(7):593–5.

242. Nassal M, Junker-Niepmann M, Schaller H. Translational inactivation of RNA function: discrimination against a subset of genomic transcripts during HBV nucleocapsid assembly. Cell. 1990;63(6):1357–63.

243. Limani SW, Mnyandu N, Ely A, Wadee R, Kramvis A, Arbuthnot P, et al. In Vivo Modelling of Hepatitis B Virus Subgenotype A1 Replication Using Adeno-Associated Viral Vectors. Viruses. 2021;13(11):2247.

244. Światowy W, Jagodziński PP. Molecules derived from tRNA and snoRNA: Entering the degradome pool. Biomed Pharmacother. 2018;108:36–42.

245. Park J, Kim M, Yi H, Baeg K, Choi Y, Lee Y suk, et al. Short poly(A) tails are protected from deadenylation by the LARP1–PABP complex. Nat Struct Mol Biol. 2023;30(3):330–8.

246. Lee Y suk, Levdansky Y, Jung Y, Kim VN, Valkov E. Deadenylation kinetics of mixed poly(A) tails at single-nucleotide resolution. Nat Struct Mol Biol. 2024;31(5):826–34.

247. Edmonds M, Vaughan MH, Nakazato H. Polyadenylic acid sequences in the heterogeneous nuclear RNA and rapidly-labeled polyribosomal RNA of HeLa cells: possible evidence for a precursor relationship. Proc Natl Acad Sci U S A. 1971;68(6):1336–40.

248. Iwamoto M, Watashi K, Tsukuda S, Aly HH, Fukasawa M, Fujimoto A, et al. Evaluation and identification of hepatitis B virus entry inhibitors using HepG2 cells overexpressing a membrane transporter NTCP. Biochem Biophys Res Commun. 2014;443(3):808–13.

249. Otoguro T, Tanaka T, Kasai H, Kobayashi N, Yamashita A, Fukuhara T, et al. Establishment of a Cell Culture Model Permissive for Infection by Hepatitis B and C Viruses. Hepatol Commun. 2021 Apr;5(4):634–49.

250. Le C, Sirajee R, Steenbergen R, Joyce MA, Addison WR, Tyrrell DL. In Vitro Infection with Hepatitis B Virus Using Differentiated Human Serum Culture of Huh7.5-NTCP Cells without Requiring Dimethyl Sulfoxide. Viruses. 2021;13(1):97.

251. Will H, Cattaneo R, Koch HG, Darai G, Schaller H, Schellekens H, et al. Cloned HBV DNA causes hepatitis in chimpanzees. Nature. 1982;299(5885):740–2.

252. Hu X, Margolis HS, Purcell RH, Ebert J, Robertson BH. Identification of hepatitis B virus indigenous to chimpanzees. Proc Natl Acad Sci USA. 2000;97(4):1661–4.

253. Dupinay T, Gheit T, Roques P, Cova L, Chevallier-Queyron P, Tasahsu S i, et al. Discovery of naturally occurring transmissible chronic hepatitis B virus infection among Macaca fascicularis from Mauritius Island. Hepatology. 2013;58(5):1610–20.

254. Walter E. Hepatitis B virus infection of tupaia hepatocytes in vitro and in vivo. Hepatology. 1996;24(1):1–5.

255. Yan RQ, Su JJ, Huang DR, Gan YC, Yang C, Huang GH. Human hepatitis B virus and hepatocellular carcinoma. I. Experimental infection of tree shrews with hepatitis B virus. J Cancer Res Clin Oncol. 1996;122(5):283–8.

256. D'Ugo E, Argentini C, Giuseppetti R, Canitano A, Catone S, Rapicetta M. The woodchuck hepatitis B virus infection model for the evaluation of HBV therapies and vaccine therapies. Expert Opin Drug Discov. 2010;5(12):1153–62.

257. Reaiche GY, Le Mire MF, Mason WS, Jilbert AR. The persistence in the liver of residual duck hepatitis B virus covalently closed circular DNA is not dependent upon new viral DNA synthesis. Virology. 2010;406(2):286–92.

258. Yang Q, Zhao X, Zang L, Fang X, Zhao J, Yang X, et al. Anti-hepatitis B virus activities of α-DDB–FNC, a novel nucleoside–biphenyldicarboxylate compound in cells and ducks, and its anti-immunological liver injury effect in mice. Antiviral Res. 2012;96(3):333–9.

259. Allweiss L, Dandri M. Experimental in vitro and in vivo models for the study of human hepatitis B virus infection. J Hepatol. 2016;64(1 Suppl):S17–31.

260. Ilan E, Burakova T, Dagan S, Nussbaum O, Lubin I, Eren R, et al. The hepatitis B virus-trimera mouse: a model for human HBV infection and evaluation of anti-HBV therapeutic agents. Hepatology. 1999;29(2):553–62.

261. Chisari FV, Pinkert CA, Milich DR, Filippi P, McLachlan A, Palmiter RD, et al. A transgenic mouse model of the chronic hepatitis B surface antigen carrier state. Science. 1985;230(4730):1157–60.

262. Chisari FV, Filippi P, McLachlan A, Milich DR, Riggs M, Lee S, et al. Expression of hepatitis B virus large envelope polypeptide inhibits hepatitis B surface antigen secretion in transgenic mice. J Virol. 1986;60(3):880–7.

263. Guidotti LG, Martinez V, Loh YT, Rogler CE, Chisari FV. Hepatitis B virus nucleocapsid particles do not cross the hepatocyte nuclear membrane in transgenic mice. J Virol. 1994;68(9):5469–75.

264. Milich DR, Jones JE, Hughes JL, Price J, Raney AK, McLachlan A. Is a function of the secreted hepatitis B e antigen to induce immunologic tolerance in utero? Proc Natl Acad Sci USA. 1990;87(17):6599–603.

265. Kim CM, Koike K, Saito I, Miyamura T, Jay G. HBx gene of hepatitis B virus induces liver cancer in transgenic mice. Nature. 1991;351(6324):317–20.

266. Koike K, Moriya K, Iino S, Yotsuyanagi H, Endo Y, Miyamura T, et al. High-level expression of hepatitis B virus HBx gene and hepatocarcinogenesis in transgenic mice. Hepatology. 1994;19(4):810–9.

267. Yu DY, Moon HB, Son JK, Jeong S, Yu SL, Yoon H, et al. Incidence of hepatocellular carcinoma in transgenic mice expressing the hepatitis B virus X-protein. J Hepatol. 1999;31(1):123–32.

268. Klein C, Bock CT, Wedemeyer H, Wüstefeld T, Locarnini S, Dienes HP, et al. Inhibition of hepatitis B virus replication in vivo by nucleoside analogues and siRNA. Gastroenterology. 2003;125(1):9–18.

269. Marimani MD, Ely A, Buff MCR, Bernhardt S, Engels JW, Scherman D, et al. Inhibition of replication of hepatitis B virus in transgenic mice following administration of hepatotropic lipoplexes containing guanidinopropyl-modified siRNAs. J Control Release. 2015;209:198–206.

270. Julander JG, Sidwell RW, Morrey JD. Characterizing antiviral activity of adefovir dipivoxil in transgenic mice expressing hepatitis B virus. Antiviral Res. 2002;55(1):27–40.

271. Weber O, Schlemmer KH, Hartmann E, Hagelschuer I, Paessens A, Graef E, et al. Inhibition of human hepatitis B virus (HBV) by a novel non-nucleosidic compound in a transgenic mouse model. Antiviral Res. 2002;54(2):69–78.

272. Julander JG, Colonno RJ, Sidwell RW, Morrey JD. Characterization of antiviral activity of entecavir in transgenic mice expressing hepatitis B virus. Antiviral Res. 2003;59(3):155–61.

273. Dandri M. Repopulation of mouse liver with human hepatocytes and in vivo infection with hepatitis B virus. Hepatology. 2001;33(4):981–8.

274. Meuleman P, Libbrecht L, De Vos R, De Hemptinne B, Gevaert K, Vandekerckhove J, et al. Morphological and biochemical characterization of a human liver in a uPA-SCID mouse chimera. Hepatology. 2005;41(4):847–56.

275. Azuma H, Paulk N, Ranade A, Dorrell C, Al-Dhalimy M, Ellis E, et al. Robust expansion of human hepatocytes in Fah−/−/Rag2−/−/Il2rg−/− mice. Nat Biotechnol. 2007;25(8):903–10.

276. Hasegawa M, Kawai K, Mitsui T, Taniguchi K, Monnai M, Wakui M, et al. The reconstituted 'humanized liver' in TK-NOG mice is mature and functional. Biochem Biophys Res Commun. 2011;405(3):405–10.

277. Brezillon NM, Dasilva L, L'hôte D, Bernex F, Piquet J, Binart N, et al. Rescue of Fertility in Homozygous Mice for the Urokinase Plasminogen Activator Transgene by the Transplantation of Mouse Hepatocytes. Cell Transplant. 2008;17(7):803–12.

278. De Crignis E, Hossain T, Romal S, Carofiglio F, Moulos P, Khalid MM, et al. Application of human liver organoids as a patient-derived primary model for HBV infection and related hepatocellular carcinoma. Elife. 2021 Jul 30;10:e60747.

279. Lim CK, Romeo O, Chilver AP, Tran BM, Flanagan DJ, Kirby EN, et al. Human Liver Organoids as a Patient-derived Model for HBV Infection and Cellular Response. bioRxiv. 2022;2022–10.

280. Yang PL, Althage A, Chung J, Chisari FV. Hydrodynamic injection of viral DNA: A mouse model of acute hepatitis B virus infection. Proc Natl Acad Sci USA. 2002;99(21):13825–30.

281. Marion PL, Salazar FH, Liittschwager K, Bordier BB, Seeger C, Winters MA, et al. A transgenic mouse lineage useful for testing antivirals targeting hepatitis B virus. In: Frontiers in Viral Hepatitis [Internet]. Elsevier; 2003 [cited 2024 May 24]. p. 197–210. Available from: https://linkinghub.elsevier.com/retrieve/pii/B9780444509864500692

282. Sabnis S, Kumarasinghe ES, Salerno T, Mihai C, Ketova T, Senn JJ, et al. A Novel Amino Lipid Series for mRNA Delivery: Improved Endosomal Escape and Sustained Pharmacology and Safety in Non-human Primates. Mol Ther. 2018;26(6):1509–19.

283. Kalehua AN, Nagel JE, Whelchel LM, Gides JJ, Pyle RS, Smith RJ, et al. Monocyte chemoattractant protein-1 and macrophage inflammatory protein-2 are involved in both excitotoxin-induced neurodegeneration and regeneration. Exp Cell Res. 2004;297(1):197–211.

284. Meeuwsen S, Bsibsi M, Persoon-Deen C, Ravid R, van Noort JM. Cultured human adult microglia from different donors display stable cytokine, chemokine and growth factor gene profiles but respond differently to a pro-inflammatory stimulus. Neuroimmunomodulation. 2005;12(4):235–45.

285. Zimmerman KA, Fischer KP, Joyce MA, Tyrrell DLJ. Zinc finger proteins designed to specifically target duck hepatitis B virus covalently closed circular DNA inhibit viral transcription in tissue culture. J Virol. 2008;82(16):8013–21.

286. Kiaie SH, Majidi Zolbanin N, Ahmadi A, Bagherifar R, Valizadeh H, Kashanchi F, et al. Recent advances in mRNA-LNP therapeutics: immunological and pharmacological aspects. J Nanobiotechnology. 2022;20(1):276.

287. Matsumura T, Takano T, Takahashi Y. Immune responses related to the immunogenicity and reactogenicity of COVID-19 mRNA vaccines. International Immunology. 2023;35(5):213–20.

288. Igyártó BZ, Qin Z. The mRNA-LNP vaccines – the good, the bad and the ugly? Front Immunol. 2024;15:1336906.

289. Schoenmaker L, Witzigmann D, Kulkarni JA, Verbeke R, Kersten G, Jiskoot W, et al. mRNA-lipid nanoparticle COVID-19 vaccines: Structure and stability. Int J Pharm. 2021;601:120586.

290. Maeki M, Okada Y, Uno S, Sugiura K, Suzuki Y, Okuda K, et al. Mass production system for RNA-loaded lipid nanoparticles using piling up microfluidic devices. Appl Mater Today. 2023;31:101754.

291. Danaei M, Dehghankhold M, Ataei S, Hasanzadeh Davarani F, Javanmard R, Dokhani A, et al. Impact of Particle Size and Polydispersity Index on the Clinical Applications of Lipidic Nanocarrier Systems. Pharmaceutics. 2018;10(2):57.

292. Clogston JD, Patri AK. Zeta potential measurement. Methods Mol Biol. 2011;697:63–70.